CORA Cork Open Research Archive
Cartlann Taighde Oscailte Chorcaí

Title	Development of sustainable biomimetic syntheses of spherical silica particles
Authors	Curley, Ricky
Publication date	2020
Original Citation	Curley, R. A. 2020. Development of sustainable biomimetic syntheses of spherical silica particles. PhD Thesis, University College Cork.
Type of publication	Doctoral thesis
Rights	© 2020, Richard A. Curley. - https://creativecommons.org/licenses/by-nc-nd/4.0/
Download date	2026-10-31 07:02:33
Item downloaded from	https://hdl.handle.net/10468/11387



UCC
University College Cork, Ireland
Coláiste na hOllscoile Corcaigh

Ollscoil na hÉireann, Corcaigh

NATIONAL UNIVERSITY OF IRELAND, CORK



Development of Sustainable Biomimetic Syntheses of Spherical Silica Particles

Thesis presented by

Richard A. Curley M.Sc.

for the degree of

Doctor of Philosophy

University College Cork

School of Chemistry

Principle supervisor: Professor Justin Holmes

Advisor: Dr. Simon Lawrence

Head of School: Dr. Humphrey Moynihan

2020

Table of Contents

Declaration iv
Acknowledgements v
List of abbreviations i
Publications i
Abstract 1
Chapter 1 2
1.1 Introduction 3
1.1.1 Overview 5
1.2 Spherical silica 7
1.2.1 Stöber process 7
1.2.2 Modified-Stöber process 9
1.2.3 Structure-directing agents 9
1.2.4 Hydrolysis and condensation 12
1.2.5 Ostwald ripening and coalescence 17
1.3 Environmental problems of Stöber silica production 19
1.4 Natural silica production 20
1.4.1 Specific biomolecules involved in biomineralisation of silica 22
1.4.2 Long-chain polyamines 22
1.4.3 Amino acids and peptides 25
1.4.4 Silaffins 29
1.5 Bridging the gap – connecting Stöber to Nature 32
1.5.1 Biopolymer physicochemical characteristics key to spherical silica synthesis 32
1.5.2 Biopolymer sources 37
1.5.3 Synthesising spherical silica particles with biopolymers 39
1.6 Conclusions and outlook 55
1.7 References 56
Chapter 2 83
2.1 Abstract 84
2.2 Introduction 85
2.3 Experimental 86
2.3.1 Materials 86
2.3.2 Method 86
2.3.3 Characterisation 87

2.4 Results and Discussion 89
2.4.1 Effect of ethanol concentration on particle size and morphology 89
2.4.2 Effect TEOS concentration on particle size and morphology 96
2.4.3 Effect of ammonium hydroxide concentration on particle size and morphology 103
2.4.4 Effect of water on particle size and morphology 109
2.5 Conclusion 115
2.6 References 117
2.7 Appendix 123
2.7.1 MATLAB sizing code 126
Chapter 3 131
3.1 Abstract 132
3.2 Introduction 133
3.3 Experimental 140
3.3.1 Materials 140
3.3.2 Silica preparation using L-α-phosphatidylcholine and soy lecithin 140
3.3.3 Characterisation 141
3.4 Results & Discussion 142
3.4.1 Silica Production via Phosphatidylcholine (PC) 146
3.4.2 Silica Synthesis via Soy Lecithin 151
3.5 Conclusion 162
3.6 References 164
3.7 Appendix 177
Chapter 4 184
4.1 Abstract 185
4.2 Introduction 186
4.3 Experimental 188
4.3.1 Materials 188
4.3.2 Silica preparation using ammonium hydroxide 188
4.3.3 Silica preparation using buffer 189
4.3.4 Silica preparation using buffer and $CaCl_2$ 190
4.3.5 Characterisation 192
4.4 Results and Discussion 193
4.4.1 Silica prepared with ammonium hydroxide 193
4.4.2 Silica prepared with acetate buffer 196
4.4.3 Silica prepared with acetate buffer and calcium chloride 203

4.5 Conclusion 219
4.6 References 220
4.7 Appendix 226
Chapter 5 234
5.1 Conclusion 235
5.2 Future Work 240

Declaration

This is to certify that the work I am submitting is my own and has not been submitted for another degree, either at University College Cork or elsewhere. All external references and sources are clearly acknowledged and identified within the contents. I have read and understood the regulations of University College Cork concerning plagiarism.

_____

Richard A. Curley

Acknowledgements

Coming to the end of my PhD, it is nice to take the opportunity to look back at the time I have spent in UCC. It is more difficult than one would think to condense the last four years – the highs, lows, and everything in between – into a few short paragraphs. Though, attempting to do so provides a catharsis which, I suppose, is a fitting end to a PhD. The significance of getting to this point is not lost on me. Growing up in a single-parent family in a council estate, one would think the odds are stacked against progression to third level education. However, with the support and backing of many people along the way, I am proud and humbled to have gotten this far. A special thanks to all the team at the UCC PLUS+ programme whose tireless work with children from disadvantaged backgrounds has helped many kids like myself realise their goal of progressing to third level education. They were a source of unwavering support throughout my time in UCC and it has been an immense source of pride when, in my later years in UCC, I was able to give back and help them run some of their many programmes, cementing the idea that kids like us can obtain college degrees.

To my supervisor Prof. Justin Holmes, thank you for all your help throughout my PhD. You have been a constant source of advice and guidance, which has been invaluable, to say the least. We have had many fruitful discussions – science-related and otherwise – which I will always remember. To all the members of the MCAG group, thank you – especially Tim, who always delighted in helping anyone and everyone, and never gave a second thought in doing so.

To everyone at the ERI, where I spent the majority of my time during my PhD, thank you for all your help and for making my time there memorable. To Dr. Paul Bolger, manager of the ERI, and one of the nicest people you will ever meet, thank you for your everything. To all the Glantreo team – Joe T, Tommy, Aoibhín, Daithí, Victor, Joe, John H – it has been a pleasure working with you for the last number of years. To Dr. John Hanrahan, thank you for giving me the opportunity to work with you and for all your help and guidance over the years, it has been a great experience, one I will never forget. To all the staff at UCC – too many to mention – who have given their help and support over the years, thank you.

To Russell, thank you for all your help throughout the years. From tea breaks to lab work, you were always on hand, and never faltered in offering support and friendship. I'm delighted you've finished your PhD, no one deserves it more.

The person who has done more than anyone to help me over the last four years, and for whom words alone will consistently fail to describe just how much, is Dr. Eoin Flynn. There is no arrangement, nor combination, of words that can begin to describe my sincere thanks and utter admiration for what you have done. These words that I have arranged can only suffice as a conduit, beginning, but never wholly, relaying just how much of an inspiration you have been. Your moral character, steadfast stoicism, and wisdom has influenced me greatly. Many of the things I have learned from you are intangible; things which cannot be taught by dictation, only through example. You took me under your wing, spent countless hours correcting, revising, advising, and guiding my work; sacrificing your own free time in the process. What you have done is beyond what anyone could ask, and for this I am eternally grateful.

To Anne-May, you've been a constant source of support throughout my PhD. Enduring the lows, and underscoring the highs. Yours was an integral part, one which you may not realise, but you've helped in more ways than you can imagine.

Finally, the greatest thanks and appreciation is reserved for my mother. Raising three kids by yourself is tough. Raising three kids and putting all of us through college is awe-inspiring. It is an astounding achievement and a great source of pride for you, I know. Again, I am lost for words. There are none that can describe the sacrifice you've made over the years in getting all three of us this far. You've always pushed us to be the best that we can be. Without you, none of this would have been possible. Thank you.

List of abbreviations

BET – Brunauer-Emmett-Teller

BSA – Bovine Serum Albumin

CTAB – Cetyltrimethylammonium Bromide

CMC – Critical Micelle Concentration

DLS – Dynamic Light Scattering

EDX – Energy-dispersive X-ray Spectroscopy

EtOH – Ethanol

FWHM – Full Width at Half Maximum

LCPA – Long-chain Polyamine

NaCas – Sodium Caseinate

PC – Phosphatidylcholine

PDI – Polydispersity Index

PSD – Particle Size Distribution

RSD – Relative Standard Deviation

SDA – Structure-directing Agent

SEM – Scanning Electron Microscopy

SL – Soy Lecithin

SNP – Silica Nanoparticle

SO – Soybean Oil

SS – Sodium Silicate

TEOS – Tetraethyl Orthosilicate

XPS – X-ray photoelectron Spectroscopy

Publications

Published

Curley, R., Banta, R.A., Garvey, S., Holmes, J.D. & Flynn, E.J. Spherical Silica Particle Production By Combined Biomimetic-Stöber Synthesis Using Renewable Sodium Caseinate Without Petrochemical Agents. *Applied Nanoscience*, DOI: 10.1007/s13204-021-01762-2.

Submitted Publications

Curley, R., Holmes, J.D. & Flynn, E.J. Can Sustainable Monodisperse Spherical Silica Be Produced From Biopolymers? A Review.

Curley, R., Banta, R.A., Garvey, S., Holmes, J.D. & Flynn, E.J. Biomimetic Spherical Silica Production using Phosphatidylcholine and Soy Lecithin.

Co-authored Publications

Banta, R.A., Collins, T.W., Curley, R., Young, P.W., Holmes, J.D. & Flynn, E.J. Nanopatterned protein-polysaccharide thin films by humidity regulated phase separation. *Journal of Colloid and Interface Science*, **532**, 171-181 (2018)

Banta, R.A., Collins, T.W., Curley, R., O'Connell, J.J., Young, P.W., Holmes, J.D. & Flynn, E.J. Regulated Phase Separation in Nanopatterned Protein-Polysaccharide Thin Films by Spin Coating. *Colloids and Surfaces B: Biointerfaces*, **190**, 110967 (2020)

Conferences

"**Silica production from biopolymers**" – 24th Annual Green Chemistry & Engineering Conference, online conference, June 15th – 19th, 2020. (Presentation)

Abstract

The work in this thesis concerns the development of processes to produce monodisperse and spherical silica particles using more sustainable and environmentally benign means. Spherical silica is widely used and is integral to many advanced applications. A major problem, however, is that current silica production methods are inherently unsustainable. Contemporary silica production can be rendered more sustainable by optimising for efficiency, an approach used in Chapter 2, when analysing a process used by Glantreo Ltd. However, optimisation of such processes eventually leads to stalemate, in which no further increase in sustainability is possible. This is due to the fundamentally unsustainable nature of the reagents used in such processes – petrochemical surfactants, organic solvents, and certain alcohols. Therefore, to create spherical silica in a sustainable and environmentally benign way, the work in this thesis lays out possible development routes for spherical silica manufacturing research into biomimetic processes which use biopolymers, mild conditions, and water-based chemistries to synthesise silica particles.

Chapter 1

Introduction

This chapter has been submitted for publication as a review article.

Curley, R., Holmes, J.D. & Flynn, E.J. Can Sustainable Monodisperse Spherical Silica Be Produced From Biopolymers? A Review.

1.1 Introduction

Spherical silica is one of the most important contemporary industrial materials. It has many integral uses across a diverse range of areas such as catalysis, adsorption, chromatography, sensors, and drug delivery, to name just a fraction.[1–5] However, like many industrial materials that are fundamental to modernity, there are issues with how spherical silica is currently produced. Since the Industrial Revolution, rates of anthropogenic pollution have rapidly increased in tandem with, and with profound causal links to, the innovation and advancement of industrial production. Throughout this period, right up to the present day, little regard in industry has been given to environmental consequences of inefficiencies and wastes of industrial processes.

In an attempt to address this failing the concept of Green Chemistry was formalised in the 1990s. One of its key facets is the "design of chemical products and processes to reduce or eliminate the use and generation of hazardous substances."[6] In essence, this means developing processes that are more sustainable, through the use of reagents which cause minimal environmental damage. Ideally, these reagents come from natural and renewable sources, that are either biodegradable or environmentally benign. This must become the guiding principal for industrial development, and silica manufacturing is no exception.

The ubiquity of spherical silica necessitates the manufacture of vast quantities of it annually to meet worldwide demand. The global market for precipitated silica, including spherical silica, was valued at USD 1.96 billion in 2018 and is expected to continue to grow.[7] However, industrial spherical silica production methods currently use vast quantities of environmentally damaging reagents such as alcohols, alkoxysilanes, and oil-derived surfactants.[8–10] These embedded environmental costs render the processes

unsustainable. Thus, finding environmentally friendly alternative production methods for spherical silica is critical. Learning from nature's own silica production method, *biomineralisation,* may offer the means to do so.

Biomineralisation is the process by which certain plants and animals create complex, hierarchical, mineral structures, often out of silica, from simple starting materials.[11] For hundreds of millions of years plants have been using silica for structural supports and pathogen defense.[12] Animals also use silica on a vast scale, with radiolaria, sponges, molluscs, and diatoms among those which have mastered the biomineralisation process.[13–16] Diatoms are particularly interesting to materials scientists. These creatures are single-celled algae that can construct labyrinthine structures out of silica with ease. They have become model organisms for studying the silica biomineralisation process. The level of detail and control achieved in diatom silica structures has not been matched by materials science. The complexity of the bottom-up silica production processes of diatoms makes *in vitro* replication of their silica constructs profoundly difficult. But biomimetic materials research has attained some understanding of the fundamentals of biomineralisation processes. This knowledge can be used to produce biosilica – silica particles synthesised via biomimetic processes – using environmentally friendly means.

Since the discovery and isolation of the biomolecules responsible for biomineralisation there have been numerous attempts to use this knowledge to replicate the process in vitro to create various silica structures.[17–20] While some of these studies have attempted to produce spherical silica particles, discrete and monodisperse particles produced via a truly sustainable biomimetic synthesis is still difficult. Identifying the parallels between biomineralisation and the current industrial methods of silica production, based upon the

Stöber process and its derivatives, may be the key to this morphological control. Another key advantage of synthesising spherical silica biomimetically is the reduced environmental impact, due to the relatively mild synthesis conditions, compared to the current methods.[19] When the Stöber processes use templating agents to control the particle morphology, these are often petrochemical surfactants. Extraction and refinement of fossil fuels, such as petroleum – from which traditional surfactants are derived – causes severe damage to ecosystems, local environments, and the climate.[21,22] Biopolymers offer a less problematic alternative. They are renewable, naturally occurring, environmentally benign, and their production and use generates less CO_2.[23] As with traditional polymers, there is a great, and ever growing, variety of highly refined biopolymers available. This stems from their widespread use in many materials science applications,[24–28] and particularly in the medical field, for drug delivery and wound healing applications.[29–33] Biopolymers have also been extensively used in food technology, mainly as films, coatings, and emulsion stabilisers.[34–37] Now, green chemistry aspirations are accelerating the use of biopolymers into further fields.

1.1.1 Overview

Chapter 1 introduces key concepts of traditional spherical silica production and the natural production of silica via biomineralisation. The similarities between these processes are highlighted and detailed, and studies using biomolecules to synthesise spherical silica in a sustainable and environmentally benign way are explored. **Chapter 2** focuses on analysing a process used by Glantreo Ltd., which synthesises silica industrially, to create non-porous spherical silica particles based on the traditional Stöber process. Glantreo Ltd. needed to optimise the process in order to control the dimensions

of the particles in the nanometre range based on the input concentrations of reagents. The ability to control the dimensions of these particles gave Glantreo Ltd. the base knowledge to scale up this process in an efficient manner. Statistical analysis of the process allowed for the determination of particle size and yield based on input reagent concentrations which improved the efficiency of the process by only using the necessary amounts of reagents and energy required to get a specific particle size. **Chapter 3** follows on from the work in **Chapter 2** and focuses on making spherical silica particles in a biomimetic and sustainable way using the Stöber process as a starting point. The biomolecules phosphatidylcholine and soy lecithin are used to synthesise spherical silica particles using a green methodology. **Chapter 4** expands on this work further by using sodium caseinate to synthesise spherical silica particles using statistical analysis and design of experiments methodologies. A regression equation is obtained allowing the prediction of particle size based on input reagent concentrations. **Chapter 5** concludes this thesis with some overarching conclusions and a future outlook on potential avenues for research into sustainable silica production.

This thesis lays out the parallels between the established Stöber processes and the emerging field of biomimetic silica, with a view to bridging the gap between the two. The focus will be on the physicochemical characteristics of the specific biomolecules responsible for biomineralisation in creatures such as diatoms and how they relate to the surfactants used in the Stöber processes. These properties are then used to identify biopolymers readily available from sustainable sources that may fulfil the role of the surfactants in the Stöber processes and enable the synthesis of spherical silica particles. Spherical silica is a material of great importance, and there is a growing need for its

production to be sustainable. While the process of biomineralisation, with its complex structures and granular control, and the Stöber processes may seem distinct from one another, the underlying formation process is strikingly similar (section **1.4**). This thesis looks at whether the unsustainable traditional spherical silica syntheses can be replaced with sustainable, biopolymer-based ones. In the first chapter, firstly we will focus on a background of spherical silica formation in the Stöber processes, and the inherent environmental problems associated with them. Secondly, explaining biomineralisation, the biomolecules responsible for the formation of silica in vivo, and physicochemical properties of biopolymers which are conducive to this. Thirdly, the parallels between the Stöber processes and biomineralisation are investigated and highlighted, and examples are given of attempts to produce silica in a biomimetic way using these parallels. Lastly, the future outlook is given on using biopolymers to create sustainable spherical silica, looking at specific examples of attempts to create spherical silica using biopolymers, and any potential barriers to this are explored.

1.2 Spherical silica

There are a number of key ways in which natural silica production in organisms is paralleled by industrial silica production. One can use biopolymers to take advantage of those parallels to make silica more sustainably. But, to do this, one must first understand current industrial spherical silica production methods. There is a single historical point of origin for all modern spherical silica manufacture – *the Stöber process.*

1.2.1 Stöber process

The origins of spherical silica production begin in 1968 when Stöber *et al*.[38] reported a process for the controlled growth of spherical non-porous silica particles of uniform size.

Since then, the field has grown drastically to include modified versions of this process to give highly porous, high surface area silica particles, which extends the applications into areas such as drug delivery and high performance liquid chromatography.[39,40] The particles obtained via this method ranged in size from 50 nm to 2000 nm in diameter. The relatively simple procedure involves mixing a silica precursor, an alkyl silicate, with ammonia, in a water/alcohol solution. The alkyl silicate is hydrolysed to give silicic acid, which subsequently condenses to yield monodisperse silica particles. Ammonia is used as a base catalyst and influences the morphology of the particles to render them spherical. A key aspect of the Stöber process is the ability to produce monodisperse particle sizes by altering the reaction conditions, i.e., type of alcohol/alkyl silicate and concentrations of the various reagents. During their systematic study of these conditions, Stöber *et al*. found that the rate of hydrolysis and condensation is fastest in methanol, giving smaller particles, and slowest in n-butanol, giving larger particles. The choice of alkyl silicate also influences particle size. Fastest reaction rate and smallest particle sizes were observed with tetramethyl orthosilicate, while slowest reaction rate and larger, fewer uniform particles were observed for tetrapentyl orthosilicate. The reason for this is that smaller alkyl chains are more sterically accessible, while larger chains are sterically hindered. The concentration of water influences the rate of hydrolysis and thus, the final particle size. Ammonia affects the morphology of the final particles. Absence of ammonia leads to irregularly shaped particles, indicating that it acts as a morphological catalyst. Control of particle size and morphology was a key step forward in silica production. Thus, key to forming discreet spherical silica particles is the presence of a morphological-control agent, aka, structure-directing agent (SDA). In this case, the SDA is ammonia. But as the

process for creating spherical silica evolved, petrochemical surfactants such as CTAB were used as the SDA. The reason why, and mechanism by which, these surfactants work is explained subsequently, but for now it suffices to say that it is these same properties that allow certain biopolymers to also create spherical silica particles.

1.2.2 Modified-Stöber process

After Stöber's seminal work on non-porous particles, surfactants were incorporated into the synthesis to create porous particles. These modified-Stöber processes broaden the utility of the particles by opening new applications. The role of the surfactants is to control the morphology, size, and porosity of the particles. This surfactant-templated approach enables a high degree of control of the these physical properties.[41] The most commonly used templating agents are long-chain amine molecules such as hexadecylamine (HDA) and cationic surfactants such as cetyltrimethylammonium bromide (CTAB), which is even more widely used. The surfactants form micelles in solution and under basic conditions the negatively charged silica oligomers interact with the positively charged or neutral surfactants. The surfactant acts as a structure-directing agent (SDA), which controls the formation of the pores and size of the particles.[42] The surfactant is then removed post-synthesis by calcination to reveal the pores. The synthesis can also be done in acidic conditions with triblock copolymer templates.[43] In either case mesoporous silica particles are formed.

1.2.3 Structure-directing agents

The structure and shape of the silica particles is highly dependent on the interactions between the silicate species and SDA during synthesis. The SDA controls the morphology of the final silica particles. In the case of the Stöber synthesis, the morphological control

comes from the ammonium hydroxide. Under basic conditions the surface of the forming particles is negatively charged and the cationic ammonium ion is electrostatically attracted to the surface. This attraction prevents aggregation of the particles and allows discrete spherical particles to grow. Such colloidal stability is generally well described by DVLO theory,[44] which describes the interaction of particles in a liquid medium as the sum of van der Waals and double layer interactions. The van der Waals forces arise from the fluctuating dipoles of atoms and molecules,[45] and are typically attractive forces. The electrical double layer forms on the surface of the particles with the first layer consisting of NH_4^+ ions attracted to the negatively charged silica surface and the second layer being made up of negatively charged ions such as OH^-. Thus the electrical double layer describes the repulsion force between particles because when two double layers overlap, electrostatic repulsion increases.[46] Whether particles aggregate together, or remain stable and do not aggregate, depends on the net potential energy, which is a sum of the van der Waals and double layer forces. If van der Waals forces dominate, the particles will aggregate, and if the double layer forces dominate, the particles will be repulsed. Ionic strength, pH, and surfactants have a direct influence on these forces, and therefore, colloidal stability.[47]

In modified-Stöber syntheses, the principle is the same although the way in which the structure-directing agent acts differs slightly. As mentioned, non-ionic or cationic surfactants are typically used in modified-Stöber syntheses. At high concentration, the surfactant forms micelles to lower the system entropy.[48] The concentration above which these micelles form is known as the critical micelle concentration (cmc). Inside the micelle core, which is essentially liquid hydrocarbon, there is greater freedom for

movement and so the entropy associated with the hydrocarbon tails also increases, which promotes the formation of micelles.[49] The electrostatic interaction between the surfactant and the growing network of silica depends on the pH of the reaction conditions. **Figure 1.1** shows three of these possible interactions.

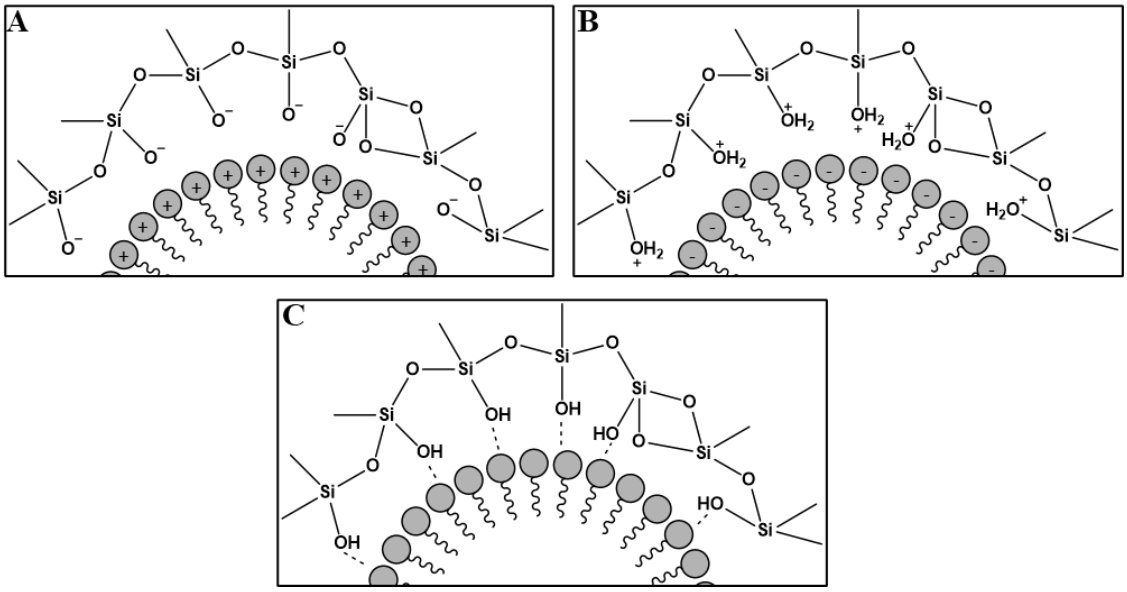


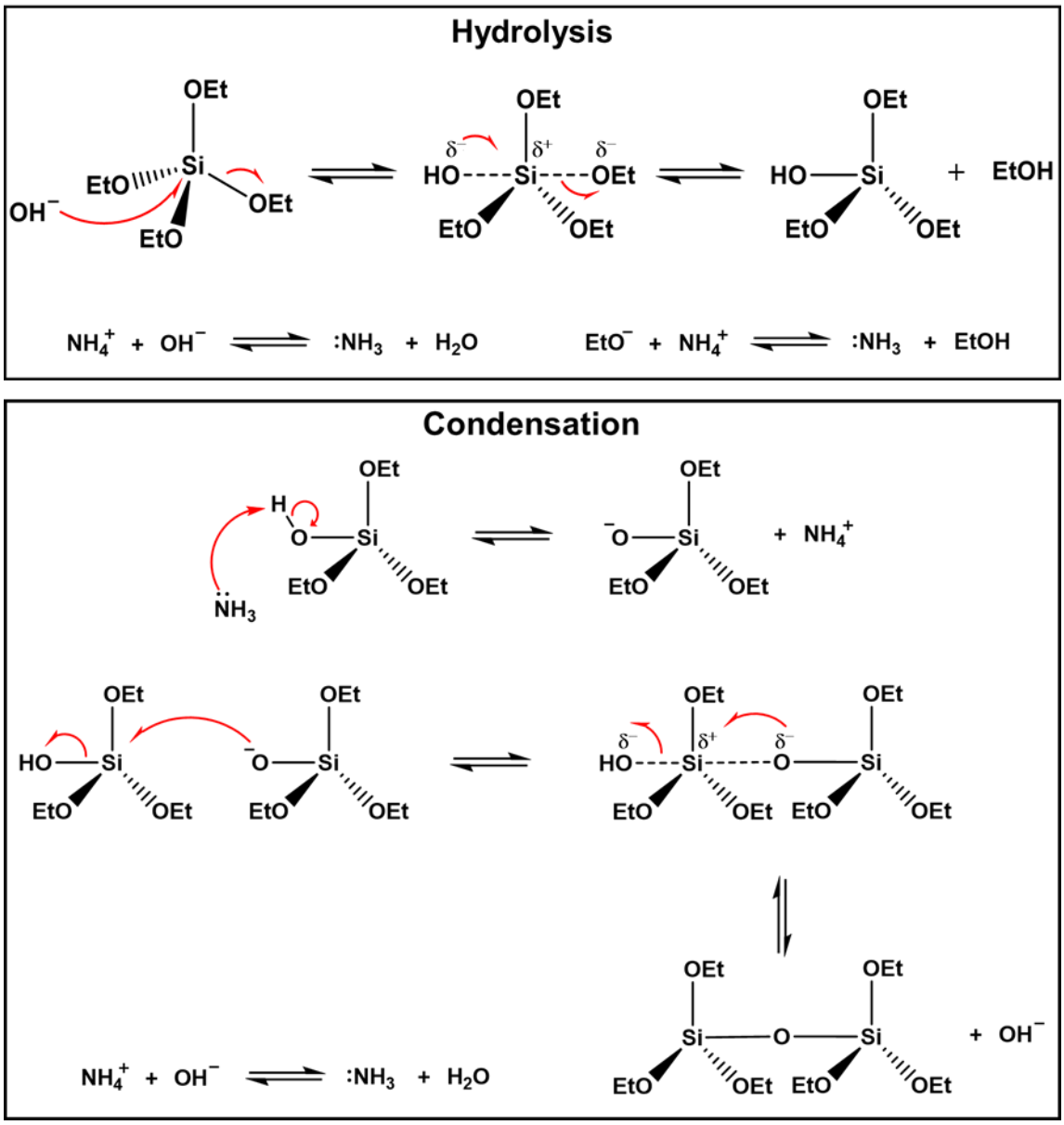
Figure 1.1 *Example of (a) interaction of cationic surfactant with negatively charged silicate species in basic conditions, (b) interaction of anionic surfactant with positively charged silicate species in acidic conditions and (c) interaction of non-ionic surfactant with silica through hydrogen bonding. Note: other types of interactions exist, shown here are the three most common. Adapted from Alothman.*[49]

The electrostatic interactions bring the silica oligomers into greater proximity with each other and as a result the silica network condenses around the surfactant micelles (see **Figure 1.3**). These electrostatic interactions also prevent aggregation of the particles and discreet monodisperse particles are produced. Non-ionic surfactants such as HDA interact with the silica surface through hydrogen bonding. This hydrogen bonding occurs between the amine hydrogen and the oxygen, and the hydroxyl hydrogen and the nitrogen.[50] Again

the silica condenses around the surfactant, while preventing aggregation. A more detailed explanation of the growth mechanism is provided in the proceeding sections.

1.2.4 Hydrolysis and condensation

The growth of silica particles in the Stöber process is, at its most fundamental, controlled by two reactions: (1) the hydrolysis of TEOS [$Si(OEt)_4 \rightarrow Si(OEt)_{4-x}(OH)_x$], where x = 1 – 4, and (2) condensation of the $Si(OEt)_{4-x}(OH)_x$ monomers into the siloxane network. **Scheme 1.1** shows the mechanism of the hydrolysis and condensation processes. The hydrolysis of the silica precursor can take place under acidic or basic conditions. At basic pH, the formation of spherical particles is promoted, while silica gels generally form under acidic pH.[51] The reason for this difference is that under acidic conditions, the forming silica particles bear little surface charge and aggregation into a gel network is more likely.[52] Whereas under basic conditions, electrostatic repulsion inhibits aggregation. The Stöber process uses ammonium hydroxide as the base catalyst to accelerate the hydrolysis and condensation of TEOS, as shown in **Scheme 1.1**. The initial hydrolysis step is the slowest and rate-determining step, but the rate increases as more ethoxy groups are removed due to increased positive charge of the silicon and reduced steric hindrance around the silicon.[53] The condensation reaction is similar to the hydrolysis reaction in that it involves a nucleophilic substitution reaction transitioning through a pentacoordinate intermediate which forms the siloxane network. The hydrolysis and condensation reactions, and the degree to which either one dominates, have a significant impact on the size and morphology of the final particles, as discussed below.



Scheme 1.1 *Mechanism of hydrolysis and condensation of TEOS in the presence of ammonia (Stöber process). TEOS is hydrolysed to give the oligomeric precursor species. Note that the hydrolysed precursor shown here is only one of the possible structures formed. For a more detailed description of these intermediaries, see Trinh et al.*[54] *Condensation of these oligomers leads to the generation of small primary seed/sub-particles. These nucleation events precede the formation of the final particles. The final particles are formed typically via coalescence and/or Ostwald ripening of the seed particles. Mechanism adapted from Ghimire et al.*[53]

Two prominent mechanisms have been proposed to describe the growth of the silica particles – the monomer addition,[55,56] and aggregation models.[57,58] Briefly, the monomer addition model suggests that monomers continue to form until above a certain critical supersaturation level, a burst nucleation event occurs. This nucleation event consumes the monomers until the concentration of monomers falls below the nucleation threshold. After this, monomers preferentially deposit onto the growing siloxane network resulting in particle growth. The aggregation model suggests that particle growth occurs via the aggregation of particles that are formed during nucleation. Smaller particles are colloidally unstable due to their high interfacial energy and therefore aggregate together, resulting in particle growth. These two models provide two distinct growth mechanisms, however they may not be mutually exclusive.

Recent research by Han *et al.*[59] has tried to reconcile the relationship between the two growth models by looking at the kinetic balance between them. They describe two pathways (see **Figure 1.2**) to growth in the Stöber process, Pathway I: hydrolysis of the silica precursor into silanol monomers which initially nucleate to form seeds for growth; and Pathway II: condensation of newly-formed silanol monomers onto the seeds formed in Pathway I, which results in augmentation of the silica particles. They found that monodisperse silica nanoparticles were only formed in concentrated ammonia solutions (≥0.95 M), which increased the hydrolysis of the silica precursor. At lower ammonia concentrations, the hydrolysis rate is slowed and polydisperse particles are formed.

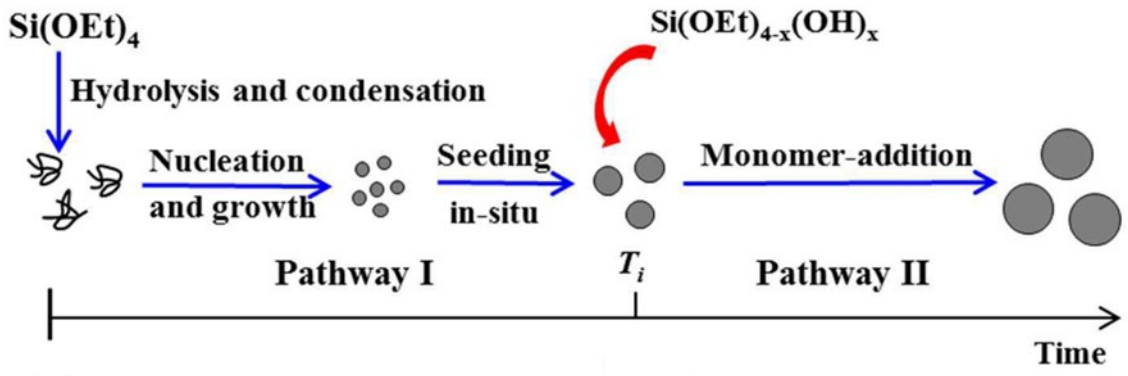


Figure 1.2 *From Han et al.*[59] *Particle growth can be divided into two consecutive stages, Pathway I (nucleation-growth) and Pathway II (monomer addition) at high ammonia concentration (≥0.95 M); or Pathway I (nucleation-growth), Pathway I+II (continuous nucleation and monomer addition) at low ammonia concentration (< 0.95 M).*

The growth mechanism for silica particles in the presence of an SDA such as CTAB can be described by similar monomer addition and aggregation models. **Figure 1.3** shows these two pathways. The monomer addition (upper pathway) describes the adsorption of silicate anions onto the surface of the micelles followed by condensation around the micelle, forming primary particles. Growth then occurs by addition of monomeric or oligomeric silica and surfactant molecules, with mesophase structuring occurring through rearrangement of the aggregated species from a non-ordered agglomerate.[60] The aggregation model (lower pathway) describes the adsorption of polymeric silica onto individual micelles (primary particles) which then aggregate together to form the mesostructure.[61] In both cases, the adsorption of silicate species onto the surface of the micelle reduces electrostatic repulsion between the micelles, allowing them to aggregate and subsequently form particles. CTAB has also been shown to form bilayers on the surface of silica particles, which allows for charge stabilisation.[62,63] This provides colloidal stability to the particles, similar to the way in which NH_4^+ acts in the Stöber synthesis.

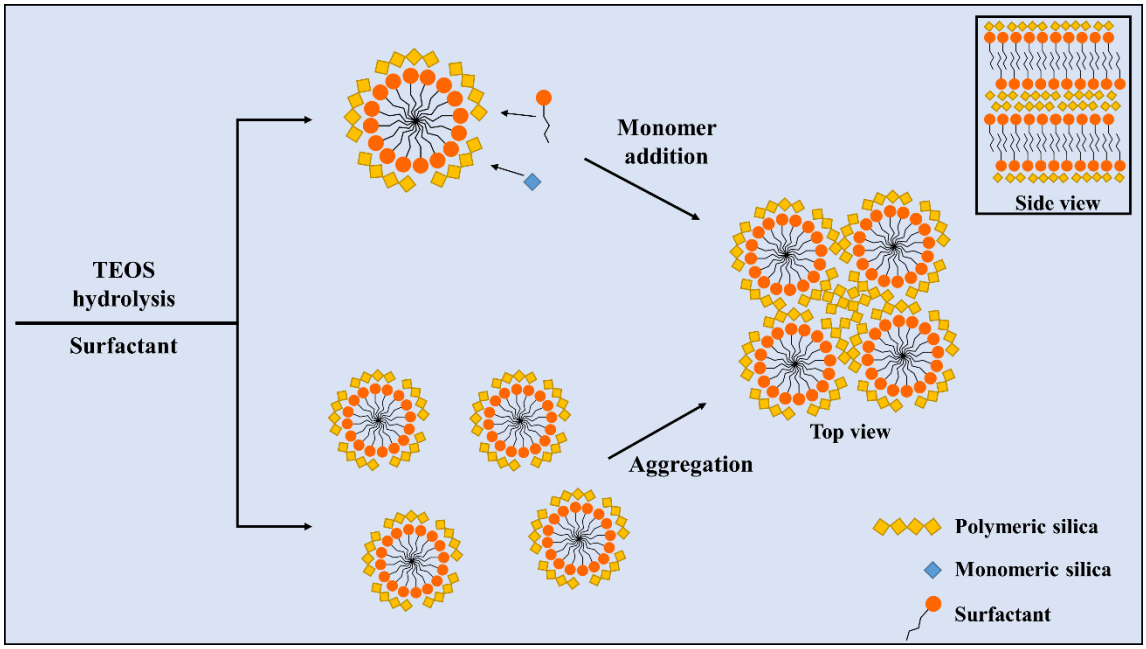


Figure 1.3 *Proposed mechanisms for the formation of surfactant-templated silica. The upper pathway corresponds to a monomeric silica addition mechanism. The lower pathway corresponds to aggregation of seed particles to form larger particles. Adapted from Nooney et al.*[61]

Another proposed mechanism for particle growth is through a phase-separation process. Initially, TEOS is located in the core of the surfactant micelle due to its immiscibility with water. The ethanol used in the synthesis is thought to act as a cosurfactant inside the surfactant micelles, involved in the formation of phase-separated seed particles.[60] Then the ethanol acts as a cosolvent decreasing the rate of hydrolysis of TEOS. This decreased hydrolysis rate slows down the production of anionic silicate species, which allows the electrostatic repulsion between surfactant headgroups to increase, elongating the micelles.[64] These elongated micelles then aggregated together, resulting in particle growth. However, SANS and molecular simulation data indicate that the likely mechanism of formation follows that of **Figure 1.3**.[65,66]

1.2.5 Ostwald ripening and coalescence

A complementary process of particle growth occurs via Ostwald ripening, which is a coarsening process which occurs in the late stage of phase transformation.[67] In general, when particles are formed from a homogeneous solution, a phase transition occurs. This transition causes an interfacial area to be created between the solid and liquid phases. Smaller particles have a higher surface-to-volume ratio than larger particles, and thus have higher surface energies associated with them. As such, any process which produces larger particles at the expense of smaller particles will be thermodynamically favourable. In order to grow, reactive units (either monomers or small aggregates) must diffuse to the surface, followed by subsequent reaction at the surface, of the particles. The coarsening can be described as occurring via diffusion-limited growth or reaction-limited growth. The most prominent Ostwald ripening process is that of diffusion-limited growth which was given a mathematical description by Lifshitz and Slyozov[68] and Wagner[69], the so-called LSW theory. Ostwald ripening can be identified in particle size distributions by a characteristic Gaussian curve. Coalescence is the fusion of two or more particles together, leading to particle growth. This process is also results in a lowering of the interfacial energy between the particles and the solution. However unlike Ostwald ripening which tends to produce size-monodisperse particles, coalescence tends to produce polydisperse particles. This is due to the non-homogenous fusion of particles and is characterised by a log-normal curve in particle size distributions. Ostwald ripening dominates in typical silica production methods. **Figure 1.4** shows some example silica particles prepared via the Stöber process.

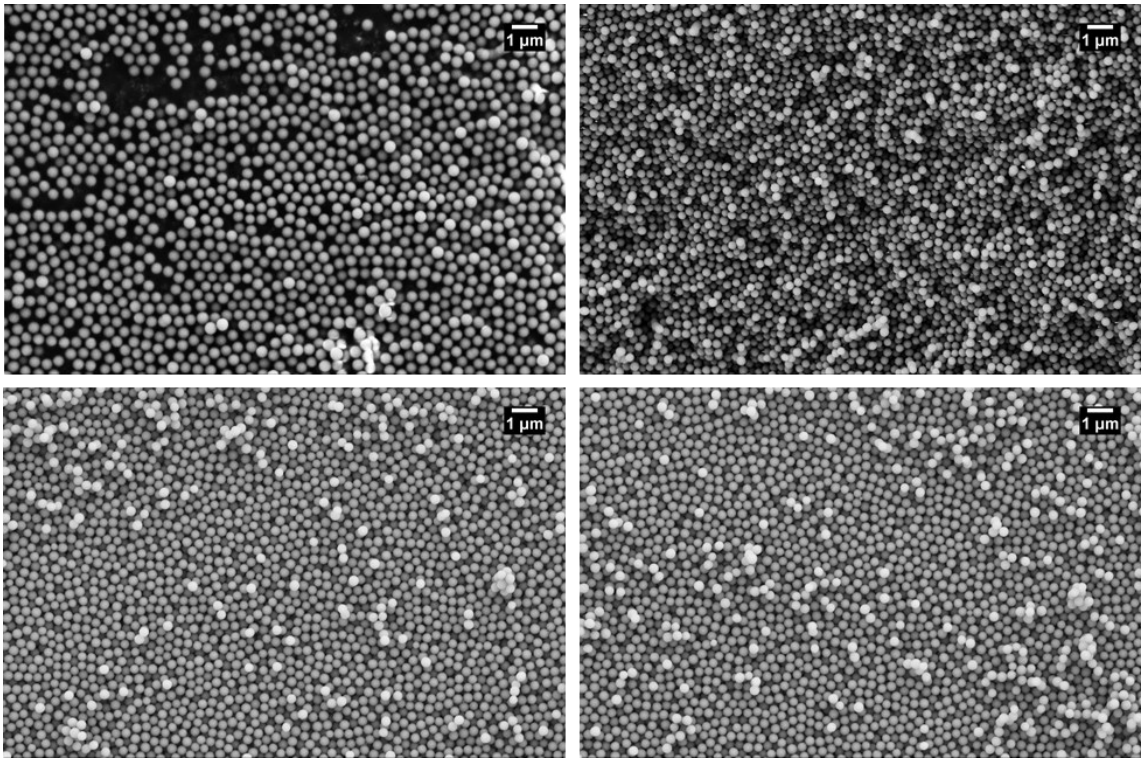


Figure 1.4 *Scanning electron microscopy images of silica nanoparticles prepared via the Stöber process. Scale bar = 1µm. Images from author's own work.*

In summary, spherical silica particles can be readily achieved via Stöber processes. The key additive that enables and promotes the spherical morphology is an SDA. The silica precursor is first hydrolysed and the SDA interacts with the hydrolysed silicate species primarily through electrostatic and/or hydrogen bonding interactions. These interactions, along with the growth mechanisms described above, promote the formation of spherical silica. The SDA also prevents aggregation of the forming particles through these same electrostatic and/or hydrogen bonding interactions, as discussed previously.

1.3 Environmental problems of Stöber silica production

While spherical silica production is important, the production process is problematic. A typical Stöber process, and its derivatives, uses some combination of the following categories of reagents: an alkoxysilane as the silica precursor, ammonia, surfactant, water, and an alcohol. The most commonly used silica precursor is tetraethyl orthosilicate (TEOS), but others such as tetramethyl orthosilicate (TMOS), tetrapropyl orthosilicate (TPOS), and tetratbutyl orthosilicate (TBOS) are also used. The main environmental problem associated with these compounds is their toxicity when they are released into the environment. This release may be accidental or deliberate, through inadequate waste disposal. Numerous studies of alkoxysilane toxicity have been conducted, with renal failure, and acute tubular necrosis, and even fatalities in some animal models among the most serious observations.[10,70–72] Ammonium hydroxide can also be toxic if released into the environment and is classed as H400 (very toxic to aquatic life) by the Globally Harmonised System of Classification and Labelling of Chemicals (GHS).[73] Ammonium hydroxide in water exists in equilibrium with the free ammonia form, which is more toxic than the ionised form.[74] Numerous studies on the effect of ammonia on aquatic life have reported an LC50 (lethal concentration, 50%) in the range of just µg/L to mg/L. A comprehensive list of these studies is available in this USEPA report.[75] Ethanol is commonly used as pesticide (microbiocide, fungicide, etc.) with a well-established toxicological profile – its use and inadequate disposal can pose ecological and environmental problems.[76] Surfactants such as cetyltrimethylammonium bromide (CTAB) and hexadecylamine (HDA) are commonly used in the manufacture of porous silica particles. These petrochemically-derived compounds pose a high risk to the

environment and health.[77,78] CTAB is listed as H400 by the GHS. HDA is also listed as H400, with further classification as H410 (very toxic to aquatic life with long lasting effects). Aside from the toxicity of these compounds, the fact they are derived from petrochemical resources means they are finite. Most synthetic surfactants are synthesised from petrochemical feedstocks,[79] alkyl silicates such as TEOS are typically produced by reaction of $SiCl_4$ with ethanol,[80] while ethanol is industrially produced by the acid-catalysed hydration of ethene, which is a petroleum product.[81] Thus, it is clear that the environmental problems associated with the manufacture of spherical silica particles need to be addressed. Aside from reducing the environmental impact of silica synthesis, biomimetic approaches also provide potential economic advantages by reducing and/or eliminating the need for organic solvents, reducing waste, and simplifying processes by using less reagents and water-based chemistries.[82] Such water-based reactions would reduce the capital expenditure needed for solvent recovery, while also reducing running costs as biomimetic silica can be produced under ambient conditions, making for a far more sustainable and economic processes at-scale. An excellent overview of ecodesign in silica synthesis is provided by Baccile *et al*.[83] The next sections look at how we can draw inspiration from the natural biomineralisation process to achieve these economic and sustainability benefits.

1.4 Natural silica production

Natural silica occurs, of course, in Earth's crust and rocks but, it is also found in plants as phytoliths, and is even utilised by certain animals. Animal uses of silica range from the complex, gene directed layering of proteins and silicates in the shells of certain molluscs,[84,85] to the intricate, fragile structures of glass sponges like the Venus flower

basket,[86,87] and incredibly diverse microalgae such as diatoms.[88,89] These applications of silica are of great interest to science because of the degrees of structural sophistication achieved through these bottom-up processes. Diatoms provide a particularly intriguing example of silica biomineralisation. These fascinating single cell creatures, though seemingly rudimentary, can create visually stunning arrays of intricate structures that even the most advanced materials science techniques cannot match. These structures are assembled by diatoms at a variety of scales, from a few nanometres up to several hundred microns.[90] The apparent ease with which these extraordinary creatures are able to create their cellular structures, acting as a protective shield while they wander the Earth's rivers and oceans, makes them especially interesting.

Diatoms are model organisms for studying biomineralisation processes. This is because the diatom species *Thalassiosira pseudonana* and *Cylindrotheca fusiformis* have been characterised in great detail.[91–95] This has enabled a greater understanding of the mechanisms by which they use biomineralisation to create such intricate structures.[96] Nanofabrication of silica in diatoms occurs under ambient conditions at slightly acidic pH and results from specific interactions between biomolecules and silicic acid derivitives.[97] Isolation and extraction of biomolecules in *T. pseudonana* and *C. fusiformis* has revealed some that are directly involved in silica fabrication. Some of the first discovered were cationically charged proteins called silaffins, all of which are rich in serine and lysine residues.[98] Other important molecules isolated from various diatoms are long-chain polyamines (LCPAs). These silaffins and LCPAs are species-specific molecules, but both have been shown to induce rapid silica condensation in vitro.[99] All these things – pH, electrostatic interactions, functional groups, condensation – play important roles in Stöber

processes too. The compounds that play these roles in diatom biomineralisation have functional equivalents in Stöber processes, though it is often not immediately apparent that this is so. The critical role to understand is that of the biomolecules. Applying that knowledge is to key to sustainable silica syntheses using biomolecules.

1.4.1 Specific biomolecules involved in biomineralisation of silica

The unravelling of the mystery behind the complex and intricate structure formation in diatoms, and other biomineralising creatures, has led to key insights into this process. Specific biomolecules have been shown to have a direct and integral role in the way these creatures shape and utilise silica. As we shall see, the underlying principle by which silica biomineralisation is conducted is not far removed from that of the Stöber processes. Evolution of the biomineralisation process over millennia has adapted and refined it into an elegant, efficient process. However, there are many lessons that can be learned to improve our own silica production methods.

1.4.2 Long-chain polyamines

The biomolecules responsible for silica synthesis in species such as diatoms contain moieties that play a crucial role. As discussed earlier, amine-containing surfactants are important for controlling condensation and particle morphology, through their structure-directing activity. The presence of the ammonium cation in the Stöber process is also critical. These amino compounds are so critical in fact, that without them, spherical silica is not formed. It is no coincidence then, that amines also play a critical role in the biomineralisation process. The role they play in biomineralisation is comparable to their role in Stöber processes. In order to draw direct parallels with the Stöber processes, the role these amines play in biomineralisation must first be explored.

Belton *et al.*[100] studied the effect that different LCPAs had on the polymerisation of silicic acid. They found that longer chain length, higher degree of methylation, and higher number of amines on the LCPAs increased the rate of condensation of the silicic acid. The authors suggest this was due to the ability of the polyamines to form microemulsions while carrying a positive charge, which provides a water-free microenvironment where the removal of water from the condensation reactions provides the driving force for the proton donor/acceptor condensation mechanism (outlined in **Scheme 1.3**)

The reason for this increase in kinetic activity is related to emulsion-forming ability of the LCPAs. This ability is directly related to how effective the amines are at preventing aggregation of the forming silica by controlling the condensation of the precursors through electrostatic interactions. They investigated the emulsion stability of the LCPAs and found that stability decreased as number of amines and amine spacing along the molecular chain decreased. Resistance to localised charging is greater when the number of amines along the molecular chain increases and their proximity decreases. This enhances the hydrophobic character of the LCPAs, thus increasing their emulsion stability. The silica can them form inside the polyamine microemulsion, which increases the condensation rate due to the hydrophobic environment providing a driving force for water removal.

Kröger *et al.*[99] isolated LCPAs from *N. angularis* and studied their morphological control of particles formed upon condensation of silicic acid. They found that LCPAs with longer chain lengths resulted in particles of 800 nm – 1 μm, while shorter chain length resulted in particles of 100 – 200 nm. While no explanation is given by the author for this difference in particle size, it is likely that it is due to the enhanced condensation rates

associated with longer chain length polyamines, as described above. An increased condensation rate would favour the formation of larger particles. Thus, silica particle size will increase with increasing chain length. Mizutani *et al.*[101] studied the catalytic effect of amines on the polymerisation of silicic acid. They found that polyamines increased polymerisation rate more so than linear amines, which had a moderate effect. Monoamines had very little effect on the polymerisation rate, while in the absence of an amine catalyst, no polymerisation occurred. The mechanism by which these amines catalyse biogenic silica polymerisation is still not clear. Some studies suggest that the process is driven by electrostatic interactions between the silica precursor and the positively charged amine groups.[102,103] Depending on the proximity of amines and their chain length, at near-neutral pH, different degrees of positive charge exist on the amines. These positive charges can then interact electrostatically with the negatively charged oligomeric silicate species, bringing them in close enough contact such that polymerisation takes place. This would explain why the monoamines had little effect on the polymerisation rate. Monoamines can only electrostatically interact with one silicate species at a time, whereas polyamines can interact with multiple, bringing them in closer proximity and facilitating polymerisation.

However, this amine-silicate interaction may proceed by a chemical mechanism also. Delak *et al.*[104] studied the effect of different length polyamines on the dimerisation of trimethylethoxysilane (TMES) – a silica precursor in which only the ethoxy bond is labile. This is significant because at pH 5.5, as used in the study, close to the pH at which biogenic silica forms, TMES is neutral. Furthermore, the intermediate product tetratmethylsilanol, is also neutral at this pH (pK_a = 12.7). This means that electrostatic

interactions cannot form the basis of the catalytic activity of these polyamines in this system. The authors propose instead that the catalytic mechanism proceeds via chemical reaction, in which a pentacoordinate intermediate is formed by nucleophilic attack of TMES by the amine. In this pentacoordinate system, the ethoxy bond of TMES is more labile and thus more susceptible to hydrolysis. Further attack by water with a transition through a hexacoordinate intermediate, followed by a condensation step proceeding through an S_N2 mechanism leads to dimerisation. While this mechanism is plausible, and under the conditions of this specific system, likely, it is not representative of the conditions of biogenic silica formation. The usual form of naturally occurring silica is silicates, in which the silicon is bonded to oxygen.[105] Therefore, naturally occurring silica species are likely negatively charged at slightly acidic pH (pKa of silicic acid = 9.8), due to silanol group deprotonation or the facile hydrolysis of labile bonds, and because of this, electrostatic interactions cannot be negated. However, there is no reason to assume that the electrostatic and chemical mechanisms contributing to polyamine catalytic activity in this context are mutually exclusive. Both mechanisms may occur together, though it remains uncertain.

1.4.3 Amino acids and peptides

Following on from the work with LCPAs, other biomolecules identified in the biomineralisation process were studied. Species-specific proteins, such as silaffins and silacidins, were isolated.[103,106] Owing to the complex nature of interactions present in the natural system, iterative investigations starting from simple molecules were carried out. The amino acids serine, lysine, proline, aspartic acid, and their homopeptides were shown to induce silicic acid polymerisation and condensation.[107] It was shown that the peptides

had a more pronounced effect than their corresponding amino acids in the polymerisation process. At low pH (4 – 7), the oligomeric silica species are negatively charged.[108] Depending on their pKa and pKb values, the amine and carboxylic acid groups of the peptides are likely positively and negatively charged, respectively. Thus, the interaction between the peptides and silica species are predominately through electrostatic interactions via the protonated amine groups. This is analogous to the Stöber process in which the ammonia plays a morphological catalyst role.

To probe this further, different chain lengths of poly-lysine and poly-arginine were investigated.[109] Again, it was shown that the positively charged amine groups of the polypeptides play a key role in the polymerisation and condensation process. Increasing the chain length of the polypeptides increased the rate of precipitation. This suggests that having more positively charged amine groups along a chain allows the negatively charged oligomeric silica precursors to be in close enough proximity for polymerisation to occur. Of course, other interactions such as hydrogen bonding may also play a key role. The overall result is that the electrostatic interactions help anchor the silica species and allow polymerisation and condensation.

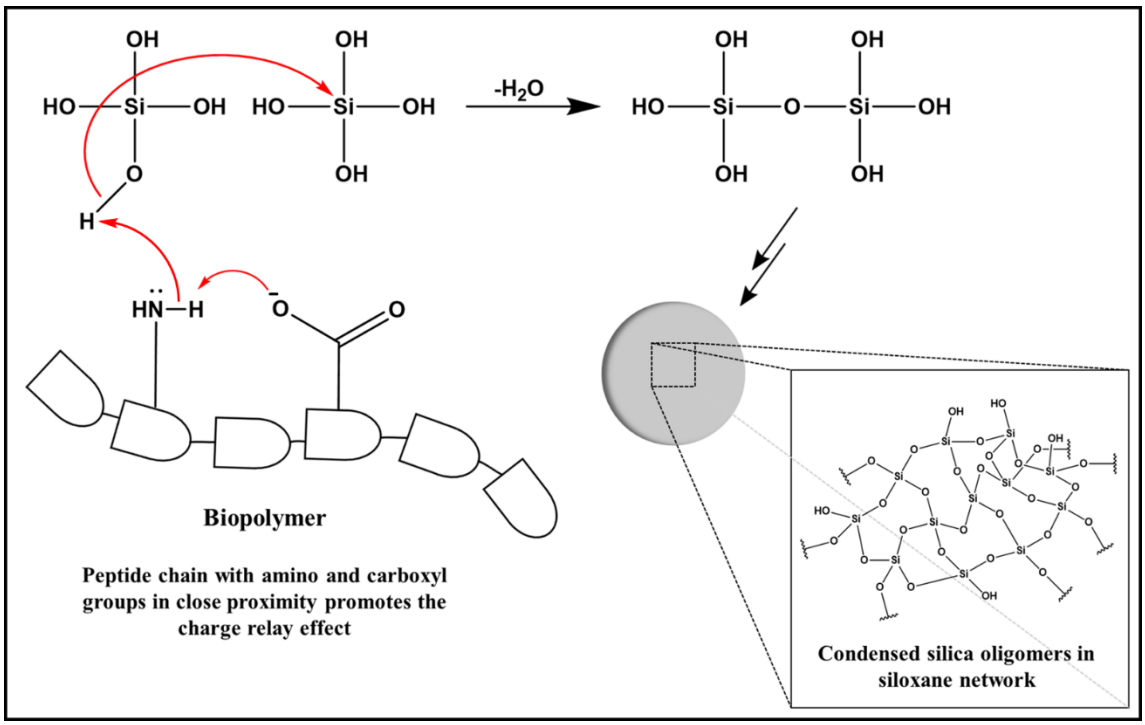
It is clear that carboxyl and amino groups play a key role in silica polymerisation by bringing the oligomeric silica species in close enough proximity for condensation to occur. This is similar to mechanism of the Stöber processes discussed in sections **1.2.3** and **1.2.4**. However, prior to polymerisation, nucleation must occur. Nucleation is the dimerisation of the silica precursor, which begins the process of polymerisation. Wallace *et al*.[110] studied the effects of carboxyl-terminated surfaces and amine-terminated surfaces on silica nucleation. They found that carboxyl-terminated surfaces were able to induce

silica nucleation under ambient conditions and at slightly acidic pH. In contrast, amine-terminated surfaces failed to induce silica nucleation under identical conditions. This is in contrast to the above studies on polymerisation, where the amine groups were more actively involved than the carboxyl groups. However, it seems during nucleation, the amine groups by themselves have little influence. Interestingly, when combining both carboxyl- and amine-terminated surfaces, it was found that the silica nucleation rate was 18× faster than carboxyl-terminated surface alone. This observation can be explained by the charge relay effect commonly seen in the active site of some enzymes. Many biomolecules such as enzymes and proteins contain what is referred to as a catalytic triad, containing three main components: acid, base, and nucleophile.[111] This triad forms the basis of the charge relay effect. In this mechanism, the base residue is activated due to polarisation from the acid residue, which is in close proximity. Once the base residue is polarised, it in turn activates the nucleophile. The activation of the nucleophile is as a result of the catalytic triad acting synergistically to lower the pKa of the nucleophile.[112] As outlined in the next paragraph, this mechanism may explain why peptides and the combined carboxyl- and amine-terminated surfaces have such an influence on the silica nucleation and polymerisation rate.

To investigate the charge relay effect and its influence on silica nucleation and polymerisation, Kuno *et al.*[113] synthesised different combinations of polypeptides using lysine (K), histidine (H), and aspartic acid (D). Homopolypeptides (K_{10} and H_{10}), block polypeptides (K_5D_5 and H_5D_5), and alternate polypeptides [$(KD)_5$ and $(HD)_5$] were used to test how individual polypeptide chains and combinations of peptides affect the nucleation and polymerisation of trimethyethoxysilane. The homopolypeptides had the

lowest catalytic activity, the block polypeptides showed around 8 – 9 % higher catalytic activity than the homopolypeptides, while the alternate polypeptides showed the highest catalytic activity which was around 11 % higher than the homopolypeptides. These results show strong evidence for the charge relay effect. In the block polypeptides, K_5D_5 and H_5D_5, only one amino acid group is adjacent to one carboxylic acid group, whereas in the alternate polypeptides, $(KD)_5$ and $(HD)_5$, each amino acid group is adjacent to one carboxylic acid group. This increased catalytic activity with neighbouring amino and carboxyl groups is what Wallace *et al.* also observed in their study. **Scheme 1.2** shows a simplified mechanism by which this process takes place with silicic acid. The carboxyl groups act as the acid which activates the amine group by deprotonation, which increases the electron density around the amine. The amine group therefore has more nucleophilic character and promotes the nucleation and polymerisation of silica as shown. Further confirmation of the importance of the charge relay effect on silica polymerisation is provided by Murai *et al.*[114] who studied the peptides Ser-His-Glu (SHE) and Val-His-Val-Glu-Val-Ser (VHVEVS) and their influence on the nucleation and polymerisation of trimethylethoxysilane. The secondary structure of SHE was found to be a random coil, while that of VHVEVS was found to be a β-sheet. This β-sheet conformation was found to increase the catalytic activity of VHVEVS by bringing the His and Glu residues into close proximity to enable the charge relay mechanism. Monolithic silica structures were prepared with both peptides, but the surface of the silica prepared with VHVEVS was smooth, while the surface of the silica prepared with SHE was rough. This indicates that the β-sheet conformation of VHVEVS exerts increased morphological control over the polymerisation process. Thus, the presence of LCPAs and peptides, and their

conformation, in silica-synthesising organisms has a major influence on the rate at which silica nucleation and polymerisation occurs and the morphology of the final structure.



Scheme 1.2 *Charge relay effect in biosilica synthesis. Here the peptide chain of the biopolymer has amino and carboxyl groups in close proximity, which is the case for many biopolymers. The oxygen of the carboxyl group hydrogen bonds to the hydrogen of the amino acid group. This pulls electron density away from the nitrogen. The lone pair on the nitrogen then activates the nucleophile, in this case a silicic acid molecule. This starts the condensation process. The silicic acid monomers condense to form a siloxane network which results in the formation of silica. The biopolymer can also act as an SDA, which can promote the formation of spherical silica particles, represented here by the grey sphere.*

1.4.4 Silaffins

One of the most intensely studied diatom species is C. *fusiformis*. This species, like many other diatoms, uses silica to make elaborate, visually arresting silicate cell walls. Pelagic sediment on the ocean floor, made up of these tiny creatures, provides a large source of bio-essential silica in the marine environment and contributes heavily to the oceanic silica

cycle. This silica cycle plays an important role in global climate regulation through the carbonate-silicate cycle,[115] showing that, while these creatures may be tiny, they have a global impact. Another recently solved mystery is how these diatoms exerts such fine control over the silica biomineralisation process. Silaffin proteins – polycationic peptides – were first discovered upon isolation from *C. fusiformis*.[116] These silaffins are responsible for the intricate and complex silica structures in the cell wall of *C. fusiformis*. Initially, silaffin-1A, silaffin-1B, and silaffin-2 were classified.[117] Named for their affinity for silica, these silaffins are highly associated with the cell wall structures of the diatoms. In order to isolate these initially, HF extraction was used. Subsequent extraction with ammonium fluoride, which does not remove amino acid modification, lead to the identification of the native silaffins; natSil-1A and natSil-1B.[106] Characterisation of these native silaffin proteins revealed extensive post-translational modification with the serine residues phosphorylated and the lysine residues modified with LCPAs.[102,118] Other amino acid residues may play a role in silica synthesis via the charge relay effect, mentioned previously. The interaction of post-translationally modified proteins and polypeptides with oligomeric silica species occurs in silica deposition vehicles (SDVs). SDVs are structures present in diatoms, as well as other organisms,[119] that mediate the growth of biogenic silica by controlling the hydrolysis and condensation of silicic acid, which proceeds in a similar way to the hydrolysis and condensation of TEOS.[120] A key similarity between silaffins and CTAB, which is used in the modified-Stöber process, is the presence of quaternary ammonium ions. These are well known to be effective structure directing agents in the synthesis of zeolites and spherical silica,[121] where longer chain alkylammonium ions, i.e., more hydrophobic molecules, showed excellent structure

directing activity. As mentioned previously, CTAB, a quaternary ammonium surfactant, is used extensively in silica synthesis due to its structure directing activity. **Figure 1.5** shows the structure of a silaffin isolated from C. *fusiformis*, which contains numerous quaternary ammonium groups. These groups are analogous to the structure of CTAB which is the SDA in modified-Stöber syntheses. In fact, silaffins isolated from diatoms have been shown to induce silica polymerisation under acidic conditions *in vitro*.[98,106] Thus, this natural biomineralisation process and the Stöber processes are directly analogous. It seems nature has already evolved molecules capable of creating complex hierarchical silica structures. The challenge now is for materials scientists to capitalise on this knowledge to improve synthesis methods for materials such as silica.

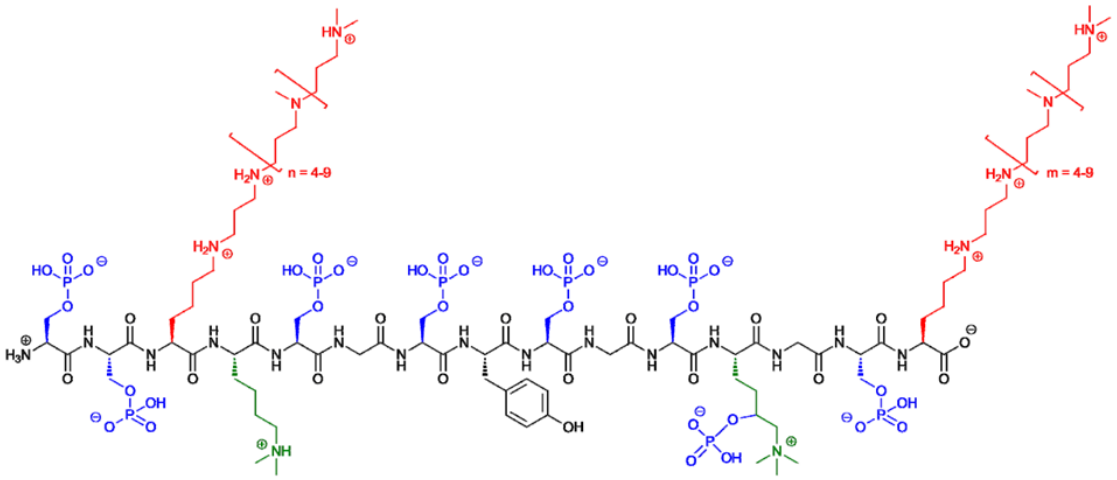


Figure 1.5 *Chemical structure of native silaffin-1A$_1$ from C. fusiformis. Reproduced from Kröger et al.*[106]

1.5 Bridging the gap – connecting Stöber to Nature

1.5.1 Biopolymer physicochemical characteristics key to spherical silica synthesis

We have seen how the extraordinary creatures like diatoms are able to create complex silica structures using specific biomolecules under ambient temperature and pH and how it relates closely to Stöber processes. The key features of these biomolecules responsible for silica biomineralisation, such as the presence of long-chain polyamines (LCPAs) and peptides, the charge relay effect, and electrostatic interactions, are strikingly similar to how spherical silica particles are formed in Stöber processes. Long-chain quaternary ammonium surfactants, like CTAB, promote the polymerisation and condensation of silica precursors through similar interactions. The following sections will look more closely at biomolecules that are not specific to the *in vivo* biomineralisation process, but contain physicochemical characteristics akin to them, and so could be used in the formation of spherical silica particles. Thus, even though the way in which traditional silica (Stöber and modified-Stöber) and biogenic silica is made is different, the underlying processes of hydrolysis and condensation, and particle growth are very similar.

Amphiphilicity

An important property of many SDAs is their amphiphilicity. Surfactants like CTAB contain a hydrophilic headgroup in the form of a quaternary ammonium cation and a hydrophobic tail group in the form of a long carbon chain. These physical characteristics allow CTAB to form micelles in solution which play a crucial role in forming spherical silica (see sections **1.2.3** and **1.2.4**). Any biopolymer replacement for CTAB should also have this structure-directing facility.

In food technology, water-in-oil (w/o) and oil-in-water (o/w) emulsions are routinely stabilised by biopolymers in order to create new foods and drinks. Emulsifiers are a specific class of surfactants and what makes emulsifiers effective is that they are amphiphilic, which helps to lower the interfacial tension and facilitate smaller droplet sizes.[122] Commonly used emulsifiers include soy lecithin and sodium caseinate. Amphiphilic biopolymers typically contain large hydrocarbon chains and ionic moieties such as carboxylates and ammoniums. As discussed earlier in sections **1.2.3** and **1.2.4**, CTAB, which is also amphiphilic, helps control particle morphogenesis through electrostatic interactions. This electrostatic interaction is the key to forming spherical particles when using surfactants such as CTAB. Electrostatic interactions between CTAB and the oligomeric silica species form the basis of the morphological control that is achieved. The amphiphilic nature of certain biopolymers should also provide this control, provided the other physicochemical characteristics, discussed next, are present.

Charge relay effect

As we have seen from the studies discussed earlier, the presence of a catalytic triad, enabling the charge relay effect, has a great effect on the silica nucleation and polymerisation rate. The presence of adjacent carboxyl and amino groups along a peptide chain of a biopolymer, together with the presence of a silica precursor, can activate and promote the nucleation and polymerisation of silica. In fact, the charge relay effect has been exploited in biocatalysis due to this catalytic behaviour.[123–126] Biomolecules which contain polypeptide chains are ideal candidates to act as SDAs in silica synthesis due to the presence of adjacent carboxyl and amino groups.

Polyamines

While the presence of LCPAs found in diatoms have been shown to play an integral role in silica biomineralisation, studies have shown that shorter chain polyamines can provide morphological control over silica polymerisation. Some of the LCPAs isolated from diatoms have complex molecular structures which can make *in vitro* replication difficult. Thus, if shorter chain polyamines are shown to behave in a similar way to LCPAs, it would simplify biomimetic silica production. The studies mentioned previously isolated biomolecules from diatoms which were subsequently shown to play a key role in the polymerisation and condensation of silicic acid. Since then there have been a few limited studies trying to replicate this process biomimetically.

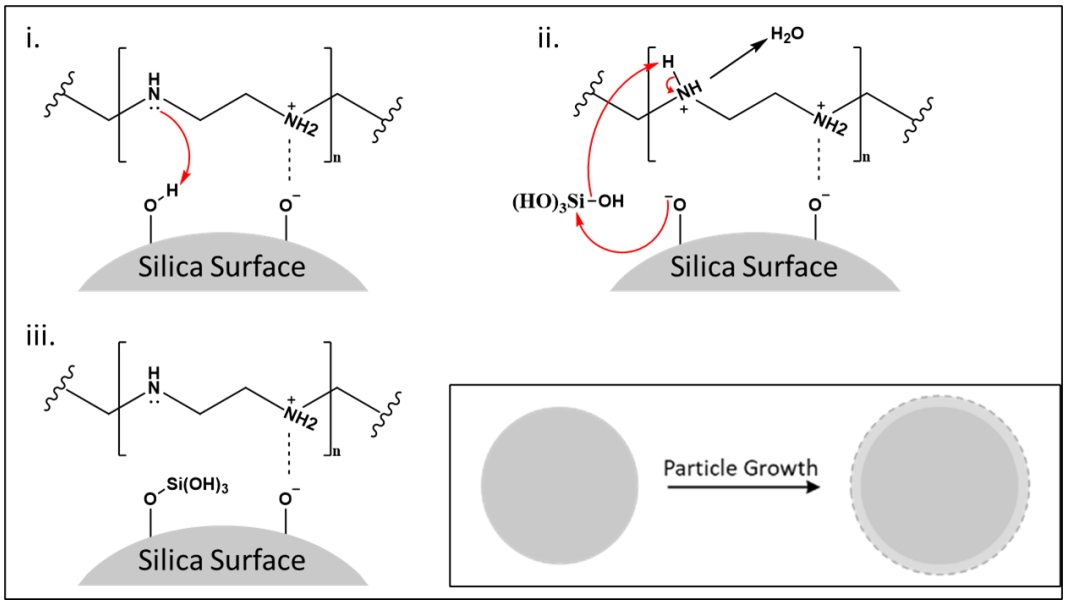
Menzel *et al.*[127] studied the effects polyamines with different lengths and branching had on silicic acid condensation. They found that diaminoethane and 1,3-diaminopropane accelerated the condensation of silicic acid the most. As the chain length of the polyamine increases the accelerating effect decreases. Linear polypropylene imine (PPI) had less of an effect on accelerating the condensation reaction that linear polyethylene imine (PEI). The methylated (branched) variants, PMPI and PMEI, both showed similar effects and did not accelerate the reaction as much as the non-branched variants. In the absence of any amine, the condensation reaction was the slowest.

It is clear from this study that polyamines speed up the condensation of silicic acid, with shorter, unbranched polyamines accelerating the reaction more than longer, branched polyamines, which indicates branching has a retarding effect. A faster condensation rate could promote particle growth.[128,129] Other work probing whether this is the case was done by Belton *et al.,*[130] who studied naturally occurring polyamines – spermidine and

spermine – along with a series of linear ethyleneamine homologues. The chain length and number of amines on the homologues increased stepwise, from ethylenediamine up to pentaethylenehexamine. They found that the smaller chain length polyamines showed no distinct spherical silica structures. However, as the chain length and number of amines increased, somewhat more spherical and distinct particles were produced. Interestingly though, spermidine produced larger particles than spermine, which has a longer chain length and an extra amine. The aggregation rate of the particles was also found to generally increase with increasing chain length and number of amines, with more pronounced increases for tetraethylenpentamine and pentaethylenehexamine.

As mentioned previously, the interaction of amines, for example quaternary ammonium groups, is important for the controlled condensation and growth of spherical silica. The authors point out that at near neutral pH about 50% of the silanol groups on the surface of the forming particles are deprotonated, i.e., every second silanol is negatively charged. Therefore, the atomic distance between these deprotonated silanols is ca. 5.4 Å. The inter-amine distance of ethylenediamine is 3.9 Å. Thus, ethylenediamine is unable to bridge the gap between two deprotonated silanols, which would shield and stabilise the surface to prevent uncontrolled aggregation. As chain length and the distance between, and amount of, amines increases, this gap is easily bridged, and the amines form a surface layer on the nascent silica particles. However, at near neutral pH, not all of the amines on the polyamines are charged due to their close proximity, which increases the resistance of neighbouring amines to become charged. This can provide a mechanism for controlled growth of the silica particles. These amines are still weakly basic and can promote silica condensation. **Scheme 1.3** shows a simplified mechanism by which this takes place. The

polyamine, which is representative of those found in biomineralisation proteins (see **Figure 1.5**), electrostatically interacts with the silica surface through its quaternary ammonium groups. This brings the polyamine molecule close enough to the surface to allow the uncharged amines to deprotonate a silanol, which then attacks free silicic acid via an Sn2 mechanism. This process continues, adding more silicate to the surface, and the particles grow in a controlled manner. The parallels between this mechanism and the mechanism of action of surfactants like CTAB in the modified-Stöber process is striking. Both processes are heavily reliant on the length of the SDA – polyamine or CTAB – and the electrostatic interaction between them and the silica surface.



Scheme 1.3 *Simplified mechanism of silica particle growth in the presence of polyamines. Polyamine is attracted to the silica surface electrostatically (represented by dashed line). (i) Lone pair of electrons on uncharged amine deprotonates a silanol in close proximity. (ii) This deprotonated silanol attacks a free silicic acid molecule via Sn2 mechanism, with OH^- as the leaving group. The OH^- then attacks the protonated amine group, releasing water and reforming the uncharged amine. (iii.) Silicic acid derivative is attached to the surface. The process repeats, adding more silicate to the surface and the particle grows. Image on lower right represents this surface growth. Dark grey is the original particle, light grey is additional silica added by growth process. Dashed line around particle illustrates an increased diameter.*

This mediation of particle growth is key to forming spherical silica particles. The strong parallel between the natural biomineralisation process and the Stöber silica processes can enable the use of naturally occurring biomolecules that possess the physicochemical properties described above. This provides the possibility of designing a more sustainable process for synthesising silica at an industrial scale – one which uses environmentally benign, non-toxic, and renewable reagents. Biomolecules fulfil the sustainability aspect, and certain biomolecules possess the physicochemical properties required to control silica condensation and growth. Some limited work has been done investigating the effect of such biomolecules on silica condensation and growth.

1.5.2 Biopolymer sources

As discussed previously, the physicochemical characteristics of biopolymers can promote the polymerisation, and control the condensation, of spherical silica. The presence of polyamine and carboxylic acid groups in biopolymers can increase the nucleation and polymerisation rate of silica through the charge relay effect. Their amphiphilicity can prevent aggregation of nanomaterials by absorbing onto their surface during growth. These properties can bring together the advantages of Stöber processes – facile production of spherical silica – and biomineralisation processes, which provides a sustainable way to produce spherical silica. One of the key advantages of using biopolymers as SDAs over petrochemical surfactants like CTAB is that they are renewable, biodegradable, and readily available from sustainable sources.

Biopolymers originate in living organisms and are a key class of molecules which fulfil the criteria described by the Green Chemistry concept. Biopolymers are also renewable. By contrast, most current industrial polymers are petrochemicals, i.e. they are derived

from an infamously finite, environmentally damaging source – crude oil. The vast majority biopolymers are available from a variety of natural, renewable sources, and a small but growing percentage are produced through various biotechnological methods. An attractive feature of many biopolymers is their biodegradability.[131] This is preferable because it mitigates, or completely solves, the issue of persistence of plastic waste in the environment.[132,133]

Many of the sources of biopolymers are forms of biomass like sugars and starch. But first-generation sources are associated with increased food costs and deforestation because they compete with food production resources.[134] As such, these biopolymer sources cannot realistically be recommended as a solution to industrial production sustainability issues. However, there are some first-generation sources, such as algae, that do not require arable land or freshwater for cultivation and are not currently a major food source. Algae are already a promising source of biofuels for the same reasons.[135] Second-generation biopolymer sources are typically waste streams. These are an immediately superior candidate source of biopolymers as the use of wastes is an inherently more sustainable practice. For example, chicken feathers, a by-product of the poultry industry, can be used as a source of highly utilitarian keratins.[136] Casein, a major component of waste streams from milk production and spoilage, can be extracted and used in food technology and textiles.[137,138] This valorisation of waste streams greatly improves the sustainability, economically and environmentally, of these sources compared to first generation feedstocks. The next sections look at the limited work that has been done utilising such sustainable biopolymers with the aim of synthesising silica in a biomimetic way.

1.5.3 Synthesising spherical silica particles with biopolymers

The knowledge garnered from studying silica biomineralising creatures such as diatoms has provided opportunities to create biomimetic silica in a sustainable way. The key physicochemical characteristics that have been shown to be crucial for controlling silica nucleation and polymerisation in biomineralisation can be adapted and used to improve the Stöber processes. The presence of adjacent amino and carboxyl groups to promote the charge relay effect, the presence of quaternary ammonium groups and their electrostatic interaction with oligomeric silica species, and amphiphilicity, are all key physicochemical attributes that are needed if a biopolymer is to promote and control silica nucleation and polymerisation. Furthermore, synthesis of biomimetic silica with these biopolymers under ambient conditions of temperature and pH vastly increases the sustainability of the process compared to the traditional Stöber processes. There has been little work on using these kinds of biopolymers to synthesise silica. However, there is evidence that it can be achieved.

Biopolymers as SDAs for spherical silica

There is evidence in the literature that biopolymers can be used to effectively direct the formation of spherical particles in nucleation and growth processes. Biopolymer SDAs have been successfully used to control the morphogenesis of iron oxide, silver, and gold nanoparticles. For example, iron oxide nanoparticles have been synthesised with a variety of different biopolymers. The polysaccharide dextran has been used to control the morphology and size of the iron oxide particles.[139–141] Dextran interacts with the iron oxide surface through chelation and hydrogen bonding, with the strength of the hydrogen bonding increasing with chain length of dextran.[142] Alginate has also been used to

synthesise iron oxide particles.[143,144] Alginate has many carboxyl groups which complex to the iron ions enabling mediation of particle growth.[145] Silver nanoparticles have also been produced using biopolymers such as starch as stabilising, and structure-control, agents.[146–148] Starch contains many hydroxyl groups which have good metal complexation properties and enable the morphological and size control of the silver nanoparticles.[149] Gold nanoparticles have been prepared using chitosan as the stabilising agent.[150–152] The polyelectrolyte properties of chitosan stabilise the gold nanoparticles through electrostatic interactions.[153] It is clear from these studies that biopolymers can readily control and stabilise the growth of nanomaterials. However, using biopolymers to synthesise monodisperse spherical silica nanoparticles has scarcely been explored. Applying the knowledge of the physicochemical properties required for biomineralisation and the structure-directing ability of some biopolymers in producing nanomaterials can bridge the gap between these similar processes.

There is some evidence that biopolymers can also act as an SDA in the synthesis of spherical silica. Coradin *et al*.[108] studied the effects of bovine serum albumin (BSA) and lysozyme on sodium silicate solutions. Lysozyme, a small enzyme, and BSA, a large protein, contain high percentages of acidic and basic groups such as lysine and aspartic acid. The ratio of amino acids-to-silica was used to compare the reactivity of both proteins. They found that under different respective pH, lysozyme and BSA were able to induce silica condensation. The formed solids were shown to have an interspersed network of protein and silica. This suggests that the interaction of protein and silicate is important for condensation. At pH 7.2, lysozyme is positively charged and interacts electrostatically with the negatively charged silicate species to induce condensation. At

this pH, BSA is negatively charged and no silica was formed, highlighting the importance of electrostatic interactions in silica formation. At pH 4.7, where BSA is positively charged, silica formation occurred. Surprisingly, even though lysozyme is also positively charged at this pH, no silica formation occurred. At this pH, the lysine groups of lysozyme are fully protonated, reducing its net positive charge. Further, at this acidic pH, the oligomeric silicate species are less negatively charged. Thus the overall result is a weaker electrostatic interaction between lysozyme and the silicate species. This further highlights the importance of electrostatic interactions between proteins and silica precursors in silica formation. This becomes a key consideration when using proteins to form spherical silica particles. (It can be argued that the charge relay effect is, at least partially, responsible for this influence.)

Another study by Coradin *et al.*[154] looked at the influence of gelatin on silica formation. Different concentrations of gelatin and sodium silicate were tested and the morphology of the silica was characterised. They found that at the concentrations studied, silica precipitation occurred. However, at higher gelatin concentration, silica nanoparticles became embedded in the polymer network. The influence of gelatin on the size and shape of these nanoparticles was studied at pH 5 and pH 7. At pH 7, highly agglomerated silica particles were observed. At pH 5, less agglomerated, slightly spherical silica particles were observed. As mentioned previously, at pH 7, the oligomeric silicate species bear high negative charges, which increases the electrostatic interaction between them and the gelatin. In fact this study showed via thermogravimetric analysis that at pH 7, the silicate species bind twice as much gelatin as at pH 5. In this case though, this means that the gelatin lost its structure-directing ability and a composite precipitate with highly

agglomerated silica particles is produced. The presence of more well-defined silica nanoparticles at pH 5 however is explained by the authors in terms of a stabilising effect of gelatin. They posit that negative charges on the carboxylate groups in the side chain of gelatin allow particle growth to proceed without aggregation of the particles. Sodium ions could prevent particle growth by stabilising surface charge. It is suggested that the carboxylate groups of the gelatin interact with the sodium ions preventing this. The fact that larger, less agglomerated particles are produced at pH 5, while smaller, aggregated particles are produced at pH 7 suggests this theory might be correct. In any case the electrostatic interactions between the biopolymer and silicate species is crucial in determining the final size and morphology of the final silica particles.

Probing the use of biopolymers to catalyse and control silica polymerisation, Demadis *et al.*[155] studied the influence of chitosan-based biopolymers phosphonomethylated chitosan (PCH), polyethyleneimine (PEI), and carboxymethylinulin (CMI) on solutions of sodium silicate at neutral pH. In this case, the biopolymers were chosen due to their physicochemical similarities to silaffins. The cationic polyamine and anionic phosphate groups are the main similarities, and as discussed earlier have been shown to be highly influential on the silica polymerisation process. However, the focus of this study was to understand the inhibitory effects these biopolymers have on the condensation process. For diatoms to form their hierarchical silica structures, a supply of dissolved silicon must be present. In the waters of Earth's oceans and rivers, there are vanishingly small quantities of dissolved silicon – far lower than the levels needed by diatoms to make their ornate siliceous cell walls. To solve this issue, diatoms have evolved a means of supersaturating silica within themselves, ensuring adequate supply for biomineralisation.[110] The diatoms

achieve this by inhibiting the condensation of silicic acid prior to its use in silica deposition vehicles to form the silica structures.[156] This inhibitory effect is achieved by electrostatic and/or H-bonding interactions between biopolymers and silicic acid.

In the above study, PCH contains protonated amines, PEI contains protonated polyamines, while CMI is anionic. The inhibitory effect of these biopolymers was tested over 72 hrs at various concentrations. While PEI and PCH individually, and together, showed good inhibitory effects towards silica condensation, CMI had less of an effect due to its anionic nature. However, in all cases, the inhibitory effects of the biopolymers could not prevent the condensation of silicic acid, instead the differing degrees of retardation resulted in structural differences in the silica precipitates. At 40 ppm and 150 ppm PCH, the morphology of the particles is quasi-spherical with size ranging between 300 – 500 nm after 72 hrs of growth, eventually forming aggregates ca. 2 μm after 4 weeks. At 20 ppm PEI, which showed comparable inhibitory effects to 40 ppm PCH, the particles were larger. PEI contains polyamine chains, which can mediate particle growth as shown in **Scheme 1.3**. PCH does not contain these polyamine chains, which may explain the difference in particle size. A combination of 20 ppm PEI and 40 ppm PCH resulted in particles of 150 – 200 nm in size.

Although the authors point out that no synergistic effect between PCH and PEI occurs in relation to the inhibition of silicic acid polymerisation, it seems there is one for particle growth. Smaller more spherical particles are formed with PEI and PCH in combination, as opposed to quasi-spherical with PCH alone, or larger particles with PEI alone. A combination of PCH and CMI results in the formation of aggregated spherical particles, while increasing the concentration of CMI results in even larger aggregates.

Further evidence for the importance of electrostatic interactions between biopolymers and silicate is given by Gautier *et al.*[157], who studied the effects of cationic gelatin and anionic alginic acid on sodium silicate polymerisation at pH 5. They found that with only alginate present, no silica is formed unless left for an extended period. In which case, a composite is formed with a small amount of alginate incorporated into the silica network. However, sodium silicate is known to polymerise in acidic solution and the small amount of alginate incorporated into the silica network could be explained by very weak interactions between the alginate and anionic silicate species. When cationic gelatin is added along with alginate, silica polymerisation occurs rapidly. The electrostatic interaction between gelatin and the silicate species brings the polypeptide chain of the gelatin in close enough proximity to induce silica polymerisation. As discussed earlier, the studies by Wallace *et al.*[110] and Kuno *et al.*[113] show that having carboxyl and amine groups in close proximity, as they are in peptides, along with alternating groups of polypeptides, greatly increases catalytic activity of the biopolymer.

While these studies are excellent examples of using the knowledge gleaned from the biomineralisation process to synthesise silica *in vitro*, the resulting silica is not comparable to that produced in Stöber processes. Aggregation and lack of sphericity, parameters easily controlled in Stöber processes, means there is still some way to go until biomimetic silica achieves parity with Stöber processes. **Table 1.1** shows a comparison of the silica formed when using various biomolecules in a biomimetic synthesis. In all cases, silica was formed, however, the morphology was either non-spherical, agglomerated, or both.

Table 1.1 *Comparison of different biopolymer SDAs and their influence on silica morphology.*

SDA[a]	Particle Size (nm)	Morphology	Refs.
BSA/lysozyme	50 – 200/ non-spherical	Non-spherical	[108]
Lysine/arginine	< 100	Non-spherical/agglomerated	[109]
Gelatin	50 - 300	Non-spherical	[154]
PCH PEI CMI	300 - 2000	Non-spherical	[155]
Gelatin/alginic acid	10 – 50	Non-spherical/agglomerated	[157]
Gelatin	Non-spherical	Non-spherical	[158]

[a]SDA, structure-directing agent; BSA, bovine serum albumin, PCH, phosphonomethylated chitosan; PEI, polyethyleneimine; CMI, carboxymethylinulin.

It is clear from the above studies that the physicochemical properties of the biopolymers plays an important role in the formation of spherical silica particles. Depending on the functionality present in a given biopolymer, condensation rate can be affected (inhibited or promoted), as can morphological control exerted on the forming particles. Therefore, it is imperative that biopolymers with potential to act as an SDA in spherical silica syntheses have physicochemical properties which promote condensation while also maximising morphological control.

Ideal biopolymer SDA candidates

Here we highlight some biopolymer candidates which, based on the physicochemical characteristics described previously, show potential to be used as SDAs in the synthesis of spherical silica. The studies described in the previous section, which used biopolymers as an SDA to produce silica, produced non-spherical or agglomerated particles. To compete with the established Stöber processes, a biopolymer SDA needs to be able to create discrete spherical particles with acceptable size-monodispersity. Ideal biomolecule

SDA candidates need to meet all the criteria described in the previous sections in order to achieve this goal. We have identified two candidates that fulfil these criteria – casein and lecithin.

Caseins

The majority protein component of milk is a family of phosphoproteins called casein. Differing primary structure and degrees of phosphorylation give rise to four distinct types, α_{s1}-, α_{s2}-, β-, and κ-casein. The caseins contain relatively high levels of the amino acid proline and as such generally lack secondary and tertiary structures, which results in high surface hydrophobicity, owing to their hydrophobic residues being exposed.[159] The caseins adopt an association complex in milk often termed casein micelles. These casein micelles are not fully analogous to traditional surfactant micelles which form reversible and ordered aggregates. Early spectroscopic data suggested casein had a random coil structure.[160] Later, Holt *et al.* [161] performed sequence alignment procedures on casein and described the protein as having a dynamic structure and called it a rheomorphic protein. It is well know that casein is a transporter of calcium and phosphate[162]. Calcium phosphate nanoclusters interact with the casein micelle and bind primarily to the phospheryl residues of the proteins. Studies by McMahon *et al.*[163] show that these calcium phosphate nanoclusters play an integral part in the casein micelle synthesis and subsequent stabilisation. Another contributing factor to the stability of the casein micelle is the presence of κ-casein on the surface. According to Holt *et al.*,[164] the C-terminal macropeptides of some of the κ-casein molecules form a negatively charged diffuse outer layer on the surface. This makes the surface hydrophilic and also prevents micelle aggregation, while the interior of the casein micelle is hydrated.[165] Caseins structure is

made up of a variety of amino acid residues, with many carboxyl and amino groups adjacent to each other.[138] The amphiphilic nature of casein along with its adjacent carboxyl and amino groups, which enable the charge relay effect detailed earlier, make casein an ideal candidate to function as an SDA in silica polymerisation. Sodium caseinate is a common form of casein which is often used in food manufacturing as an additive for its high protein content. It is produced by acid precipitation and resuspension under alkaline conditions. During this process the calcium phosphate is removed, which leads to the destabilisation of the casein micelles, resulting in individual caseinate molecules or small aggregates.[166] However, reintroduction of calcium can reform and stabilise the casein micelle.[165] Another, more promising, source of casein is from milk wastes generated dairy and milk processing.[167,168] This casein-containing waste is a more sustainable source of casein. Valorisation of waste-streams is a key tenet of the circular economy and use of such casein in spherical silica synthesis fulfils the requirements for sustainable SDAs detailed earlier.

A lot of the work involving sodium caseinate/casein has focused on its emulsifying properties. This surfactant-type property of proteins is due to their amphiphilic nature and it enables the stabilising of oil-in-water system which are common in many food products. Aside from this, casein is an ideal candidate to act as an SDA in the synthesis of spherical silica due to its micelle-forming ability and also the presence of amino and carboxyl groups in its peptide chain, all key properties that have been deemed essential in creating spherical silica.

While the literature provides some examples of casein being used in somewhat of an SDA role in synthesising nanocomposite particles, there are no reports of casein being used

solely as an SDA in synthesising discreet spherical silica particles. However, there is no reason that insights gathered from these studies on nanocomposites cannot be transferred into spherical silica synthesis. Xu *et al.*[169] produced core-shell casein-silica nanocomposites using caprolactam-modified casein, polyacrylate, and TEOS. The emulsifying properties of casein were exploited to solvate and stabilise the hydrophobic acrylate monomers. Addition of an initiator, which starts the polymerisation of the acrylate, and TEOS allows for a double in situ preparation of the core-shell casein silica nanocomposite particles. The resultant particles had a spherical morphology, meaning that the polymerisation of the acrylate and TEOS occurred in a controlled manner. The FTIR spectrum of the casein showed large intensity peaks for both amine and carboxyl groups, which, as we have seen, is essential for SDA activity.

Further evidence for the potential of casein to act as an SDA in silica synthesis is provided by Ma *et al.*[170] who also prepared core-shell casein silica nanocomposites. The procedure was similar to that of Xu *et al.* where the casein was modified with caprolactam followed by subsequent in situ polymerisation of TEOS and acrylate, resulting in the formation of spherical nanocomposite particles. Again, the polymerisation was controlled by the action of casein. Thus, the micelle-forming ability, along with the presence of amino and carboxyl groups, of casein can be used to direct and control the polymerisation of silica. In fact, there is evidence to support the specific interaction of the peptide chains of casein with silica. Tiberg *et al.*[171] used neutron reflectometry to study the adsorption of β-casein on the surface of silica and suggested that a positive charge surplus in the hydrophobic domain of β-casein may electrostatically interact with the negatively charged silica surface, facilitating adsorption. They also note that hydrophobic and hydrogen bonding

may also play a role in this adsorption behaviour. This coupled with the micelle-forming ability of casein, and the charge relay effect promoted by the presence of adjacent amino and carboxyl groups on the peptide chain, make casein an ideal candidate for use as an SDA in spherical silica synthesis.

Lecithin

Lecithin is a mixture of acetone insoluble phospholipids, containing mainly phosphatidylcholine (PC), phosphatidylethanolamine (PE), phosphatidylinositol (PI), minor compounds such as phosphatidic acid (PA) and other substances (triglycerides, carbohydrates, etc.).[172] Many of these phospholipids exhibit good emulsifying properties due to their amphiphilic nature. Lecithin is a waste product generated from soybean oil production. It can be obtained from this crude waste by a process called degumming.[173] Therefore, lecithin, like casein, can be obtained through valorisation of waste-streams, which increases their inherent sustainability.

Figure 1.6 shows the structures of the main components of lecithin (and CTAB for reference). In fact, the major application of lecithin is in the food industry as emulsifying agents, which is analogous to the surfactant role of CTAB.. Some more advanced uses of lecithin that have exploited this inherent nature have been in drug delivery. Lecithin organogels form when lecithin is dissolved in an organic medium and small amounts of water are added. Upon addition of water, the lecithin molecules form reverse micelles with further water addition converting these to three-dimensional, long, tubular networks.[174] Lecithin can also form bilayers in aqueous solution. Lecithin and PC contain long-chain fatty acid residues and quaternary ammonium headgroups, which are

structurally similar to the head and tail groups of CTAB. The formation of spherical silica particles is highly role of CTAB, as discussed in sections **1.2.3** and **1.2.4**.

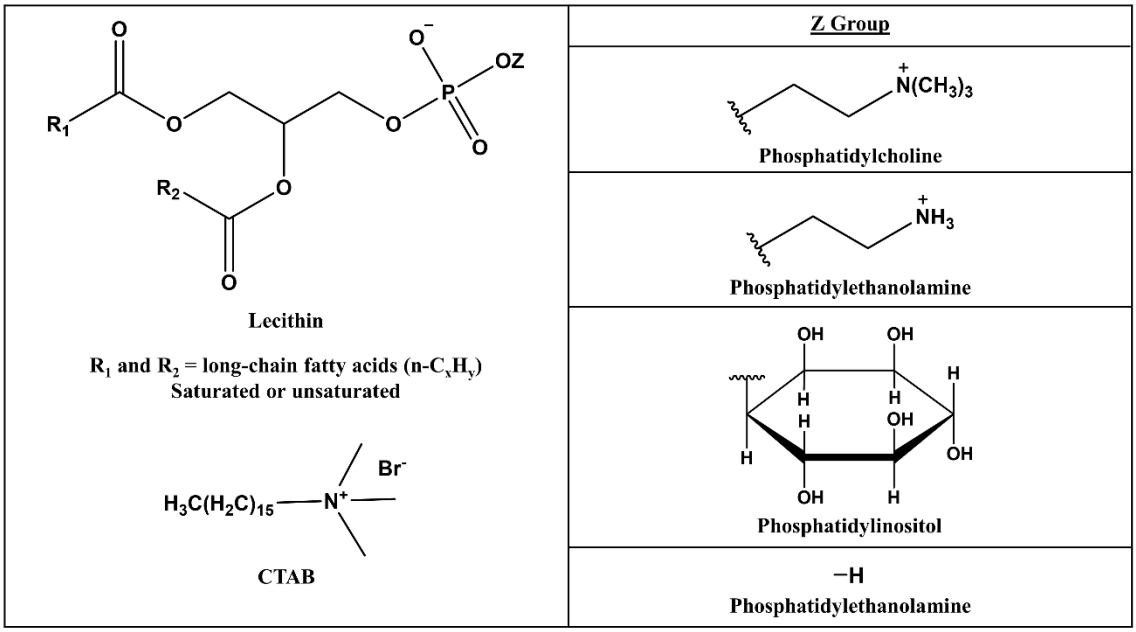


Figure 1.6 *General structure of lecithin (top left) and it's variations (right column). R_1 and R_2 = fatty acid residues. CTAB is shown (bottom left) for structural comparison. Notice the similarities between the quaternary ammonium headgroups of phosphatidylcholine and phosphatidylethanolamine and that of CTAB. The long-chain fatty acid residues of lecithin are also structurally and chemically similar to the long carbon tail of CTAB.*

Phospholipids are an important component of the cellular membrane in both plants and animals and are highly abundant and renewable. The hydrophobic tails are the R_1 and R_2 groups (see **Figure 1.6** above), which are long-chain fatty acid residues with varying chain length and degree of saturation. The phosphate head is the hydrophilic part of the phospholipid, with the Z group varying depending on the derivative. These zwitterionic phospholipids have surfactant properties just like CTAB, which allow them to stabilise emulsions. This property has made lecithin useful in the food industry, but lecithin has

also found limited use in controlling the morphology of silica. This propensity could allow lecithin to replace CTAB in spherical silica synthesis.

The literature shows some limited investigation of lecithin as a means to control silica polymerisation. Galarneau *et al.*[175] exploited the surface active agency of lecithin to form sponge mesoporous silica using lecithin/dodecylamine mixed-micelles in ethanol/water. Han *et al.*[176] used calcium phosphate to coat the surface of lecithin micelles. These micelles were used to encapsulate perflurocarbon, which is used as an artificial oxygen carrier. The calcium phosphate coated lecithin micelles showed enhanced stability.

These studies show the ability and facility of lecithin to form micelles/bilayer structures. This is important when it is used to mimic biosilica formation. Surfactants like CTAB, which are used in Stöber processes, form micelles, their ability as structure directing agents has a significant influence on the size and morphology of the resulting silica particles. To date, there have been no reports in the literature of using lecithin as an SDA in the synthesis of spherical silica using a biomimetic approach. The notably similar physicochemical properties of lecithin and CTAB – bilayer structure and quaternary ammonium headgroups – make lecithin an ideal candidate as an SDA. As we have seen, until now the attempts to use biomolecules as SDAs in the synthesis of spherical silica particles has not yielded great success. Finding biomolecules, such as lecithin and casein, which closely match the physicochemical characteristics detailed previously would finally bridge the gap between the Stöber processes and Nature.

Biopolymers as porogens

A major aspect of spherical silica particle production is rendering particles porous on occasion. This is done for specific applications. This necessitates the use of porogens in syntheses. Biopolymers have potential functionality in this role too. Apart from employing biopolymers to act as SDAs to control morphogenesis, biopolymers have also been used as porogens to create meso- and micropores in various materials. This dual role of biopolymers is the same as that of CTAB which controls the morphology of silica particles but also, depending on reaction conditions, reveals pores upon its removal.

Jia *et al.*[158] produced microporous silica gel using tetramethyl orthosilicate (TMOS) templated by gelatin, which was removed post-synthesis via calcination. They found that as the concentration of gelatin increased, the surface area and pore volume of the silica also increased. Gelatin interacts with the silicate species produced during hydrolysis via H-bonding and covalent interactions through the amino acid hydroxyproline.[177] This enables the gelatin to be incorporated into the forming silica gel network, with its subsequent removal revealing the porous structure, similar to CTAB. Sabarish *et al.*[178] used sodium alginate and tetrapropylammonium hydroxide (TPAOH) to create mesopores in the zeolite silicalite-1. The sodium alginate was removed by calcination and found that compared to conventional silicalite-1, mesopores were formed instead of micropores when sodium alginate was used as the porogen. Sodium alginate is a homopolymer composed of guluronic and mannuronic acid, both of which contain hydroxyl and carboxyl groups. The quaternary ammonium TPAOH likely electrostatically interacts with the alginate and the silicate species which enables a dual template-porogen role. This interaction and role of the quaternary ammonium cation is discussed in previous sections.

Sodium alginate was also used as a porogen by Abramson *et al.*[179] to synthesise millimetre-sized magnetic silica beads. In this case, alginate beads were formed first and a solution of hydrolysed TEOS was subsequently added. The hydrolysed TEOS then diffused into the alginate beads and polymerised. Subsequent washing with water and nitric acid removed the alginate template, leaving behind the mesoporous magnetic silica beads.

The above studies exemplify how biopolymers can have a dual role as a porogen and an SDA. Depending on the physicochemical characteristics of the biopolymer, some biopolymers can behave in the same way that the traditional surfactant CTAB does in spherical silica synthesis.

Comparison of experimental conditions of biopolymer-based silica synthesis versus Stöber processes

As we have seen, Nature has evolved the biomineralisation process to be a highly sustainable and efficient process. The synthesis of silica in diatoms and other creatures occurs under ambient conditions of temperature and pH in aqueous media. *In vitro* replication of this biomineralisation process can be conducted under similar ambient conditions. Contrast this to the typical synthesis conditions in the Stöber and modified-Stöber process outlined in **Table 1.2**. A typical Stöber synthesis is conducted at temperatures between 10 – 80 °C, but in order to get smaller particles which are more desirable, higher temperatures are needed. The Stöber process also needs ethanol as a solvent because TEOS is insoluble in water, therefore, ethanol acts as a mutual solvent for these. Post-processing of the particles typically involves washing with water and acetone. A typical modified-Stöber synthesis using CTAB is run at temperatures between

10 – 40 °C. Again, smaller particles are achieved at higher temperatures. The modified-Stöber process also uses ethanol for the same reason as the Stöber process. Post-processing of the particles synthesised using the modified-Stöber process requires calcination at very high temperatures to remove the CTAB. Chemical extraction of the CTAB is also possible but requires the use of acid/alcohol mixtures which also require heating.

Table 1.2 *Comparison of experimental conditions of biopolymer-based silica synthesis with Stöber and modified-Stöber processes.*

Production Process	Precursor	Temperature (°C)	Solvent	Post-processing	Refs.
Biopolymer-based	Sodium silicate	Ambient	Water	Washing	108,109,154, 155,157,158
Stöber	TEOS	10 – 80	Ethanol/ water	Washing	38,180–185
Modified-Stöber	TEOS	10 – 40	Ethanol/ water	Calcination > 500 °C or chemical extraction	5,49,186–190

The above table provides a simple yet effective outline of the advantages of a biopolymer-based silica synthesis over the traditional Stöber processes. Compared to the biopolymer-based silica syntheses, which use biodegradable and sustainable SDAs, water-based chemistries, minimal post-processing, and ambient experimental conditions, the Stöber processes are unsustainable and highly energy-intensive.

1.6 Conclusions and outlook

The outlook on the use of biopolymers to synthesise spherical silica is bright. The use of sustainable and renewable reagents, ambient reaction conditions, and environmentally friendly methods, offers significant advantages over the traditional, established methods. However, the one area which has perhaps hindered the adoption of such biopolymer-based silica syntheses is their failure to produce monodisperse silica particles thus far. The widespread use of Stöber and modified-Stöber processes is due to the ease, and consistency, with which they are able to produce discrete and monodisperse silica particles. Various applications, such as chromatography and drug-delivery, require monodisperse silica particles, and as such, it is an essential physical property to control. However, there has been decades of work and refinement since Stöber first reported the synthesis of monodisperse particles. Synthesising such particles using biomimetic methods is much more recent. It has already been shown that using Nature as an inspiration, biomimetic silica can successfully be synthesised *in vitro*. Further optimisation of this process, to control monodispersity, would lead to parity between the Stöber and biopolymer-based processes. These optimisations should focus on the physicochemical characteristics discussed previously – amphiphilicity, adjacent carboxyl and amino groups (charge relay effect), polyamines, and quaternary amines – and the reaction conditions which are conducive to such biopolymers acting as an SDA, because the structure-directing role of a biopolymer is crucial to forming discrete monodisperse spherical silica. By these means, truly sustainable production of spherical silica particles to meet the needs of the modern world is possible.

1.7 References

1. Narayanan, R. & El-Sayed, M. A. Effect of catalysis on the stability of metallic nanoparticles: Suzuki reaction catalyzed by PVP-palladium nanoparticles. *J. Am. Chem. Soc.* **125**, 8340–8347 (2003) DOI: 10.1021/ja035044x.

2. Miyake, Y., Hanaeda, M. & Asada, M. Separation of organic compounds by spherical mesoporous silica prepared from W/O microemulsions of tetrabutoxysilane. *Ind. Eng. Chem. Res.* **46**, 8152–8157 (2007) DOI: 10.1021/ie0705047.

3. Brown, P. R. High-performance liquid chromatography. Past developments, present status, and future trends. *Anal. Chem.* **62**, 995A-1008A (1990) DOI: 10.1021/ac00218a001.

4. Pagliaro, M. *Silica Based Material for Advanced Chemical Applications*. (2009).

5. Slowing, I. I., Vivero-Escoto, J. L., Wu, C.-W. & Lin, V. S.-Y. Y. Mesoporous silica nanoparticles as controlled release drug delivery and gene transfection carriers. *Adv. Drug Deliv. Rev.* **60**, 1278–1288 (2008) DOI: 10.1016/j.addr.2008.03.012.

6. Anastas, P. & Eghbali, N. Green chemistry: Principles and practice. *Chem. Soc. Rev.* **39**, 301–312 (2010) DOI: 10.1039/b918763b.

7. Grand View Research. *Precipitated Silica Market Size & Analysis, Industry Report, 2019-2025*. (2019).

8. Isomaa, B., Reuter, J. & Djupsund, B. M. The subacute and chronic toxicity of

cetyltrimethylammonium bromide (CTAB), a cationic surfactant, in the rat. *Arch. Toxicol.* **35**, 91–96 (1976) DOI: 10.1007/BF00372762.

9. Nałęcz-Jawecki, G., Grabińska-Sota, E. & Narkiewicz, P. The toxicity of cationic surfactants in four bioassays. *Ecotoxicol. Environ. Saf.* **54**, 87–91 (2003) DOI: 10.1016/S0147-6513(02)00025-8.

10. Nakashima, H., Omae, K., Sakai, T., Yamazaki, K. & Sakurai, H. Acute and subchronic inhalation toxicity of tetraethoxysilane (TEOS) in mice. *Arch. Toxicol.* **68**, 277–283 (1994) DOI: 10.1007/s002040050069.

11. Mann, S. *Biomineralization: Principles and Concepts in Bioinorganic Materials Chemistry*. (Oxford University Press, 2001).

12. Trembath-Reichert, E., Wilson, J. P., McGlynn, S. E. & Fischer, W. W. Four hundred million years of silica biomineralization in land plants. *Proc. Natl. Acad. Sci.* **112**, 5449–5454 (2015) DOI: 10.1073/pnas.1500289112.

13. Knoll, A. H. Biomineralization and Evolutionary History. *Rev. Mineral. Geochemistry* **54**, 329–356 (2003) DOI: 10.2113/0540329.

14. Tang, Q., Wan, B., Yuan, X., Muscente, A. D. & Xiao, S. Spiculogenesis and biomineralization in early sponge animals. *Nat. Commun.* **10**, 3348 (2019) DOI: 10.1038/s41467-019-11297-4.

15. Schoeppler, V. *et al.* Biomineralization as a Paradigm of Directional Solidification: A Physical Model for Molluscan Shell Ultrastructural Morphogenesis. *Adv. Mater.* **30**, 1803855 (2018) DOI: 10.1002/adma.201803855.

16. Hildebrand, M. Diatoms, Biomineralization Processes, and Genomics. *Chem. Rev.* **108**, 4855–4874 (2008) DOI: 10.1021/cr078253z.

17. Piletska, E. *et al.* Biomimetic Silica Nanoparticles Prepared by a Combination of Solid-Phase Imprinting and Ostwald Ripening. *Sci. Rep.* **7**, 11537 (2017) DOI: 10.1038/s41598-017-12007-0.

18. Coradin, T., Lopez, P. J., Gautier, C. & Livage, J. From biogenic to biomimetic silica. *Comptes Rendus Palevol* **3**, 443–452 (2004) DOI: 10.1016/j.crpv.2004.07.002.

19. Jackson, E. *et al.* Protein-Templated Biomimetic Silica Nanoparticles. *Langmuir* **31**, 3687–3695 (2015) DOI: 10.1021/la504978r.

20. Wang, F. *et al.* In situ Synthesis of Biomimetic Silica Nanofibrous Aerogels with Temperature-Invariant Superelasticity over One Million Compressions. *Angew. Chemie Int. Ed.* **59**, 8285–8292 (2020) DOI: 10.1002/anie.202001679.

21. Höök, M. & Tang, X. Depletion of fossil fuels and anthropogenic climate change—A review. *Energy Policy* **52**, 797–809 (2013) DOI: 10.1016/j.enpol.2012.10.046.

22. Rebello, S., Asok, A. K., Mundayoor, S. & Jisha, M. S. Surfactants: toxicity, remediation and green surfactants. *Environ. Chem. Lett.* **12**, 275–287 (2014) DOI: 10.1007/s10311-014-0466-2.

23. Hayes, D. G. & Smith, G. A. Biobased Surfactants: Overview and Industrial State of the Art. in *Biobased Surfactants* 3–38 (Elsevier, 2019). doi:10.1016/B978-0-12-812705-6.00001-0 DOI: 10.1016/B978-0-12-812705-6.00001-0.

24. Yu, L. *et al.* Carbohydrate-Derived Hydrothermal Carbons: A Thorough Characterization Study. *Langmuir* **28**, 12373–12383 (2012) DOI: 10.1021/la3024277.

25. Alatalo, S.-M. *et al.* Versatile Cellulose-Based Carbon Aerogel for the Removal of Both Cationic and Anionic Metal Contaminants from Water. *ACS Appl. Mater. Interfaces* **7**, 25875–25883 (2015) DOI: 10.1021/acsami.5b08287.

26. Li, X.-H., Kurasch, S., Kaiser, U. & Antonietti, M. Synthesis of Monolayer-Patched Graphene from Glucose. *Angew. Chemie Int. Ed.* **51**, 9689–9692 (2012) DOI: 10.1002/anie.201203207.

27. White, R. J., Yoshizawa, N., Antonietti, M. & Titirici, M.-M. A sustainable synthesis of nitrogen-doped carbon aerogels. *Green Chem.* **13**, 2428 (2011) DOI: 10.1039/c1gc15349h.

28. Mann, S. *et al.* Crystallization at Inorganic-organic Interfaces: Biominerals and Biomimetic Synthesis. *Science (80-.).* **261**, 1286–1292 (1993) DOI: 10.1126/science.261.5126.1286.

29. Patil, G. V. Biopolymer albumin for diagnosis and in drug delivery. *Drug Dev. Res.* **58**, 219–247 (2003) DOI: 10.1002/ddr.10157.

30. Park, S. Bin, Lih, E., Park, K. S., Joung, Y. K. & Han, D. K. Biopolymer-based functional composites for medical applications. *Prog. Polym. Sci.* **68**, 77–105 (2017) DOI: 10.1016/j.progpolymsci.2016.12.003.

31. Oh, J. K., Lee, D. I. & Park, J. M. Biopolymer-based microgels/nanogels for drug

delivery applications. *Prog. Polym. Sci.* **34**, 1261–1282 (2009) DOI: 10.1016/j.progpolymsci.2009.08.001.

32. Tematio, C. *et al.* Design and characterization of conductive biopolymer nanocomposite electrodes for medical applications. *Mater. Sci. Forum* **879**, 1921–1926 (2017) DOI: 10.4028/www.scientific.net/MSF.879.1921.

33. Kogan, G., Šoltés, L., Stern, R. & Gemeiner, P. Hyaluronic acid: A natural biopolymer with a broad range of biomedical and industrial applications. *Biotechnol. Lett.* **29**, 17–25 (2007) DOI: 10.1007/s10529-006-9219-z.

34. Othman, S. H. Bio-nanocomposite Materials for Food Packaging Applications: Types of Biopolymer and Nano-sized Filler. *Agric. Agric. Sci. Procedia* **2**, 296–303 (2014) DOI: 10.1016/j.aaspro.2014.11.042.

35. Scholten, E., Moschakis, T. & Biliaderis, C. G. Biopolymer composites for engineering food structures to control product functionality. *Food Struct.* **1**, 39–54 (2014) DOI: 10.1016/j.foostr.2013.11.001.

36. Ghanbarzadeh, B., Oleyaei, S. A. & Almasi, H. Nanostructured Materials Utilized in Biopolymer-based Plastics for Food Packaging Applications. *Crit. Rev. Food Sci. Nutr.* **55**, 1699–1723 (2015) DOI: 10.1080/10408398.2012.731023.

37. Tang, X. Z., Kumar, P., Alavi, S. & Sandeep, K. P. Recent Advances in Biopolymers and Biopolymer-Based Nanocomposites for Food Packaging Materials. *Crit. Rev. Food Sci. Nutr.* **52**, 426–442 (2012) DOI: 10.1080/10408398.2010.500508.

38. Stöber, W., Fink, A. & Bohn, E. Controlled growth of monodisperse silica spheres in the micron size range. *J. Colloid Interface Sci.* **26**, 62–69 (1968) DOI: 10.1016/0021-9797(68)90272-5.

39. Liberman, A., Mendez, N., Trogler, W. C. & Kummel, A. C. Synthesis and surface functionalization of silica nanoparticles for nanomedicine. *Surf. Sci. Rep.* **69**, 132–158 (2014) DOI: 10.1016/j.surfrep.2014.07.001.

40. Hayes, R., Ahmed, A., Edge, T. & Zhang, H. Core-shell particles: Preparation, fundamentals and applications in high performance liquid chromatography. *J. Chromatogr. A* **1357**, 36–52 (2014) DOI: 10.1016/j.chroma.2014.05.010.

41. Anderson, M. T., Martin, J. E., Odinek, J. G. & Newcomer, P. P. Effect of methanol concentration on CTAB micellization and on the formation of surfactant-templated silica (STS). *Chem. Mater.* **10**, 1490–1500 (1998) DOI: 10.1021/cm970240m.

42. Hoffmann, F., Cornelius, M., Morell, J. & Fröba, M. Silica-based mesoporous organic-inorganic hybrid materials. *Angew. Chemie - Int. Ed.* **45**, 3216–3251 (2006) DOI: 10.1002/anie.200503075.

43. Zhao, D. *et al.* Triblock copolymer syntheses of mesoporous silica with periodic 50 to 300 angstrom pores. *Science (80-.).* **279**, 548–52 (1998) DOI: 10.1126/science.279.5350.548.

44. Trefalt, G., Ruiz-Cabello, F. J. M. & Borkovec, M. Interaction Forces, Heteroaggregation, and Deposition Involving Charged Colloidal Particles. *J. Phys. Chem. B* **118**, 6346–6355 (2014) DOI: 10.1021/jp503564p.

45. Luo, Y., Zhao, R. & Pendry, J. B. van der Waals interactions at the nanoscale: The effects of nonlocality. *Proc. Natl. Acad. Sci.* **111**, 18422–18427 (2014) DOI: 10.1073/pnas.1420551111.

46. Trefalt, G., Behrens, S. H. & Borkovec, M. Charge Regulation in the Electrical Double Layer: Ion Adsorption and Surface Interactions. *Langmuir* **32**, 380–400 (2016) DOI: 10.1021/acs.langmuir.5b03611.

47. Zareei, M., Yoozbashizadeh, H. & Madaah Hosseini, H. R. Investigating the effects of pH, surfactant and ionic strength on the stability of alumina/water nanofluids using DLVO theory. *J. Therm. Anal. Calorim.* **135**, 1185–1196 (2019) DOI: 10.1007/s10973-018-7620-1.

48. Zhao, X. S., Lu, G. Q. (Max) & Millar, G. J. Advances in Mesoporous Molecular Sieve MCM-41. *Ind. Eng. Chem. Res.* **35**, 2075–2090 (1996) DOI: 10.1021/ie950702a.

49. Alothman, Z. A Review: Fundamental Aspects of Silicate Mesoporous Materials. *Materials (Basel).* **5**, 2874–2902 (2012) DOI: 10.3390/ma5122874.

50. Spencer, J. N., Wolbach, W. S., Hovick, J. W., Ansel, L. & Modarress, K. J. Hydrogen bonding by alcohols and amines. *J. Solution Chem.* **14**, 805–814 (1985) DOI: 10.1007/BF00646002.

51. Iler, R. K. *The Chemistry of Silica: Solubility, Polymerization, Colloid and Surface Properties, and Biochemistry. Wiley-Interscience* (Wiley: New York, 1979).

52. Hench, L. *Sol- Gel Silica: Properties, Processing and Technology Transfer*.

(1998).

53. Ghimire, P. P. & Jaroniec, M. Renaissance of Stöber method for synthesis of colloidal particles: New developments and opportunities. *J. Colloid Interface Sci.* **584**, 838–865 (2021) DOI: 10.1016/j.jcis.2020.10.014.

54. Trinh, T. T., Jansen, A. P. J. & Van Santen, R. A. Mechanism of oligomerization reactions of silica. *J. Phys. Chem. B* **110**, 23099–23106 (2006) DOI: 10.1021/jp063670l.

55. Matsoukas, T. & Gulari, E. Dynamics of growth of silica particles from ammonia-catalyzed hydrolysis of tetra-ethyl-orthosilicate. *J. Colloid Interface Sci.* **124**, 252–261 (1988) DOI: 10.1016/0021-9797(88)90346-3.

56. Matsoukas, T. & Gulari, E. Monomer-addition growth with a slow initiation step: A growth model for silica particles from alkoxides. *J. Colloid Interface Sci.* **132**, 13–21 (1989) DOI: 10.1016/0021-9797(89)90210-5.

57. Bogush, G.H.; Zukoski, C. F. Uniform Silica Particle Precipitation: An Aggregative Growth Model. *J. Colloid Interface Sci.* **142**, 19–34 (1991).

58. Bogush, G. H. & Zukoski IV, C. F. Studies of the kinetics of the precipitation of uniform silica particles through the hydrolysis and condensation of silicon alkoxides. *J. Colloid Interface Sci.* **142**, 1–18 (1991) DOI: 10.1016/0021-9797(91)90029-8.

59. Han, Y. *et al.* Unraveling the growth mechanism of silica particles in the stöber method: In situ seeded growth model. *Langmuir* **33**, 5879–5890 (2017) DOI:

10.1021/acs.langmuir.7b01140.

60. Edler, K. J. Current Understanding of Formation Mechanisms in Surfactant-Templated Materials. *Aust. J. Chem.* **58**, 627 (2005) DOI: 10.1071/CH05141.

61. Nooney, R. I., Thirunavukkarasu, D., Chen, Y., Josephs, R. & Ostafin, A. E. Synthesis of Nanoscale Mesoporous Silica Spheres with Controlled Particle Size. *Chem. Mater.* **14**, 4721–4728 (2002) DOI: 10.1021/cm0204371.

62. Zhang, T., Xu, G., Puckette, J. & Blum, F. D. Effect of Silica on the Structure of Cetyltrimethylammonium Bromide. *J. Phys. Chem. C* **116**, 11626–11634 (2012) DOI: 10.1021/jp303338t.

63. Liu, Y., Tourbin, M., Lachaize, S. & Guiraud, P. Silica nanoparticles separation from water: Aggregation by cetyltrimethylammonium bromide (CTAB). *Chemosphere* **92**, 681–687 (2013) DOI: 10.1016/j.chemosphere.2013.03.048.

64. Lebedev, O. I., Van Tendeloo, G., Collart, O., Cool, P. & Vansant, E. F. Structure and microstructure of nanoscale mesoporous silica spheres. *Solid State Sci.* **6**, 489–498 (2004) DOI: 10.1016/j.solidstatesciences.2004.01.013.

65. Hollamby, M. J. *et al.* Growth of Mesoporous Silica Nanoparticles Monitored by Time-Resolved Small-Angle Neutron Scattering. *Langmuir* **28**, 4425–4433 (2012) DOI: 10.1021/la203097x.

66. Chien, S.-C. *et al.* Molecular Simulations of the Synthesis of Periodic Mesoporous Silica Phases at High Surfactant Concentrations. *J. Phys. Chem. C* **121**, 4564–4575 (2017) DOI: 10.1021/acs.jpcc.6b09429.

67. Ostwald, W. Über die vermeintliche Isomerie des roten und gelben Quecksilberoxyds und die Oberflächenspannung fester Körper. *Zeitschrift für Phys. Chemie* **34U**, (1900) DOI: 10.1515/zpch-1900-3431.

68. Lifshitz, I. M. & Slyozov, V. V. The kinetics of precipitation from supersaturated solid solutions. *J. Phys. Chem. Solids* **19**, 35–50 (1961) DOI: 10.1016/0022-3697(61)90054-3.

69. Wagner, C. Theorie der Alterung von Niederschlägen durch Umlösen (Ostwald-Reifung). *Berichte der Bunsengesellschaft für Phys. Chemie* **65**, 581–591 (1961) DOI: 10.1002/BBPC.19610650704.

70. Nakashima, H., Omae, K., Yamazaki, K., Sakai, T. & Sakurai, H. Toxicity of Intraperitoneally Administrated Silicon Tetraalkoxides in Male ICR Mice. *Keio J. Med.* **42**, 122–124 (1993) DOI: 10.2302/kjm.42.122.

71. Nakashima, H. Time course of effects of tetraethoxysilane (TEOS) on the kidney and blood silicon concentration in mice. *Arch. Toxicol.* **69**, 59–64 (1994) DOI: 10.1007/s002040050138.

72. OKAMURA, T. Acute urinary tract toxicity of tetraethylorthosilicate in rats. *Fundam. Appl. Toxicol.* **18**, 425–441 (1992) DOI: 10.1016/0272-0590(92)90141-4.

73. United Nations. *Globally Harmonized System of Classification and Labelling of Chemicals (GHS) 8th Revised Edition*. (2019).

74. Thurston, R. V., Chakoumakos, C. & Russo, R. C. Effect of fluctuating exposures

on the acute toxicity of ammonia to rainbow trout (Salmo gairdneri) and cutthroat trout (S. clarki). *Water Res.* **15**, 911–917 (1981) DOI: 10.1016/0043-1354(81)90147-0.

75. *Ambient Water Quality Criteria for Ammonia. United States Environmental Protection Agency (USEPA)*. (1998).

76. U.S. Environmental Protection Agency. *Enironmental Laws Applicable to Construction and Operation of Ethanol Plants*. (2007).

77. Final Report on the Safety Assessment of Cetrimonium Chloride, Cetrimonium Bromide, and Steartrimonium Chloride. *Int. J. Toxicol.* **16**, 195–220 (1997) DOI: 10.1080/109158197227152.

78. Timmer, N., Gore, D., Sanders, D., Gouin, T. & Droge, S. T. J. Toxicity mitigation and bioaccessibility of the cationic surfactant cetyltrimethylammonium bromide in a sorbent-modified biodegradation study. *Chemosphere* **222**, 461–468 (2019) DOI: 10.1016/j.chemosphere.2019.01.152.

79. Knepper, T. P. & Berna, J. L. Surfactants: Properties, production, and environmental Aspects. in 1–49 (2003). doi:10.1016/S0166-526X(03)40004-4 DOI: 10.1016/S0166-526X(03)40004-4.

80. Sánchez-Ramírez, E. *et al.* Reactive Distillation Column Design for Tetraethoxysilane (TEOS) Production: Economic and Environmental Aspects. *Ind. Eng. Chem. Res.* **57**, 5024–5034 (2018) DOI: 10.1021/acs.iecr.7b05058.

81. Scully, S. M. & Orlygsson, J. Biological Production of Alcohols. in *Advanced*

Bioprocessing for Alternative Fuels, Biobased Chemicals, and Bioproducts 83–108 (Elsevier, 2019). doi:10.1016/B978-0-12-817941-3.00005-X DOI: 10.1016/B978-0-12-817941-3.00005-X.

82. Patwardhan, S. V. Biomimetic and bioinspired silica: recent developments and applications. *Chem. Commun.* **47**, 7567 (2011) DOI: 10.1039/c0cc05648k.

83. Baccile, N., Babonneau, F., Thomas, B. & Coradin, T. Introducing ecodesign in silica sol–gel materials. *J. Mater. Chem.* **19**, 8537 (2009) DOI: 10.1039/b911123a.

84. Kaplan, D. L. Mollusc shell structures: novel design strategies for synthetic materials. *Curr. Opin. Solid State Mater. Sci.* **3**, 232–236 (1998) DOI: 10.1016/S1359-0286(98)80096-X.

85. McDougall, C. & Degnan, B. M. The evolution of mollusc shells. *Wiley Interdiscip. Rev. Dev. Biol.* **7**, e313 (2018) DOI: 10.1002/wdev.313.

86. Sundar, V. C., Yablon, A. D., Grazul, J. L., Ilan, M. & Aizenberg, J. Fibre-optical features of a glass sponge. *Nature* **424**, 899–900 (2003) DOI: 10.1038/424899a.

87. Birkbak, M. E., Guizar-Sicairos, M., Holler, M. & Birkedal, H. Internal structure of sponge glass fiber revealed by ptychographic nanotomography. *J. Struct. Biol.* **194**, 124–128 (2016) DOI: 10.1016/j.jsb.2016.02.006.

88. Malviya, S. *et al.* Insights into global diatom distribution and diversity in the world's ocean. *Proc. Natl. Acad. Sci.* **113**, E1516–E1525 (2016) DOI: 10.1073/pnas.1509523113.

89. Piredda, R. *et al.* Diatom diversity through HTS-metabarcoding in coastal

European seas. *Sci. Rep.* **8**, 18059 (2018) DOI: 10.1038/s41598-018-36345-9.

90. Lopez, P., Gautier, C., Livage, J. & Coradin, T. Mimicking Biogenic Silica Nanostructures Formation. *Curr. Nanosci.* **1**, 73–83 (2006) DOI: 10.2174/1573413052953156.

91. Brembu, T., Chauton, M. S., Winge, P., Bones, A. M. & Vadstein, O. Dynamic responses to silicon in Thalasiossira pseudonana - Identification, characterisation and classification of signature genes and their corresponding protein motifs. *Sci. Rep.* **7**, 4865 (2017) DOI: 10.1038/s41598-017-04921-0.

92. Sumper, M. & Brunner, E. Silica Biomineralisation in Diatoms: The Model Organism Thalassiosira pseudonana. *ChemBioChem* **9**, 1187–1194 (2008) DOI: 10.1002/cbic.200700764.

93. Hildebrand, M., Dahlin, K. & Volcani, B. E. Characterization of a silicon transporter gene family in Cylindrotheca fusiformis: sequences, expression analysis, and identification of homologs in other diatoms. *Mol. Gen. Genet. MGG* **260**, 480–486 (1998) DOI: 10.1007/s004380050920.

94. Magaletti, E., Urbani, R., Sist, P., Ferrari, C. R. & Cicero, A. M. Abundance and chemical characterization of extracellular carbohydrates released by the marine diatom Cylindrotheca fusiformis under N- and P-limitation. *Eur. J. Phycol.* **39**, 133–142 (2004) DOI: 10.1080/0967026042000202118.

95. Bertermann, R., Kröger, N. & Tacke, R. Solid-state 29Si MAS NMR studies of diatoms: structural characterization of biosilica deposits. *Anal. Bioanal. Chem.* **375**, 630–634 (2003) DOI: 10.1007/s00216-003-1769-5.

96. Kröger, N. Prescribing diatom morphology: toward genetic engineering of biological nanomaterials. *Curr. Opin. Chem. Biol.* **11**, 662–669 (2007) DOI: 10.1016/j.cbpa.2007.10.009.

97. Sumper, M., Lorenz, S. & Brunner, E. Biomimetic Control of Size in the Polyamine-Directed Formation of Silica Nanospheres. *Angew. Chemie - Int. Ed.* **42**, 5192–5195 (2003) DOI: 10.1002/anie.200352212.

98. Pamirsky, I. E. & Golokhvast, K. S. Silaffins of diatoms: From applied biotechnology to biomedicine. *Mar. Drugs* **11**, 3155–3167 (2013) DOI: 10.3390/md11093155.

99. Kröger, N., Deutzmann, R., Bergsdorf, C. & Sumper, M. Species-specific polyamines from diatoms control silica morphology. *Proc. Natl. Acad. Sci.* **97**, 14133–14138 (2000) DOI: 10.1073/pnas.260496497.

100. Belton, D. J., Patwardhan, S. V., Annenkov, V. V., Danilovtseva, E. N. & Perry, C. C. From biosilicification to tailored materials: Optimizing hydrophobic domains and resistance to protonation of polyamines. *Proc. Natl. Acad. Sci.* **105**, 5963–5968 (2008) DOI: 10.1073/pnas.0710809105.

101. Mizutani, T., Nagase, H., Fujiwara, N. & Ogoshi, H. Silicic Acid Polymerization Catalyzed by Amines and Polyamines. *Bull. Chem. Soc. Jpn.* **71**, 2017–2022 (1998) DOI: 10.1246/bcsj.71.2017.

102. Sumper, M. & Kröger, N. Silica formation in diatoms: The function of long-chain polyamines and silaffins. *J. Mater. Chem.* **14**, 2059–2065 (2004) DOI: 10.1039/b401028k.

103. Wenzl, S., Hett, R., Richthammer, P. & Sumper, M. Silacidins: Highly acidic phosphopeptides from diatom shells assist in silica precipitation in vitro. *Angew. Chemie - Int. Ed.* **47**, 1729–1732 (2008) DOI: 10.1002/anie.200704994.

104. Delak, K. M. & Sahai, N. Amine-catalyzed biomimetic hydrolysis and condensation of organosilicate. *Chem. Mater.* **17**, 3221–3227 (2005) DOI: 10.1021/cm048355v.

105. Fairbridge, R. W. Silica, silicate. in *Encyclopedia of Planetary Science* 737–737 (Kluwer Academic Publishers, 1997). doi:10.1007/1-4020-4520-4_365 DOI: 10.1007/1-4020-4520-4_365.

106. Kröger, N., Lorenz, S., Brunner, E. & Sumper, M. Self-Assembly of Highly Phosphorylated Silaffins and Their Function in Biosilica Morphogenesis. *Science (80-.).* **298**, 584–586 (2014) DOI: 10.1126/science.1076221.

107. Coradin, T. & Livage, J. Effect of some amino acids and peptides on silicic acid polymerization. *Colloids Surfaces B Biointerfaces* **21**, 329–336 (2001) DOI: 10.1016/S0927-7765(01)00143-6.

108. Coradin, T., Coupé, A. & Livage, J. Interactions of bovine serum albumin and lysozyme with sodium silicate solutions. *Colloids Surfaces B Biointerfaces* **29**, 189–196 (2003) DOI: 10.1016/S0927-7765(02)00208-4.

109. Coradin, T., Durupthy, O. & Livage, J. Interactions of amino-containing peptides with sodium silicate and colloidal silica: A biomimetic approach of silicification. *Langmuir* vol. 18 2331–2336 (2002) DOI: 10.1021/la011106q.

110. Wallace, A. F., DeYoreo, J. J. & Dove, P. M. Kinetics of silica nucleation on carboxyl- and amine-terminated surfaces: Insights for biomineralization. *J. Am. Chem. Soc.* **131**, 5244–5250 (2009) DOI: 10.1021/ja809486b.

111. Brumlik, M. J. & Buckley, J. T. Identification of the catalytic triad of the lipase/acyltransferase from Aeromonas hydrophila. *J. Bacteriol.* **178**, 2060–2064 (1996) DOI: 10.1128/jb.178.7.2060-2064.1996.

112. Ekici, Ö. D., Paetzel, M. & Dalbey, R. E. Unconventional serine proteases: Variations on the catalytic Ser/His/Asp triad configuration. *Protein Sci.* **17**, 2023–2037 (2008) DOI: 10.1110/ps.035436.108.

113. Kuno, T., Nonoyama, T., Hirao, K. & Kato, K. Influence of the charge relay effect on the silanol condensation reaction as a model for silica biomineralization. *Langmuir* **27**, 13154–13158 (2011) DOI: 10.1021/la202576v.

114. Murai, K., Higuchi, M., Kuno, T. & Kato, K. Silica mineralization by a peptide template having a high charge relay effect. *Chempluschem* **79**, 531–535 (2014) DOI: 10.1002/cplu.201300321.

115. Berner, R. A. Weathering, plants, and the long-term carbon cycle. *Geochim. Cosmochim. Acta* **56**, 3225–3231 (1992) DOI: 10.1016/0016-7037(92)90300-8.

116. Thamatrakoln, K., Alverson, A. J. & Hildebrand, M. COMPARATIVE SEQUENCE ANALYSIS OF DIATOM SILICON TRANSPORTERS: TOWARD A MECHANISTIC MODEL OF SILICON TRANSPORT. *J. Phycol.* **42**, 822–834 (2006) DOI: 10.1111/j.1529-8817.2006.00233.x.

117. Kröger, N., Deutzmann, R. & Sumper, M. Silica-precipitating peptides from diatoms: The chemical structure of silaffin-1A from Cylindrotheca fusiformis. *J. Biol. Chem.* **276**, 26066–26070 (2001) DOI: 10.1074/jbc.M102093200.

118. Kröger, N., Deutzmann, R. & Sumper, M. Polycationic peptides from diatom biosilica that direct silica nanosphere formation. *Science (80-.).* **286**, 1129–1132 (1999) DOI: 10.1126/science.286.5442.1129.

119. Simpson, T. L. & Volcani, B. E. *Silicon and Siliceous Structures in Biological Systems*. (Springer New York, 1981). doi:10.1007/978-1-4612-5944-2 DOI: 10.1007/978-1-4612-5944-2.

120. Belton, D. J., Deschaume, O., Patwardhan, S. V. & Perry, C. C. A Solution Study of Silica Condensation and Speciation with Relevance to in Vitro Investigations of Biosilicification. *J. Phys. Chem. B* **114**, 9947–9955 (2010) DOI: 10.1021/jp101347q.

121. Goretsky, A. V., Beck, L. W., Zones, S. I. & Davis, M. E. Influence of the hydrophobic character of structure-directing agents for the synthesis of pure-silica zeolites. *Microporous Mesoporous Mater.* **28**, 387–393 (1999) DOI: 10.1016/S1387-1811(98)00307-2.

122. Ghasemi, H., Mazloomi, H. & Hajipour, H. Stabilization of multiple emulsions using natural surfactants. (2017).

123. Nothling, M. D. *et al.* Simple Design of an Enzyme-Inspired Supported Catalyst Based on a Catalytic Triad. *Chem* **2**, 732–745 (2017) DOI: 10.1016/j.chempr.2017.04.004.

124. Gruber, K. & Kratky, C. Biopolymers for biocatalysis: Structure and catalytic mechanism of hydroxynitrile lyases. *J. Polym. Sci. Part A Polym. Chem.* **42**, 479–486 (2004) DOI: 10.1002/pola.10845.

125. Anobom, C. D. *et al.* From Structure to Catalysis: Recent Developments in the Biotechnological Applications of Lipases. *Biomed Res. Int.* **2014**, 1–11 (2014) DOI: 10.1155/2014/684506.

126. Amrein, B. A. *et al.* Expanding the Catalytic Triad in Epoxide Hydrolases and Related Enzymes. *ACS Catal.* **5**, 5702–5713 (2015) DOI: 10.1021/acscatal.5b01639.

127. Menzel, H. *et al.* Chemical properties of polyamines with relevance to the biomineralization of silica. *Chem. Commun.* **3**, 2994–2995 (2003) DOI: 10.1039/b310201g.

128. Greasley, S. L. *et al.* Controlling particle size in the Stöber process and incorporation of calcium. *J. Colloid Interface Sci.* **469**, 213–223 (2016) DOI: 10.1016/j.jcis.2016.01.065.

129. Yokoi, T. *et al.* Mechanism of formation of uniform-sized silica nanospheres catalyzed by basic amino acids. *Chem. Mater.* **21**, 3719–3729 (2009) DOI: 10.1021/cm900993b.

130. Belton, D. J., Patwardhan, S. V. & Perry, C. C. Spermine, spermidine and their analogues generate tailored silicas. *J. Mater. Chem.* **15**, 4629–4638 (2005) DOI: 10.1039/b509683a.

131. Niaounakis, M. N. *Biopolymers: Applications and Trends*. *Engineering* vol. 42 (Elsevier, 2016). DOI: 10.1016/C2014-0-00936-7.

132. Thompson, R. C., Moore, C. J., vom Saal, F. S. & Swan, S. H. Plastics, the environment and human health: current consensus and future trends. *Philos. Trans. R. Soc. B Biol. Sci.* **364**, 2153–2166 (2009) DOI: 10.1098/rstb.2009.0053.

133. Thompson, R. C. Microplastics in the Marine Environment: Sources, Consequences and Solutions. in *Marine Anthropogenic Litter* 185–200 (Springer International Publishing, 2015). doi:10.1007/978-3-319-16510-3_7 DOI: 10.1007/978-3-319-16510-3_7.

134. Niaounakis, M. *Biopolymers : Reuse, Recycling, and Disposal*. (Technology & Engineering, 2013).

135. Tabassum, M. R., Xia, A. & Murphy, J. D. Potential of seaweed as a feedstock for renewable gaseous fuel production in Ireland. *Renew. Sustain. Energy Rev.* **68**, 136–146 (2017) DOI: 10.1016/j.rser.2016.09.111.

136. Sinkiewicz, I., Śliwińska, A., Staroszczyk, H. & Kołodziejska, I. Alternative Methods of Preparation of Soluble Keratin from Chicken Feathers. *Waste and Biomass Valorization* **8**, 1043–1048 (2017) DOI: 10.1007/s12649-016-9678-y.

137. Rasmussen, L. K. & Petersen, T. E. Purification of disulphide-linked α s2 - and κ-casein from bovine milk. *J. Dairy Res.* **58**, 187–193 (1991) DOI: 10.1017/S0022029900029733.

138. Huppertz, T., Fox, P. F. & Kelly, A. L. *The caseins: Structure, stability, and*

functionality. *Proteins in Food Processing: Second Edition* (Elsevier Ltd., 2018). doi:10.1016/B978-0-08-100722-8.00004-8 DOI: 10.1016/B978-0-08-100722-8.00004-8.

139. Predescu, A. M. *et al.* Synthesis and characterization of dextran-coated iron oxide nanoparticles. *R. Soc. Open Sci.* **5**, 171525 (2018) DOI: 10.1098/rsos.171525.

140. Naha, P. C. *et al.* Dextran-Coated Iron Oxide Nanoparticles as Biomimetic Catalysts for Localized and pH-Activated Biofilm Disruption. *ACS Nano* **13**, 4960–4971 (2019) DOI: 10.1021/acsnano.8b08702.

141. Hradil, J., Pisarev, A., Babič, M. & Horák, D. Dextran-modified iron oxide nanoparticles. *China Particuology* **5**, 162–168 (2007) DOI: 10.1016/j.cpart.2007.01.003.

142. Laurent, S. *et al.* Magnetic Iron Oxide Nanoparticles: Synthesis, Stabilization, Vectorization, Physicochemical Characterizations, and Biological Applications. *Chem. Rev.* **108**, 2064–2110 (2008) DOI: 10.1021/cr068445e.

143. Finotelli, P. V., Sampaio, D. A., Morales, M. A., Rossi, A. M. & Rocha-Leão, M. H. Ca alginate as scaffold for iron oxide nanoparticles synthesis. *Brazilian J. Chem. Eng.* **25**, 759–764 (2008) DOI: 10.1590/S0104-66322008000400013.

144. Wu, K. *et al.* Functionalized magnetic iron oxide/alginate core-shell nanoparticles for targeting hyperthermia. *Int. J. Nanomedicine* 3315 (2015) doi:10.2147/IJN.S68719 DOI: 10.2147/IJN.S68719.

145. SHEARS, G. E., LEDWARD, D. A. & NEALE, R. J. Iron complexation to

carboxyl groups in a bovine serum albumin digest. *Int. J. Food Sci. Technol.* **22**, 265–272 (2007) DOI: 10.1111/j.1365-2621.1987.tb00487.x.

146. Kumar, S. V. *et al.* High conversion synthesis of <10 nm starch-stabilized silver nanoparticles using microwave technology. *Sci. Rep.* **8**, 5106 (2018) DOI: 10.1038/s41598-018-23480-6.

147. Salaheldin, H. I. Optimizing the synthesis conditions of silver nanoparticles using corn starch and their catalytic reduction of 4-nitrophenol. *Adv. Nat. Sci. Nanosci. Nanotechnol.* **9**, 025013 (2018) DOI: 10.1088/2043-6254/aac4eb.

148. Yakout, S. M. & Mostafa, A. A. A novel green synthesis of silver nanoparticles using soluble starch and its antibacterial activity. *Int. J. Clin. Exp. Med.* **8**, 3538–44 (2015).

149. Raghavendra, G. M., Jung, J., Kim, D. & Seo, J. Step-reduced synthesis of starch-silver nanoparticles. *Int. J. Biol. Macromol.* **86**, 126–128 (2016) DOI: 10.1016/j.ijbiomac.2016.01.057.

150. Sun, L. *et al.* One pot synthesis of gold nanoparticles using chitosan with varying degree of deacetylation and molecular weight. *Carbohydr. Polym.* **178**, 105–114 (2017) DOI: 10.1016/j.carbpol.2017.09.032.

151. Adlim, A. & Bakar, M. A. Preparation of chitosan-gold nanoparticles: Part 2. The role of chitosan. *Indones. J. Chem.* **8**, 320–326 (2010) DOI: 10.22146/ijc.21585.

152. Huang, H. & Yang, X. Synthesis of Chitosan-Stabilized Gold Nanoparticles in the Absence/Presence of Tripolyphosphate. *Biomacromolecules* **5**, 2340–2346 (2004)

DOI: 10.1021/bm0497116.

153. Mohan, C. O., Gunasekaran, S. & Ravishankar, C. N. Chitosan-capped gold nanoparticles for indicating temperature abuse in frozen stored products. *npj Sci. Food* **3**, 2 (2019) DOI: 10.1038/s41538-019-0034-z.

154. Coradin, T., Bah, S. & Livage, J. Gelatine/silicate interactions: From nanoparticles to composite gels. *Colloids Surfaces B Biointerfaces* **35**, 53–58 (2004) DOI: 10.1016/j.colsurfb.2004.02.008.

155. Demadis, K. D., Pachis, K., Ketsetzi, A. & Stathoulopoulou, A. Bioinspired control of colloidal silica in vitro by dual polymeric assemblies of zwitterionic phosphomethylated chitosan and polycations or polyanions. *Adv. Colloid Interface Sci.* **151**, 33–48 (2009) DOI: 10.1016/j.cis.2009.07.005.

156. Kotzsch, A. *et al.* Silicanin-1 is a conserved diatom membrane protein involved in silica biomineralization. *BMC Biol.* **15**, 9–11 (2017) DOI: 10.1186/s12915-017-0400-8.

157. Gautier, C. *et al.* Biomimetic dual templating of silica by polysaccharide/protein assemblies. *Colloids Surfaces B Biointerfaces* **65**, 140–145 (2008) DOI: 10.1016/j.colsurfb.2008.03.005.

158. Jia, J., Zhou, X., Caruso, R. A. & Antonietti, M. Synthesis of Microporous Silica Templated by Gelatin. *Chem. Lett.* **33**, 202–203 (2004) DOI: 10.1246/cl.2004.202.

159. Fox, P. F. Milk Proteins: General and Historical Aspects. in *Advanced Dairy Chemistry---1 Proteins: Part A & B* (eds. Fox, P. F. & McSweeney, P. L. H.) 1–48

(Springer US, 2003). doi:10.1007/978-1-4419-8602-3_1 DOI: 10.1007/978-1-4419-8602-3_1.

160. Ono, T., Yada, R., Yutani, K. & Nakai, S. Comparison of conformations of κ-casein, para-κ-casein and glycomacropeptide. *Biochim. Biophys. Acta (BBA)/Protein Struct. Mol.* **911**, 318–325 (1987) DOI: 10.1016/0167-4838(87)90072-0.

161. Holt, C. & Sawyer, L. Caseins as rheomorphic proteins: Interpretation of primary and secondary structures of the αs1-, β- and κ-caseins. *J. Chem. Soc. Faraday Trans.* **89**, 2683–2692 (1993) DOI: 10.1039/FT9938902683.

162. De Kruif, C. G. & Holt, C. Casein Micelle Structure, Functions and Interactions. in *Advanced Dairy Chemistry—1 Proteins* vol. 1 233–276 (Springer US, 2003). DOI: 10.1007/978-1-4419-8602-3_5.

163. McMahon, D. J. & Oommen, B. S. Supramolecular Structure of the Casein Micelle. *J. Dairy Sci.* **91**, 1709–1721 (2008) DOI: 10.3168/jds.2007-0819.

164. Holt, C. & Horne, D. S. The hairy casein micelle: Evolution of the concept and its implications for dairy technology. *Netherlands Milk Dairy J.* **50**, 85–111 (1996).

165. McMahon, D. J. & Oommen, B. S. Casein Micelle Structure, Functions, and Interactions. in *Advanced Dairy Chemistry* 185–209 (Springer US, 2013). doi:10.1007/978-1-4614-4714-6_6 DOI: 10.1007/978-1-4614-4714-6_6.

166. Smialowska, A., Merino, L. M.-, Ingham, B. & Carr, A. J. Effect of calcium on the aggregation behaviour of caseinates. *Colloids Surfaces A Physicochem. Eng. Asp.*

(2017) doi:10.1016/j.colsurfa.2017.02.074 DOI: 10.1016/j.colsurfa.2017.02.074.

167. Gopinatha Kurup, G., Adhikari, B. & Zisu, B. Recovery of proteins and lipids from dairy wastewater using food grade sodium lignosulphonate. *Water Resour. Ind.* **22**, 100114 (2019) DOI: 10.1016/j.wri.2019.100114.

168. Ryder, K., Ali, M. A., Carne, A. & Billakanti, J. The potential use of dairy by-products for the production of nonfood biomaterials. *Crit. Rev. Environ. Sci. Technol.* **47**, 621–642 (2017) DOI: 10.1080/10643389.2017.1322875.

169. Xu, Q., Ma, J., Zhou, J., Wang, Y. & Zhang, J. Bio-based core–shell casein-based silica nano-composite latex by double-in situ polymerization: Synthesis, characterization and mechanism. *Chem. Eng. J.* **228**, 281–289 (2013) DOI: 10.1016/j.cej.2013.04.079.

170. Ma, J. *et al.* Synthesis and biological response of casein-based silica nano-composite film for drug delivery system. *Colloids Surfaces B Biointerfaces* **111**, 257–263 (2013) DOI: 10.1016/j.colsurfb.2013.06.011.

171. Tiberg, F., Nylander, T., Su, T. J., Lu, J. R. & Thomas, R. K. β-Casein Adsorption at the Silicon Oxide−Aqueous Solution Interface. *Biomacromolecules* **2**, 844–850 (2001) DOI: 10.1021/bm0155221.

172. Cabezas, D. M., Diehl, B. W. K. & Tomás, M. C. Sunflower lecithin: Application of a fractionation process with absolute ethanol. *JAOCS, J. Am. Oil Chem. Soc.* **86**, 189–196 (2009) DOI: 10.1007/s11746-008-1336-5.

173. Ceci, L. N., Constenla, D. T. & Crapiste, G. H. Oil recovery and lecithin production

using water degumming sludge of crude soybean oils. *J. Sci. Food Agric.* **88**, 2460–2466 (2008) DOI: 10.1002/jsfa.3363.

174. Raut, S. *et al.* Lecithin organogel: A unique micellar system for the delivery of bioactive agents in the treatment of skin aging. *Acta Pharm. Sin. B* **2**, 8–15 (2012) DOI: 10.1016/j.apsb.2011.12.005.

175. Galarneau, A. *et al.* Synthesis of sponge mesoporous silicas from lecithin/dodecylamine mixed-micelles in ethanol/water media: A route towards efficient biocatalysts. *Microporous Mesoporous Mater.* **104**, 103–114 (2007) DOI: 10.1016/j.micromeso.2007.01.017.

176. Han, K.-B., Takagi, C., Wu, C.-J., Mizukami, H. & Ostafin, A. Synthesis of Calcium Phosphate Controllable Coating Thickness on Oil-in-Water Nanoemulsion with Performance of Oxygen Release as Oxygen Carrier. *J. Biomater. Nanobiotechnol.* **07**, 55–63 (2016) DOI: 10.4236/jbnb.2016.72007.

177. Watzke, H. J. & Dieschbourg, C. Novel silica-biopolymer nanocomposites: the silica sol-gel process in biopolymer organogels. *Adv. Colloid Interface Sci.* **50**, 1–14 (1994) DOI: 10.1016/0001-8686(94)80021-9.

178. Sabarish, R. & Unnikrishnan, G. Novel biopolymer templated hierarchical silicalite-1 as an adsorbent for the removal of rhodamine B. *J. Mol. Liq.* **272**, 919–929 (2018) DOI: 10.1016/j.molliq.2018.10.093.

179. Abramson, S. *et al.* Highly porous and monodisperse magnetic silica beads prepared by a green templating method. *J. Mater. Chem.* **20**, 4916 (2010) DOI: 10.1039/c000525h.

180. Wang, X. *et al.* Synthesis of Ordered Mesoporous Silica with Tunable Morphologies and Pore Sizes via a Nonpolar Solvent-Assisted St??ber Method. *Chem. Mater.* **28**, 2356–2362 (2016) DOI: 10.1021/acs.chemmater.6b00499.

181. Bogush, G. H., Tracy, M. A. & Zukoski, C. F. Preparation of monodisperse silica particles: Control of size and mass fraction. *J. Non. Cryst. Solids* **104**, 95–106 (1988) DOI: 10.1016/0022-3093(88)90187-1.

182. Harris, M. T., Brunson, R. R. & Byers, C. H. The base-catalyzed hydrolysis and condensation reactions of dilute and concentrated TEOS solutions. *J. Non. Cryst. Solids* **121**, 397–403 (1990) DOI: 10.1016/0022-3093(90)90165-I.

183. Meier, M., Ungerer, J., Klinge, M. & Nirschl, H. Synthesis of nanometric silica particles via a modified Stöber synthesis route. *Colloids Surfaces A Physicochem. Eng. Asp.* **538**, 559–564 (2018) DOI: 10.1016/j.colsurfa.2017.11.047.

184. Qi, D., Lin, C., Zhao, H., Liu, H. & Lü, T. Size regulation and prediction of the SiO 2 nanoparticles prepared via Stöber process. *J. Dispers. Sci. Technol.* **38**, 70–74 (2017) DOI: 10.1080/01932691.2016.1143373.

185. Nozawa, K. *et al.* Smart Control of Monodisperse Stöber Silica Particles: Effect of Reactant Addition Rate on Growth Process. *Langmuir* **21**, 1516–1523 (2005) DOI: 10.1021/la048569r.

186. Zhao, Z. *et al.* Facile, low-cost, and scalable fabrication of particle size and pore structure tuneable monodisperse mesoporous silica nanospheres as supports for advanced solid acid catalysts. *RSC Adv.* **6**, 9072–9081 (2016) DOI: 10.1039/c5ra26432d.

187. Luo, L., Liang, Y., Erichsen, E. S. & Anwander, R. Monodisperse mesoporous silica nanoparticles of distinct topology. *J. Colloid Interface Sci.* **495**, 84–93 (2017) DOI: 10.1016/j.jcis.2017.01.107.

188. Yi, Z. *et al.* A New Insight into Growth Mechanism and Kinetics of Mesoporous Silica Nanoparticles by in Situ Small Angle X-ray Scattering. *Langmuir* **31**, 8478–8487 (2015) DOI: 10.1021/acs.langmuir.5b01637.

189. Stovpiaga, E. Y., Kurdyukov, D. A., Kukushkina, Y. A., Sokolov, V. V. & Yagovkina, M. A. Monodisperse spherical silica particles with controlled-varied diameter of micro- and mesopores. *Glas. Phys. Chem.* **41**, 316–323 (2015) DOI: 10.1134/S1087659615030153.

190. Möller, K. & Bein, T. Talented Mesoporous Silica Nanoparticles. *Chem. Mater.* acs.chemmater.6b03629 (2016) doi:10.1021/acs.chemmater.6b03629 DOI: 10.1021/acs.chemmater.6b03629.

Chapter 2

Synthesis of Non-Porous Spherical Silica Particles with Controllable Dimensions

2.1 Abstract

The influence of ethanol, tetraethyl orthosilicate (TEOS), ammonium hydroxide, and water concentrations on the size of silica nanoparticles prepared using a Glantreo Ltd. method based on the Stöber process was investigated univariately. From this data a table of particle sizes was produced, allowing particles ranging in size from 149 – 511 nm to be easily synthesised depending on input parameters. Increasing ethanol concentration increased particle size, with smallest particles of 156 nm and largest particles of 511 nm being formed. Increasing TEOS concentration increased particle size, with smallest particles of 222 nm and largest particles of 394 nm being formed. Increasing ammonium hydroxide concentration increased particle size up to 5.1 M, with smallest particles of 149 nm and largest particles of 491 nm being formed. Increasing water concentration increased particle size up to 0.8 ml, with a decrease in particle size beyond this, with smallest particles of 190 nm and largest particles of 377 nm were formed.

2.2 Introduction

The preparation of non-porous silica nanoparticles (SNPs) is a vibrant area of research due to their unique physical and chemical properties, such as colloidal stability, facile surface modification, and bioinertness.[1–3] Applications of SNPs are diverse and include more specialised use, such as drug delivery vehicles in biomedicine, and more general use, such as food additives.[4–6] Other important uses of these SNPs is in insulation materials for buildings[7,8] and superhydrophobic coatings for substrates.[9,10] The particle size and size uniformity (dispersity) influences the quality and therefore, the scope of application of the particles. For more specialised uses, it is desirable to have the ability to synthesise SNPs with high size monodispersity. The National Institute of Standards and Technology (NIST) defines monodispersity as particles of nearly the same size, forming a narrow distribution about an average value. Specifically, NIST guidelines state that 90 % of the distribution lies within ± 5 % of the average size,[11] which equates to a relative standard deviation (RSD) of around 3 %. However, even with these guidelines, there seems to be a lack of consensus in the silica literature as to the accepted RSD value that defines monodisperse. Reported values of RSD that are considered monodisperse vary greatly, though an RSD of ≤ 10 % is generally regarded as being monodisperse,[12–17] and will be the definition used here.

However, it is also important to be able to tune the synthesis to prepare particles with a specific mean size, which broadens their application. Having the ability to tune the synthesis for different particle sizes, while also keeping monodispersity high is advantageous. Stöber *et al.*[18] first reported the process for the controlled growth of spherical non-porous silica particles of uniform size. The growth of silica particles in the

Stöber process is, at its most fundamental, controlled by two reactions: (1) the hydrolysis of tetraethyl orthosilicate (TEOS) [$Si(OEt)_4 \rightarrow Si(OEt)_{4-x}(OH)_x$], where x = 1 – 4, and (2) condensation of the $Si(OEt)_{4-x}(OH)_x$ monomers into the siloxane network. The size and morphology of the synthesised particles is dependent on the rates of hydrolysis and condensation. These can be controlled by altering the reaction conditions. Here we report a tuneable synthesis of non-porous silica nanoparticles in the diameter range between 150 – 500 nm. This tuneable synthesis allows for precise control of particle diameter along with size monodispersity.

2.3 Experimental

2.3.1 Materials

Tetraethyl orthosilicate (TEOS) (98 % purity), ammonium hydroxide (assay: 28 – 30 % NH_3 basis) were purchased from Sigma Aldrich. Ethanol was purchased from Carbon Group. Milli-Q water (> 18.2 MΩ.cm) was used for all reactions.

2.3.2 Method

Non-porous silica nanoparticles were prepared using a Glantreo Ltd. process which is based on the Stöber process. The reaction conditions can be found in **Table 2.1**. The requisite amounts of water, ethanol and ammonium hydroxide were placed in a 10 ml reaction vial with a magnetic stirrer and placed on a temperature-controlled heating block. This solution was allowed stir for 1 hr at 250 rpm. The required amount of TEOS was then introduced and the reaction flask was left to stir overnight. The clear solution began to turn milky-white 1-3 min after TEOS addition. The reaction mixture was centrifuged at 14,000 rpm for 10 mins and the solids were washed with water and acetone. The solids

were then dried in an oven overnight and characterised by scanning electron microscopy (SEM).

2.3.3 Characterisation

Scanning Electron Microscopy (SEM) was used to obtain images of the silica nanospheres. The SEM analyses were carried out on a high-resolution FEI Inspect, operated at either 10 or 15 kV. Each sample was adhered to a stainless-steel stub (stage) via double-sided carbon tape. Particle diameters were determined using an automated statistical method performed using MATLAB software, further details and limitations of which are provided in section **2.7 Appendix**. Multiple SEM images were obtained for each sample and the number of particles measured per sample was ≥ 10,000 for the majority of samples. RSD was calculated from the mean diameter of the total sample. Statistical analyses were done in OriginLab OriginPro 9.0 software.

Table 2.1 *Synthesis conditions for obtaining silica nanoparticles of various sizes. T = 25 °C.*

EtOH (ml)	H_2O (ml)	NH_4OH (M)	TEOS (ml)	Mean Particle Size (nm)	SD[a] (nm)	RSD[b] (%)
5	1.12	1.2	0.7	149	20.2	13.5
5	0.4	6.3	0.7	190	31.2	16.5
5	1.12	3.2	0.2	222	48.3	21.7
5	1.12	3.2	0.3	245	50.7	20.7
1	1.12	3.2	0.555	256	35.4	13.8
5	0.5	5.6	0.7	263	43.6	16.6
5	1.12	3.2	0.4	270	39.8	14.7
5	1.12	3.2	0.5	292	51.5	17.7
5	0.6	5.0	0.7	297	50.4	17.0
5	1.12	3.2	0.555	359	48	13.5
5	1.12	3.2	0.7	317	49.5	15.6
3	1.12	3.2	0.555	322	59.4	18.5
4	1.12	3.2	0.555	340	46.5	13.7
5	1.1	3.2	0.7	327	44.5	13.6
5	1.12	3.2	0.8	339	50.0	14.7
5	1.12	2.2	0.7	340	32.6	9.6
5	1.12	3.2	0.9	359	50.2	14.0
5	1.0	3.4	0.7	360	53.8	14.9
5	0.9	3.7	0.7	372	56.1	15.1
5	1.12	3.2	0.6	377	47.4	12.6
6	1.12	3.2	0.555	378	51	13.6
5	0.8	4.1	0.7	377	58.1	15.4
5	1.12	3.1	0.7	389	26.9	6.9
5	1.12	3.2	1.0	392	48.2	12.3
5	1.12	3.2	1.1	394	54.2	13.8
5	1.12	5.6	0.7	399	54.1	13.6
2	1.12	3.2	0.555	425	62.4	14.7
7	1.12	3.2	0.555	449	25.2	5.6
5	1.12	6.1	0.7	452	72.2	16.0
5	0.7	4.5	0.7	370	62.6	16.9
5	1.12	3.8	0.7	469	25.6	5.5
5	1.12	4.5	0.7	484	43.5	9.0
5	1.12	5.1	0.7	491	31.7	6.5
8	1.12	3.2	0.555	511	31.3	6.1

[a]SD, standard deviation
[b]RSD, relative standard deviation

2.4 Results and Discussion

2.4.1 Effect of ethanol concentration on particle size and morphology

Table 2.2 *Experimental conditions and size data for ethanol variation.*

EtOH (ml)	H_2O (ml)	NH_4OH (M)	TEOS (ml)	Mean Particle Size (nm)	SD[a] (nm)	RSD[b] (%)
1	1.12	3.2	0.555	256	35.4	13.8
2	1.12	3.2	0.555	425	62.4	14.7
3	1.12	3.2	0.555	322	59.4	18.5
4	1.12	3.2	0.555	340	46.5	13.7
5	1.12	3.2	0.555	359	48	13.5
6	1.12	3.2	0.555	378	51	13.6
7	1.12	3.2	0.555	449	25.2	5.6
8	1.12	3.2	0.555	511	31.3	6.1

[a]SD, standard deviation
[b]RSD, relative standard deviation

The volume of ethanol was varied while keeping all other reactants constant. **Table 2.2** shows the experimental conditions and size data for ethanol variation. **Figure 2.1** shows SEM images of the particles obtained upon varying the ethanol volume. In all cases, spherical nanoparticles were formed. According to Sadasivan *et al.*[19] alcohols used as solvents in TEOS hydrolysis affects the formation of silica in two major ways. High solvent viscosity and a lower self-diffusion coefficient for the nucleophile in higher carbon-chain alcohols contribute to steric hindering and results in a slower hydrolysis reaction. Conversely, the weaker hydrogen bonding in higher carbon-chain alcohols can enhance the hydrolysis rate. These two opposing factors can influence the particle size depending on what type of alcohol is used. This would suggest that lower carbon-chain alcohols such as methanol would give larger particles than higher carbon-chain alcohols such as ethanol. This is contrary to what Stöber *et al.*[18] observed who found that the

reaction rate was fastest in methanol, giving smallest particle sizes, and slowest in n-butanol, giving largest particle sizes. This could be explained by the polarity of the solvent. Methanol is relatively polar and the polarity of alcohols decreases with increasing chain length. Colloidal stability is achieved more readily with small particles in highly polar solvents, while it is achieved with larger particles in low polarity solvents. While the effects of different solvents on particle morphology have been studied,[20] the effect of different concentrations of the same solvent on particle morphology is less understood.

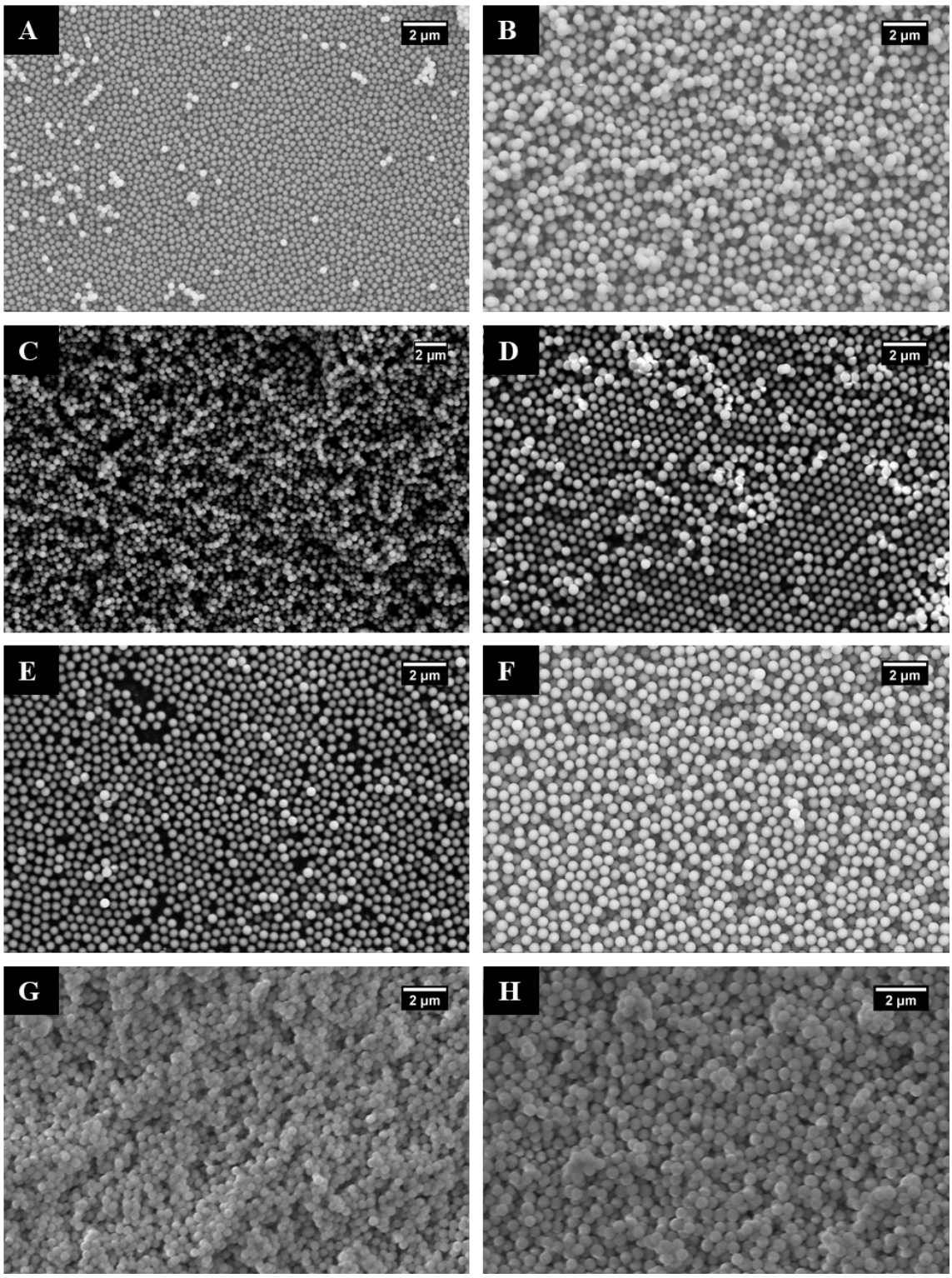


Figure 2.1 *SEM images of silica nanoparticles synthesised by varying amount of ethanol. (a) 1 ml EtOH, (b) 2 ml EtOH, (c) 3 ml EtOH, (d) 4 ml EtOH, (e) 5 ml EtOH, (f) 6 ml EtOH, (g) 7 ml EtOH, and (h) 8 ml EtOH. All other reactants kept constant.*

Figure 2.2 shows the particle size distributions (PSDs) of the nanoparticles prepared when EtOH is varied. **Figure 2.2A** shows a single peak at 256 nm (1 ml EtOH) fitted with a Gaussian function (R^2 = 0.99, RSD = 13.8 %). **Figure 2.2B** shows a single peak at 435 nm (2 ml EtOH) fitted with a Gaussian function (R^2 = 0.98, RSD = 14.7 %). **Figure 2.2C** shows a single peak at 322 nm also fitted with a Gaussian function (R^2 = 0.99, RSD = 18.5 %). **Figure 2.2D** shows a single peak at 340 nm (4 ml EtOH) fitted with a Gaussian function (R^2 = 0.99, RSD = 13.7 %). Gaussian fittings are characteristic of a growth process occurring via Ostwald ripening.[21] Smaller particles are typically thermodynamically unstable and redissolve into the bulk solution. Growth occurs via material transfer from the bulk solution onto the surface the larger particles. A mathematical description of this process was provided by Lifshitz and Slyozov[22], and Wagner.[23] Their description included a boundary constraint in which no particle could have a diameter greater than 1.5 times the mean particle diameter, which resulted in a left-skewed particle size distribution. However, in real systems this constraint does not exist, therefore, a Gaussian distribution better describes the Ostwald ripening process. **Figure 2.2A-D** show particle size distributions which are indicative of an Ostwald ripening process. **Figure 2.2E** shows a peak at 343 nm (5 ml EtOH) fitted with a Gaussian function and a peak at 407 nm fitted with a log-normal function (R^2 = 0.99, RSD = 13.5 %). A log-normal function is characteristic of a growth process occurring via coalescence. Coalescence occurs when particles of different sizes fuse together into a single particle. This leads to a characteristic right-skewed particle size distribution. Ostwald ripening and coalescence can therefore be differentiated by the shape of the particle size distribution.

In general, particles that grow via an Ostwald ripening process are more monodisperse than those that grow via coalescence.

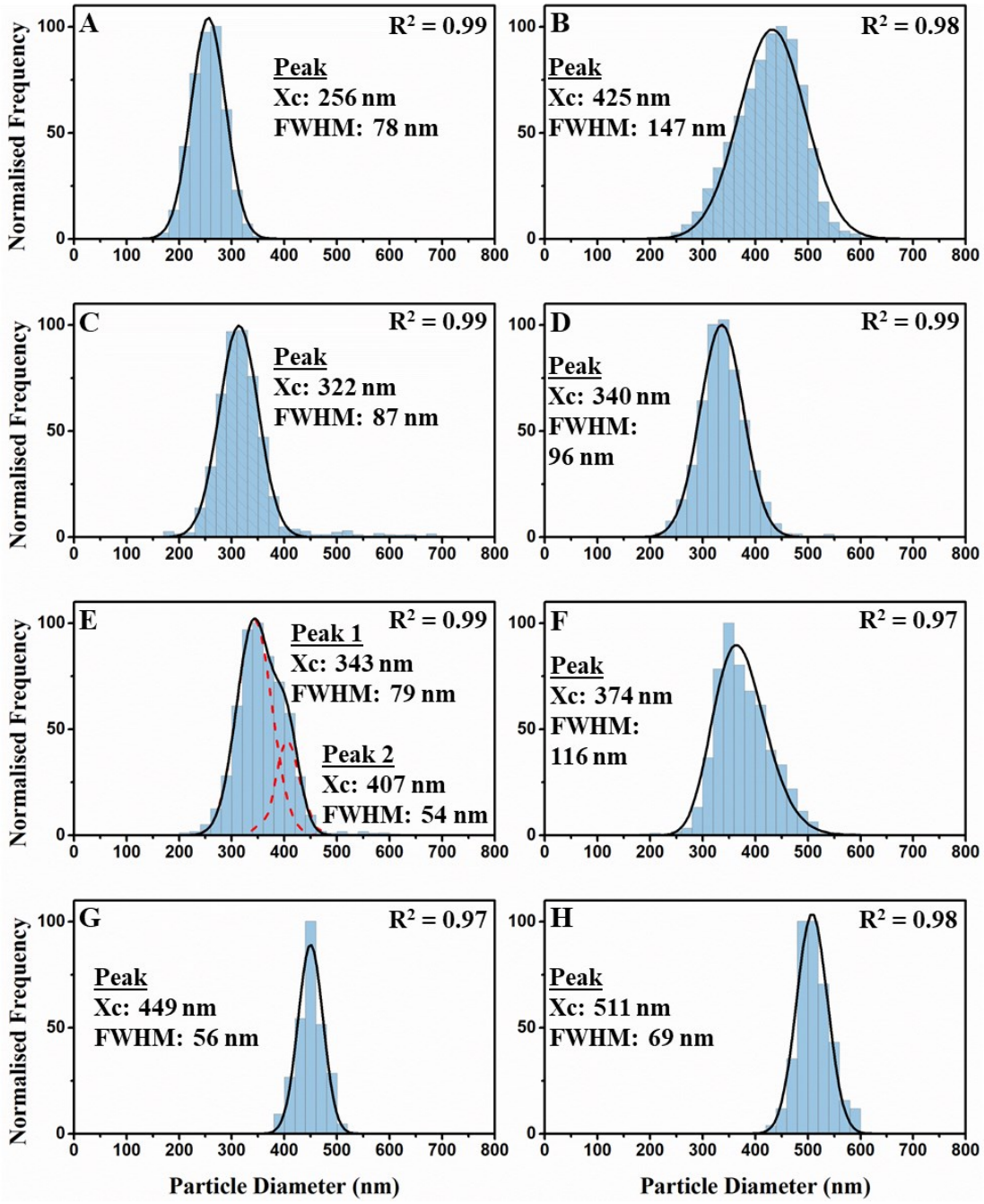


Figure 2.2 *PSDs of silica nanoparticles synthesised by varying amount of ethanol. (a) 1 ml EtOH, (b) 2 ml EtOH, (c) 3 ml EtOH, (d) 4 ml EtOH, (e) 5 ml EtOH, (f) 6 ml EtOH, (g) 7 ml EtOH, and (h) 8 ml EtOH. All other reactants kept constant.*

Figure 2.2F shows a single peak at 374 (6 ml EtOH) fitted with a log-normal function (R^2 = 0.97, RSD = 13.6 %). **Figure 2.2G** shows a single peak at 449 nm (7 ml EtOH) fitted with a Gaussian function (R^2 = 0.97, RSD = 5.6 %). **Figure 2.2H** shows a single peak at 511 nm (8 ml EtOH) fitted with a Gaussian function (R^2 = 0.98, RSD = 6.1 %).

Figure 2.3 shows that increasing the amount of EtOH results in an increase in particle size, with the smallest mean diameter seen at 1 ml EtOH and the largest mean diameter seen at 8 ml EtOH. While EtOH is not directly involved in the hydrolysis and condensation reactions, its concentration affects them. Increasing the EtOH concentration reduces the relative concentration of water and TEOS. A lower concentration of water and TEOS means hydrolysis is slower than condensation, resulting in larger particles. A higher concentration of water and TEOS means hydrolysis is faster than condensation, resulting in smaller particles. Previous work has shown that particle size is dependent on the relative concentration of water and TEOS, and follows this same trend.[24–26] At the lowest (1 ml, 2 ml, 3 ml, and 4 ml) and the highest (7 ml and 8 ml) amounts of EtOH, the growth process occurs via Ostwald ripening only, resulting in good size monodispersity, as seen in the low RSDs and represented by the red shaded area in **Figure 2.3**. At 5 and 6 ml EtOH, a mixture of Ostwald ripening and coalescence is seen. The percentage yield decreases when the volume of EtOH is increases, with the yield dropping to ca. 60 % at 4 ml EtOH. The highest yield is observed at 1 ml EtOH (97.5 %), followed by 2 ml (94.7 %) and 3 ml (93.4 %) EtOH. Therefore, the data indicate that the highest level of monodispersity and yield is achieved at lower EtOH concentrations.

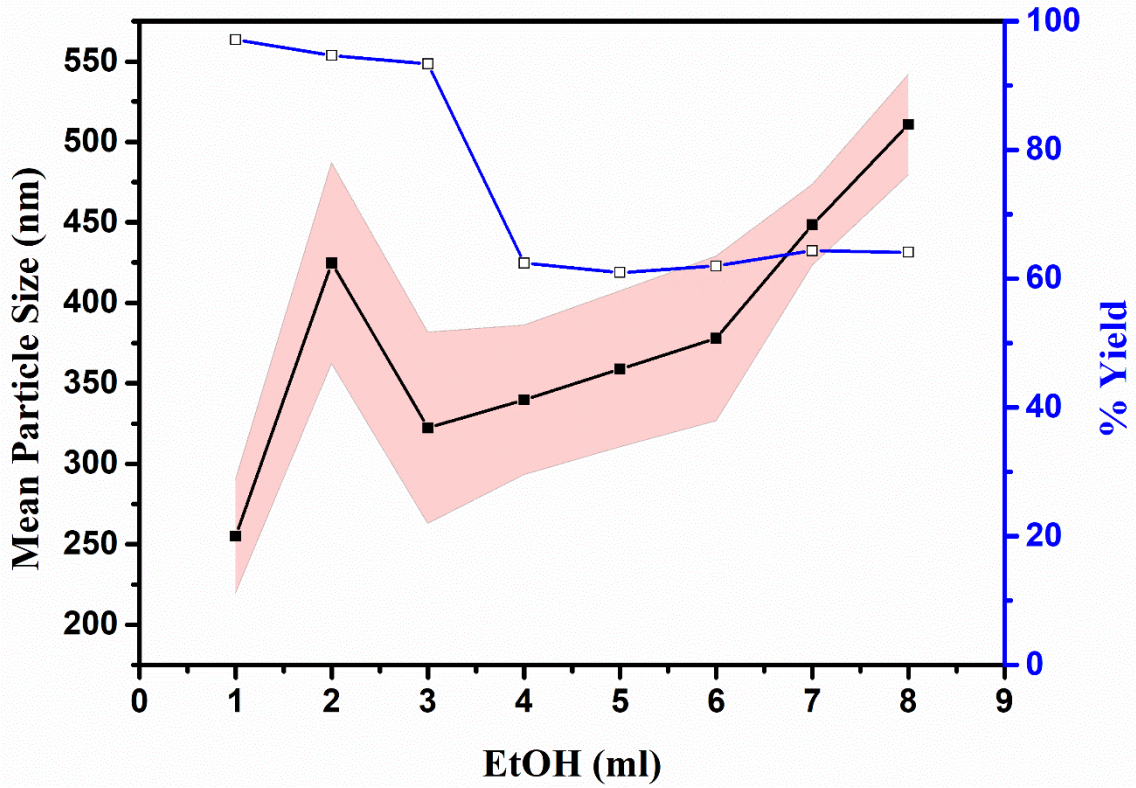


Figure 2.3 *Effect of ethanol volume on mean particle size (—■—) and percent yield (—□—). Red shaded area is the standard deviation of mean particle size.*

2.4.2 Effect TEOS concentration on particle size and morphology

Table 2.3 *Experimental conditions and size data for TEOS variation.*

EtOH (ml)	H_2O (ml)	NH_4OH (M)	TEOS (ml)	Mean Particle Size (nm)	SD[a] (nm)	RSD[b] (%)
5	1.12	3.2	0.2	222	48.3	21.7
5	1.12	3.2	0.3	245	50.7	20.7
5	1.12	3.2	0.4	270	39.8	14.7
5	1.12	3.2	0.5	292	51.5	17.7
5	1.12	3.2	0.6	377	47.4	12.6
5	1.12	3.2	0.7	317	49.5	15.6
5	1.12	3.2	0.8	339	50.0	14.7
5	1.12	3.2	0.9	359	50.2	14.0
5	1.12	3.2	1.0	392	48.2	12.3
5	1.12	3.2	1.1	394	54.2	13.8

[a]SD, standard deviation
[b]RSD, relative standard deviation

Table 2.3 shows the experimental conditions and size data for TEOS variation. TEOS is the most commonly studied silica precursor in the literature and systems employing this are well established.[27–29] The amount of TEOS in the reaction influences the rate of hydrolysis and therefore the particle size. When the concentration of TEOS is low, hydrolysis is faster than condensation and the increased concentration of hydrolysed monomer increases the nucleation rate, resulting in more particles of smaller size. When the concentration of TEOS is high, hydrolysis becomes the rate-limiting step.[30] In this scenario the rate of condensation dominates and particle growth is favoured, as observed in our case. **Figure 2.4** shows SEM images of silica nanoparticles obtained when varying TEOS concentration. **Figure 2.5** shows the particle size distributions of these particles. As expected, increasing the concentration of TEOS results in an increase in particles size.

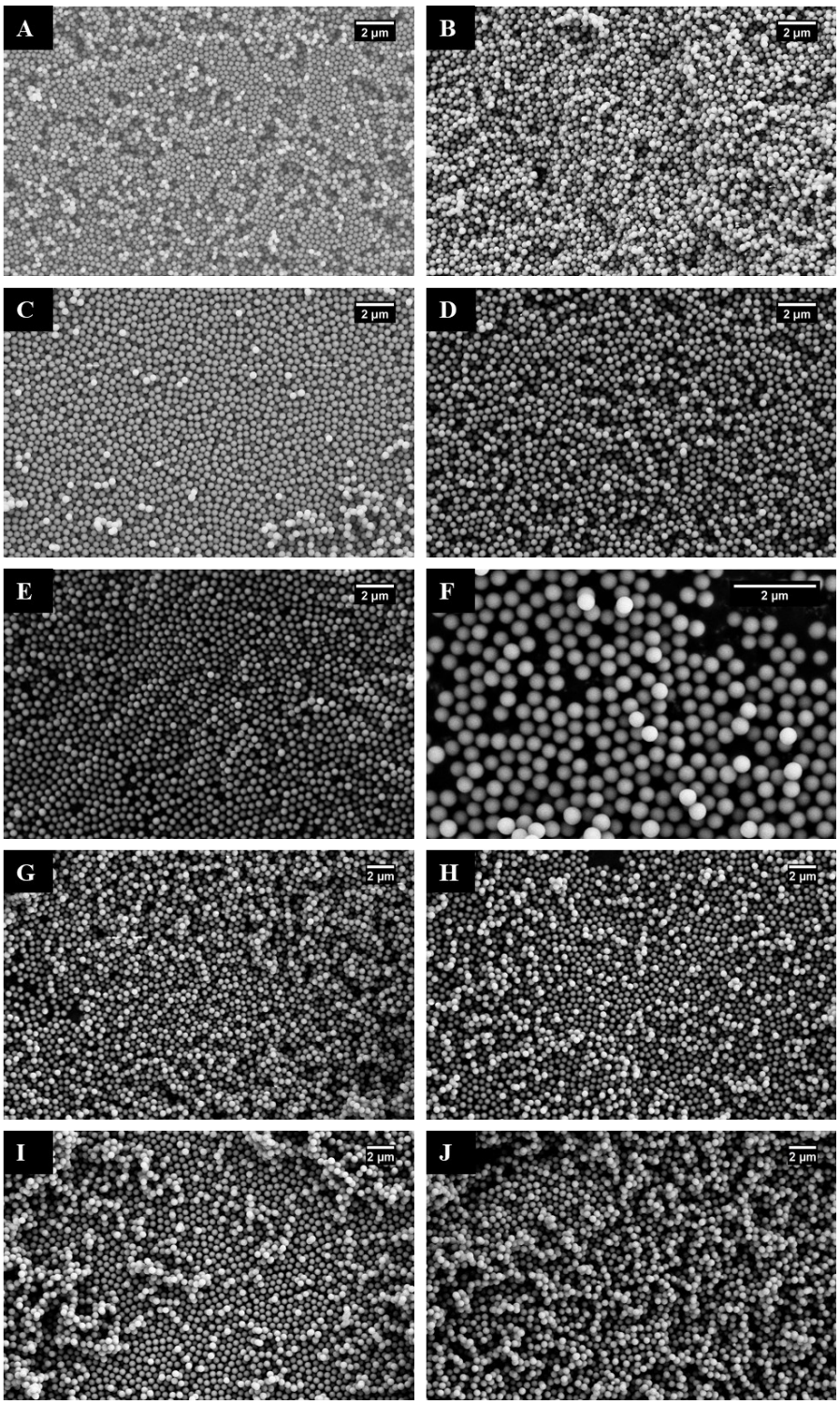


Figure 2.4 *SEM images of silica nanoparticles synthesised by varying amount of TEOS. (a) 0.2 ml TEOS, (b) 0.3 ml TEOS, (c) 0.4 ml TEOS, (d) 0.5 ml TEOS, (e) 0.6 ml TEOS, (f) 0.7 ml TEOS, (g) 0.8 ml TEOS, (h) 0.9 ml TEOS, (i) 1 ml TEOS, and (j) 1.1 ml TEOS. All other reactants kept constant.*

Figure 2.5 shows the PSDs of the nanoparticles prepared when TEOS is varied. **Figure 2.5A** shows a single peak at of 222 nm (0.2 ml TEOS) fitted with a Gaussian function (R^2 = 0.99, RSD = 21.7 %), indicating Ostwald ripening. **Figure 2.5B** shows a peak at 189 nm (0.3 ml TEOS) fitted with a log-normal function and a peak at 267 nm fitted with a Gaussian function (R^2 = 0.99, RSD = 20.7 %), indicating that a mixture of coalescence and Ostwald ripening is occurring. **Figure 2.5C** shows a peak at 234 nm (0.4 ml TEOS) fitted with a log-normal function and a peak at 281 nm fitted with a Gaussian function (R^2 = 0.99, RSD = 14.7 %). **Figure 2.5D** shows a peak at 232 nm (0.5 ml TEOS) fitted with a log-normal function and a peak at 311 nm fitted with a Gaussian function (R^2 = 0.99, RSD = 17.7 %). While **Figure 2.5B-D** show that a mixture of coalescence and Ostwald ripening is occurring, the log-normal peak decreases in frequency as the TEOS volume is increased. The peaks also begin to shift to larger diameter. This is characteristic of Ostwald ripening, where the smaller diameter particles decrease in number, while the larger particles grow in size. Therefore, as the TEOS volume is increased from 0.3 ml to 0.5 ml, Ostwald ripening begins to dominate. This is seen in **Figure 2.5E** (0.6 ml TEOS) where the log-normal peak disappears and two peaks at 350 and 445 nm fitted with Gaussian functions are seen (R^2 = 0.95, RSD = 12.6 %). However, **Figure 2.5F** shows a single peak at 311 nm (0.7 ml TEOS) fitted with a log-normal function (R^2 = 0.99, RSD = 15.6 %), which indicates that coalescence is occurring. **Figure 2.5G** shows a single peak at 339 nm (0.8 ml TEOS) fitted with a Gaussian function (R^2 = 0.99, RSD = 14.7 %), which indicates that the growth process has reverted back to Ostwald ripening. **Figure 2.5H** displays two peaks at 344 and 416 nm (0.9 ml TEOS) fitted with Gaussian functions (R^2 = 0.99, RSD = 14 %). **Figure 2.5I** shows a single peak at 395 nm (1 ml TEOS) fitted

with a log-normal distribution (R^2 = 0.99, RSD = 12.3 %), indicating that the growth process has reverted back to coalescence. **Figure 2.5J** shows two peaks at 388 and 438 nm (1.1 ml TEOS) fitted with Gaussian functions (R^2 = 0.99, RSD = 13.8 %).

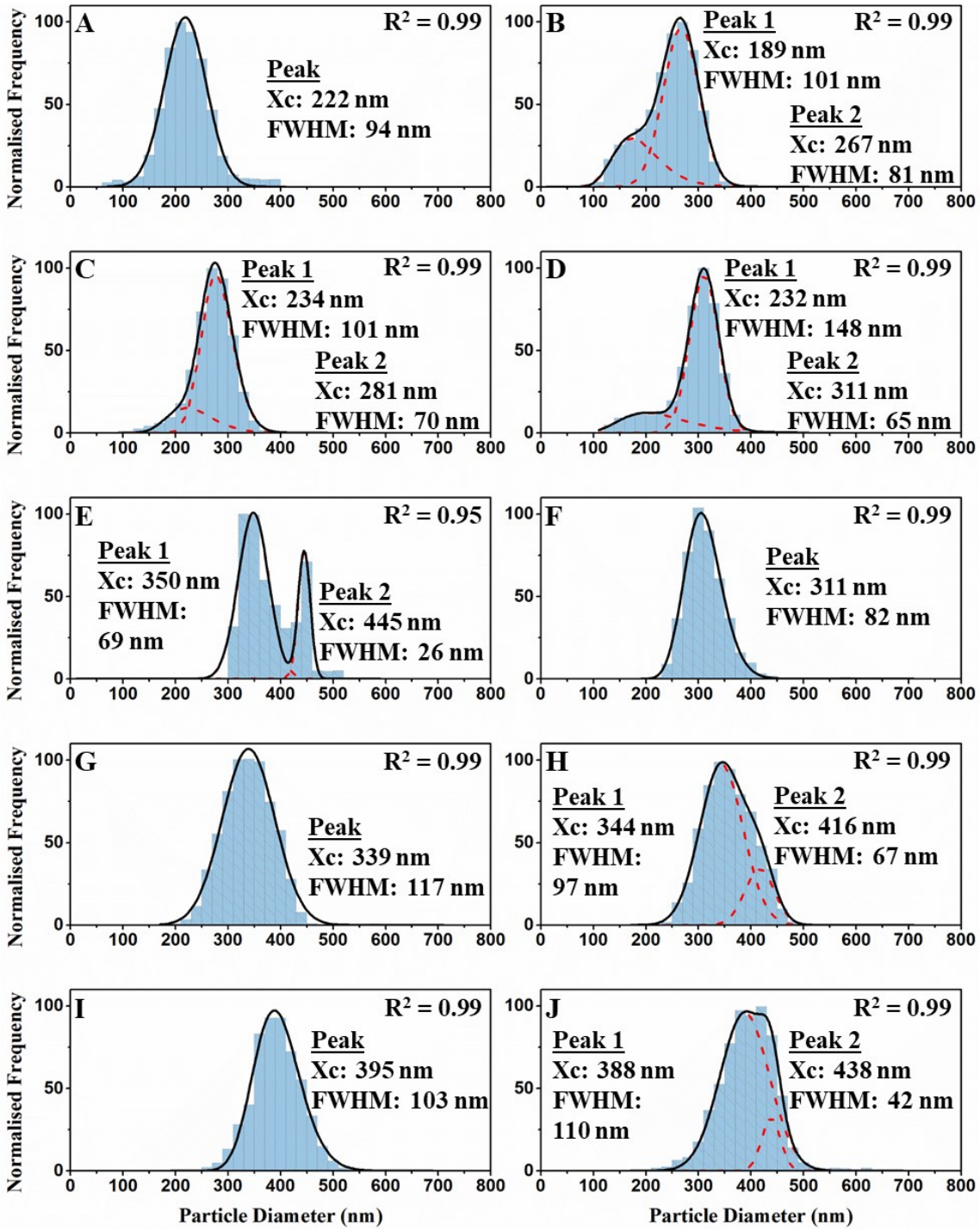


Figure 2.5 *PSDs of silica nanoparticles synthesised by varying amount of TEOS. (a) 0.2 ml TEOS, (b) 0.3 ml TEOS, (c) 0.4 ml TEOS, (d) 0.5 ml TEOS, (e) 0.6 ml TEOS, (f) 0.7 ml TEOS, (g) 0.8 ml TEOS, (h) 0.9 ml TEOS, (i) 1 ml TEOS, and (j) 1.1 ml TEOS. All other reactants kept constant.*

The data show that at the lowest volume of TEOS tested (0.2 ml) the growth process occurs via Ostwald ripening. As the volume of TEOS is increased the growth process shifts to a mixture of Ostwald ripening and coalescence. As the volume of TEOS increases from 0.3 to 0.5 ml, the log-normal peak in the PSDs begins to shrink while the Gaussian peak shifts to larger diameters. This indicates that Ostwald ripening begins to dominate. Further increasing the volume of TEOS to 0.6 ml shows that Ostwald ripening is the dominant process. However, further increases in the volume of TEOS causes the growth process to alternate between coalescence and Ostwald ripening. **Figure 2.6** shows that overall, the mean particle size increases as the volume of TEOS is increased. Similar studies in the literature also show an increase in particle size with increasing TEOS concentration.[31–33] The RSD also decreases as the volume of TEOS increases, going from 21.7 % at 0.2 ml TEOS to 13.8 % at 1.1 ml TEOS. However, the percentage yield decreases slightly as the volume of TEOS is increased. The highest percentage yield was 94.7 % (0.2 ml TEOS) and the lowest was 91.6 % (1.1 ml TEOS).

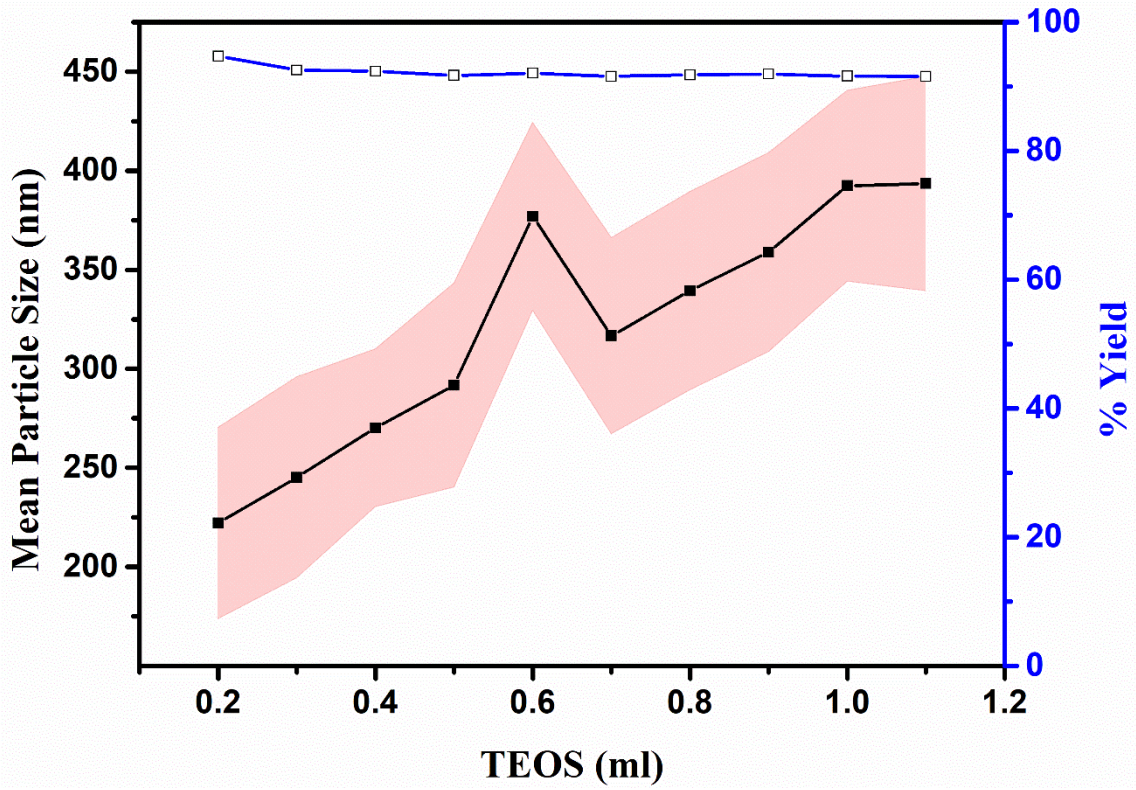


Figure 2.6 *Effect of TEOS volume on mean particle size (—■—) and percent yield (—□—). Red shaded area is the standard deviation of mean particle size.*

2.4.3 Effect of ammonium hydroxide concentration on particle size and morphology

Table 2.4 *Experimental conditions and size data for ammonium hydroxide variation.*

EtOH (ml)	H_2O (ml)	NH_4OH (M)	TEOS (ml)	Mean Particle Size (nm)	SD[a] (nm)	RSD[b] (%)
5	1.12	1.2	0.7	149	20.2	13.5
5	1.12	2.2	0.7	340	32.6	9.6
5	1.12	3.1	0.7	389	26.9	6.9
5	1.12	3.8	0.7	469	25.6	5.5
5	1.12	4.5	0.7	484	43.5	9.0
5	1.12	5.1	0.7	491	31.7	6.5
5	1.12	5.6	0.7	399	54.1	13.6
5	1.12	6.1	0.7	452	72.2	16.0

[a]SD, standard deviation
[b]RSD, relative standard deviation

Table 2.4 shows the experimental conditions and size data for ammonium hydroxide variation. **Figure 2.7** shows SEM images of the nanoparticles prepared when ammonium hydroxide concentration is varied. In all cases, spherical particles were formed. Ammonium hydroxide is used a base-catalyst in the Stöber process. The hydrolysis and condensation rate of TEOS depends on the concentration of ammonium hydroxide and it is expected that increasing this concentration should increase the nucleation rate, resulting in increased particle size.[34] **Figure 2.8** shows the PSDs of the nanoparticles prepared when varying ammonium hydroxide. **Figure 2.8A** shows a single peak at 149 nm (1.2 M NH_4OH) fitted with a Gaussian function (R^2 = 0.99, RSD = 13.5 %). **Figure 2.8B** shows a single peak at 340 nm (2.2 M NH_4OH) fitted with a Gaussian function (R^2 = 0.99, RSD = 9.6 %). **Figure 2.8C** shows a single peak at 389 nm (3.1 M NH_4OH) fitted with a Gaussian function (R^2 = 0.99, RSD = 6.9 %). **Figure 2.8D** shows a single peak at 469 nm (3.8 M NH_4OH) fitted with a Gaussian function (R^2 = 0.96, RSD = 5.5 %). At ammonium

hydroxide concentrations of 1.2 to 3.8 M, the growth process occurs via Ostwald ripening. **Figure 2.8E** shows a peak at 463 nm (4.5 M NH_4OH) fitted with a log-normal function and a peak at 494 nm fitted with a Gaussian function (R^2 = 0.99, RSD = 9 %). A mixture of Ostwald ripening and coalescence is occurring at this concentration of ammonium hydroxide. **Figure 2.8F** shows a single peak at 491 nm (5.1 M NH_4OH) fitted with a Gaussian function (R^2 = 0.99, RSD = 6.5 %). **Figure 2.8G** shows three peaks at 327, 398, and 457 nm (5.6 M NH_4OH) fitted with Gaussian functions (R^2 = 0.99, RSD = 13.6 %). **Figure 2.8H** shows four peaks at 341, 446, 497, and 542 nm (6.1 M NH_4OH) fitted with Gaussian functions (R^2 = 0.99, RSD = 16 %). At ammonium hydroxide concentrations above 4.5 M, the growth process reverts to Ostwald ripening. However, at concentrations above 5.1 M, the particles begin to show increased polydispersity, represented by an increase in number of peaks and an increase in the RSD.

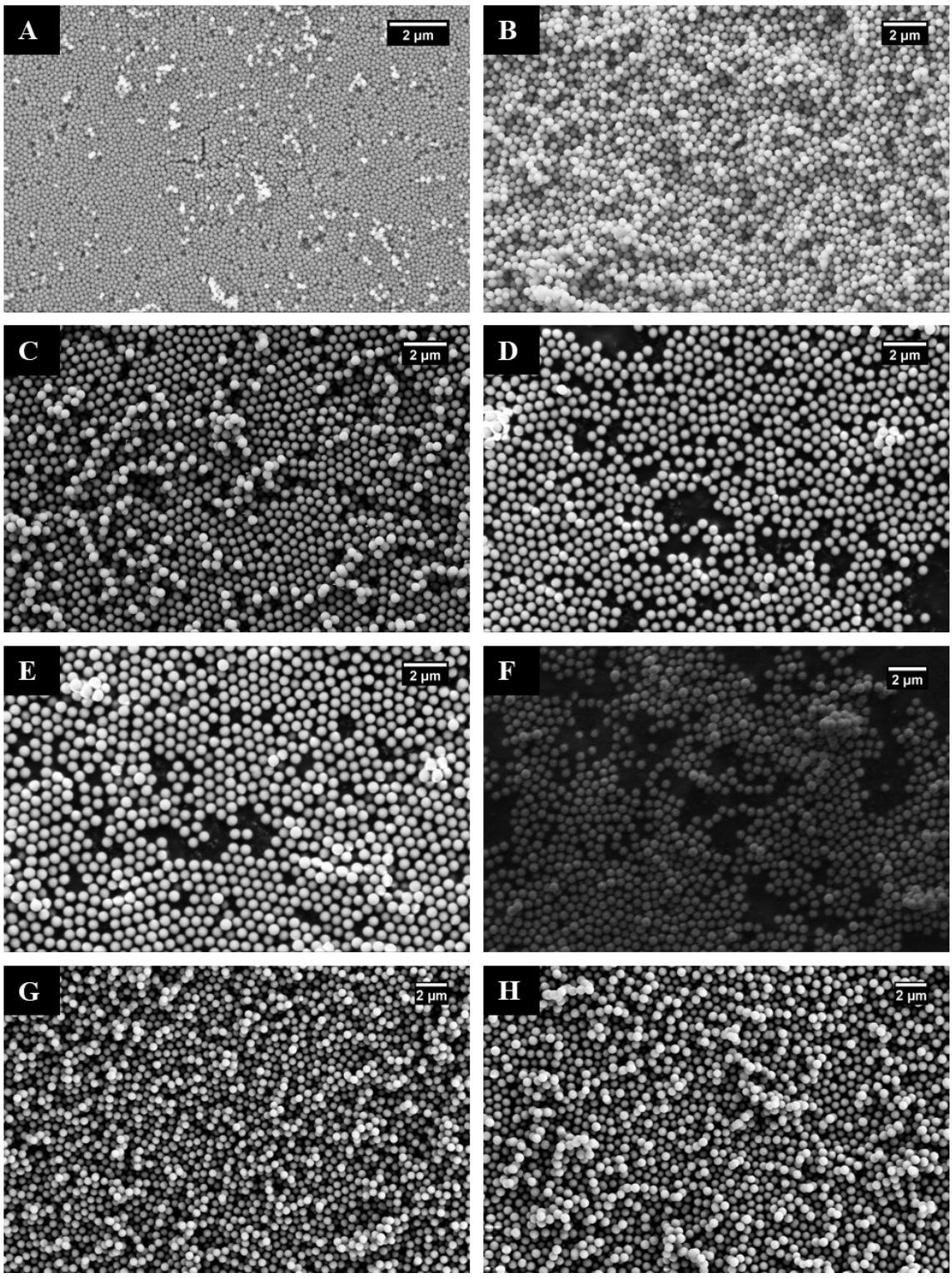


Figure 2.7 *SEM images of silica nanoparticles synthesised by varying ammonium hydroxide concentration. (a) 1.2 M NH_4OH, (b) 2.2 M NH_4OH, (c) 3.1 M NH_4OH, (d) 3.8 M NH_4OH, (e) 4.5 M NH_4OH, (f) 5.1 M NH_4OH, (g) 5.6 M NH_4OH, and (h) 6.1 M NH_4OH.*

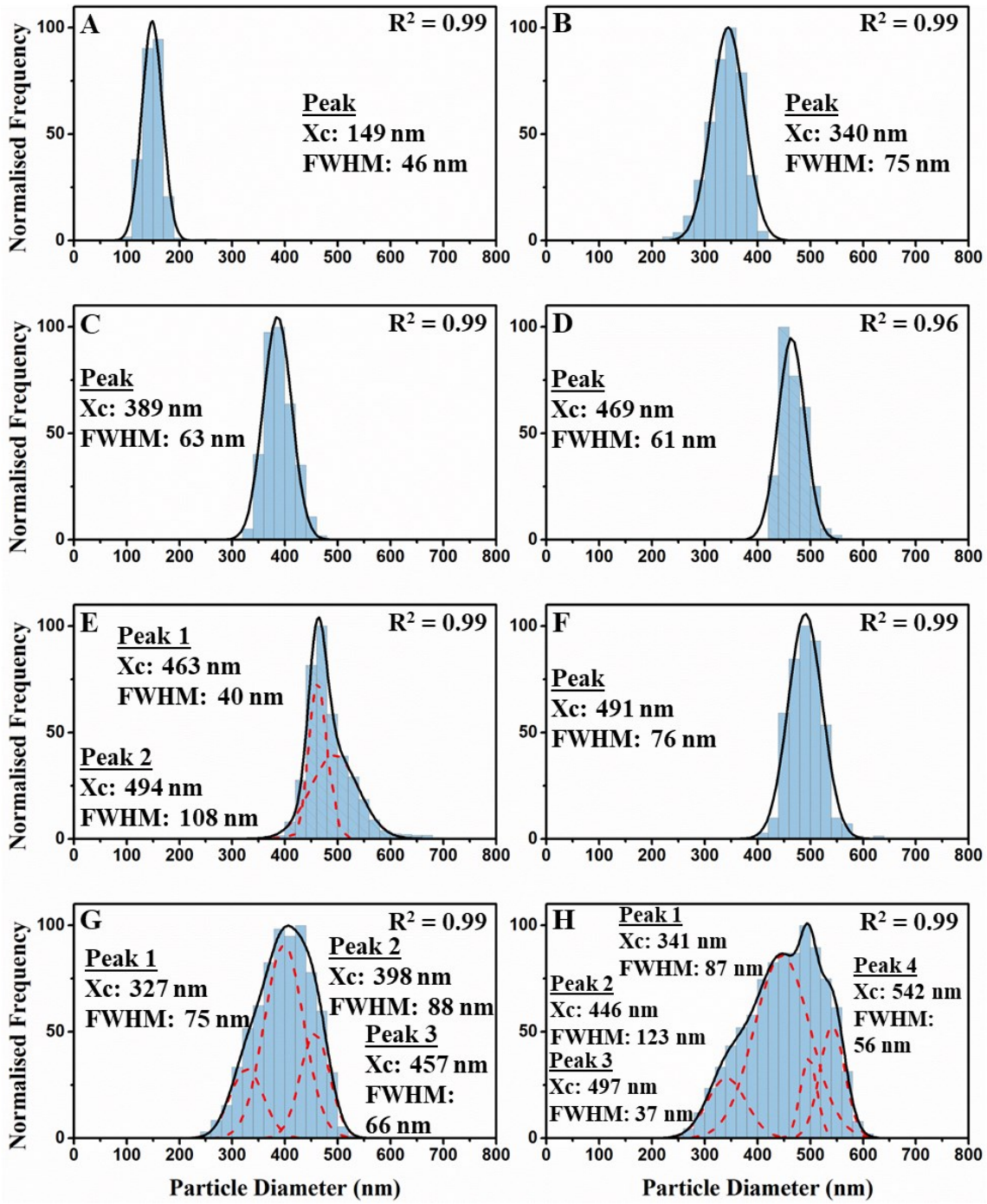


Figure 2.8 *PSDs of silica nanoparticles prepared by varying amount of ammonia. (a) 1.2 M NH_4OH, (b) 2.2 M NH_4OH, (c) 3.1 M NH_4OH, (d) 3.8 M NH_4OH, (e) 4.5 M NH_4OH, (f) 5.1 M NH_4OH, (g) 5.6 M NH_4OH, and (h) 6.1 M NH_4OH. All other reactants kept constant.*

Figure 2.9 shows the effect of ammonium hydroxide concentration on mean particle size and percent yield. The percent yield remains stable ca. 90 % at all ammonium hydroxide concentrations tested. Increasing the ammonium hydroxide concentration leads to an increase in particle size up to 5.1 M. Further increases resulted in a decrease in the particle size. The initial increase can be attributed to the ammonium hydroxide acting as a catalyst for the hydrolysis and condensation reactions. At higher ammonium hydroxide concentrations, the rate of hydrolysis of TEOS proceeds rapidly. This fast consumption of TEOS at the beginning of the reaction produces highly reactive anionic silanol monomers, such as $Si(OEt)_2(OH)(O^-)$ and $Si(OEt)(OH)_2(O^-)$, which are more reactive than $Si(OEt)_3(O^-)$. These highly reactive monomers preferentially condense onto the surface of already formed particles rather than diffuse into the siloxane network, thus promoting the growth of the particles.[35] At ammonium hydroxide concentrations > 5.1 M, it is likely that the conductivity of the solution is so high that these highly reactive monomers are prevented from reaching the surface of the already formed particles due to the high negative surface charge and screening from the NH_3^+. This results in smaller particles being formed but also an increase in polydispersity because condensation is impeded by the high conductivity. Faster hydrolysis and condensation of the silica precursor contributes to the growth in particle size. The decrease in particle size at 6.5 M NH_4OH can be explained by the stabilising effect of the NH_4^+ ions on the newly forming silica surface. The increased positive ion concentration stabilises the negatively charged surface and inhibits particle growth. Higher concentrations of NH_4OH also increase the polydispersity of the particles, as represented by the increase in the RSD. Our results show

that increasing ammonium hydroxide concentration increases particle size, which is in agreement with other studies in the literature.[32,36]

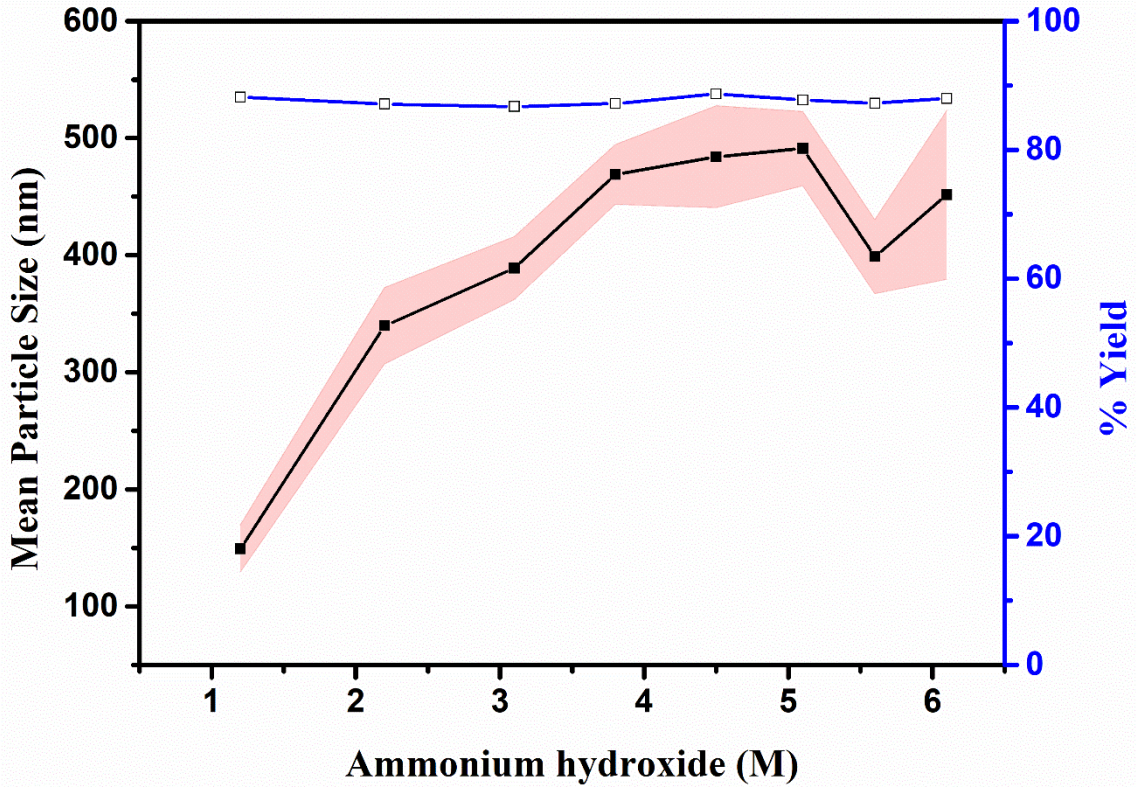


Figure 2.9 *Effect of ammonium hydroxide concentration on mean particle size (—■—) and percent yield (—□—). Red shaded area is the standard deviation of mean particle size.*

2.4.4 Effect of water on particle size and morphology

Table 2.5 *Experimental conditions and size data for water variation.*

EtOH (ml)	H_2O (ml)	NH_4OH (M)	TEOS (ml)	Mean Particle Size (nm)	SD[a] (nm)	RSD[b] (%)
5	0.4	6.3	0.7	190	31.2	16.5
5	0.5	5.6	0.7	263	43.6	16.6
5	0.6	5.0	0.7	297	50.4	17.0
5	0.7	4.5	0.7	370	62.6	16.9
5	0.8	4.1	0.7	377	58.1	15.4
5	0.9	3.7	0.7	372	56.1	15.1
5	1.0	3.4	0.7	360	53.8	14.9
5	1.1	3.2	0.7	327	44.5	13.6

[a]SD, standard deviation
[b]RSD, relative standard deviation

Table 2.5 shows the experimental conditions and size data for water variation. **Figure 2.10** shows SEM images of the nanoparticles prepared when the amount of water is varied. In all cases, spherical particles were formed. **Figure 2.11** shows the PSDs of the nanoparticles prepared when the amount of water was varied. **Figure 2.11A** shows a single peak at 190 nm (0.4 ml H_2O) fitted with a Gaussian function (R^2 = 0.98, RSD = 16.5 %), indicating that Ostwald ripening is taking place. **Figure 2.11B** shows a peak at 247 nm (0.5 ml H_2O) fitted with a log-normal function and a peak at 353 nm fitted with a Gaussian function (R^2 = 0.99, RSD = 16.6 %). **Figure 2.11C** shows a peak at 247 nm (0.6 ml H_2O) fitted with a log-normal function and a peak at 340 nm fitted with a Gaussian function (R^2 = 0.95, RSD = 17 %). At 0.5 ml H_2O, a mixture of coalescence and Ostwald ripening is occurring, with coalescence being the dominant process as seen in the larger log-normal peak. At 0.6 ml H_2O, a mixture of coalescence and Ostwald ripening is also occurring, however, Ostwald ripening is greater than at 0.5 ml H_2O, as seen in the larger Gaussian peak. **Figure 2.11D** shows a peak at 370 nm (0.7 ml H_2O) fitted with a Gaussian

function (R^2 = 0.96, RSD = 16.9 %), indicating that Ostwald ripening is the dominant process compared to 0.6 ml H_2O. **Figure 2.11E** shows a peak at 321 nm (0.8 ml H_2O) fitted with a log-normal function and a peak at 401 nm fitted with a Gaussian function (R^2 = 0.99, RSD = 15.4 %), indicating that a mixture of coalescence and Ostwald ripening is occurring. **Figure 2.11F** shows two peaks at 353 and 435 nm (0.9 ml H_2O) fitted with Gaussian functions (R^2 = 0.99, RSD = 15.1 %), indicating that Ostwald ripening is the dominant process. **Figure 2.11G** shows a single peak at 360 nm (1 ml H_2O) fitted with a Gaussian function (R^2 = 0.99, RSD = 14.9 %). **Figure 2.11H** shows a single peak at 328 nm (1.1 ml H_2O) fitted with a log-normal function (R^2 = 0.99, RSD = 13.6%), indicating that coalescence is the dominant process.

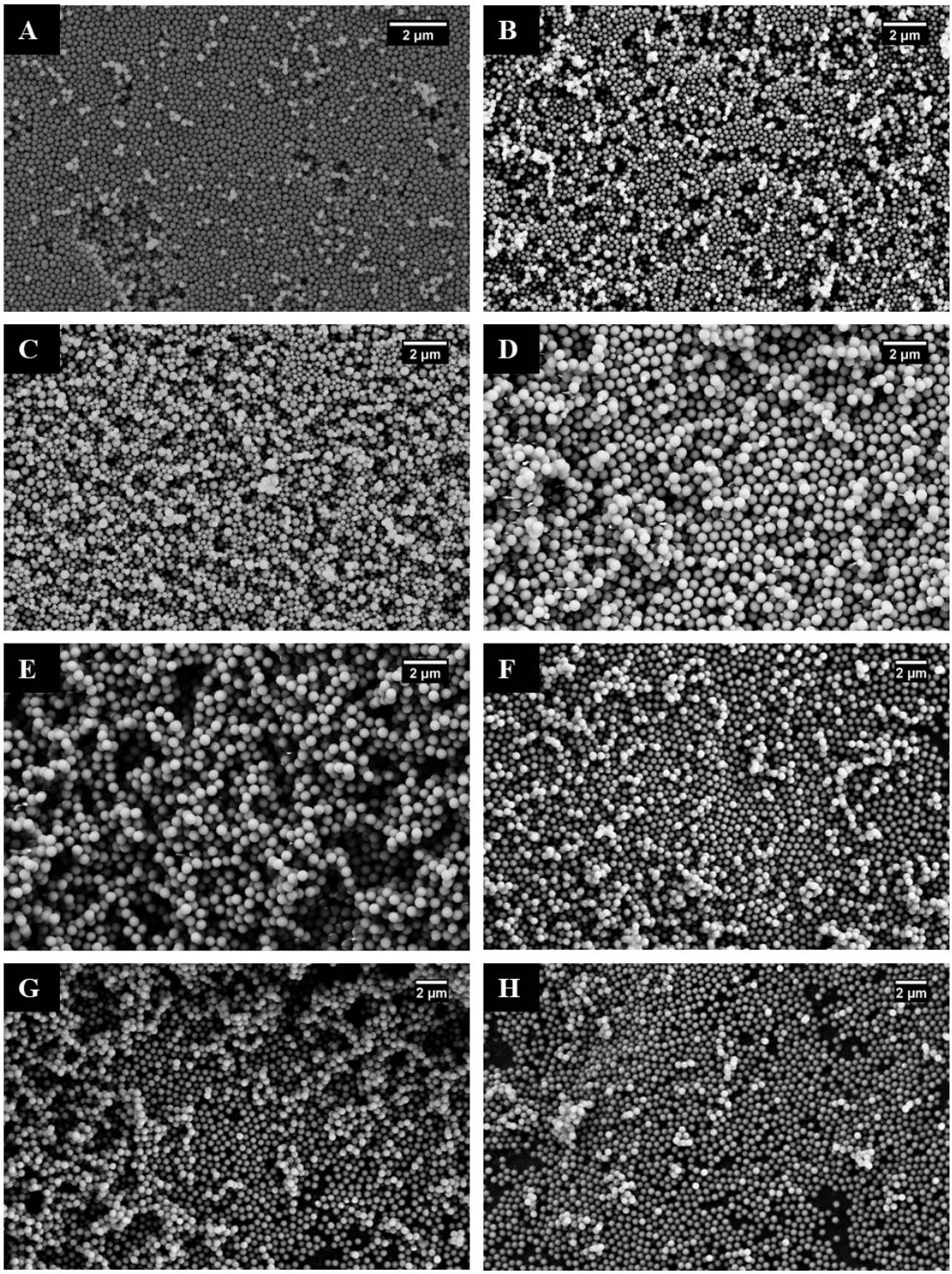


Figure 2.10 *SEM images of silica nanoparticles synthesised by varying amount of water. (a) 0.4 ml H_2O, (b) 0.5 ml H_2O, (c) 0.6 ml H_2O, (d) 0.7 ml H_2O, (e) 0.8 ml H_2O, (f) 0.9 ml H_2O, (g) 1 ml H_2O, and (h) 1.1 ml H_2O.*

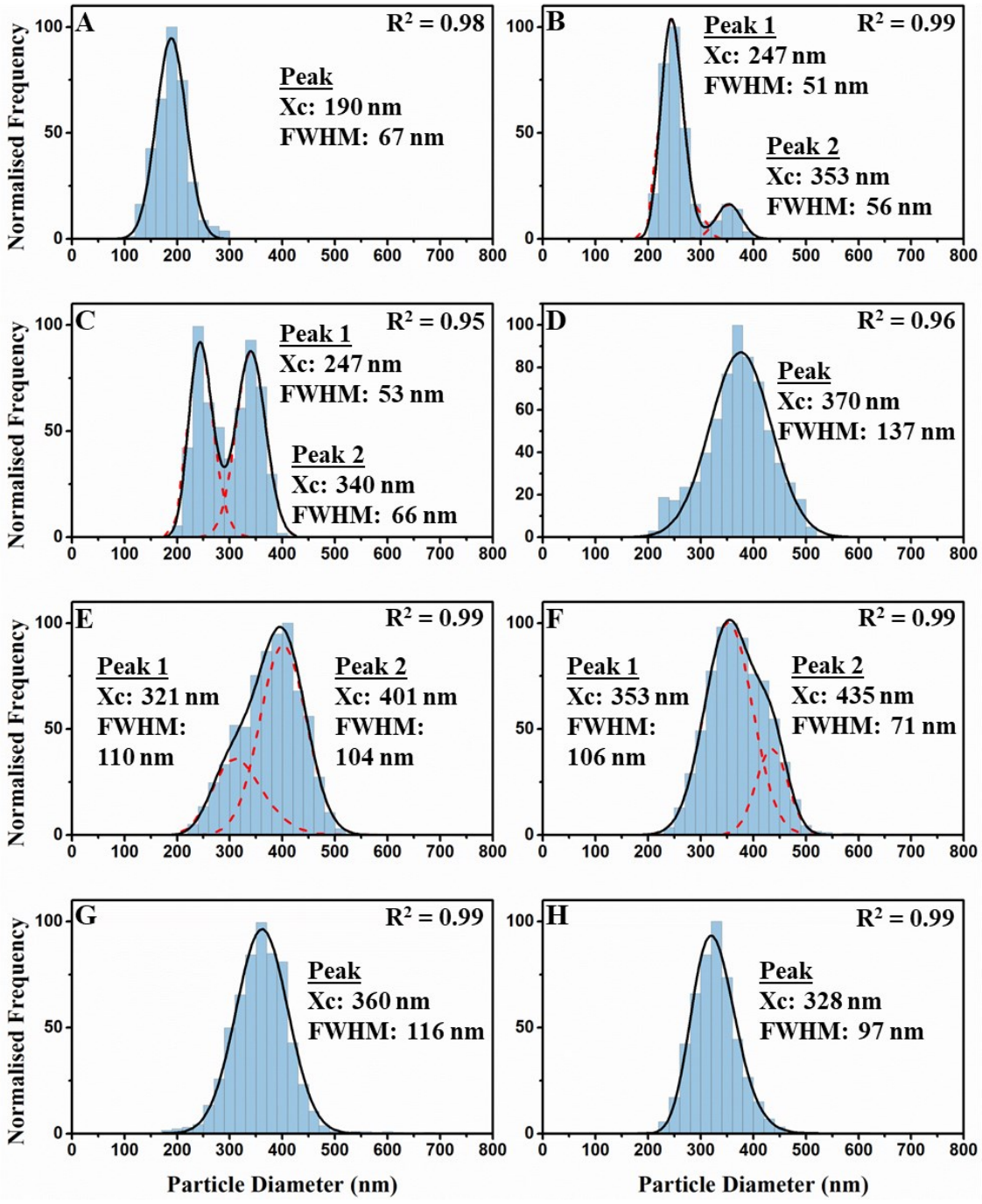


Figure 2.11 *PSDs of silica nanoparticles synthesised by varying amount of water. (a) 0.4 ml H_2O, (b) 0.5 ml H_2O, (c) 0.6 ml H_2O, (d) 0.7 ml H_2O, (e) 0.8 ml H_2O, (f) 0.9 ml H_2O, (g) 1 ml H_2O, and (h) 1.1 ml H_2O.*

Figure 2.12 shows the effect of the amount of water has on mean particle size and percent yield. The percent yield remains stable ca. 90 % across all volumes of water tested. At low volumes of water, the particle increases as the water volume increases. This is in contrast to our earlier results when studying EtOH concentration, where the particle size increased as the relative concentration of water and TEOS decreased. However, here TEOS concentration remains constant because EtOH concentration remains constant. Initially small particles are formed, but as the concentration of water increases, larger particles are formed up to 0.8 ml water. Previous studies have also shown that increasing water concentration increases particle size.[37,38] Recent research suggests that below a threshold concentration of water, the condensation reaction, which releases water, is accelerated due to the sustained consumption of water in the hydrolysis reaction, thus promoting particle growth.[39] Beyond this threshold, the condensation reaction is inhibited and the high water content system stabilises the particles earlier. This is a possible explanation for the decrease in particle size we see in our data beyond 0.8 ml water. Another possible explanation for this is a decrease in stability of the oligomeric silica species formed during the hydrolysis. At low volumes of water, a homogenous single-phase mixture with ethanol was formed. At higher volumes of water, this homogeneity is likely no longer present and a two-phase mixture is possible. The oligomeric species formed during hydrolysis will have differing solubilities and therefore migration to a particle surface can be hindered in a two-phase system at higher volumes of water.[38] The overall result is an increase in mean particle size up to 0.8 ml water, while also increasing monodispersity (lower RSD). Further increasing the volume of water results in a decrease in mean particle size with an increase in polydispersity (higher RSD).

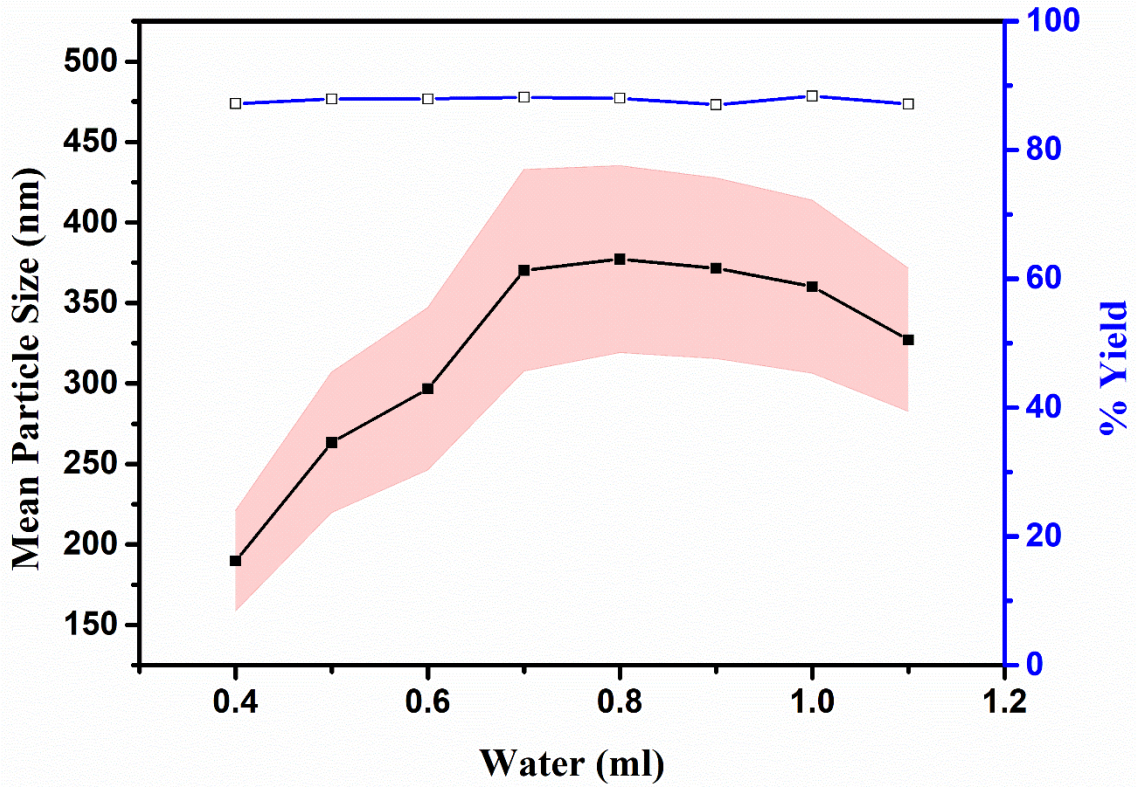


Figure 2.12 *Effect of water volume on mean particle size (–■–) and percent yield (–□–). Red shaded area is the standard deviation of mean particle size.*

2.5 Conclusion

The effect of ethanol, TEOS, ammonium hydroxide, and water, each had on the particle size of silica particles prepared using a Glantreo Ltd. method based on the Stöber process was investigated. A table of particle sizes was successfully produced allowing for the easy synthesis of non-porous silica particles between 149 – 511 nm in size. Increasing the amount of ethanol results in an increase in particle size. At very low and very high ethanol concentrations, the growth process occurs via Ostwald ripening only, resulting in good monodispersity. The percent yield drops to ca. 60 % from 3 ml ethanol onwards. Increasing the amount of TEOS results in an increase in particle size. At the lowest volume of TEOS (0.2 ml) the growth process occurs via Ostwald ripening, however this shifts to a mixture of coalescence and Ostwald ripening as the amount of TEOS is increased. At 0.7 ml TEOS and above, the growth process alternates between coalescence and Ostwald ripening. The percent yield was highest for 0.2 ml TEOS (94.7 %) and lowest for 1.1 ml TEOS (91.6 %). Increasing the concentration of ammonium hydroxide leads to an increase in particle size up to 5.1 M. Further increase beyond 5.1 M ammonium hydroxide leads to a decrease in particle size. The percent yield for all tested concentrations of ammonium hydroxide remained constant at ca. 90 %. At low volumes of water, the particle size increases as the volume of water increases. Above 0.8 ml water, the particle size decreases with increasing volume of water. The percent yield remained constant at ca. 90 % across all volumes of water tested. The statistical analysis of this Glantreo Ltd. process enabled the synthesis of silica nanoparticles of controllable dimension, a key requirement for Glantreo Ltd. to subsequently scale-up this process. Information acquired during this analysis allowed for an efficient and high-yielding scale-

up. Overall, the results presented here agree with numerous studies that have investigated changing reaction parameters and their influence on particle size.

2.6 References

1. Iler, R. K. *The Chemistry of Silica: Solubility, Polymerization, Colloid and Surface Properties, and Biochemistry. Wiley-Interscience* (Wiley: New York, 1979).

2. Rahman, I. A. & Padavettan, V. Synthesis of Silica nanoparticles by Sol-Gel: Size-dependent properties, surface modification, and applications in silica-polymer nanocompositesa review. *J. Nanomater.* **2012**, (2012) DOI: 10.1155/2012/132424.

3. Möller, K. & Bein, T. Talented Mesoporous Silica Nanoparticles. *Chem. Mater.* acs.chemmater.6b03629 (2016) doi:10.1021/acs.chemmater.6b03629 DOI: 10.1021/acs.chemmater.6b03629.

4. Lu, J., Liong, M., Li, Z., Zink, J. I. & Tamanoi, F. Biocompatibility, biodistribution, and drug-delivery efficiency of mesoporous silica nanoparticles for cancer therapy in animals. *Small* **6**, 1794–1805 (2010) DOI: 10.1002/smll.201000538.

5. Slowing, I. I., Vivero-Escoto, J. L., Wu, C.-W. & Lin, V. S.-Y. Y. Mesoporous silica nanoparticles as controlled release drug delivery and gene transfection carriers. *Adv. Drug Deliv. Rev.* **60**, 1278–1288 (2008) DOI: 10.1016/j.addr.2008.03.012.

6. Contado, C., Ravani, L. & Passarella, M. Size characterization by Sedimentation Field Flow Fractionation of silica particles used as food additives. *Anal. Chim. Acta* **788**, 183–192 (2013) DOI: 10.1016/j.aca.2013.05.056.

7. Mohamed, A. T. Experimental enhancement for dielectric strength of polyethylene insulation materials using cost-fewer nanoparticles. *Int. J. Electr. Power Energy*

Syst. **64**, 469–475 (2015) DOI: 10.1016/j.ijepes.2014.06.075.

8. Gangåssæter, H. F., Jelle, B. P. & Mofid, S. A. Synthesis of Silica-Based Nano Insulation Materials for Potential Application in Low-Energy or Zero Emission Buildings. *Energy Procedia* **122**, 949–954 (2017) DOI: 10.1016/j.egypro.2017.07.435.

9. Gu, H., Zhang, Q., Gu, J., Li, N. & Xiong, J. Facile preparation of superhydrophobic silica nanoparticles by hydrothermal-assisted sol–gel process and effects of hydrothermal time on surface modification. *J. Sol-Gel Sci. Technol.* **87**, 478–485 (2018) DOI: 10.1007/s10971-018-4731-x.

10. Naderizadeh, S., Athanassiou, A. & Bayer, I. S. Interfacing superhydrophobic silica nanoparticle films with graphene and thermoplastic polyurethane for wear/abrasion resistance. *J. Colloid Interface Sci.* **519**, 285–295 (2018) DOI: 10.1016/j.jcis.2018.02.065.

11. Hackley, V. A. & Ferraris, C. F. *NIST Recommended Practice Guide: The Use of Nomenclature in Dispersion Science and Technology*. (2001).

12. Henry, R. A., Ross, P., Betz, W. R., Parmar, G. & Way, W. K. The Importance of Monodisperse Silica in the Evolution of UHPLC and HPLC Column Performance. *American Laboratory* https://www.americanlaboratory.com/914-Application-Notes/171558-The-Importance-of-Monodisperse-Silica-in-the-Evolution-of-UHPLC-and-HPLC-Column-Performance/ (2015).

13. Chen, C.-N., Lin, H.-P., Tsai, C.-P. & Tang, C.-Y. Synthesis of Artificial Opals with Uniform Mesoporous Silica Spheres. *Chem. Lett.* **33**, 838–839 (2004) DOI:

10.1246/cl.2004.838.

14. Vasileva, P., Dakova, I., Yordanova, T. & Karadjova, I. New composite sorbent for speciation analysis of soluble chromium in textiles. *Open Chem.* **17**, 1095–1104 (2019) DOI: 10.1515/chem-2019-0115.

15. English, M. D. & Waclawik, E. R. A novel method for the synthesis of monodisperse gold-coated silica nanoparticles. *J. Nanoparticle Res.* **14**, 650 (2012) DOI: 10.1007/s11051-011-0650-2.

16. Choi, J. Y., Kim, C. H. & Kim, D. K. Formation and Characterization of Monodisperse, Spherical Organo-Silica Powders from Organo-Alkoxysilane-Water System. *J. Am. Ceram. Soc.* **81**, 1184–1188 (2005) DOI: 10.1111/j.1151-2916.1998.tb02466.x.

17. Xia, L. *et al.* Fundamental method for controlling monodisperse silica nanoparticles dimension assisted by lysine. *J. Sol-Gel Sci. Technol.* **92**, 134–145 (2019) DOI: 10.1007/s10971-019-05087-z.

18. Stöber, W., Fink, A. & Bohn, E. Controlled growth of monodisperse silica spheres in the micron size range. *J. Colloid Interface Sci.* **26**, 62–69 (1968) DOI: 10.1016/0021-9797(68)90272-5.

19. Sadasivan, S., Dubey, A. K., Li, Y. & Rasmussen, D. H. Alcoholic solvent effect on silica synthesis - NMR and DLS investigation. *J. Sol-Gel Sci. Technol.* **12**, 5–14 (1998) DOI: 10.1023/A:1008659708390.

20. Harris, M. T., Brunson, R. R. & Byers, C. H. The base-catalyzed hydrolysis and

condensation reactions of dilute and concentrated TEOS solutions. *J. Non. Cryst. Solids* **121**, 397–403 (1990) DOI: 10.1016/0022-3093(90)90165-I.

21. *Emulsions: Structure, Stability and Interactions, Volume 4*. (Academic Press, 2004).

22. Lifshitz, I. M. & Slyozov, V. V. The kinetics of precipitation from supersaturated solid solutions. *J. Phys. Chem. Solids* **19**, 35–50 (1961) DOI: 10.1016/0022-3697(61)90054-3.

23. Wagner, C. Theorie der Alterung von Niederschlägen durch Umlösen (Ostwald-Reifung). *Berichte der Bunsengesellschaft für Phys. Chemie* **65**, 581–591 (1961) DOI: 10.1002/BBPC.19610650704.

24. Green, D. L. *et al.* Size, volume fraction, and nucleation of Stober silica nanoparticles. *J. Colloid Interface Sci.* **266**, 346–358 (2003) DOI: 10.1016/S0021-9797(03)00610-6.

25. Fernandes, R. S., Raimundo, I. M. & Pimentel, M. F. Revising the synthesis of Stöber silica nanoparticles: A multivariate assessment study on the effects of reaction parameters on the particle size. *Colloids Surfaces A Physicochem. Eng. Asp.* **577**, 1–7 (2019) DOI: 10.1016/j.colsurfa.2019.05.053.

26. Chen, Q., Ge, Y., Granbohm, H. & Hannula, S.-P. Effect of Ethanol on Ag@Mesoporous Silica Formation by In Situ Modified Stöber Method. *Nanomater. (Basel, Switzerland)* **8**, (2018) DOI: 10.3390/nano8060362.

27. H. E. Bergna, W. O. R., Bergna, H. E. & Roberts, W. O. *COLLOIDAL SILICA*

Fundamentals and Applications. *Surfactant Science Series* vol. 131 (CRC Press, 2005).

28. Buckley, A. & Greenblatt, M. The sol-gel preparation of silica gels. *J. Chem. Educ.* **71**, 599–602 (1994) DOI: 10.1021/ed071p599.

29. Neville, F., Mohd. Zin, A., Jameson, G. J. & Wanless, E. J. Preparation and characterization of colloidal silica particles under mild conditions. *J. Chem. Educ.* **89**, 940–942 (2012) DOI: 10.1021/ed200684s.

30. Matsoukas, T. & Gulari, E. Dynamics of growth of silica particles from ammonia-catalyzed hydrolysis of tetra-ethyl-orthosilicate. *J. Colloid Interface Sci.* **124**, 252–261 (1988) DOI: 10.1016/0021-9797(88)90346-3.

31. Greasley, S. L. *et al.* Controlling particle size in the Stöber process and incorporation of calcium. *J. Colloid Interface Sci.* **469**, 213–223 (2016) DOI: 10.1016/j.jcis.2016.01.065.

32. Meier, M., Ungerer, J., Klinge, M. & Nirschl, H. Synthesis of nanometric silica particles via a modified Stöber synthesis route. *Colloids Surfaces A Physicochem. Eng. Asp.* **538**, 559–564 (2018) DOI: 10.1016/j.colsurfa.2017.11.047.

33. Hristov, D. R., Mahon, E. & Dawson, K. A. Controlling aqueous silica nanoparticle synthesis in the 10–100 nm range. *ChemComm* **51**, 17420–17423 (2015) DOI: 10.1039/C5CC06598D.

34. Wang, X. D. *et al.* Preparation of spherical silica particles by Stöber process with high concentration of tetra-ethyl-orthosilicate. *J. Colloid Interface Sci.* **341**, 23–29

(2010) DOI: 10.1016/j.jcis.2009.09.018.

35. Han, Y. *et al.* Unraveling the growth mechanism of silica particles in the stöber method: In situ seeded growth model. *Langmuir* **33**, 5879–5890 (2017) DOI: 10.1021/acs.langmuir.7b01140.

36. Zeng, D., Zhang, H., Wang, B., Sang, K. & Yang, J. Effect of Ammonia Concentration on Silica Spheres Morphology and Solution Hydroxyl Concentration in Stober Process. *J. Nanosci. Nanotechnol.* **15**, 7407–7411 (2015) DOI: 10.1166/jnn.2015.10595.

37. Van Helden, A. K., Jansen, J. W. & Vrij, A. Preparation and characterization of spherical monodisperse silica dispersions in nonaqueous solvents. *J. Colloid Interface Sci.* **81**, 354–368 (1981) DOI: 10.1016/0021-9797(81)90417-3.

38. Bourebrab, M. A. *et al.* Influence of the initial chemical conditions on the rational design of silica particles. *J. Sol-Gel Sci. Technol.* **88**, 430–441 (2018) DOI: 10.1007/s10971-018-4821-9.

39. Zhao, X. *et al.* The Influence of Water Content on the Growth of the Hybrid-Silica Particles by Sol-Gel Method. *Silicon* (2020) doi:10.1007/s12633-020-00756-z DOI: 10.1007/s12633-020-00756-z.

2.7 Appendix

Code written by: Dr. Timothy W. Collins
Input and testing by: Ricky Curley

Image analysis procedure:

The code used to analyse the SEM images shown below is run in using MATLAB programming language and computing environment developed by Mathworks (see https://uk.mathworks.com/help/images/ref/imfindcircles.html for a more detailed explanation of the mathematical arguments on which this code is based). Briefly, the SEM image is captured and saved in TIFF format (code can be altered to accommodate different formats). The filename of the image is appended with '-xxxxx' with xxxxx being the horizontal field width in nanometres. The image is converted to grayscale. 2-D median filtering is applied to this grayscale image. A minimum and maximum radius is defined and a circular Hough transform is applied. This transform finds the spheres in the specified image with radii in the specified range. The output argument contains the radii obtained using the Hough transform. The number of spheres and their corresponding diameters are then output in tabular form which can be statistically analysed.

The two parameters within the code that have the greatest influence on the ability of the code to determine particle diameters are 'Sensitivity – Sensitivity factor' and 'EdgeThreshold – Edge gradient threshold'.

[centres , radii] = imfindcircles(img , [radius_min radius_max]

*,'ObjectPolarity' , 'bright' , '**Sensitivity**', 0.97, '**EdgeThreshold**',0.15);*

Sensitivity factor is the sensitivity for the circular Hough transform accumulator array, specified as the comma-separated pair consisting of 'Sensitivity' and a number in the range [0,1]. As you increase the sensitivity factor, *imfindcircles* detects more circular objects, including weak and partially obscured circles. Higher sensitivity values also increase the risk of false detection. Edge gradient threshold sets the gradient threshold for determining edge pixels in the image, specified as the comma-separated pair consisting of 'EdgeThreshold' and a number in the range [0, 1]. Specify 0 to set the threshold to zero-gradient magnitude. Specify 1 to set the threshold to the maximum gradient magnitude. *imfindcircles* detects more circular objects (with both weak and strong edges) when you set the threshold to a lower value. It detects fewer circles with weak edges as you increase the value of the threshold (ref: see link above).

The adjustment of these two parameters enables the code to be fine-tuned to improve the accuracy of the data obtained from the image. A possible source of error that must be acknowledged is when multiple layers of particles are present in the SEM image. The slight variation in height of the particles from the surface of the carbon tape will introduce a small error in the size analysis due to this difference in perspective. However, this difference is so small that it becomes negligible when thousands of data points are generated for each image, as is the case here. Nonetheless, it is worth keeping this fact in mind.

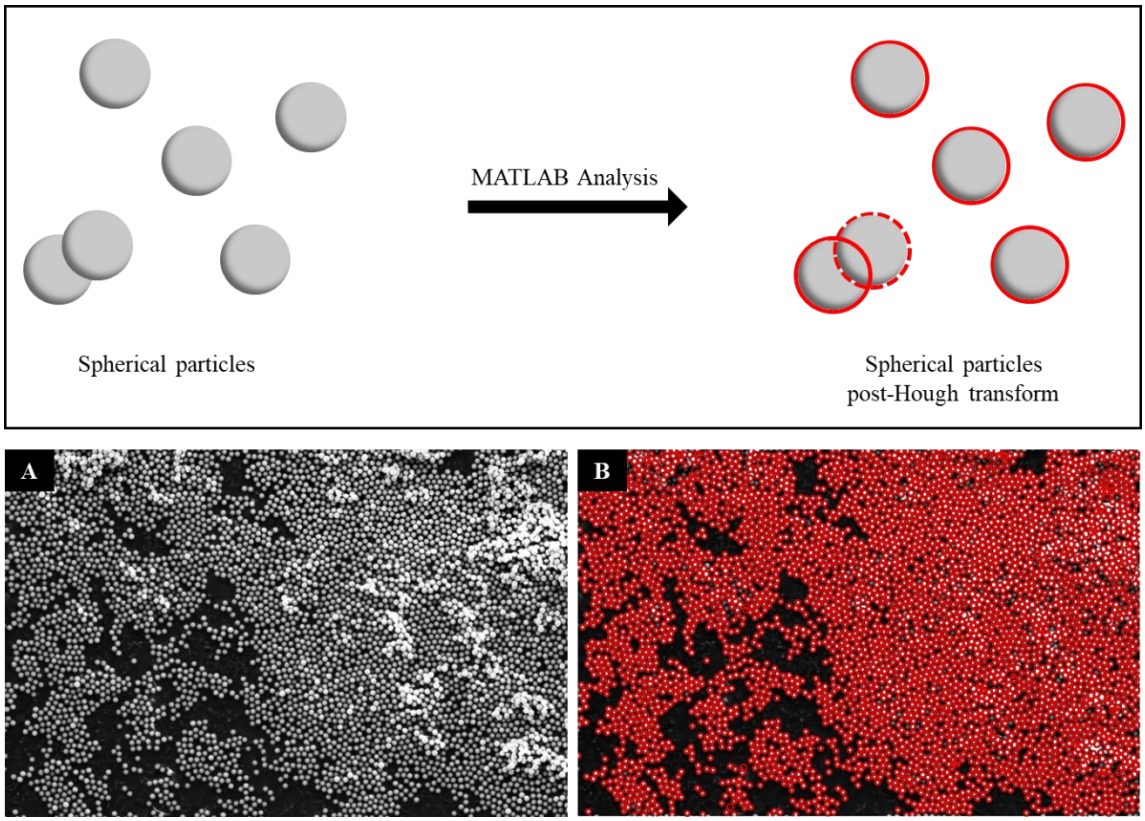


Figure A2.1 *Simplified representation (top) of the fundamental analysis taking place. Spherical particles are identified in the SEM image by parameters defined in the Hough transform. Note how overlapping particles can also be individually identified. Post-transformation, these particles are shown in the output image encased in red circles. (a) SEM image before processing. (b) SEM image post-processing.*

2.7.1 MATLAB sizing code

```
clear all;
clf;
clear all;

location = '';
% location of images on drive
cd(location);

contents = dir('*.tif');
% or whatever the filename extension is

% Set up the initial 00 table for reference

Title = {0};
CD_mean = 0;
CD_median = 0;
CD_std = 0;
CD_3sig = 0;
CD_mad = 0;
CD_mad_3sig = 0;
no_centres = 0;
gauss_centre = 0;
gauss_sig = 0;
logn_center = 0;
logn_sig = 0;

Row_1 = 'Na';
T = table(Title,CD_mean,CD_median,CD_std,CD_3sig,CD_mad,CD_mad_3sig,...
    no_centres,gauss_centre,gauss_sig,logn_center,logn_sig);


for r = 1:numel(contents)

  filename = contents(r).name;
  % loads each image in turn

  Ic = imread(filename);

  [path, name_1] = fileparts(filename);
  % gets the filename

Names = strsplit(name_1,'-');
% splits the name % suffix after '-' needs to be horizontal field width in whatever units
desired e.g. nm
```

```
name = char(Names(1,1));
% load the first part as the image name

image_width = str2num(char(Names(1,2)));
% reference the matrix for Names
% and convert to numeric; % image width in nm

tolerance = 300;
% tolerance for two circles to be the same circle

mkdir(name);

Io = rgb2gray(Ic); % ERI_SEM
% Io = Ic; % Tyndall_SEM

[height,width] = size(Io);

% I = imcrop(Io,[0 0 width (height*0.87)]);

I = imcrop(Io,[0 0 width (height*0.87)]);

I2 = imadjust(I);

nm_px = (image_width/width);
% nm per pixel ratio!
tol= (tolerance/nm_px);
% tolerance (in pixels)

f_radius = round((150/nm_px));
% if the nm_px ratio is too high, the filter radius will round to 0, is which case try using
1 or skipping as necessary
domain=fspecial('disk',f_radius)>0;
img = ordfilt2(I2,round(0.5*numel(find(domain))),domain);

   img = medfilt2(I2);

radius_min = round(200/nm_px);
% Minimum CD = half diameter (radius) = 320nm
radius_max = round(350/nm_px);
% Maximum CD  = half diameter (radius) = 700nm
% can change radius_min and radius_max as necessary

[centres , radii] = imfindcircles( img , [radius_min radius_max] ,'ObjectPolarity' , 'bright'
, 'Sensitivity', 0.97, 'EdgeThreshold',0.15);
 % find circles, save results in centres, radii
```

```
% Look at http://www.mathworks.co.uk/help/images/examples/detect-and-measure-circular-objects-in-an-image.html?prodcode=IP&language=en

% stop any double counting
for i=1:length(centres)
   for j=i+1:length(centres)
      if( ( abs( centres(i,1) - centres(j,1) ) < tol ) && ( abs( centres(i,2) - centres(j,2) ) < tol ) )
         radii(j)=0;
         centres(j,1)=0;
         centres(j,2)=0;
      end
   end
end

radii( all(~radii,2), : ) = [];
centres( all(~centres,2), : ) = [];

% show detected features
figure(1);
imshow(Ic)
title('Input image');
loc1 = strcat(name,'\Input.png');
saveas(gcf,loc1);

figure(2);
imshow(img)
h = viscircles (centres , radii);
% overlay the circles found
title('Detected features');
loc2 = strcat(name,'\Features.png');
saveas(gcf,loc2);

% how many spheres
no_centres = length(centres);

radii_nm = (radii*nm_px);
diameter = radii_nm*2;

D_loc = strcat(location,'\',name,'\diameters.xlsx');
xlswrite(D_loc,diameter);


% descriptive statistics
CD_mean = mean(diameter);
CD_median = median(diameter);
```

```
CD_std = (std(diameter));
CD_3sig = (std(diameter))*3;
CD_mad = mad(diameter);
CD_mad_3sig = (mad(diameter))*1.253*3;

% generate histogram
[hi_dia,diametercentres] = hist(diameter, 50);
his_dia = [diametercentres(1,:);hi_dia(1,:)];
histogram_d = (his_dia.');
indices_d = find(histogram_d(:,2)==0);
histogram_d(indices_d,:) = [];

H_loc = strcat(location,'\',name,'\histograms.xlsx');
xlswrite(H_loc,histogram_d);

% fit histograms to gaussian plot
figure(3);
[gauss_d,gof_d] = fit(histogram_d(:,1),histogram_d(:,2),'gauss1');
coeff1 = coeffvalues(gauss_d);
strg = sprintf('Gaussian with Xc = %f',coeff1(1,2));
plot(gauss_d,histogram_d(:,1),histogram_d(:,2));
xlabel('Diameter/nm');
ylabel('frequency');
title(strg);

loc3 = strcat(name,'\Gaussian.png');
saveas(gcf,loc3);

% fit Lognormal and gaussian for combined plot
[parmhat,parmci] = lognfit(diameter);
[mu,s,muci,sci] = normfit(diameter);

% plot graph and overlay
figure(6);
scatter(histogram_d(:,1),histogram_d(:,2),'g');
hold on
SF = 6;
% the 6 in the line here is a scaling factor to the line plots match up with the scatter plot,
may need to be adjusted.
plot(histogram_d(:,1),SF*no_centres*normpdf(histogram_d(:,1),mu,s),'b');
hold on
plot(histogram_d(:,1),SF*no_centres*lognpdf(histogram_d(:,1),parmhat(1),parmhat(2)),
'r');
str = sprintf('Gaussian Xc %f, LogN Xc %f',mu,exp(parmhat(1)));
title(str);
xlabel('Diameter/nm');
```

```
ylabel('frequency');
legend('scatter','Gaussian','Lognormal');

loc6 = strcat(name,'\Gauss&LogN.png');
saveas(gcf,loc6);

% Trying manual input equation
% figure(4);
% gaussLogn = 'a*exp(-((x-b)/c)^2)+d*exp(-((log(x-e))/f)^2)+g';
% Lognfit = 'a*exp(-((log(x-b))/c)^2)';
% startPoints = coeffvalues(gauss_d);
% fit1 = fit(histogram_d(:,1),histogram_d(:,2),Lognfit,'Start', startPoints);
% coeffvals = coeffvalues(fit1);
% plot(fit1,histogram_d(:,1),histogram_d(:,2));

% more stats
gauss_centre = mu;
gauss_sig = s;
logn_center = exp(parmhat(1));
logn_sig = exp(parmhat(2));

% write stats to table
Title = {name};
T1 = table(Title,CD_mean,CD_median,CD_std,CD_3sig,CD_mad,CD_mad_3sig,...
    no_centres,gauss_centre,gauss_sig,logn_center,logn_sig,'Rownames',Title);

T = [T;T1];

% save data to location
T1_loc = strcat(location,'\',name,'\Statistics.xlsx');
writetable(T1, T1_loc);

figure(5);
imshow(img)
title('Enhanced image');
loc5 = strcat(name,'\Enhanced image.png');
saveas(gcf,loc5);

close all
clearvars -except location contents T

end

% save data to location
T_l = strcat(location,'\Stats.xlsx');
writetable(T, T_l);
```

Chapter 3

Biomimetic Spherical Silica Production using Phosphatidylcholine and Soy Lecithin

This chapter has been submitted for publication. Consequently, sections of the chapter such as the abstract and introduction may contain repeating concepts and paragraphs.

Curley, R., Banta, R.A., Garvey, S., Holmes, J.D. & Flynn, E.J. Biomimetic Spherical Silica Production using Phosphatidylcholine and Soy Lecithin.

3.1 Abstract

Spherical silica particles are traditionally made via Stöber and modified-Stöber processes, which commonly use environmental toxins as reagents. Here we report a process to synthesise spherical silica particles using environmentally friendly biomolecules (phosphatidylcholine and soy lecithin) and employing water and soybean oil as a solvents, rather than potentially harmful organic solvents. The spherical silica particles we synthesised are among the most monodisperse of any silica particles produced through biomolecule templating agents in the literature to date. This scalable method represents an important step towards sustainable industrial silica syntheses. Under mildly acidic conditions phosphatidylcholine and soy lecithin can control the condensation of sodium silicate to form discrete, spherical silica particles. Silica particles with diameters ranging between 329 nm to 2232 nm were readily produced using phosphatidylcholine as the templating agent and soybean oil as the solvent in the presence of sodium silicate. Narrower size distributions (262 nm – 1272 nm) were achieved using soy lecithin as the templating agent in an aqueous acetate buffer solution containing sodium silicate. Silica particles grown using low concentrations of phosphatidylcholine and soy lecithin as templating agents formed by a combination of coalescence and Ostwald ripening, whilst particles grown at high concentrations predominantly formed through Ostwald ripening behaviour.

3.2 Introduction

Finding sustainable and environmentally friendly alternative routes to produce spherical silica is critical. Spherical silica particles are one of the most important and versatile mineral materials produced industrially with many integral uses in catalysis, adsorption, chromatography, sensors and drug delivery.[1–8] However, production of spherical silica currently relies on environmentally damaging and unsustainable processes (namely Stöber and modified-Stöber processes), such as ammonium hydroxide, quaternary ammonium surfactants, *e.g.* cetyltrimethylammonium bromide (CTAB), alcoholic solvents, and various alkoxysilanes. Ammonium hydroxide and CTAB control the morphology of the particles by acting as structure-directing agents (SDAs) and the way in which they act is described in detail in sections **1.2.3** and **1.2.4**. However, these reagents have adverse environmental effects due to their toxicity.[9–11] Nevertheless, these SDAs are required to form spherical particles. Therefore, any sustainable process for producing spherical silica particles needs to address the inherent environmental issues of the Stöber processes while also maintaining the ability to control the morphology of the particles.

Biomineralisation, the process by which biological systems create complex, hierarchical, mineral structures, often out of silica, from simple starting materials may offer the solution to forming particles in an environmentally friendly process.[12] Synthesis of bioinspired nanomaterials is a vibrant area of research.[13–16] Within the natural World's producers of complex, hierarchical, silica structures, *diatoms* have been widely studied.[17–20] These tiny creatures can create intricate cell walls made of silica nanoparticles arranged in highly ordered structures over a variety of scales, from nanometres up to several hundred microns.[21] Nanofabrication of silica in diatoms occurs under ambient conditions at

slightly acidic pH and results from specific interactions between biomolecules and silicic acid derivitives.[22] Some of the first discovered biomolecules that were responsible for controlling silica polymerisation were cationically charged polypeptides called silaffins.[23] Other important molecules isolated from various diatoms are long-chain polyamines (LCPAs). These silaffins and LCPAs are species-specific molecules, but both have been shown to induce rapid silica condensation *in vitro*.[18]

How these biomolecules exert such fine control over the biomineralisation process is still not fully understood. Early studies focused on small biomolecules such as amino acids and peptides to provide insight into this process. Wallace *et al*.[24] studied the effects of carboxyl-terminated surfaces and amine-terminated surfaces on silica nucleation in vitro. They found that carboxyl-terminated surfaces were able to induce silica nucleation under ambient conditions and at slightly acidic pH. In contrast, amine-terminated surfaces failed to induce silica nucleation under identical conditions. When combining both carboxyl- and amine-terminated surfaces, they found that the silica nucleation rate was 18 times faster than carboxyl-terminated surface alone, indicating that molecules, such as peptides and proteins, that contain carboxyl and amine groups in close proximity, play a crucial role in silica formation. The mechanism of how peptides induce nucleation of silica can be explained by looking at the charge relay effect of enzymes. Enzymes such as transferases contain what is referred to as a catalytic triad, containing three main components: acid, base, and nucleophile.[25] The mechanism of this catalytic triad charge relay mechanism is as follows: the base residue is activated due to deprotonation from the acid residue, which is in close proximity. Once the base residue is activated, it in turn activates the nucleophile. The activation of the nucleophile is a result of the catalytic triad

acting synergistically to lower the pK_a of the nucleophile.[26] For the above study, the carboxyl groups act as the acid which activates the amine group. The amine group then induces the polymerisation of silica by acting as a nucleophilic catalyst. This behaviour of the charge relay effect and its influence on silica condensation was studied in detail by Kuno *et al*.[27] They synthesised homopolypeptides of lysine (K_{10}) and histidine (H_{10}); and block polypeptides of lysine/aspartic acid (K_5D_5) and histidine/aspartic acid (H_5D_5), consisting of two chains of each peptide linked together; and alternate polypeptides of lysine/aspartic acid [$(KD)_5$] and histidine/aspartic acid[$HD)_5$], consisting of an alternating chain of two peptides. They found that the catalytic activity of the alternate polypeptides was higher because the acid and base residues were in close proximity and could more readily induce silica condensation via the charge relay mechanism.

There have been numerous attempts to synthesise silica biomimetically using the knowledge obtained from silica biomineralising organisms. Use of amino acids and polyamines has been extensively studied due to the discovery that such compounds play an integral role in silica biomineralisation *in vivo*. [28–30] The interaction of the amines with oligomeric silicate species is thought to occur via electrostatic interactions and/or chemical reaction depending on the reaction conditions used. However, many of these studies, while successfully employing biomimetic principles to synthesis silica, use TEOS, ammonia and ethanol, which as mentioned are not conducive to a sustainable synthesis. Furthermore, they use various polyamines and cyclic amines which are not naturally occurring and must be synthesised synthetically. The ultimate goal of synthesising silica biomimetically is to use renewable reagents and environmentally

benign synthesis conditions. Naturally occurring biomolecules can provide this opportunity.

To date, there are fewer scientific reports on producing spherical silica particles from more complex biomolecules through methods that seek to mimic natural processes. Most studies using biopolymers specifically have resulted in agglomerated and highly size-polydisperse and non-spherical particles. For example, Demadis *et al*.[31] studied silica formation from sodium silicate in the presence of phosphonomethylated chitosan, polyethyleneimine, and carboxymethylinulin. They found that in all cases, silica precipitation was observed with a size range of 150 nm – 2 μm. However, discrete and spherical particles were never obtained. Gautier *et al*.[32] investigated the influence of gelatin/alginate mixtures on sodium silicate condensation. Again, silica precipitation occurred, but the silica structures generated were undefined and agglomerated. Jia *et al*.[33] also used gelatin to form silica from tetramethyl orthosilicate, however spherical silica particles were not produced, only porous, agglomerated structures. In two separate studies, Coradin *et al.*[34,35] explored the interaction of bovine serum albumin (BSA) and lysozyme on sodium silicate solutions, and the interaction of amino-containing peptides on sodium silicate solutions. In both studies, the biopolymers were able to produce silica from sodium silicate solutions. While some degree of sphericity could be discerned from the SEM images of the particles produced with BSA and lysozyme, the particles were non-uniform and are highly agglomerated. Furthermore, no size analysis was performed on these particles. Similarly, their silica prepared using peptides consisted of non-spherical agglomerates.

The studies discussed above show that morphological control is possible with certain biomolecules depending on their physicochemical properties. Detailed summaries on the role these biomolecules play in biomineralisation are provided elsewhere.[36–38] These biomolecules are able to induce silica polymerisation while also controlling morphology. The role surfactants, such as CTAB, play in the condensation of silica has been thoroughly investigated.[39–43] They act as SDAs, controlling the silica particle morphology during synthesis which arrange themselves into micelles when a critical micelle concentration (cmc) is reached. In traditional CTAB and tetraethyl orthosilicate (TEOS)-based modified-Stöber reaction systems, alcohol acts as a mutual solvent for both water and TEOS. Thus, hydrolysis and condensation of silica occurs at the shell of the SDA micelles. Once TEOS is hydrolysed, oligomeric silicate species are produced. These negatively charged species interact electrostatically with the positively charged quaternary ammonium SDAs.[40] Electrostatic interactions mediate particle growth, while also preventing agglomeration of the particles, yielding discrete, spherical silica particles.

Using biomineralisation as a starting point, we identified phosphatidylcholine (PC) and soy lecithin (SL) as ideal candidates to replace CTAB in the Stöber processes. These biomolecules contain carboxyl and amine groups in close proximity, which, as mentioned above, improves the nucleation rate of silica greatly. Phosphorylation present in proteins responsible for biosilicification has been shown to be integral for silica polymerisation.[23,44] PC and SL contain structurally similar phosphoryl groups. They also contain large hydrophobic tails of fatty acids and hydrophilic headgroups similar to CTAB. Specifically, the presence of quaternary ammonium cations in the headgroup of PC and SL, like CTAB, is important for morphological control. **Figure 1.6** shows the

structural similarities between PC, SL, and CTAB. Yokoi *et al.*[45] studied the effects that lysine had on the polymerisation of TEOS and found that the lysine acted as a weak base catalyst promoting the hydrolysis of TEOS. The lysine was subsequently adsorbed onto the forming silica surface through electrostatic interaction between the $-NH_4^+$ groups of the lysine and the OH^- groups of the silica surface, enabling morphological control of the particles by preventing agglomeration. Similar studies investigating the effects of polyamines on silica polymerisation suggest electrostatic interactions along with their emulsion droplet formation play an integral role in the morphological control of the silica.[18,46,47] However, this amine-silicate interaction can also proceed through chemical reaction. Delak *et al.*[48] chose tetramethylethoxysilane (TMES) as the silica precursor because at the pH used in the study (pH 5.5), TMES, and its hydrolysed intermediate tetramethylsilanol, is neutral. Therefore, electrostatic interactions between the amines and the silicate species cannot occur. However, the amines catalytic activity was still evident. The lone pair on the nitrogen is thought to chemically attack the silica precursor, forming a pentacoordinate intermediate which increases the lability of ethoxy bond of TMES, making hydrolysis more facile. Subsequent condensation and morphological control achieved through the emulsion stability provided by the amines leads to silica formation. Further evidence for this chemical mechanism is provided by Masse *et al.*[49] It is clear that the emulsion stability provided by these amines along with the electrostatic interactions and/or chemical catalysis plays an integral role in silica polymerisation.

Lecithin is widely used as an emulsion stabiliser in food products and it also contains quaternary ammonium groups similar to CTAB and the amines responsible for silica biomineralisation. Therefore, lecithin has potential to act as an SDA in spherical silica

synthesis. For example, Galarneau *et al*.[50] used lecithin/dodecylamine mixed micelles to synthesis sponge mesoporous silica in which lecithin was directly involved in silica morphogenesis. Furthermore, Chung *et al.*[51] highlighted the important emulsion-stabilising property of lecithin in oil-in-water emulsions. They found that the emulsion droplets were highly stable in the presence of lecithin between pH 5-7 (the pH used in this study is 5.92) due to electrostatic repulsion preventing agglomeration of the droplets. It is likely that these properties are the reason that silica is formed so readily in the presence of lecithin, while in its absence no particles are formed. Therefore, in order for our proposed biomolecule replacements for CTAB – PC and SL – to function as SDAs, they must be capable of forming structures in the reaction solvent which promote and control silica polymerisation.

SL is a waste product obtained from crude soy oil after degumming. Valorisation of waste streams is an important aspect of the circular economy aimed at reducing waste, while utilising renewable resources. This is in stark contrast to petrochemical surfactants such as CTAB, which are non-renewable and environmentally damaging. Furthermore, we use buffered media as the catalyst for hydrolysis, eliminating the need for ammonium hydroxide. The use of such biomolecules permits further reductions in the environmental impact of the Stöber silica production process, as such biomolecules can be processed using water-based chemistries and so permit the greatly reduced use of petrochemically derived solvents; which can be highly toxic, can damage environments and ecosystems, and come with large embedded environmental costs due to their methods of manufacture and source material, *i.e.* oil.

3.3 Experimental

3.3.1 Materials

Sodium silicate (10.6 % Na_2O, 26.5 % SiO_2) from Sigma Aldrich was used as the silicic acid source, as it is analogous to the natural form of soluble silica. Soy Lecithin (SL) was purchased from Modernist Pantry. Buffer solution was 0.05 M acetate (pH 5.92) and was prepared in distilled water. L-α-Phosphatidylcholine (PC) (assay: ≥ 40 % phosphatidylcholine, TLC; ≥ phosphatides (as acetone insolubles)) and soybean oil were purchased from Sigma Aldrich.

3.3.2 Silica preparation using L-α-phosphatidylcholine and soy lecithin

Sodium silicate was added to 50 ml soybean oil under stirring. Aliquots of L-α-phosphatidylcholine stock solution (10 mg ml^{-1} of L-α-phosphatidylcholine in an aqueous solution of 0.05 M acetate buffer, pH 5.92) were subsequently added. For preparation using soy lecithin, the procedure is similar except 50 ml acetate buffer (0.05 M, pH 5.92) was used as the reaction medium and aliquots of soy lecithin stock solution (20 mg ml^{-1} soy lecithin in an aqueous solution of 0.05 M acetate buffer, pH 5.92) were used. The reaction solution was stirred in a closed vessel at room temperature and left to age overnight. This solution was then centrifuged at 14,000 rpm in an Eppendorf® MiniSpin Plus microcentrifuge and washed using minimal water, ethanol, and acetone. The sample was then dried. **Table 3.1** shows the experimental conditions for silica preparation using L-α-phosphatidylcholine and soy lecithin.

Table 3.1 *Experimental conditions of syntheses using PC and soybean oil, and SL. Replicated in triplicate and data combined.*

	SO (ml)	SS (µL)	PC (mg)	PC (mg ml^{-1})		Acetate Buffer [0.05 M] (ml)	SS (µL)	SL (mg)	SL (mg ml^{-1})
PC1	50	500	1	0.02	**SL1**	50	820	0.2	0.004
PC2	50	500	5	0.1	**SL2**	50	820	2	0.04
PC3	50	500	10	0.2	**SL3**	50	820	4	0.08
PC4	50	500	20	0.4	**SL4**	50	820	100	1.8

SO, soybean oil; SS, sodium silicate; PC, phosphatidylcholine; SL, soy lecithin

3.3.3 Characterisation

Scanning Electron Microscopy (SEM) was used to obtain images of the silica particles. SEM analyses were carried out on an FEI Inspect and Quanta 650, operated at either 10 or 15 kV. Each sample was adhered to a stainless-steel stub (stage) via double-sided carbon tape.

Elemental characterisation was acquired using energy-dispersive x-ray spectroscopy (EDX) on the FEI Quanta 650 instrument using Oxford Instruments INCA software. Particle diameters were determined using ImageJ image analysis software and statistical analyses were done in OriginLab OriginPro 9.0 software.

Dynamic light scattering (DLS) measurements were conducted on a Malvern Panalytical Zetasizer Nano ZSP using non-invasive backscattering (NIBS) technology. The scattering angle was set at 173° and the measurement temperature was set to 20 °C. Samples were dispersed in ethanol and sonicated to give a stable solution prior to analysis. Mean size and polydispersity index (PDI) were determined using Cumulant analysis.

X-Ray Photoelectron Spectroscopy (XPS) spectra were acquired on an Oxford Applied Research Escabase XPS 230 System equipped with a CLASS VM 100 mm mean radius

hemispherical electron energy analyser with multichannel detectors in an analysis chamber with a base pressure of 5.0×10^{-9} mbar. A pass energy of 50 eV, a step size of 0.7 eV and a dwell of 0.3 s was used for survey spectra which were swept twice. All core level scans were acquired with a step size of 0.1 eV, a dwell time of 0.1 s and a pass energy of 20 eV averaged over 10 scans. A non-monochromated Al-Kα X-ray source (1486.58 eV) at 100 W power (10 mA, 10 kV) was used for all scans. All spectra were acquired at a take-off angle of 90° with respect to the analyser axis and were charge corrected with respect to the C 1s photoelectric line at 284.8 eV. Synthetic peaks are Gaussian in shape. The relative sensitivity factors used are from a CasaXPS library containing Scofield cross-sections.

Nitrogen sorption measurements were performed on a Micromeritics TriStar II surface area analyser (Micromeritics, Norcross, GA, USA). Samples were pre-treated by heating at 200 °C under nitrogen for 12 hours. Surface area was measured using the Brunauer-Emmett-Teller (BET) method. Pore volume and pore diameter data was calculated using the Barrett, Joyner and Halenda (BJH) method. Specific surface areas were calculated from the measured relative pressure in the range of $P/P_0 = 0.01$ to $P/P_0 = 0.3$.

3.4 Results & Discussion

Molecules like CTAB, which function as SDAs in modified-Stöber processes, produce spherical silica particles by forming micelles in the reaction solvent, promoting silica condensation at the surface of the micelles. The SDA controls the rates of hydrolysis and condensation and controls the shape by adsorbing onto the surface of the growing particle.[7,42,52–54] The long-chain, hydrophobic, hydrocarbon tail group combined with the charged headgroup of CTAB permits this micellar activity. Both PC and SL contain

structural features akin to CTAB – hydrophobic, long-chain fatty acid residues, and quaternary ammonium headgroups, which are functionally similar to CTAB's head and tail groups (see **Figure 1.6**). In the same way these properties enable CTAB to form micelles in solution, PC and SL can form similar structures via bilayers.[50,55–57] To test this, we obtained DLS data of PC and SL in solution. Dynamic light scattering (DLS) was used to analyse bilayer formation of PC and SL in the reaction solvent (aqueous solution of 0.05 M acetate buffer at pH 5.92). **Figure 3.1A** shows that PC forms possible bilayer aggregates at all concentrations tested in acetate buffer solution. Increasing the concentration of PC had little effect on the structure size. At all concentrations of PC, the peak 1 mean is relatively consistent (see **Table A3.1** in section **3.7 Appendix**). Peak 2 is due to the formation of large aggregates which commonly form in biomolecule solutions. However, the effect of these large aggregates on the determination of the structure size (peak 1) is negligible at such low intensity.[58] The polydispersity index (PDI) for each concentration also did change much (see **Table A3.1** in section **3.7 Appendix**). The mean PDI for PC was 0.349.

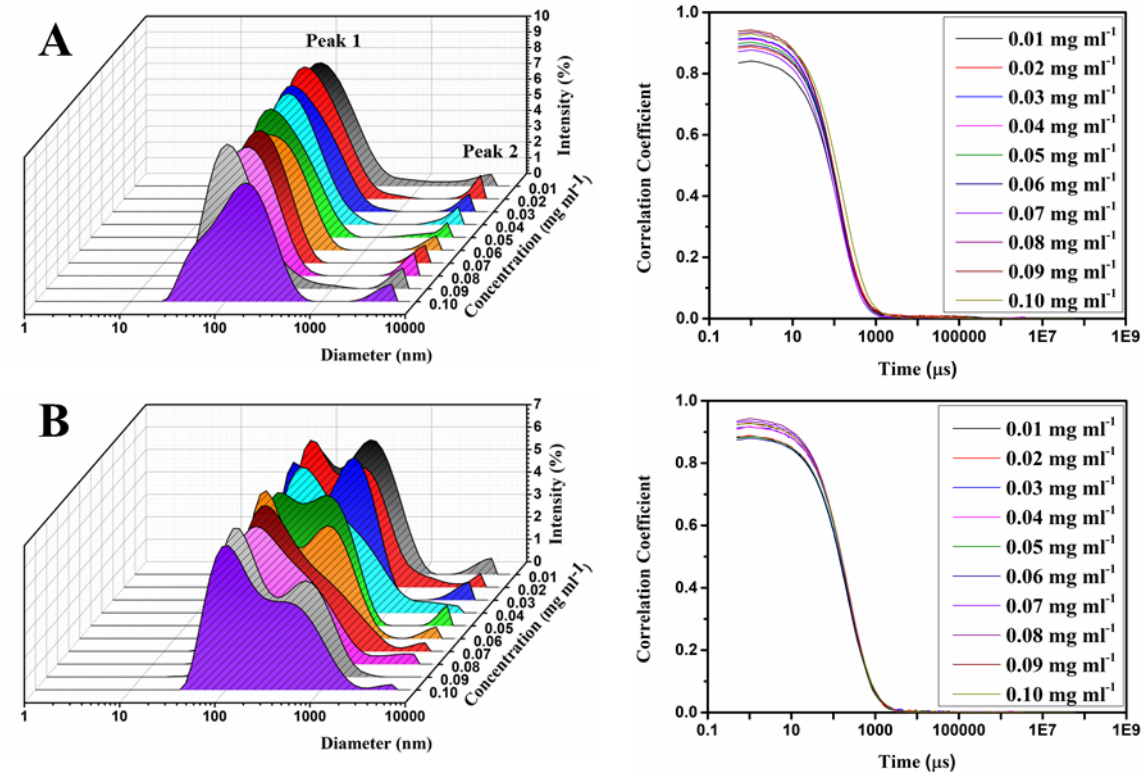


Figure 3.1 *PSD data and correlograms from DLS measurements of (a) phosphatidylcholine in acetate buffer (0.05 M, pH 5.92) and (b) soy lecithin in acetate buffer (0.05 M, pH 5.92) at various concentrations.*

Similarly, DLS data (**Figure 3.1B**) shows that SL likely forms bilayer aggregates at all concentrations tested in acetate buffer solution. The PSD for SL in acetate buffer (**Figure 3.1B**) shows a bimodal distribution which varies depending on concentration. **Table A3.1** (section **3.7 Appendix**) shows how the peak means change with concentration. The average PDI is 0.423, which is higher than for PC in the same system and the same concentrations. In fact, **Table A3.1** (section **3.7 Appendix**) shows that the PDI for SL is higher than that of PC at all concentrations. This difference in peak shape and PDI is expected because SL is less refined than PC and contains a higher number of different phospholipids. The greater variety of fatty acid chain length contributes to larger variation if the aggregate size, hence higher polydispersity. However, DLS is highly sensitive to

sample preparation techniques and the method used to analyse the method used to analyse the correlation function. Cumulant analysis, such as used here is most commonly used as it is a simple model and gives a good general estimate of the distributions. If more precise detail about the size distribution is required then more complex analysis methods such as CONTIN can be used but require that prior assumptions are made about the size distribution. However, for the purposes required here of acquiring a general estimate of the biopolymer size distributions, Cumulant analysis is sufficient.

Figure A3.1 (section **3.7 Appendix**) shows results from control experiments in which no PC or SL was used in the reaction system. In the absence of the biomolecules no spherical silica particles are formed, only unstructured monoliths. Based upon the results of these control experiments we could draw the following conclusions: (i) Spherical silica particles could not form under our proposed reaction conditions, without the presence of a structural directing agent in the reaction (ammonium hydroxide loses its structure-directing ability at this acidic pH). (ii) CTAB is known to function as a structural directing agent for formation of silica particles and the shape of the particles is influenced by the CTAB micelles along with the its quaternary ammonium headgroup.[40,41,54] PC and SL both contain quaternary ammonium headgroups similar to CTAB. As discussed earlier, the presence of these groups have been shown to be integral in biomineralisation by catalysing and directing silica formation.

3.4.1 Silica Production via Phosphatidylcholine (PC)

To test the ability of SL to form spherical silica particles in our proposed process, we first performed syntheses using PC in soybean oil and buffered solution. Lecithin is a mixture phospholipids, containing mainly PC, phosphatidylethanolamine (PE), phosphatidylinositol (PI), minor compounds such as phosphatidic acid (PA), and other substances (triglycerides, carbohydrates, etc.).[59] PC is the lecithin component most structurally similar to CTAB. PC took the place of CTAB as the structure-directing agent. Sodium silicate, which undergoes hydrolysis under acidic conditions to form $Si(OH)_4$, was used as the silica precursor, and was chosen as it is water-soluble and a close analogue to natural silicates. In dilute solutions, silicic acid undergoes polymerisation and condensation to form silica particles.[34] Zwitterionic compounds, such as PC, can electrostatically interact with the negatively charged oligomeric silicate species formed upon hydrolysis of sodium silicate. Acetate buffer was used as the catalyst for hydrolysis, in place of ammonium hydroxide. Soybean oil was used as the reaction medium, in place of ethanol, in this first experimental iteration.

Spherical particles were successfully produced using PC (**Figure 3.2**). Given the results of our control experiments without an SDA present, we can conclude that the spherical particles are due to the presence of PC in the system. At 0.02 mg ml^{-1} PC, spherical particles were observed with some agglomeration present (**Figure 3.2A**). At 0.1 mg ml^{-1} PC, spherical particles were also observed but with increased agglomeration (**Figure 3.2B**). At 0.2 mg ml^{-1} PC, spherical particles were observed with no agglomeration (**Figure 3.2C**). At 0.4 mg ml^{-1} PC, spherical particles were observed with some

agglomeration (**Figure 3.2D**). From these observations, it is clear that 0.2 mg ml^{-1} PC produced the most discrete particles.

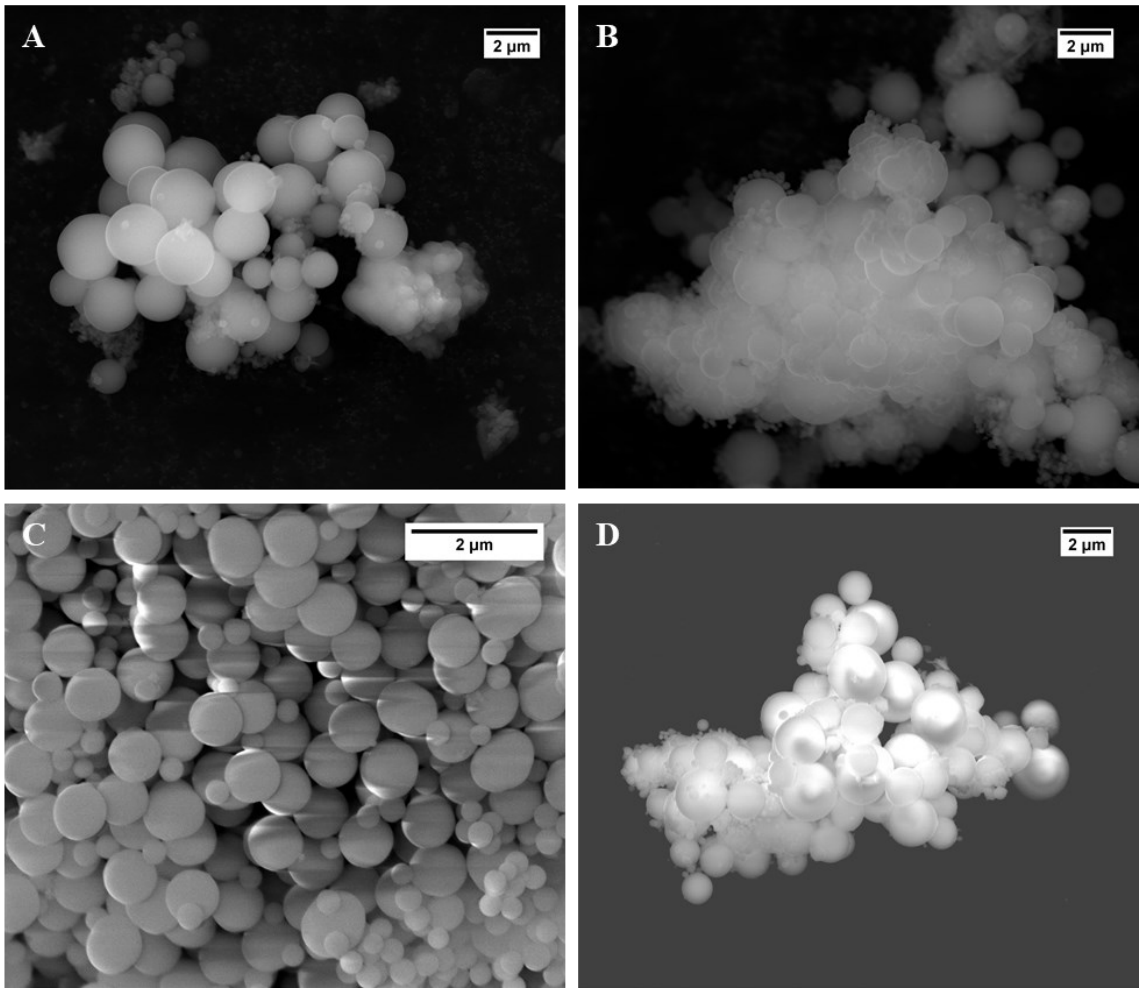


Figure 3.2 *SEM micrographs of silica particles produced using phosphatidylcholine. (a) 0.02 mg ml^{-1} PC (PC1), (b) 0.1 mg ml^{-1} PC (PC2), (c) 0.2 mg ml^{-1} PC (PC3), and (d) 0.4 mg ml^{-1} PC (PC4). All reactions done in 50 ml soybean oil with 500 µL sodium silicate at room temperature. Scale bars are 2µm.*

PSDs obtained when using PC (**Figure 3.3**) show that the silica particles formed were polydisperse (multiple peaks). **Figure 3.3A** shows a relatively broad particle size range and three distinct, widely separated, peaks at 329 nm, 1326 nm, and 2132 nm at 0.02 mg ml^{-1} PC. Note also that **Figure 3.3A** exhibits log-normal characteristics at small diameters,

indicating coalescence at 0.02 mg ml^{-1} PC. Coalescence is the fusion of smaller particles to form larger particles, resulting in a reduction in surface energy. Larger particles have a lower, stabler, more favoured energy state than smaller particles and this is what drives the process. Coalescence can be identified in the PSD by a log-normal distribution. Combination of particles of different sizes to form particles of larger size results in right-skewed distribution, *i.e.*, log-normal. Increasing PC concentration from 0.02 mg ml^{-1} to 0.1 mg ml^{-1} (**Figure 3.3B)** results in an increase in particle diameter and polydispersity, represented by an increase in number of peaks at 0.1 mg ml^{-1} PC (6 peaks) in comparison to 0.02 mg ml^{-1} PC (3 peaks). These six peaks at 0.1 mg ml^{-1} PC are at 380 nm, 557 nm, 886 nm, 1407 nm, 1730 nm, and 2232 nm. This wide range of diameters, indicates decreased morphological control, resulting in high polydispersity at 0.1 mg ml^{-1} PC. Further increasing the concentration of PC to 0.2 mg ml^{-1} sees a reduction in size range and in the number of peaks observed (3 peaks) (**Figure 3.3C**) indicating greater control of particle size at this PC concentration. These three peaks have means of 344 nm, 618 nm, and 849 nm. These peaks at 0.2 mg ml^{-1} PC are similar to those observed at 0.1 mg ml^{-1} except the peaks at the larger diameter (1407 nm, 1730 nm, and 2232 nm) disappear, suggesting that PC is exerting greater morphological control at 0.2 mg ml^{-1} than 0.1 mg ml^{-1}. Increasing PC concentration further still, to 0.4 mg ml^{-1} (**Figure 3.3D**), the number of peaks increases to four (161 nm, 299 nm, 1353 nm, and 1589 nm). However, the FWHM of these peaks also decreases significantly, indicating that the polydispersity at these peak diameters has decreased. These changes in particle size and polydispersity broadly correlate with the DLS data. **Figure A3.2** (section **3.7 Appendix**) shows how the Z-average diameter of the bilayer structure changes with concentration of PC. At 0.02 mg

ml^{-1} PC the mean diameter is 95nm, at 0.1 mg ml^{-1} it is 115nm, at 0.2 mg ml^{-1} it is also 115nm, and at 0.4 mg ml^{-1} it is 116 nm. **Figure A3.3** (section **3.7 Appendix**) shows how the PDI changes with concentration. At 0.02 mg ml^{-1} the PDI is 0.357, at 0.1 mg ml^{-1} it is 0.394, at 0.2 mg ml^{-1} it is 0.388, and at 0.4 mg ml^{-1} it is 0.397. While the Z-average diameter increases with increasing PC concentration, this increase may be a result of aggregation or flocculation of PC at higher concentrations. Accordingly, it is difficult to determine whether this has any significant effect on particle size. Though, higher concentrations of PC do seem to reduce the level of polydispersity of the particles.

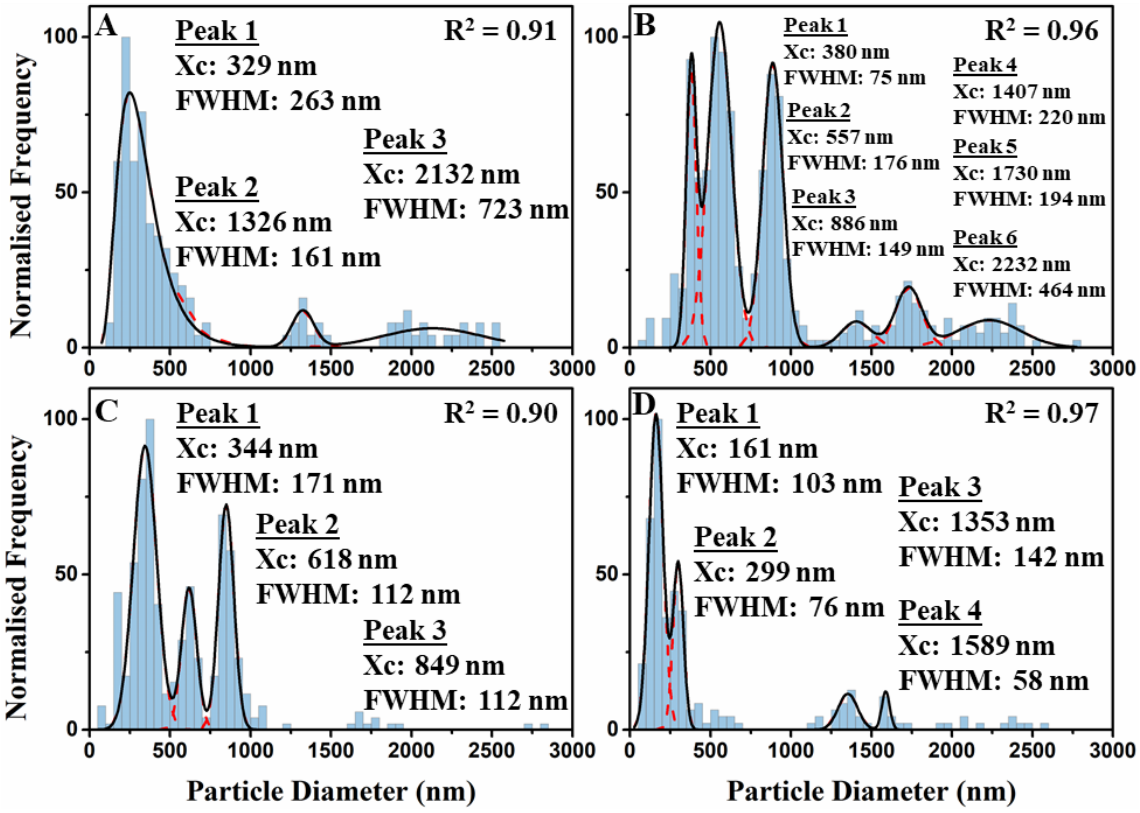


Figure 3.3 *PSDs of silica particles produced when using PC (a) 0.02 mg ml^{-1} PC (PC1), (b) 0.1 mg ml^{-1} PC (PC2), (c) 0.2 mg ml^{-1} PC (PC3), and (d) 0.4 mg ml^{-1} PC (PC4). All reactions done in 50 ml soybean oil with 500 µl sodium silicate at room temperature.*

Figure 3.3D also gives a clear indication that Ostwald ripening is occurring. The peaks on the smaller diameter side shift left, while larger particles over 1350 nm begin to emerge. Ostwald ripening is the growth of large particles at the expense of smaller particles, rather than a fusion of smaller particles, which occurs due to the unfavourably high surface energy increase associated with the phase transition from homogenous solution to solid particle.[60] In order to minimise this surface energy increase, smaller particles redissolve and reactive units (either monomers or small aggregates) diffuse to the surface of larger particles to continue growth. A mathematical description of Ostwald ripening called the *LSW model* was given by Lifshitz and Slyozov[61] and Wagner.[62] Using the precepts of this model it is possible to determine which of the growth processes, coalescence or Ostwald ripening, is the dominant one by examining PSDs.[63] Ostwald ripening occurs via the transfer of material from smaller particles to larger particles. Thus, the LSW model produces a characteristic left-skewed distribution, as seen in **Figure 3.3A**. One of the assumptions of the LSW model is that the solution is infinitely dilute. A consequence of this is that particle interaction is absent from the model and no particle greater than 1.5 times the mean particle diameter can exist. Thus, to account for particle interaction, the LSW model must be modified, and a Gaussian fit provides a better description,[60,64,65] which is precisely what we applied to our own data. Insights into the growth mechanism of silica particles can be gleaned from examination of the PSDs obtained. Post nucleation, particle growth typically occurs by Ostwald ripening and coalescence processes. There is no acute distinction between coalescence and Ostwald ripening. Both processes coexist and overlap during particle formation. By understanding how changes in experimental conditions affect particle growth processes, particularly the

extent to which coalescence or Ostwald ripening dominate, one can optimise a synthesis. Depending on which growth process dominates, the monodispersity of the final particles can be positively or negatively impacted.

One possible explanation of the data shown in **Figure 3.3** is that at low PC concentration, a mixture of coalescence and Ostwald ripening occurs, indicated by the presence of both log-normal and Gaussian peaks. However, at higher concentration, Ostwald ripening appears to become the dominant process as indicated by the presence of Gaussian peaks. The data indicate that when transitioning from a mixed (coalescence and Ostwald ripening) growth process to one dominated by Ostwald ripening, the system undergoes a brief period of instability (**Figure 3.3B**). This transition is characterised by maxima in polydispersity and particle size range. Although the spherical morphology of the particles is still maintained, indicating that PC is continuing its SDA role, the growth mechanics are not as well defined. Transition to a growth mechanism dominated by Ostwald ripening at high PC concentrations means better control of polydispersity. This is seen in the Gaussian distributions and narrow peak size (**Figure 3.3C** and **D**). As outlined above, this Gaussian distribution is preferable to a log-normal (coalescence) one that skews to larger diameter. Thus, we can possibly optimise monodispersity and size range with high PC concentration.

3.4.2 Silica Synthesis via Soy Lecithin

Next we investigated whether SL - the less refined source of PC – could function as an SDA and produce spherical particles. SL would be a more sustainable structure-directing agent to use because it requires less processing than PC. It is commonly used as a food additive and is readily available and inexpensive. Furthermore, the physicochemical

properties of SL, such as its ability to form bilayers and its structural similarities to CTAB, make it a prime candidate as an SDA in sustainable spherical silica synthesis. Based on our results with PC - the major, CTAB-like component of SL - we expected that spherical silica particles could also be formed using SL. However, in order to increase the sustainability of our process, soybean oil was no longer used as the reaction medium as its production has its own environmental costs. Instead, the ability of SL to form spherical particles in aqueous acetate buffer was investigated.

Figure 3.4 shows that spherical particles were successfully produced using SL. Given the results of our control experiments, we can conclude that the spherical particles are due to the presence of SL in the system. At 0.004 mg ml^{-1} SL, spherical particles were observed with some agglomeration present (**Figure 3.4A**). At 0.04 mg ml^{-1} SL, spherical particles were also observed with agglomeration (**Figure 3.4B**). At 0.08 mg ml^{-1} SL, spherical particles were observed with some agglomeration (**Figure 3.4C**). At 1.8 mg ml^{-1} SL, spherical particles were observed with no agglomeration (**Figure 3.4D**). From these observations, it is clear that 1.8 mg ml^{-1} SL produced the most discrete particles. It is worth noting however, that the quality of the particles is still something to be improved upon. Some non-spherical artefacts remain in the sample, therefore the PSDs were obtained by sizing the spherical particles only.

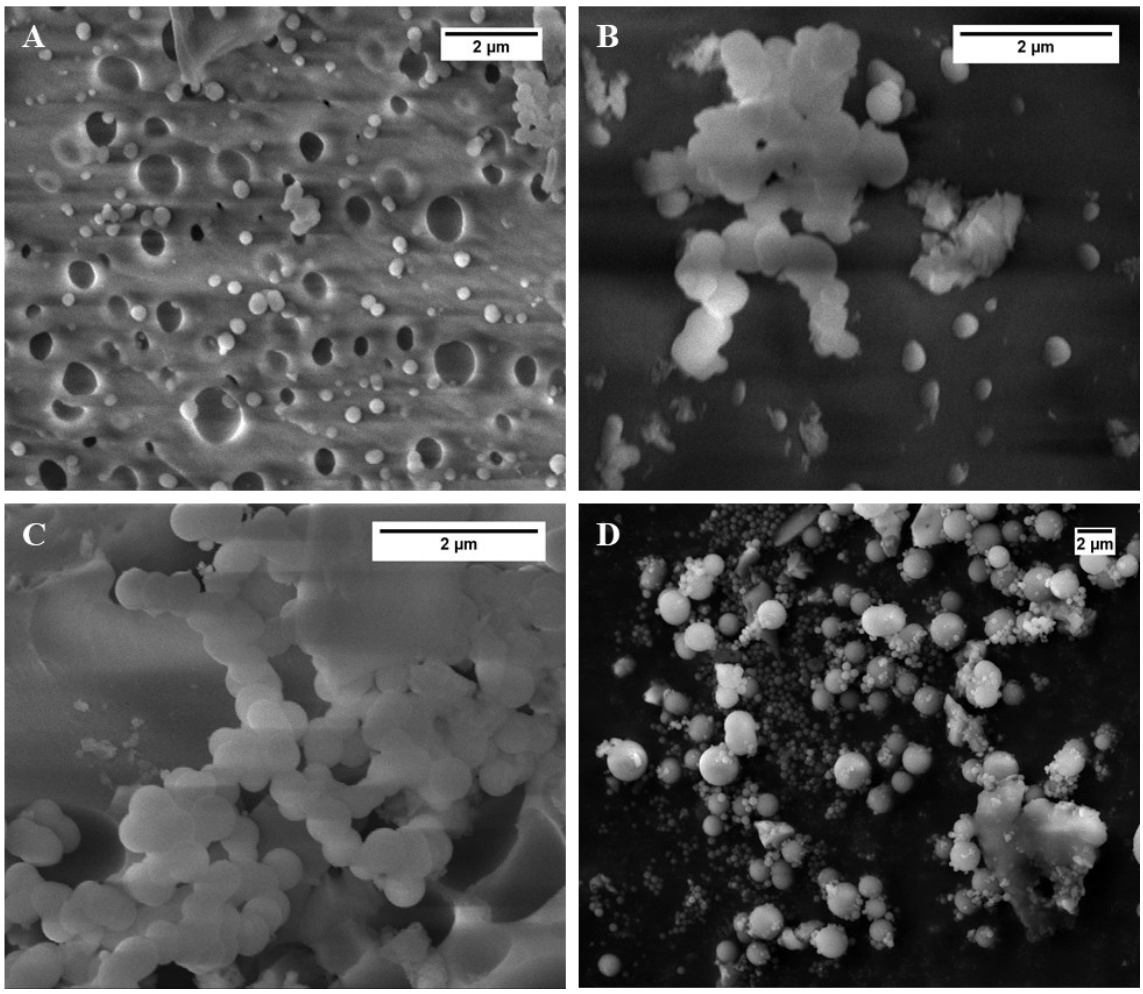


Figure 3.4 *SEM micrographs of silica particles produced when using SL with various aliquots of SL (a) 0.004 mg ml^{-1} SL (SL1), (b) 0.04 mg ml^{-1} SL (SL2), (c) 0.08 mg ml^{-1} PC (SL3), and (d) 1.8 mg ml^{-1} SL (SL4). All reactions done in 50 ml acetate buffer (0.05M, pH 5.92) with 820 µL sodium silicate at room temperature. Scale bars are 2µm. Background in (a) is carbon tape.*

PSDs of these particles were lower and had narrower size ranges, mostly below 1000 nm (**Figure 3.5**), in comparison to silica particles produced by PC. This is seen in the PSDs, where fewer peaks are present. Increasing the amount of SL from 0.004 mg ml^{-1} to 0.04 mg ml^{-1} shifts the PSD to larger diameter while also increasing the size polydispersity (**Figure 3.5A** and **B)**. **Figure 3.5A** shows a unimodal distribution with Gaussian fitting (R^2 = 0.97) with a mean particle diameter of 262 nm (0.004 mg ml^{-1} SL). **Figure 3.5B**

shows a peak with a shoulder fitted with a combination of log-normal and Gaussian curves ($R^2 = 0.75$). Fitting log-normal or Gaussian alone results in a lower R^2 value. Peak 1 has a mean of 302 nm and peak 2 has a mean of 550 nm (0.04 mg ml^{-1} SL). This suggests the onset of Ostwald ripening because there is a shift from a log-normal to a Gaussian distribution, while also resulting in a shift to larger diameter and an increase in small particles. A further increase in the amount of SL shifts the PSD to larger diameter with a decrease in polydispersity and a unimodal distribution with Gaussian fitting ($R^2 = 0.97$) with mean of 496 nm (0.08 mg ml^{-1} SL, **Figure 3.5C**). Increasing the SL concentration to 1.8 mg ml^{-1} results in two peaks with Gaussian fitting ($R^2 = 0.97$) with means 342 and 1272 nm (**Figure 3.5D**). This shift to smaller diameters and the emergence of a peak at 1272 nm suggest Ostwald ripening is taking place.[65] This trend of increasing particle size with increasing SL is similar to that seen when using PC. However, compared to the increases with PC, they are not accompanied by large increases in polydispersity, and while the particle size generally increases with SL concentration, the size range reduces to a substantially narrower range than seen for PC.

Overall, the data suggest that coalescence and Ostwald ripening are both occurring (**Figure 3.5B**). However, at higher SL concentrations the growth process transitions to one dominated by Ostwald ripening. This is comparable to the growth dynamics seen when using PC. However, the drastic transition from a mixed (coalescence and Ostwald ripening) growth process, with high polydispersity and wide particle size range, to an Ostwald ripening dominated process is not seen when using SL. This suggests that using SL grants greater control over particle growth dynamics. This is evident in the improved monodispersity of the particles produced in the SL system (**Figure 3.5**). Thus, SL

produced particles which are smaller and more size monodisperse than those produced using PC. Moreover, as observed in the PC experiments, at all concentrations of SL used spherical particles were obtained.

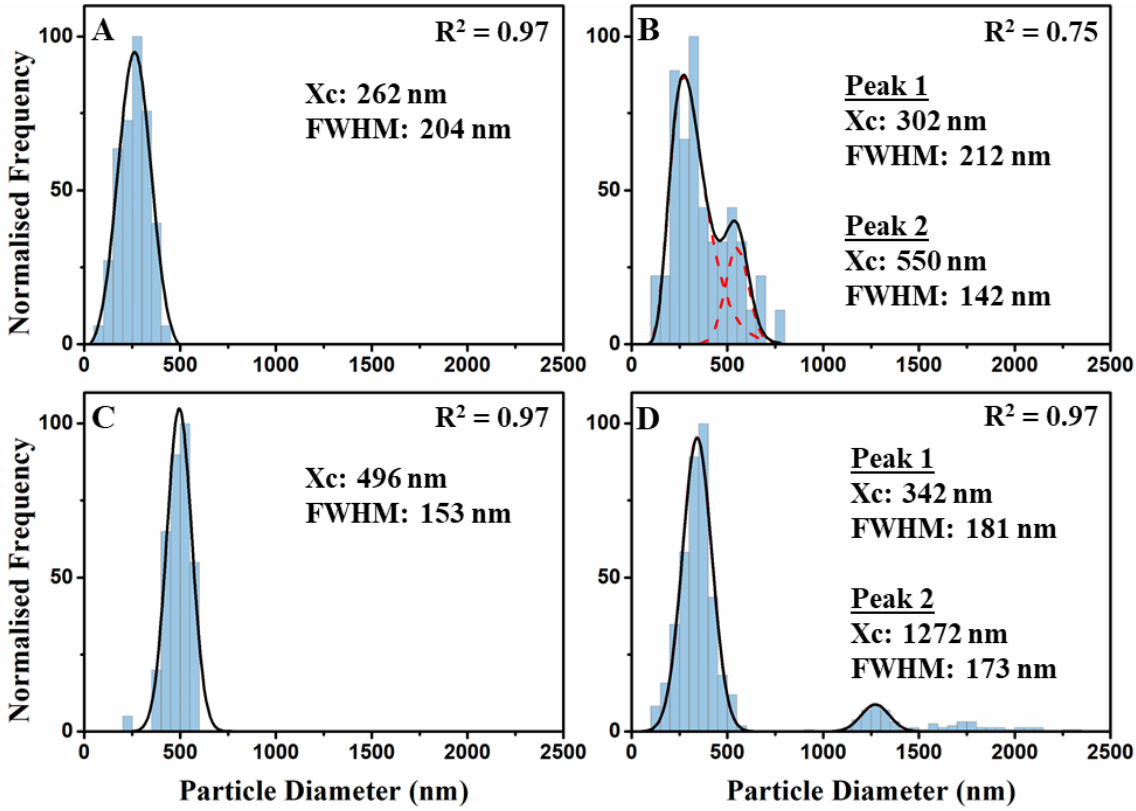


Figure 3.5 *PSDs of silica particles produced using soy lecithin (a) 0.004 mg ml^{-1} SL (SL1), (b) 0.04 mg ml^{-1} SL (SL2), (c) 0.08 mg ml^{-1} PC (SL3), and (d) 1.8 mg ml^{-1} SL (SL4). All reactions done in 50 ml acetate buffer (0.05M, pH 5.92) with 820 µL sodium silicate at room temperature.*

Figure A3.4 (section **3.7 Appendix**) shows the nitrogen sorption isotherm and the pore size distribution of silica particles prepared with 0.08 mg ml^{-1} SL (SL3). The isotherm is a Type H4 hysteresis loop, which is indicative of a mixture of both micropores and mesopores.[66] This is also confirmed in the pore size distribution, which shows pore sizes of 17 and 39 Å. Removal of CTAB post-synthesis in a typical modified-Stöber process

results in porous silica particles. Similarly, in our system, removal of SL post-synthesis also results in porosity.

Figure 3.6A(i) shows the EDX spectrograph of the spherical particles from PC2 (0.1 mg ml^{-1} PC), confirming the presence of silicon in the sample. **Figure 3.6A(ii)** shows the EDX spectrograph of the spherical particles from SL4 (1.8 mg ml^{-1} SL), confirming the presence of silicon in the sample. Oxygen and carbon peaks are also present, although these are common contaminants in EDX spectra. To confirm that these particles were SiO_2, XPS analysis was performed. **Figure 3.6B** shows the XPS spectra for PC2 (0.1 mg ml^{-1} PC). **Figure 3.6C** shows the XPS spectra for SL4 (1.8 mg ml^{-1} SL). The O 1s spectra show peaks at binding energies of 532.8 eV and 533.5 eV for PC2 (**Figure 3.6B(i)**), and 532.9 eV and 533.7 eV for SL4 (**Figure 3.6C(i)**), which correspond to Si-O-Si and Si-OH, respectively.[67–70] The small intensity peaks at 531.2 eV and 531.4 correspond to either C-O or C=O, but distinction between the two is not possible as the binding energies are closely related.[71,72] This peak is likely due to the presence of carbon contamination during the XPS analysis or small amounts of SL remaining in the particles. The sample was washed with water, ethanol, and acetone post-synthesis so that as much residual acetic acid, soybean oil, PC, and sodium acetate as possible is removed in this step. Thus, most residual carbon-containing compounds are removed from the particles. The peaks at 534.3 eV and 535.2 eV corresponds to O-H which is due to water contamination,[73] or O-H on the silica surface. The Si 2p spectra show two peaks corresponding to Si-O-Si and Si-O-H, which are indicative of SiO_2.[70,74] Overall, the EDX and XPS data confirm that the particles are made of SiO_2.

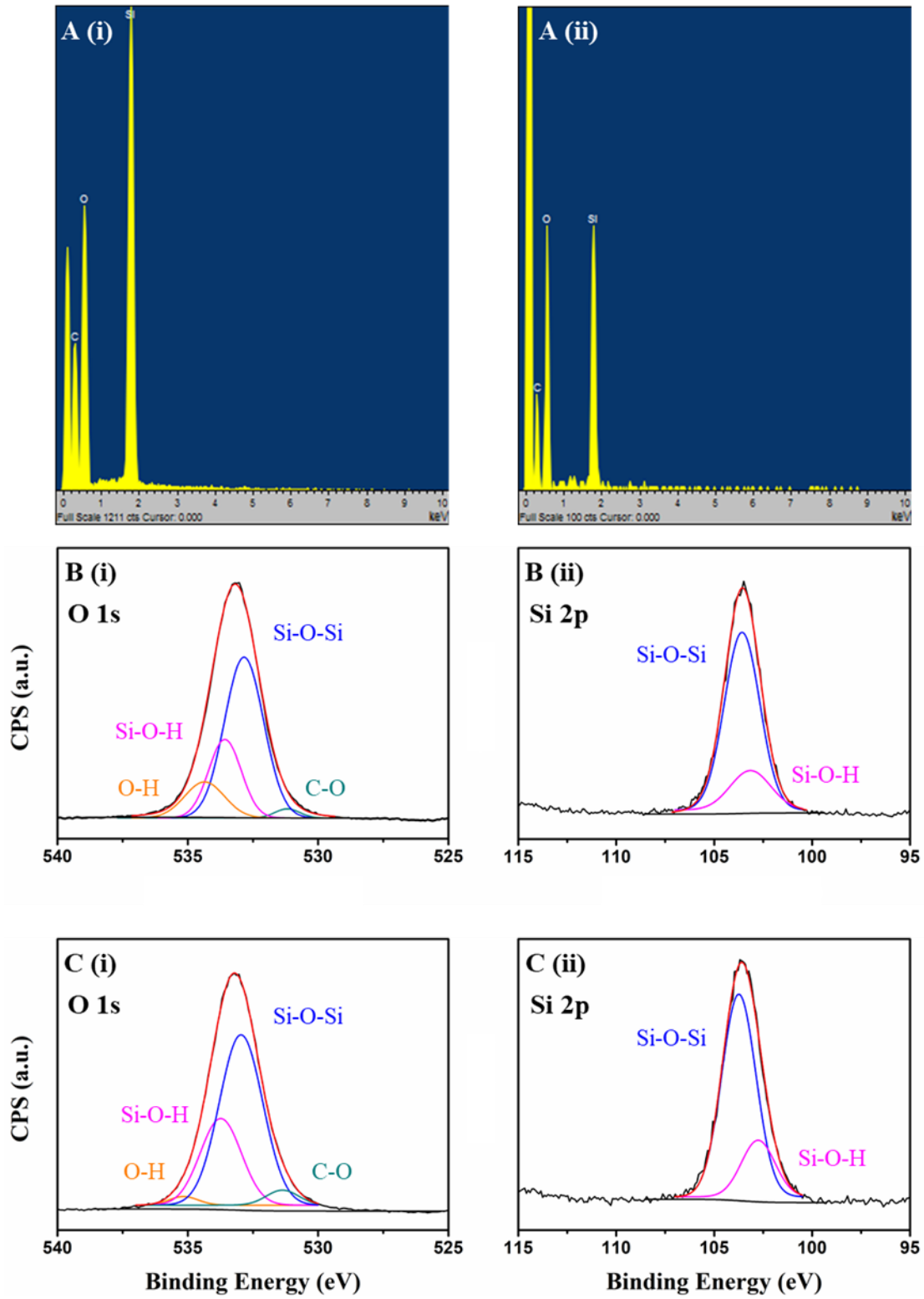


Figure 3.6 *Energy-dispersive x-ray spectra (a(i)) of PC2 (0.1 mg ml^{-1} PC), and (a(ii)) SL4 (1.8 mg ml^{-1} SL), (b) XPS spectra of O 1s and Si 2p peaks of PC2 (0.1 mg ml^{-1} PC). Red curve is the cumulative fitting, and (c) XPS spectra of O 1s and Si 2p peaks of SL4 (1.8 mg ml^{-1} SL). Red curve is the cumulative fitting.*

SL produced smaller, more size monodisperse silica particles than PC in our sustainable, biomolecule-based, modified-Stöber synthesis. Whereas the particle sizes of the silica produced using PC corelated with the DLS data for PC, the particle sizes of the silica produced when using SL did not. Based on our initial DLS data, it was expected that SL would produce larger and more polydisperse silica than PC. However, SL produced smaller and more monodisperse particles than PC. To investigate this we analysed the bilayers formed in our reaction system using SL with our silica precursor (sodium silicate) present. **Figure A3.5** (section **3.7 Appendix**) shows the temporal evolution of the mean diameter and PDI after sodium silicate addition. As time increases, the PDI decreases and the distribution becomes unimodal. The Z-average remains consistent over this time period. Our results, shown in **Figure A3.6** (section **3.7 Appendix**), show that the presence of sodium silicate reduced the size of the SL bilayer structures while also narrowing their size distribution. One possible explanation for this is that the sodium ions from the sodium silicate co-localise with the ester moeity of the phospholipids.[75] This penetration of the sodium ion into the headgoup double layer causes enhances the attractive forces between the headgroups, likely leading to a change in curvature and reduction in size. This effect is likely happening in the PC system also, but to a lesser extent as there is little difference between the particle sizes observed with PC and the bilayer structure size of PC without sodium silicate. Addition of sodium silicate to SL in acetate buffer results in a smaller bilayer structure size than without sodium silicate, precisely as seen in our DLS data, which in turn results in a smaller than initially anticipated silica particle size.

The reason PC and SL are effective at producing spherical silica, is because modified-Stöber processes have been developed using long-chain quaternary ammonium

surfactants, of which CTAB is an example.[52,76] SL's mixture of phospholipids (specifically PC) possessing quaternary ammonium cations and fatty acid residues, allow both SL and PC to behave like CTAB. Further understanding of the efficacy of our chosen biomolecules in modified-Stöber silica syntheses can be derived from studying natural silica formation. In diatoms, long-chain polyamines (LCPAs) and proteins such as silaffins and silacidins have been shown to be integral to silica formation. The LCPAs typically have a quaternary ammonium group and have been shown to have direct involvement in the structure-directing step in the biomineralisation process.[77] Silaffins are proteins which possess these LCPAs and also have a high degree of phosphorylation and quaternary ammonium structures. Indeed, phosphorylation present in silaffins has been shown to be intimately involved in the biomineralisation process, promoting silica polymerisation through electrostatic and hydrogen-bonding interactions.[78] These proteins bear similar structures to PC and SL.[44] These similarities are likely the reason PC and SL can form spherical silica particles in our system. Furthermore, silaffins and silacidins have been shown to induce silica polymerisation under acidic conditions in vitro.[44,79] To have the ability to both induce silica polymerisation (nucleation) and control its final structure (growth) means the catalyst typically required in the modified-Stöber synthesis is no longer required. The biomolecules, PC and SL, in our synthesis also have this functionality.

Regardless of the growth process, the monodispersity of the final sample is most important. Monodisperse particles are needed for advanced applications such as chromatography and drug delivery. A useful numerical descriptor of monodispersity is relative standard deviation (RSD) The lower this number, the more monodisperse the

particles. **Table 3.2** shows a comparison of the best RSD of our results (SL3; 0.08 mg ml^{-1} SL) to twelve other studies which explicitly state they have prepared monodisperse, spherical silica particles, using traditional syntheses, and three studies using biomolecules to produce silica. Other studies that synthesised silica particles biomimetically using simple molecules such as amino acids and polyamines were not included, as a direct comparison between studies that use more complex biomolecules is prudent. The lowest RSD seen was 1.2 % and the highest was 59.8 %. Our RSD value of 13.1 % compares favourably with the monodispersity of silica particles prepared with traditional methods in the literature. All of the biomolecule-based silica syntheses produced non-spherical particles and did not give any standard deviations, thus RSD calculation was not possible. The particles produced using our method are among the most monodisperse and discrete silica particles produced using biomolecules in a simple templated approach.

Table 3.2 *Comparison of SL3 (0.08 mg ml^{-1}) monodispersity with literature. The RSD was taken from the studies, where given, or calculated from the given mean particle diameter and standard deviation. Where multiple results are given, the range of RSD is shown.*

Production Process	SDA[a]	Particle Size (nm)	RSD (%)	Refs.
Biopolymer-based	Soy lecithin	496	13.1	This study
Biopolymer-based	Gelatin	Non-spherical	Non-spherical	[33]
Biopolymer-based	BSA/lysozyme	50 – 200/non-spherical	No data/non-spherical	[34]
Biopolymer-based	Lysine/arginine	< 100	Non-spherical/agglomerated	[35]
Modified-Stöber	CTAB	223 – 303	5.4 – 12	[80]
Modified-Stöber	CTAB	450	4	[81]
	DTAB	700	10	
Modified-Stöber	CTAB	37 – 130	3.5 – 29	[82]
Modified-Stöber	CTAB	100 – 1470	3.1 – 45.9	[83]
	DTAB	20 – 360	Non-spherical	
		471	22.4	
Stöber	Ethanolamine	122.4	6.1	[84]
Stöber	NH_3	10.2 – 236.4	1.7 – 59.8	[85]
Stöber	NH_3	27 – 96	7.8 – 13.3	[86]
Stöber	NH_3	15	9.3	[87]
	n-propylamine	13	11.5	
	n-butylamine	12 – 21	7.6 – 11.7	
Modified-Stöber	CTAC	21 – 111	7 – 14.8	[88]
Stöber	NH_3	100 – 870	1.2 – 18.2	[89]
Stöber	NH_3	51 – 769	3.5 – 12.9	[90]
Stöber	NH_3	245	11.4	[91]
	Diethanolamine	186	15.6	
	Triethanolamine	82	23.2	

[a]SDA, structure-directing agent; BSA, bovine serum albumin; CTAB, cetyltrimethylammonium bromide; DTAB, decyltrimethylammonium bromide; CTAC, Hexadecyltrimethylammonium chloride.

3.5 Conclusion

Biomolecules with physicochemical characteristics akin to compounds like CTAB that are traditionally used as structural directing agents (SDAs) in modified-Stöber processes, can produce small, spherical, monodisperse silica particles. Our syntheses are more environmentally sustainable than these processes. CTAB (a synthetic, amphiphilic surfactant), ethanol, and ammonium hydroxide were replaced in a modified-Stöber silica synthesis with less toxic, more sustainable equivalents: the biomolecules phosphatidylcholine (PC) or soy lecithin (SL); from a waste source, buffered water (plus soybean oil for PC), and acetate buffer respectively. PC and SL can function as SDAs in the synthesis of spherical silica particles. Long-chain polyamines and proteins, such as silaffins and silacidins are integral to silica formation in the natural silica biomineralisation processes of organisms like diatoms. SL and PC bear close similarities to these diatom biomolecules. Furthermore, the physicochemical similarities that PC and SL have with CTAB, allows them to function as substitutes for CTAB in our synthesis. A mixture of Ostwald ripening and coalescence was shown to occur at low biomolecule concentrations, while transitioning to an Ostwald ripening dominated process at high biomolecule concentrations. Higher biomolecule concentrations also tended to increase particle size. The data show that SL gives much greater control over particle size and morphology and produces smaller, more monodisperse silica particles than using PC. This emphasises the progress our research represents in harnessing biomineralisation processes for producing small, monodisperse, spherical silica particles. Our silica is among the best produced from biopolymers seen in the literature to date – it is spherical, discrete, statistically analysed, and has comparable monodispersity to silica prepared using

Stöber/modified-Stöber processes. Preliminary results also show that porosity can be achieved using these biomolecule-based syntheses, although further work is needed to optimise this. Our process is a significant step forward in evolving the traditional methods of silica manufacturing - an inherently unsustainable and environmentally damaging process - into one that is sustainable and environmentally benign. We have shown that not only can spherical silica particles be prepared using more environmentally benign and sustainable conditions along with PC and SL, but also that a much higher degree of control over the morphology and monodispersity can be achieved than has been reported previously using such systems.

3.6 References

1. Narayanan, R. & El-Sayed, M. A. Effect of catalysis on the stability of metallic nanoparticles: Suzuki reaction catalyzed by PVP-palladium nanoparticles. *J. Am. Chem. Soc.* **125**, 8340–8347 (2003) DOI: 10.1021/ja035044x.
2. Miyake, Y., Hanaeda, M. & Asada, M. Separation of organic compounds by spherical mesoporous silica prepared from W/O microemulsions of tetrabutoxysilane. *Ind. Eng. Chem. Res.* **46**, 8152–8157 (2007) DOI: 10.1021/ie0705047.
3. Brown, P. R. High-performance liquid chromatography. Past developments, present status, and future trends. *Anal. Chem.* **62**, 995A-1008A (1990) DOI: 10.1021/ac00218a001.
4. Pagliaro, M. *Silica Based Material for Advanced Chemical Applications*. (2009).
5. Slowing, I. I., Vivero-Escoto, J. L., Wu, C.-W. & Lin, V. S.-Y. Y. Mesoporous silica nanoparticles as controlled release drug delivery and gene transfection carriers. *Adv. Drug Deliv. Rev.* **60**, 1278–1288 (2008) DOI: 10.1016/j.addr.2008.03.012.
6. Hanrahan, J. P., Donovan, A., Morris, M. A. & Holmes, J. D. Synthesis and swelling of large pore diameter mesoporous silica spheres. *J. Mater. Chem.* **17**, 3881 (2007) DOI: 10.1039/b705023b.
7. Keane, D. A., Hanrahan, J. P., Copley, M. P., Holmes, J. D. & Morris, M. A. A modified Stöber process for the production of mesoporous Sub 2 micron silica microspheres; applications in HPLC. *J. Porous Mater.* **17**, 145–152 (2010) DOI: 10.1007/s10934-009-9274-7.

8. Homes, Justin; Morris, Michael; Hanrahan, John; Keane, Donal; Copley, M. A method for synthesising porous silica microparticles PCT WO 2009/010945. (2008).

9. Isomaa, B., Reuter, J. & Djupsund, B. M. The subacute and chronic toxicity of cetyltrimethylammonium bromide (CTAB), a cationic surfactant, in the rat. *Arch. Toxicol.* **35**, 91–96 (1976) DOI: 10.1007/BF00372762.

10. Nałęcz-Jawecki, G., Grabińska-Sota, E. & Narkiewicz, P. The toxicity of cationic surfactants in four bioassays. *Ecotoxicol. Environ. Saf.* **54**, 87–91 (2003) DOI: 10.1016/S0147-6513(02)00025-8.

11. Capello, C., Fischer, U. & Hungerbühler, K. What is a green solvent? A comprehensive framework for the environmental assessment of solvents. *Green Chem.* **9**, 927–934 (2007) DOI: 10.1039/b617536h.

12. Mann, S. *Biomineralization: Principles and Concepts in Bioinorganic Materials Chemistry*. (Oxford University Press, 2001).

13. Chen, Y. *et al.* Biomineralization Forming Process and Bio-inspired Nanomaterials for Biomedical Application: A Review. *Minerals* **9**, 68 (2019) DOI: 10.3390/min9020068.

14. Mann, S. *et al.* Crystallization at Inorganic-organic Interfaces: Biominerals and Biomimetic Synthesis. *Science (80-.).* **261**, 1286–1292 (1993) DOI: 10.1126/science.261.5126.1286.

15. Baccile, N., Babonneau, F., Thomas, B. & Coradin, T. Introducing ecodesign in silica sol–gel materials. *J. Mater. Chem.* **19**, 8537 (2009) DOI: 10.1039/b911123a.

16. Piletska, E. *et al.* Biomimetic Silica Nanoparticles Prepared by a Combination of

Solid-Phase Imprinting and Ostwald Ripening. *Sci. Rep.* **7**, 11537 (2017) DOI: 10.1038/s41598-017-12007-0.

17. Patwardhan, S. V., Mukherjee, N., Steinitz-Kannan, M. & Clarson, S. J. Bioinspired synthesis of new silica structures. *Chem. Commun.* **3**, 1122–1123 (2003) DOI: 10.1039/b302056h.
18. Kröger, N., Deutzmann, R., Bergsdorf, C. & Sumper, M. Species-specific polyamines from diatoms control silica morphology. *Proc. Natl. Acad. Sci.* **97**, 14133–14138 (2000) DOI: 10.1073/pnas.260496497.
19. Kröger, N., Deutzmann, R. & Sumper, M. Silica-precipitating peptides from diatoms: The chemical structure of silaffin-1A from Cylindrotheca fusiformis. *J. Biol. Chem.* **276**, 26066–26070 (2001) DOI: 10.1074/jbc.M102093200.
20. Sumper, M. & Kröger, N. Silica formation in diatoms: The function of long-chain polyamines and silaffins. *J. Mater. Chem.* **14**, 2059–2065 (2004) DOI: 10.1039/b401028k.
21. Lopez, P., Gautier, C., Livage, J. & Coradin, T. Mimicking Biogenic Silica Nanostructures Formation. *Curr. Nanosci.* **1**, 73–83 (2006) DOI: 10.2174/1573413052953156.
22. Sumper, M., Lorenz, S. & Brunner, E. Biomimetic Control of Size in the Polyamine-Directed Formation of Silica Nanospheres. *Angew. Chemie - Int. Ed.* **42**, 5192–5195 (2003) DOI: 10.1002/anie.200352212.
23. Pamirsky, I. E. & Golokhvast, K. S. Silaffins of diatoms: From applied biotechnology to biomedicine. *Mar. Drugs* **11**, 3155–3167 (2013) DOI: 10.3390/md11093155.

24. Wallace, A. F., DeYoreo, J. J. & Dove, P. M. Kinetics of silica nucleation on carboxyl- and amine-terminated surfaces: Insights for biomineralization. *J. Am. Chem. Soc.* **131**, 5244–5250 (2009) DOI: 10.1021/ja809486b.

25. Brumlik, M. J. & Buckley, J. T. Identification of the catalytic triad of the lipase/acyltransferase from Aeromonas hydrophila. *J. Bacteriol.* **178**, 2060–2064 (1996) DOI: 10.1128/jb.178.7.2060-2064.1996.

26. Ekici, Ö. D., Paetzel, M. & Dalbey, R. E. Unconventional serine proteases: Variations on the catalytic Ser/His/Asp triad configuration. *Protein Sci.* **17**, 2023–2037 (2008) DOI: 10.1110/ps.035436.108.

27. Kuno, T., Nonoyama, T., Hirao, K. & Kato, K. Influence of the charge relay effect on the silanol condensation reaction as a model for silica biomineralization. *Langmuir* **27**, 13154–13158 (2011) DOI: 10.1021/la202576v.

28. Carcouët, C. C. M. C. *et al.* Nucleation and Growth of Monodisperse Silica Nanoparticles. *Nano Lett.* **14**, 1433–1438 (2014) DOI: 10.1021/nl404550d.

29. Tilburey, G. E., Blundell, T. J., Argent, S. P. & Perry, C. C. Azamacrocycles and tertiary amines can be used to form size tuneable hollow structures or monodisperse oxide nanoparticles depending on the 'M' source. *Dalt. Trans.* **48**, 15470–15479 (2019) DOI: 10.1039/c9dt02080b.

30. Masse, S. *et al.* Modification of the stöber process by a polyazamacrocycle leading to unusual core-shell silica nanoparticles. *Langmuir* **24**, 4026–4031 (2008) DOI: 10.1021/la703828v.

31. Demadis, K. D., Pachis, K., Ketsetzi, A. & Stathoulopoulou, A. Bioinspired control of colloidal silica in vitro by dual polymeric assemblies of zwitterionic

phosphomethylated chitosan and polycations or polyanions. *Adv. Colloid Interface Sci.* **151**, 33–48 (2009) DOI: 10.1016/j.cis.2009.07.005.

32. Gautier, C. *et al.* Biomimetic dual templating of silica by polysaccharide/protein assemblies. *Colloids Surfaces B Biointerfaces* **65**, 140–145 (2008) DOI: 10.1016/j.colsurfb.2008.03.005.

33. Jia, J., Zhou, X., Caruso, R. A. & Antonietti, M. Synthesis of Microporous Silica Templated by Gelatin. *Chem. Lett.* **33**, 202–203 (2004) DOI: 10.1246/cl.2004.202.

34. Coradin, T., Coupé, A. & Livage, J. Interactions of bovine serum albumin and lysozyme with sodium silicate solutions. *Colloids Surfaces B Biointerfaces* **29**, 189–196 (2003) DOI: 10.1016/S0927-7765(02)00208-4.

35. Coradin, T., Durupthy, O. & Livage, J. Interactions of amino-containing peptides with sodium silicate and colloidal silica: A biomimetic approach of silicification. *Langmuir* vol. 18 2331–2336 (2002) DOI: 10.1021/la011106q.

36. Patwardhan, S. V. & Clarson, S. J. Silicification and biosilicification. *Silicon Chem.* 207–214 (2002).

37. Belton, D., Paine, G., Patwardhan, S. V. & Perry, C. C. Towards an understanding of (bio)silicification: the role of amino acids and lysine oligomers in silicification. *J. Mater. Chem.* **14**, 2231 (2004) DOI: 10.1039/b401882f.

38. Patwardhan, S. V., Clarson, S. J. & Perry, C. C. On the role(s) of additives in bioinspired silicification. *Chem. Commun.* 1113 (2005) doi:10.1039/b416926c DOI: 10.1039/b416926c.

39. Goretsky, A. V., Beck, L. W., Zones, S. I. & Davis, M. E. Influence of the hydrophobic character of structure-directing agents for the synthesis of pure-silica

zeolites. *Microporous Mesoporous Mater.* **28**, 387–393 (1999) DOI: 10.1016/S1387-1811(98)00307-2.

40. Alothman, Z. A Review: Fundamental Aspects of Silicate Mesoporous Materials. *Materials (Basel).* **5**, 2874–2902 (2012) DOI: 10.3390/ma5122874.

41. Büchel, G., Grün, M., Unger, K. K., Matsumoto, A. & Kazuo, T. Tailored syntheses of nanostructured silicas: Control of particle morphology, particle size and pore size. *Supramol. Sci.* **5**, 253–259 (1998) DOI: 10.1016/S0968-5677(98)00016-9.

42. Slowing, I. I., Vivero-Escoto, J. L., Trewyn, B. G. & Lin, V. S.-Y. Mesoporous silica nanoparticles: structural design and applications. *J. Mater. Chem.* **20**, 7924 (2010) DOI: 10.1039/c0jm00554a.

43. Wan, Y. & Zhao, D. On the controllable soft-templating approach to mesoporous silicates. *Chem. Rev.* **107**, 2821–2860 (2007) DOI: 10.1021/cr068020s.

44. Kröger, N., Lorenz, S., Brunner, E. & Sumper, M. Self-Assembly of Highly Phosphorylated Silaffins and Their Function in Biosilica Morphogenesis. *Science (80-.).* **298**, 584–586 (2014) DOI: 10.1126/science.1076221.

45. Yokoi, T. *et al.* Mechanism of formation of uniform-sized silica nanospheres catalyzed by basic amino acids. *Chem. Mater.* **21**, 3719–3729 (2009) DOI: 10.1021/cm900993b.

46. Belton, D. J., Patwardhan, S. V., Annenkov, V. V., Danilovtseva, E. N. & Perry, C. C. From biosilicification to tailored materials: Optimizing hydrophobic domains and resistance to protonation of polyamines. *Proc. Natl. Acad. Sci.* **105**, 5963–5968 (2008) DOI: 10.1073/pnas.0710809105.

47. Mizutani, T., Nagase, H., Fujiwara, N. & Ogoshi, H. Silicic Acid Polymerization

Catalyzed by Amines and Polyamines. *Bull. Chem. Soc. Jpn.* **71**, 2017–2022 (1998) DOI: 10.1246/bcsj.71.2017.

48. Delak, K. M. & Sahai, N. Amine-Catalyzed Biomimetic Hydrolysis and Condensation of Organosilicate. *Chem. Mater.* **17**, 3221–3227 (2005) DOI: 10.1021/cm048355v.

49. Masse, S., Laurent, G. & Coradin, T. Influence of cyclic polyamines on silica formation during the Stöber process. *Phys. Chem. Chem. Phys.* **11**, 10204–10210 (2009) DOI: 10.1039/b915428k.

50. Galarneau, A. *et al.* Synthesis of sponge mesoporous silicas from lecithin/dodecylamine mixed-micelles in ethanol/water media: A route towards efficient biocatalysts. *Microporous Mesoporous Mater.* **104**, 103–114 (2007) DOI: 10.1016/j.micromeso.2007.01.017.

51. Chung, C., Sher, A., Rousset, P. & McClements, D. J. Impact of Electrostatic Interactions on Lecithin-Stabilized Model O/W Emulsions. *Food Biophys.* **13**, 292–303 (2018) DOI: 10.1007/s11483-018-9535-6.

52. Möller, K. & Bein, T. Talented Mesoporous Silica Nanoparticles. *Chem. Mater.* acs.chemmater.6b03629 (2016) doi:10.1021/acs.chemmater.6b03629 DOI: 10.1021/acs.chemmater.6b03629.

53. Anderson, M. T., Martin, J. E., Odinek, J. G. & Newcomer, P. P. Effect of methanol concentration on CTAB micellization and on the formation of surfactant-templated silica (STS). *Chem. Mater.* **10**, 1490–1500 (1998) DOI: 10.1021/cm970240m.

54. Yi, Z. *et al.* A New Insight into Growth Mechanism and Kinetics of Mesoporous Silica Nanoparticles by in Situ Small Angle X-ray Scattering. *Langmuir* **31**, 8478–

8487 (2015) DOI: 10.1021/acs.langmuir.5b01637.

55. Murdan, S. A review of pluronic lecithin organogel as a topical and transdermal drug delivery system. *Hosp. Pharm.* **12**, 267–270 (2005).

56. Shaikh, I., Jadhav, K., Gide, P., Kadam, V. & Pisal, S. Topical Delivery of Aceclofenac from Lecithin Organogels: Preformulation Study. *Curr. Drug Deliv.* **3**, 417–427 (2006) DOI: 10.2174/156720106778559010.

57. Cabezas, D. M., Diehl, B. W. K. & Tomás, M. C. Emulsifying properties of hydrolysed and low HLB sunflower lecithin mixtures. *Eur. J. Lipid Sci. Technol.* **118**, 975–983 (2016) DOI: 10.1002/ejlt.201500182.

58. Lorber, B., Fischer, F., Bailly, M., Roy, H. & Kern, D. Protein analysis by dynamic light scattering: Methods and techniques for students. *Biochem. Mol. Biol. Educ.* **40**, 372–382 (2012) DOI: 10.1002/bmb.20644.

59. Cabezas, D. M., Diehl, B. W. K. & Tomás, M. C. Sunflower lecithin: Application of a fractionation process with absolute ethanol. *JAOCS, J. Am. Oil Chem. Soc.* **86**, 189–196 (2009) DOI: 10.1007/s11746-008-1336-5.

60. Santos, J., Calero, N., Trujillo-Cayado, L. A., Garcia, M. C. & Muñoz, J. Assessing differences between Ostwald ripening and coalescence by rheology, laser diffraction and multiple light scattering. *Colloids Surfaces B Biointerfaces* **159**, 405–411 (2017) DOI: 10.1016/j.colsurfb.2017.08.015.

61. Lifshitz, I. M. & Slyozov, V. V. The kinetics of precipitation from supersaturated solid solutions. *J. Phys. Chem. Solids* **19**, 35–50 (1961) DOI: 10.1016/0022-3697(61)90054-3.

62. Wagner, C. Theorie der Alterung von Niederschlägen durch Umlösen (Ostwald-

Reifung). *Berichte der Bunsengesellschaft für Phys. Chemie* **65**, 581–591 (1961) DOI: 10.1002/BBPC.19610650704.

63. Banta, R. A. *et al.* Nanopatterned protein-polysaccharide thin films by humidity regulated phase separation. *J. Colloid Interface Sci.* **532**, (2018) DOI: 10.1016/j.jcis.2018.07.109.

64. Ma, Y. & Ardell, A. J. Coarsening of γ (Ni–Al solid solution) precipitates in a γ′ (Ni3Al) matrix. *Acta Mater.* **55**, 4419–4427 (2007) DOI: 10.1016/j.actamat.2007.04.008.

65. Lotty, O. *et al.* Self-seeded growth of germanium nanowires: Coalescence and ostwald ripening. *Chem. Mater.* **25**, 215–222 (2013) DOI: 10.1021/cm3032863.

66. Thommes, M. Physical Adsorption Characterization of Nanoporous Materials. *Chemie Ing. Tech.* **82**, 1059–1073 (2010) DOI: 10.1002/cite.201000064.

67. Himpsel, F. J., McFeely, F. R., Taleb-Ibrahimi, A., Yarmoff, J. A. & Hollinger, G. Microscopic structure of the SiO2/Si interface. *Phys. Rev. B* **38**, 6084–6096 (1988) DOI: 10.1103/PhysRevB.38.6084.

68. Hollinger, G. & Himpsel, F. J. Probing the transition layer at the SiO 2 -Si interface using core level photoemission. *Appl. Phys. Lett.* **44**, 93–95 (1984) DOI: 10.1063/1.94565.

69. Gustus, R. *et al.* Decomposition of amorphous Si2C by thermal annealing. *Thin Solid Films* **552**, 232–240 (2014) DOI: 10.1016/j.tsf.2013.12.033.

70. Post, P., Wurlitzer, L., Maus-Friedrichs, W. & Weber, A. Characterization and Applications of Nanoparticles Modified in-Flight with Silica or Silica-Organic Coatings. *Nanomaterials* **8**, 530 (2018) DOI: 10.3390/nano8070530.

71. Sadri, R. *et al.* A bio-based, facile approach for the preparation of covalently functionalized carbon nanotubes aqueous suspensions and their potential as heat transfer fluids. *J. Colloid Interface Sci.* **504**, 115–123 (2017) DOI: 10.1016/j.jcis.2017.03.051.

72. Wang, Q. *et al.* Fluorescent carbon dots as an efficient siRNA nanocarrier for its interference therapy in gastric cancer cells. *J. Nanobiotechnology* **12**, 58 (2014) DOI: 10.1186/s12951-014-0058-0.

73. Bebensee, F., Voigts, F. & Maus-Friedrichs, W. The adsorption of oxygen and water on Ca and CaO films studied with MIES, UPS and XPS. *Surf. Sci.* **602**, 1622–1630 (2008) DOI: 10.1016/j.susc.2008.02.011.

74. Yang, H.-W., Kang, N., Myung, S.-T., Kim, J. & Kim, S.-J. Exceptional Effect of Benzene in Uniform Carbon Coating of SiO x Nanocomposite for High-Performance Li-Ion Batteries. *J. Electrochem. Soc.* **165**, A1247–A1253 (2018) DOI: 10.1149/2.0291807jes.

75. Le, C. T. M., Houri, A., Balage, N., Smith, B. J. & Mechler, A. Interaction of Small Ionic Species With Phospholipid Membranes: The Role of Metal Coordination. *Front. Mater.* **5**, (2019) DOI: 10.3389/fmats.2018.00080.

76. Prasomsri, T., Jiao, W., Weng, S. Z. & Garcia Martinez, J. Mesostructured zeolites: bridging the gap between zeolites and MCM-41. *Chem. Commun.* **51**, 8900–8911 (2015) DOI: 10.1039/C4CC10391B.

77. Lechner, C. C. & Becker, C. F. W. Silaffins in silica biomineralization and biomimetic silica precipitation. *Mar. Drugs* **13**, 5297–5333 (2015) DOI: 10.3390/md13085297.

78. Sprenger, K. G., Prakash, A., Drobny, G. & Pfaendtner, J. Investigating the Role of Phosphorylation in the Binding of Silaffin Peptide R5 to Silica with Molecular Dynamics Simulations. *Langmuir* **34**, 1199–1207 (2018) DOI: 10.1021/acs.langmuir.7b02868.

79. Wenzl, S., Hett, R., Richthammer, P. & Sumper, M. Silacidins: Highly acidic phosphopeptides from diatom shells assist in silica precipitation in vitro. *Angew. Chemie - Int. Ed.* **47**, 1729–1732 (2008) DOI: 10.1002/anie.200704994.

80. Luo, L., Liang, Y., Erichsen, E. S. & Anwander, R. Monodisperse mesoporous silica nanoparticles of distinct topology. *J. Colloid Interface Sci.* **495**, 84–93 (2017) DOI: 10.1016/j.jcis.2017.01.107.

81. Stovpiaga, E. Y., Kurdyukov, D. A., Kukushkina, Y. A., Sokolov, V. V. & Yagovkina, M. A. Monodisperse spherical silica particles with controlled-varied diameter of micro- and mesopores. *Glas. Phys. Chem.* **41**, 316–323 (2015) DOI: 10.1134/S1087659615030153.

82. Zhao, Z. *et al.* Facile, low-cost, and scalable fabrication of particle size and pore structure tuneable monodisperse mesoporous silica nanospheres as supports for advanced solid acid catalysts. *RSC Adv.* **6**, 9072–9081 (2016) DOI: 10.1039/c5ra26432d.

83. Trofimova, E. Y. *et al.* Monodisperse spherical mesoporous silica particles: Fast synthesis procedure and fabrication of photonic-crystal films. *Nanotechnology* **24**, (2013) DOI: 10.1088/0957-4484/24/15/155601.

84. Meier, M., Ungerer, J., Klinge, M. & Nirschl, H. Synthesis of nanometric silica particles via a modified Stöber synthesis route. *Colloids Surfaces A Physicochem.*

Eng. Asp. **538**, 559–564 (2018) DOI: 10.1016/j.colsurfa.2017.11.047.

85. Park, S. K., Kim, K. Do & Kim, H. T. Preparation of silica nanoparticles: Determination of the optimal synthesis conditions for small and uniform particles. *Colloids Surfaces A Physicochem. Eng. Asp.* **197**, 7–17 (2002) DOI: 10.1016/S0927-7757(01)00683-5.

86. Huang, Y. & Pemberton, J. E. Synthesis of uniform, spherical sub-100nm silica particles using a conceptual modification of the classic LaMer model. *Colloids Surfaces A Physicochem. Eng. Asp.* **360**, 175–183 (2010) DOI: 10.1016/j.colsurfa.2010.02.031.

87. Wang, J. *et al.* Two-phase synthesis of monodisperse silica nanospheres with amines or ammonia catalyst and their controlled self-assembly. *ACS Appl. Mater. Interfaces* **3**, 1538–1544 (2011) DOI: 10.1021/am200104m.

88. Lv, X., Zhang, L., Xing, F. & Lin, H. Controlled synthesis of monodispersed mesoporous silica nanoparticles: Particle size tuning and formation mechanism investigation. *Microporous Mesoporous Mater.* **225**, 238–244 (2016) DOI: 10.1016/j.micromeso.2015.12.024.

89. Nozawa, K. *et al.* Smart Control of Monodisperse Stöber Silica Particles: Effect of Reactant Addition Rate on Growth Process. *Langmuir* **21**, 1516–1523 (2005) DOI: 10.1021/la048569r.

90. Plumeré, N., Ruff, A., Speiser, B., Feldmann, V. & Mayer, H. A. Stöber silica particles as basis for redox modifications: Particle shape, size, polydispersity, and porosity. *J. Colloid Interface Sci.* **368**, 208–219 (2012) DOI: 10.1016/j.jcis.2011.10.070.

91. Nandy, S., Kundu, D. & Naskar, M. K. Synthesis of mesoporous Stöber silica nanoparticles: the effect of secondary and tertiary alkanolamines. *J. Sol-Gel Sci. Technol.* **72**, 49–55 (2014) DOI: 10.1007/s10971-014-3420-7.

3.7 Appendix

Table A3.1 *DLS data of PC and SL at various concentrations. Micelle size represented by peak means along with polydispersity index (PDI).*

PC in acetate buffer (0.05 M, pH 5.92)				
Concentration (mg ml^{-1})	**Peak 1 mean** (nm)	**Peak 2 mean** (nm)	**PDI**	
0.01	150	3790	0.342	
0.02	129	4915	0.357	
0.03	128	4804	0.349	
0.04	123	4587	0.349	
0.05	124	4199	0.351	
0.06	127	4726	0.328	
0.07	116	4716	0.303	
0.08	119	4747	0.349	
0.09	132	4656	0.339	
0.1	165	4427	0.394	
SL in acetate buffer (0.05 M, pH 5.92)				
Concentration (mg ml^{-1})	**Peak 1 mean** (nm)	**Peak 2 mean** (nm)	**Peak 3 mean** (nm)	**PDI**
0.01	89	360	4459	0.401
0.02	110	475	4714	0.414
0.03	97	376	4500	0.415
0.04	406	-	-	0.418
0.05	101	370	4923	0.404
0.06	105	479	4672	0.418
0.07	332	4511	-	0.424
0.08	302	3811		0.431
0.09	123	640	-	0.449
0.1	338	4545	-	0.430

Figure A3.1 shows SEM images of structurally undirected, crystalline monoliths of widely varying sizes and shapes that formed in the absence of PC or SL. These monoliths were formed when using acetate buffer (0.05 M, pH 5.92) and sodium silicate. There are three possible explanations for what these monoliths are: (1) sodium metal from the reduction of Na^+, (2) Na_2O from the sodium silicate, and (3) SiO_2. The formed solids were a white powder. This observation, along with the high reduction potential required to reduce Na^+, means these solids are highly unlikely to be sodium metal. Thus these white solids are either Na_2O or SiO_2. SiO_2 can be formed because sodium silicate slowly hydrolyses under acidic conditions, such as seen here. However, without any structure-directing agent the subsequent silica polymerisation is uncontrolled. These white solids are likely are a mixture of Na_2O and SiO_2. However, no spherical particles are formed. Thus, we conclude that the conditions of our silica synthesis require the presence of structure directing agent to form spherical silica particles.

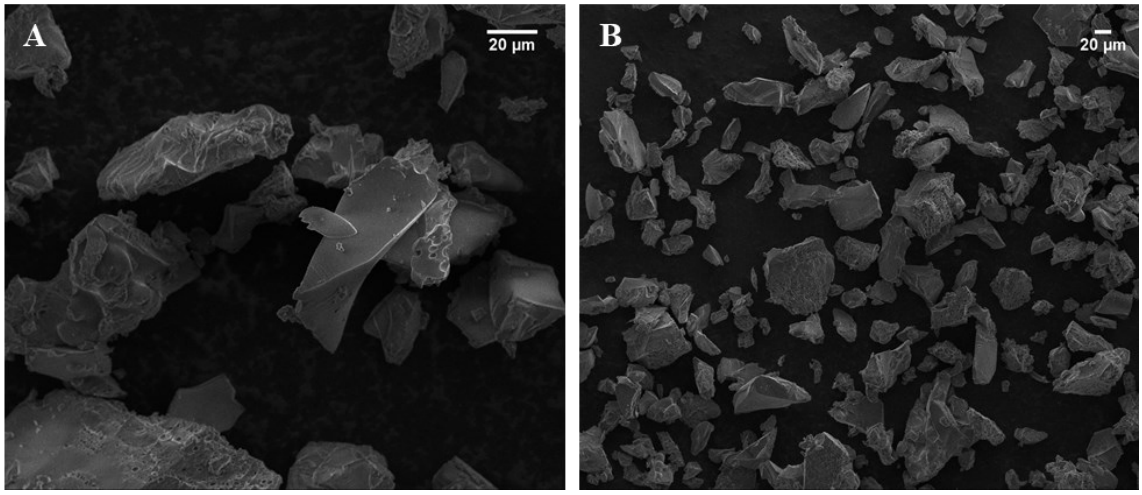


Figure A3.1 *Monoliths formed when (a) no PC and (b) no SL is present in the synthesis.*

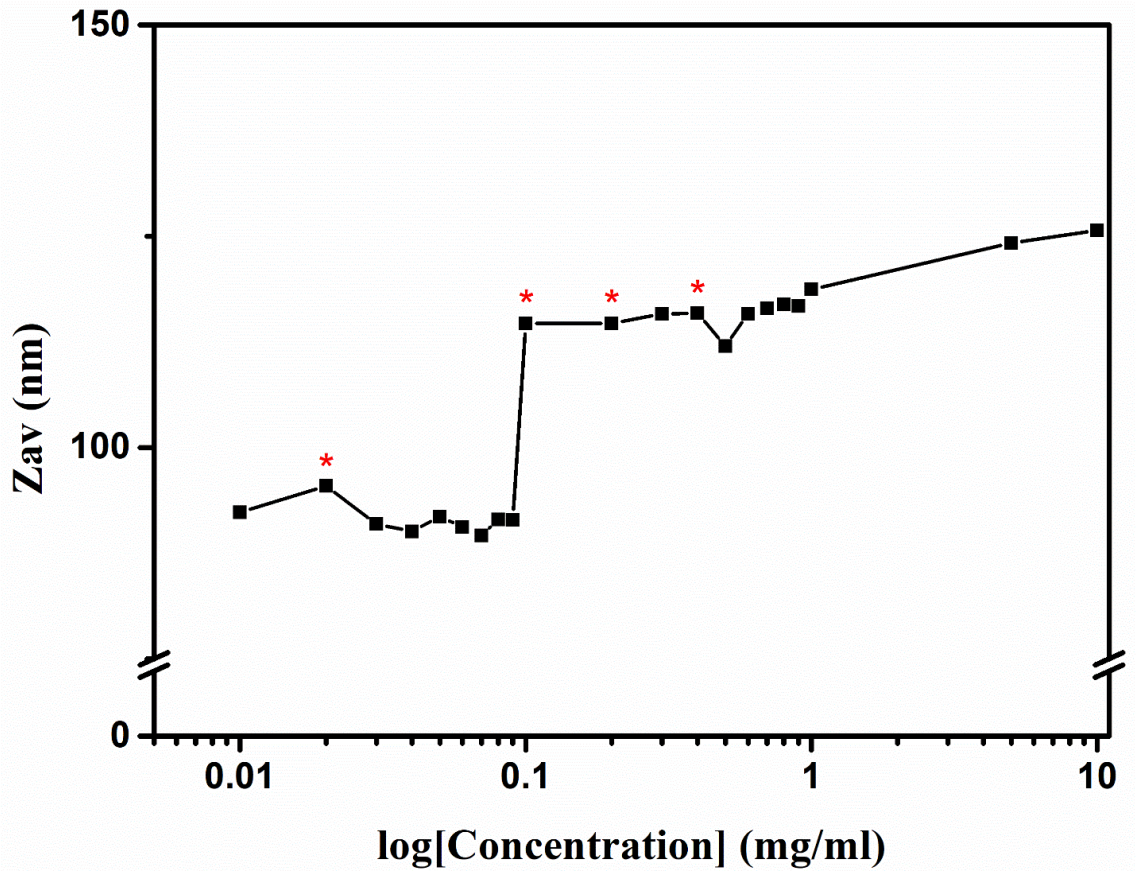


Figure A3.2 *Z-average for PC in acetate buffer (0.05M, pH 5.92) over a wider concentration range. PC1, PC2, PC3, and PC4 are marked with* (*).

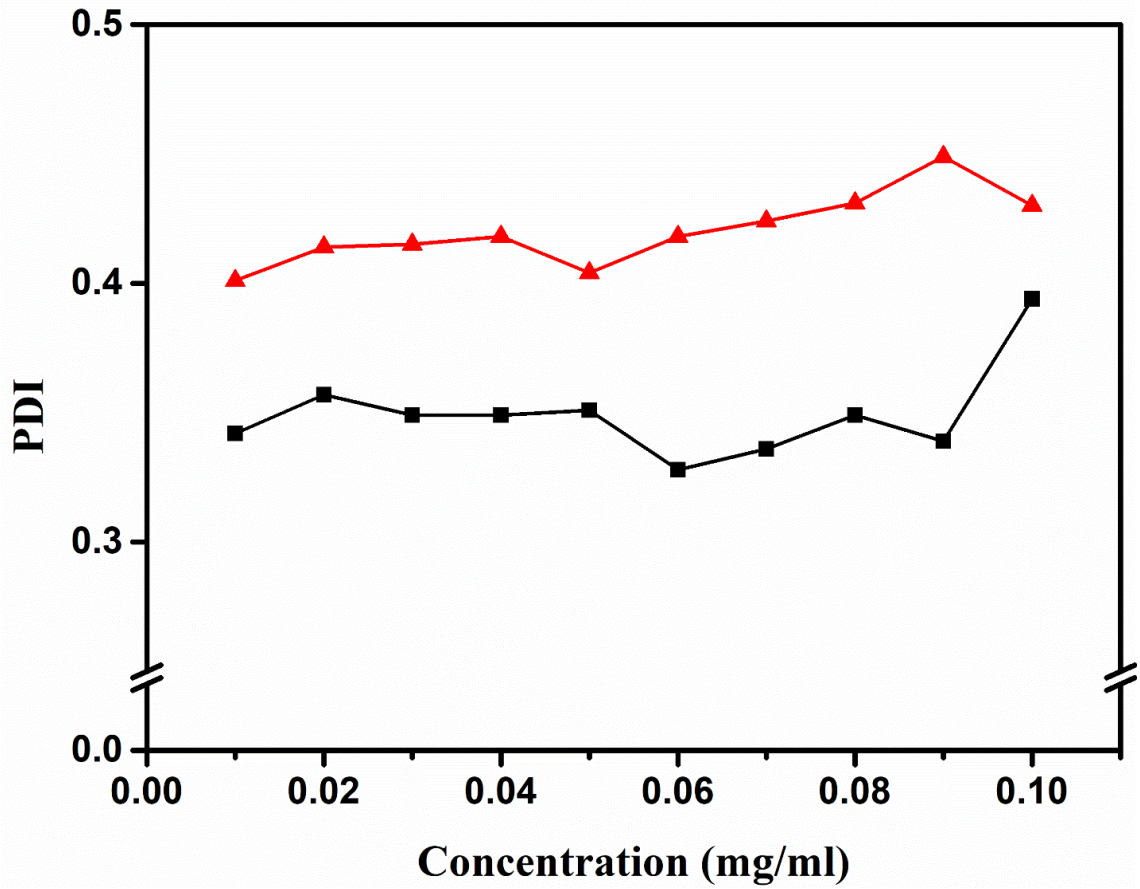


Figure A3.3 *PDI for PC (■) and SL (▲) in acetate buffer (0.05M, pH 5.92) at various concentrations (from DLS data).*

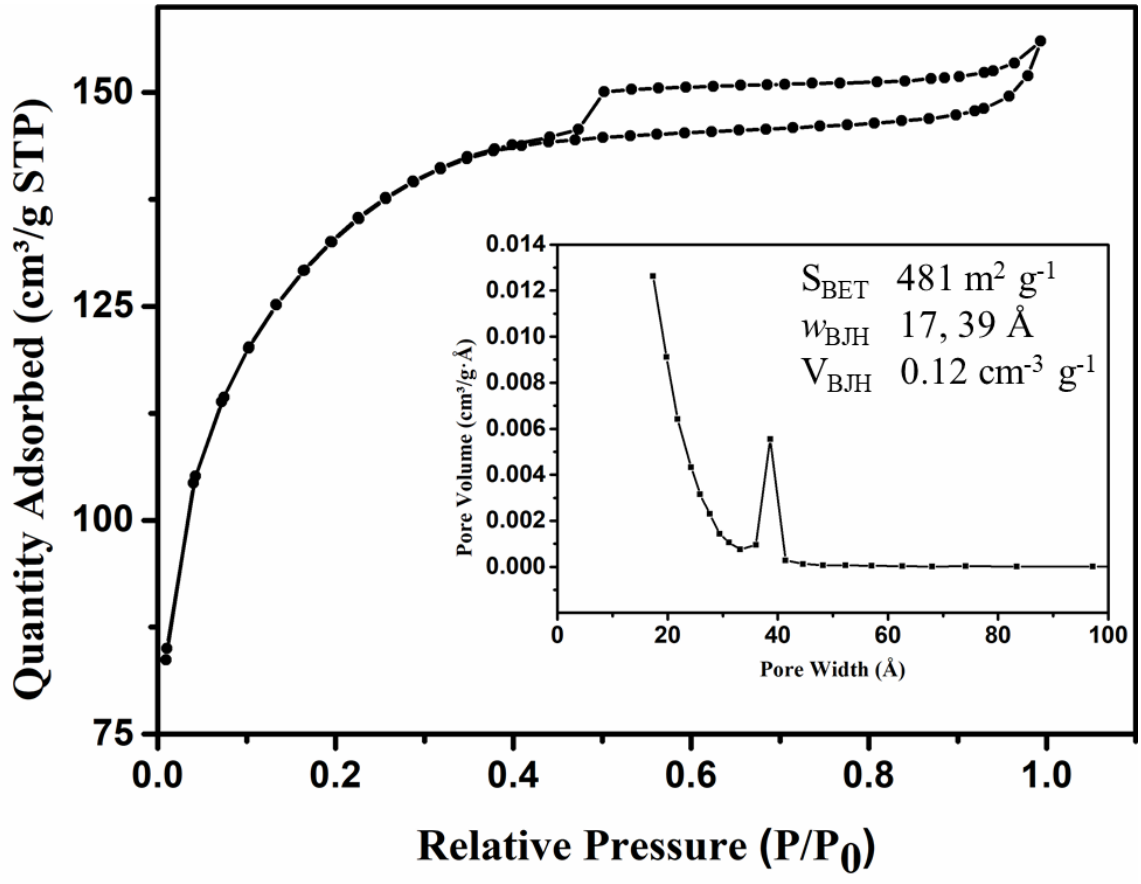


Figure A3.4 *N_2 sorption isotherm and pore size distribution (inset) of silica particles produced with 0.08 mg ml^{-1} SL (SL3).*

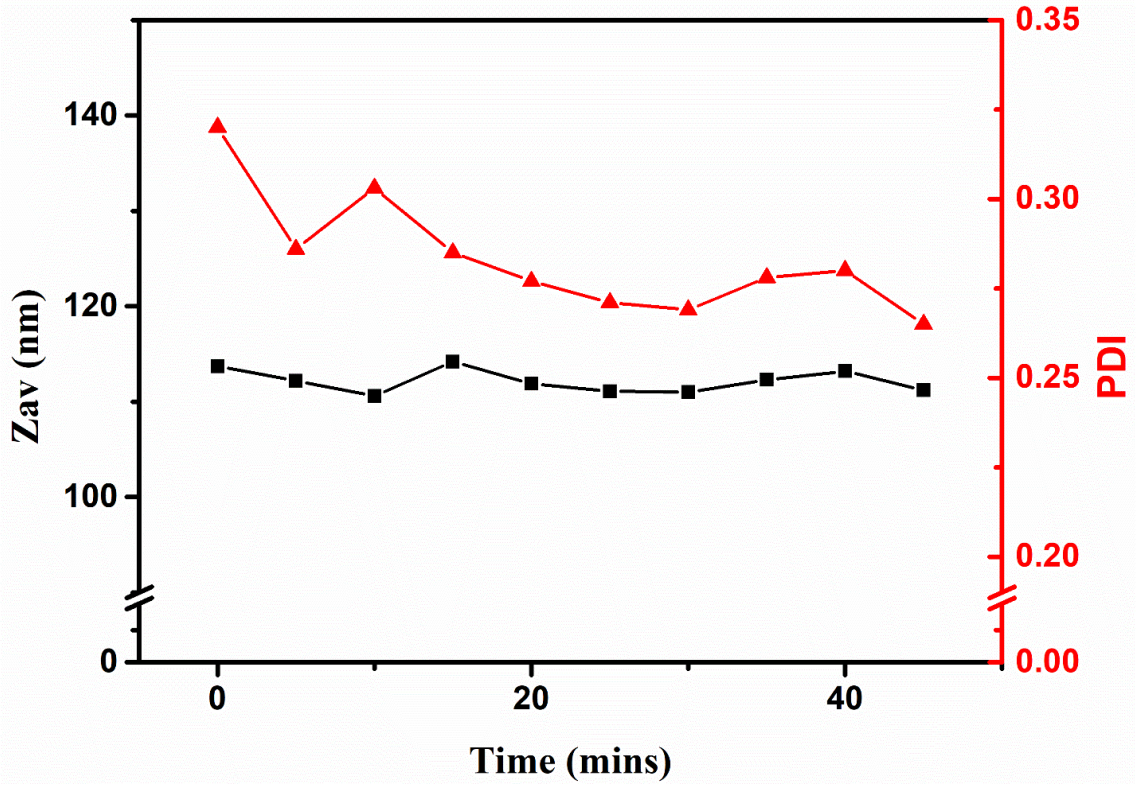


Figure A3.5 *Temporal evolution of Z-average (■) and PDI (▲) of 0.1 mg ml^{-1} SL in acetate buffer (0.05M, pH 5.92) with 10 µL sodium silicate.*

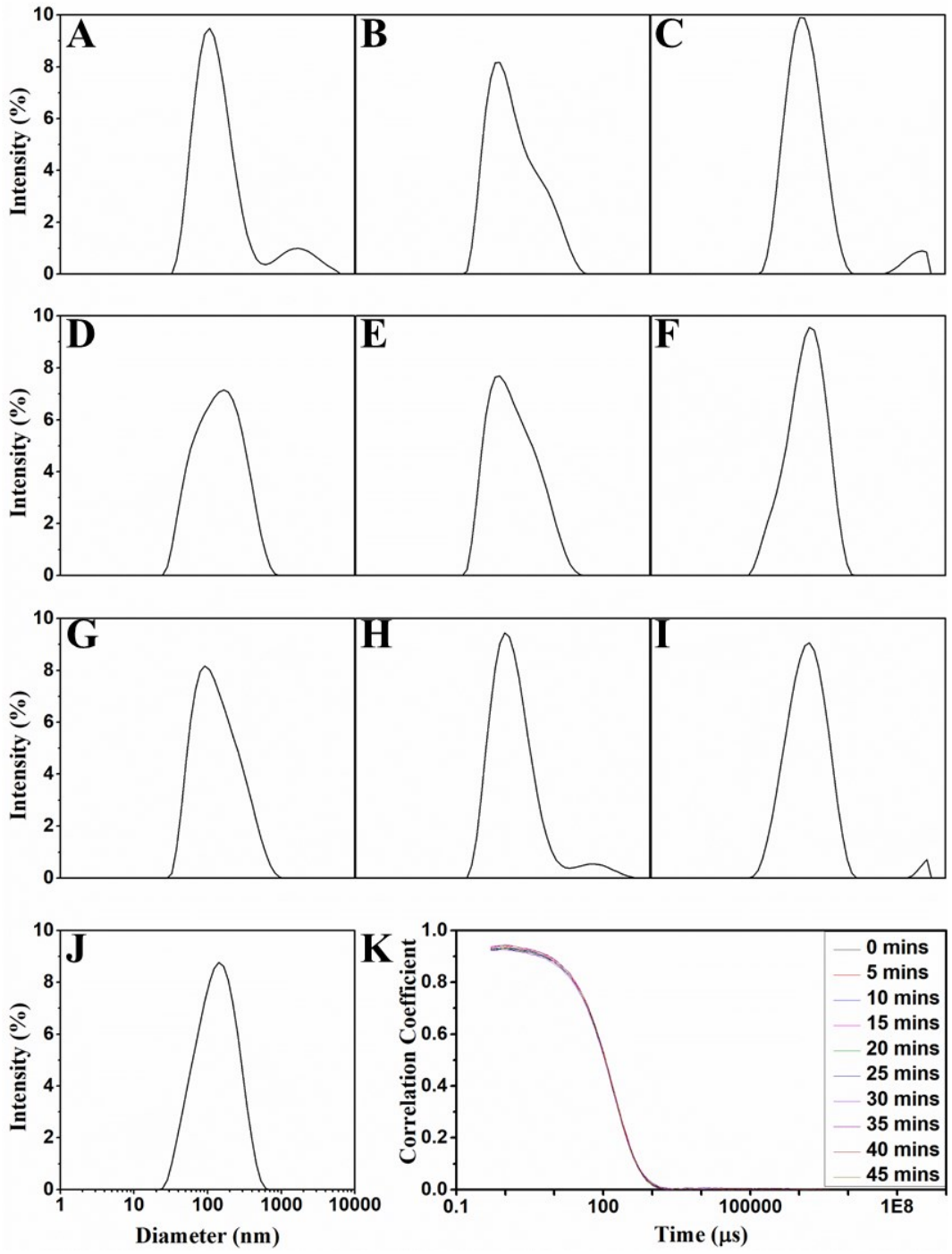


Figure A3.6 *Temporal PSD data from DLS measurements of 0.1 mg ml^{-1} soy lecithin in acetate buffer (0.05 M, pH 5.92) with 10 µL sodium silicate. (a) 0 mins after sodium silicate addition, (j) 45 mins after sodium silicate addition, increment is 5 mins. (k) Correlograms for a-j. As time increases, the distribution becomes unimodal, showing the effect that added sodium silicate has on the SL stability.*

Chapter 4

Spherical Silica Particle Production By Combined Biomimetic-Stöber Synthesis Using Renewable Sodium Caseinate Without Petrochemical Agents

This chapter has been published in Applied Nanoscience. Consequently, sections of the chapter such as the abstract and introduction may contain repeating concepts and paragraphs.

Curley, R., Banta, R.A., Garvey, S., Holmes, J.D. & Flynn, E.J. Spherical Silica Particle Production By Combined Biomimetic-Stöber Synthesis Using Renewable Sodium Caseinate Without Petrochemical Agents.

DOI: 10.1007/s13204-021-01762-2

4.1 Abstract

Spherical silica particles are typically made via Stöber and modified-Stöber processes. However, these processes are environmentally unsustainable. Here we report a process to synthesise spherical silica particles in a more sustainable way using sodium caseinate. Initial experiments showed that sodium caseinate can replace the typical industrial structural directing agents used to produce spherical particles. Upon further optimisation, particles with diameters ranging between 124 nm and 1590 nm, were readily produced using sodium caseinate, sodium silicate, and acetate buffer. Higher concentrations of sodium caseinate and low concentrations of sodium silicate promoted Ostwald ripening. Low concentrations of sodium caseinate and high concentrations of sodium silicate promoted coalescence. Subsequent optimisation of the dispersity using a statistical design of experiments yielded silica particles between 172 and 340 nm, that showed good monodispersity, using sodium caseinate, calcium chloride, sodium silicate, and acetate buffer. Analysis of variance (ANOVA) and regression analyses were used to determine and quantify the relationship between reagent concentrations and particle size. A regression equation was calculated, which predicts particle size based on reagent concentration. Predicted particle sizes and experimentally determined particle sizes showed good agreement. These spherical silica particles are the most discreet and monodisperse produced to date using a sustainable method with biopolymers.

4.2 Introduction

Spherical silica is one of the most important and widely used materials in the world, however, the production methods (Stöber and modified-Stöber) combined with the industrial scale at which spherical silica is made, is inherently environmentally unsustainable. The environmental impact of its production will continue to grow as demand for the material increases. The main problems associated with the large-scale production of silica is the use of environmentally damaging and toxic precursors. Alcoholic solvents and synthetic surfactants, such as cetyltrimethylammonium bromide (CTAB), are typically used and these have been shown to have adverse effects on the environment.[1–3] Industrially, synthetic surfactants and alcohols such as ethanol are mostly produced from petrochemical feedstocks.[4,5] In order to address these problems while meeting the demand for spherical silica, a new method of production needs to be devised. Using the natural process of biomineralisation may offer a possible solution.[6–9]

Limited work has been done on trying to replicate the biomineralisation process in vitro using biopolymers to synthesise spherical silica particles. However, thus far, a lot of this work has only yielded silica particles that are non-spherical, agglomerated, or both.[10–14] In **Chapter 3** we successfully synthesised spherical silica particles using phosphatidylcholine and soy lecithin, however particle quality still needed to be improved. Here, we have identified sodium caseinate (NaCas) as an ideal candidate to act as a structure-directing agent (SDA) in synthesising spherical silica particles. NaCas is a widely used as an emulsion stabiliser in food products[15–17] as it provides stabilisation against coalescence via electrostatic and steric interactions.[18] Casein is a family of phosphoproteins of four distinct types: α_{s1}-, α_{s2}-, β-, and κ-casein. The α_s-caseins are

calcium sensitive and the κ-casein is calcium insensitive.[19] The casein micelles are stabilised by steric stabilisation, with κ-casein forming a brush on the surface of the micelles, preventing agglomeration. Caseins can associate into small clusters via their hydrophobic sections. **Figure A4.1** shows the possible structure of the casein micelle. This surfactant-like behaviour can be exploited for use as an SDA in silica synthesis. Under acidic conditions, the carboxylic acid groups of the sodium caseinate sub-micelles are neutralised, increasing the attractive forces between the proteins, resulting in larger micelle-like aggregate structures.[20] Furthermore, addition of calcium to a solution of NaCas has been shown to stabilise the aggregate structures into micelles of ca. 100 nm.[21] This stabilisation effect is thought to occur via crosslinking by ionic calcium, which prevents flocculation of the micelle structures.[22] The role of amphiphilic CTAB is to control the condensation of silica to form spherical particles via these micelles. As described in sections **1.2.3** and **1.2.4** silica condensation occurs around these micelles, which then aggregate together to produce spherical particles.[23–26] NaCas has this same physical property and could be used in the same way. Using a biopolymer such as NaCas as the SDA along with environmentally benign reagents could make the process for producing silica more sustainable by replacing the need to use petrochemically-derived reagents such as CTAB, tetraethyl orthosilicate (TEOS), and ethanol.

The objective of the current work was to produce sustainable silica nanoparticles using NaCas, as the SDA, and water-based chemistry. A new sustainable process was created, starting from the traditional modified-Stöber process. Initially, the ability of NaCas to function as an SDA to form spherical particles was tested. Once this ability was confirmed, optimisation of the process was performed which used NaCas, sodium silicate

and acetate buffer. The particle size distributions were analysed for coalescence and Ostwald ripening. Further optimisation improved the monodispersity of the particles. The optimised and sustainable process uses NaCas, calcium chloride, sodium silicate, and acetate buffer. Thus, the most environmentally hazardous reagents that are typically used to produce silica were replaced with environmentally benign and sustainable ones. The environmental impact of producing spherical silica nanoparticles is greatly reduced by using this biopolymer-based approach.

4.3 Experimental

4.3.1 Materials

Sodium silicate (10.6 % Na_2O, 26.5 % SiO_2) from Sigma Aldrich was used as the silicic acid source. Ammonium hydroxide (assay: 28-30 % NH_3 basis), sodium caseinate (NaCas), sodium acetate, and acetic acid were all purchased from Sigma Aldrich. Acetate buffer solution (0.05 M, pH 5.94) was prepared in distilled water.

4.3.2 Silica preparation using ammonium hydroxide

Initial experiments used a traditional modified-Stöber synthesis which was adapted for use with NaCas.[27] The experimental conditions, denoted by NC, are shown in **Table 4.1**. In a 100 ml flask, NaCas was added to distilled water under stirring and temperature was set to 50 °C. After dissolution of NaCas, ammonium hydroxide was added. Finally, sodium silicate was added and the resulting solution was left to react overnight in a closed vessel. The reaction mixture was then centrifuged at 14,000 rpm in an Eppendorf MiniSpin Plus microcentrifuge and the solids were washed with water, ethanol, and acetone. The sample was then dried in an oven and characterised by SEM.

Table 4.1 *Experimental conditions of syntheses using NaCas, sodium silicate, and ammonia. Experiments are denoted by NC.*

	H_2O (ml)	Sodium Silicate (ml)	NH_4OH (ml)	NaCas (mg)	T (°C)
NC1	25	3.2	12	0.32	50
NC2	25	6.4	12	0.32	50
NC3	25	6.4	6	0.64	50
NC4	50	6.4	6	0.64	50

4.3.3 Silica preparation using buffer

After initial testing, it was found that high volumes of sodium silicate were not needed, with microlitres being sufficient to form the particles. This is of added benefit as less reagent is required. The experimental conditions, denoted by BF, are shown in **Table 4.2**. The required amount of NaCas stock solution (100 mg ml^{-1} NaCas in 0.05 M acetate buffer, pH 5.94) was added to 50 ml of acetate buffer (0.05 M, pH 5.94). Sodium silicate was subsequently added and the reaction solution was stirred in a closed vessel overnight at room temperature. The reaction solution was then centrifuged at 14,000 rpm in an Eppendorf MiniSpin Plus microcentrifuge and the solids were washed with water, ethanol, and acetone. The sample was then dried in an oven and characterised by SEM.

Table 4.2 *Experimental conditions of syntheses using NaCas and sodium silicate. Experiments were repeated under identical conditions with distilled water instead of acetate buffer. All experiments repeated in triplicate and data combined. Experiments are denoted by BF.*

	Acetate Buffer [0.05 M, pH 5.94] (ml)	Sodium Silicate (µL)	NaCas (mg ml^{-1})
BF1	50	81	0.2
BF2	50	81	0.4
BF3	50	162	0.2
BF4	50	810	0.2

4.3.4 Silica preparation using buffer and $CaCl_2$

An experimental design (**Table 4.3**) was created using Minitab statistical software. A full factorial (2^3) design was used with all terms free from aliasing. The design was replicated twice in two blocks with one centre point per block. The input factors (NaCas, sodium silicate, $CaCl_2$) had two levels and their effect on the response variable (particle size) was analysed using ANOVA. Regression analysis was used to obtain a regression equation which could predict values of the response variable based on the input factors. Experimentally, the required amount of NaCas stock solution (20 mg ml^{-1} NaCas in 0.05 M acetate buffer, pH 5.94) was added to 50 ml acetate buffer (0.05 M, pH 5.94). Aliquots of 100 mM $CaCl_2$ were added to this solution to give the required concentration of $CaCl_2$ as shown in **Table 4.3**. Finally, sodium silicate was added and the reaction was stirred in a closed vessel overnight. This procedure was also used for experiments conducted at pH 4.94, denoted by BC (**Table 4.4**). The reaction solution was then centrifuged at 14,000 rpm in an Eppendorf MiniSpin Plus microcentrifuge and the solids were washed with water, ethanol, and acetone. The sample was then dried in an oven and characterised by dynamic light scattering.

Table 4.3 *Experimental conditions for 2^3 full factorial design with 2 replicates, 2 blocks, and 1 centre per block. Factors: sodium silicate, NaCas; sodium caseinate, $CaCl_2$. Response variable: PS; particle size. Each factor has two levels and each centre point is midway between these levels. All terms are free from aliasing. Block generators are the replicates.*

Run Order	Centre Point	Blocks	Sodium Silicate (µL)	NaCas (mg)	$CaCl_2$ (mM)
1	1	1	486	60	6
2	1	1	486	20	12
3	1	1	729	20	6
4	1	1	486	20	6
5	1	1	486	60	12
6	1	1	729	20	12
7	1	1	729	60	12
8	1	1	729	60	6
9	0	1	607	40	9
10	1	2	486	60	6
11	1	2	486	20	6
12	1	2	729	60	12
13	0	2	607	40	9
14	1	2	729	20	12
15	1	2	486	60	12
16	1	2	729	60	6
17	1	2	486	20	12
18	1	2	729	20	6

Table 4.4 *Experimental conditions of syntheses using NaCas, sodium silicate and calcium chloride at pH 4.94. Experiments are denoted by BC.*

	Acetate Buffer [0.05 M, pH 4.94] (ml)	Sodium Silicate (µL)	NaCas (mg)	$CaCl_2$ (mM)
BC1	50	729	40	8
BC2	50	729	80	8
BC3	50	729	120	8
BC4	50	729	160	8

4.3.5 Characterisation

Scanning Electron Microscopy (SEM) was used to obtain images of the silica particles. The SEM analyses were carried out on an FEI Inspect and Quanta 650, operated at either 10 or 15 kV. Each sample was adhered to a stainless-steel stub (stage) via double-sided carbon tape.

Elemental characterisation was acquired using energy-dispersive x-ray spectroscopy (EDX) on the FEI Quanta 650 instrument using Oxford Instruments INCA software.

Particle diameters were determined using ImageJ image analysis software and statistical analyses were done in OriginLab OriginPro 9.0 software.

Dynamic light scattering (DLS) measurements were conducted on a Malvern Panalytical Zetasizer Nano ZSP, using non-invasive backscattering (NIBS) technology. The scattering angle was set at 173° and the measurement temperature was set to 20 °C. Samples were dispersed in ethanol and sonicated to give a stable solution prior to analysis. Mean size and polydispersity index (PDI) were determined using Cumulant analysis.

X-Ray Photoelectron Spectroscopy (XPS) spectra were acquired on an Oxford Applied Research Escabase XPS 230 System equipped with a CLASS VM 100 mm mean radius hemispherical electron energy analyser with multichannel detectors in an analysis chamber with a base pressure of 5.0×10^{-9} mbar. A pass energy of 50 eV, a step size of 0.7 eV and a dwell of 0.3 s was used for survey spectra which were swept twice. All core level scans were acquired with a step size of 0.1 eV, a dwell time of 0.1 s and a pass energy of 20 eV averaged over 10 scans. A non-monochromated Al-Kα X-ray source (1486.58 eV) at 100 W power (10 mA, 10 kV) was used for all scans. All spectra were

acquired at a take-off angle of 90° with respect to the analyser axis and were charge corrected with respect to the C 1s photoelectric line at 284.8 eV. Synthetic peaks are Gaussian in shape. The relative sensitivity factors used are from a CasaXPS library containing Scofield cross-sections.

Nitrogen sorption measurements were performed on a Micromeritics TriStar II surface area analyser (Micromeritics, Norcross, GA, USA). Samples were pre-treated by heating at 200 °C under nitrogen for 12 hours. The surface area was measured using the Brunauer-Emmett-Teller (BET) method. The pore volume and pore diameter data was calculated using the Barrett, Joyner and Halenda (BJH) method. Specific surface areas were calculated from the measured relative pressure in the range of P/P_0= 0.01 to P/P_0= 0.3.

4.4 Results and Discussion

4.4.1 Silica prepared with ammonium hydroxide

The ultimate goal is to make the synthesis of spherical silica more sustainable. We replaced CTAB with NaCas to investigate whether NaCas could function as an SDA In order to use NaCas, ethanol could not be used as it can cause denaturation of the protein,[28] so water was used as the solvent. Without ethanol, TEOS could also no longer be used because it is water-insoluble. Instead we chose water-soluble sodium silicate, which has the added benefit of being akin to the usual form of soluble silica found in nature.[13,29] A catalyst was still required. The use of NaCas as an SDA necessitated the change of multiple components in the original synthesis. Thus, ammonium hydroxide was retained as the catalyst to minimise the number of changes made to the original system as much as

possible . This new system was assessed , with a view to further modifying it to create a totally sustainable process if successful.

We produced spherical particles using NaCas, sodium silicate, water and ammonium hydroxide (**Figure 4.1)**. The particles are spherical, but exhibit polydispersity. NC1 and NC3 show agglomeration, while NC2 shows some agglomeration and NC4 shows discrete particles. The particle diameters range between 283-1349 nm. These initial results were promising, as it showed that our modified system could indeed produce spherical particles. Control experiments conducted with sodium silicate, water, and ammonium hydroxide showed that no spherical particles were formed (see **Figure A4.2** in section **4.7 Appendix**). This is expected as there is no effective morphological control agent present in the system to control the morphology of the particles. The fact that spherical particles are only formed when NaCas is present suggests that NaCas acts as an effective SDA.

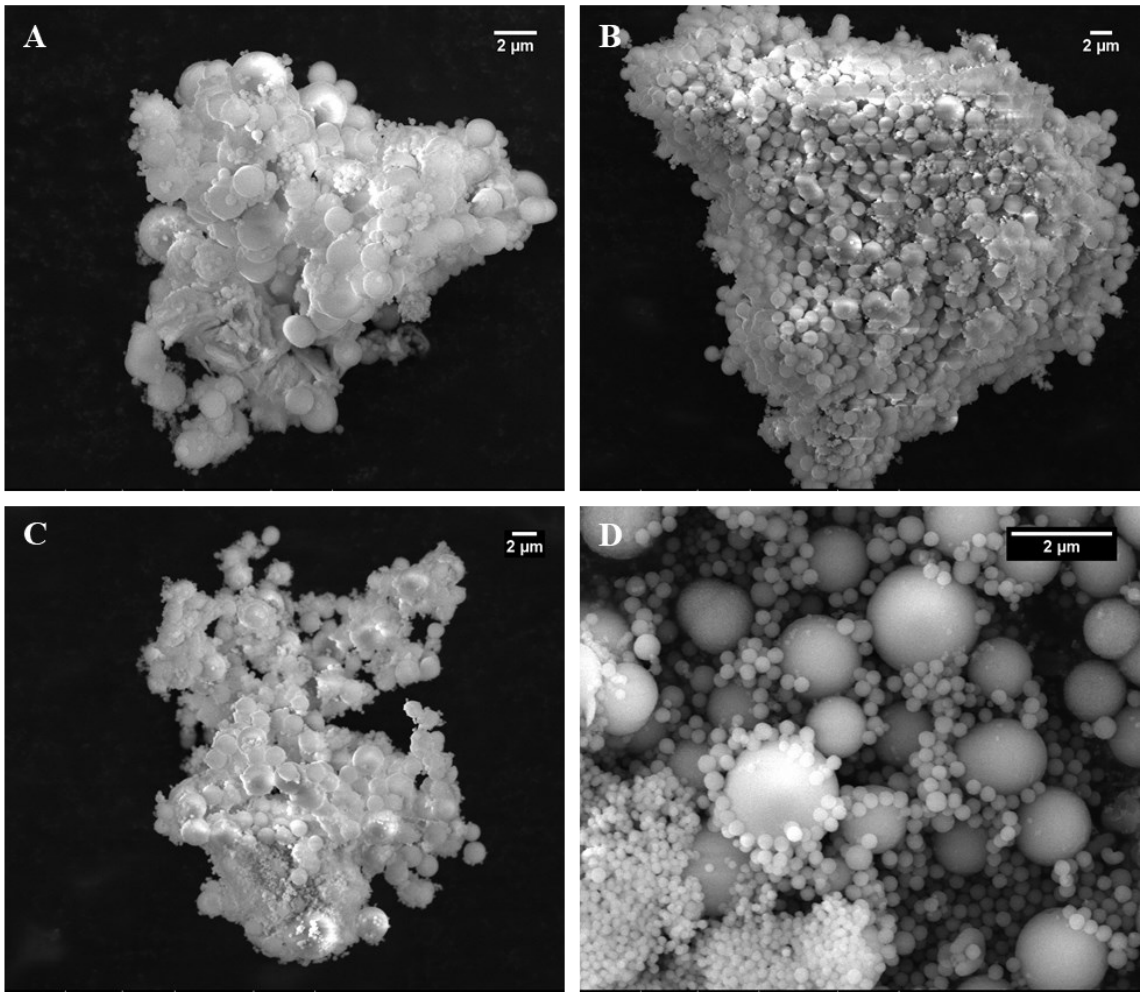


Figure 4.1 *SEM micrographs (a) NC1 and (b) NC2, (c) NC3, and (d) NC4. T = 50°C.*

These sets of experiments show that our modified system can produce spherical silica particles. Ammonium hydroxide was needed here as the catalyst to initiate the hydrolysis of sodium silicate. Two conclusions were drawn from these experiments: (1) in the absence of an effective morphological control agent, no spherical particles are formed in our system, and (2) in the presence of NaCas, spherical particles are formed in our system. Knowing that NaCas functions as an effective SDA in our system, we proceeded to further modify our system to increase its sustainability. Our next set of experiments used an acid

catalyst in the form of acetate buffer to replace ammonium hydroxide and the role NaCas plays is investigated in detail in this new sustainable system.

4.4.2 Silica prepared with acetate buffer

Based on the results of our previous experiments, our next set of experiments focused on maximising the sustainability of our process. As before, sodium silicate and NaCas were used as the silica source and SDA, respectively. There was still a need to catalyse the hydrolysis of sodium silicate. Simply removing ammonium hydroxide from the system would retard silica formation. Thus, in place of ammonium hydroxide we used acetate buffer because sodium silicate hydrolyses readily in acidic media.[30] This three component system has now eliminated the most toxic and unsustainable reagents of the modified-Stöber process; namely ethanol, ammonium hydroxide, CTAB, and TEOS. Our system uses sodium silicate as the silica source, NaCas as the SDA, and acetate buffered water, which has twofold benefit of being an environmentally benign solvent, while also promoting the hydrolysis of sodium silicate.

Our initial experiments showed that NaCas can act as an effective SDA to produce spherical particles. This was followed by experiments conducted in acetate buffer without the remaining environmentally problematic compound in the modified-Stöber process – ammonium hydroxide.

To investigate the precise role that NaCas plays in our sustainable system DLS measurements of NaCas in acetate buffer were obtained. **Figure 4.2** shows DLS data of NaCas in acetate buffer (0.05 M, pH 5.94). The data show that at all concentrations tested, NaCas forms micelles, however in some cases they are multimodal, and showing

polydispersity. Furthermore, large aggregate peaks ca. 3000 nm are seen at 0.2, 0.4, and 0.6 mg ml^{-1} NaCas and free proteins are also seen at all concentrations (< 100 nm). This polydispersity could translate into the final particles and is a likely explanation of the polydispersity seen when using the ammonium hydroxide system. Knowing that NaCas forms micelle structures in acetate buffer, we attempted to synthesise spherical silica particles using NaCas, sodium silicate, and acetate buffer.

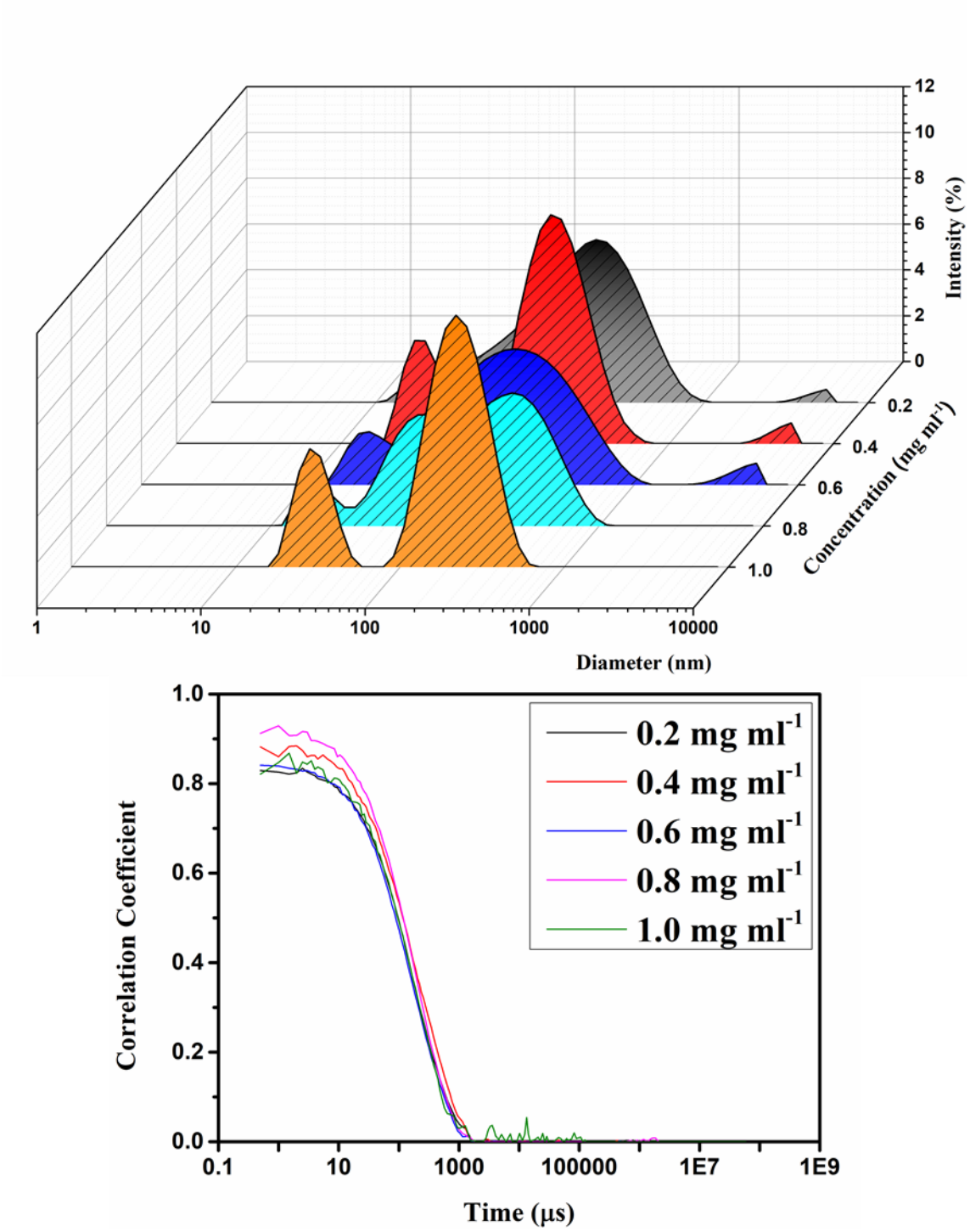


Figure 4.2 *DLS measurements of sodium caseinate in acetate buffer (0.05 M, pH 5.94) at various concentrations (top). Correlograms (bottom).*

Figure 4.3 shows SEM images of the spherical particles obtained with this new system. Interestingly, when these experiments were replicated using distilled water as the reaction medium, as opposed to acetate buffer, no spherical particles are formed. Instead, monoliths with no defined structure are formed (see **Figure A4.3** in section **4.7 Appendix**). This suggests the acidic pH promotes the conformational changes required of NaCas to form micelles. The SEM images show that the samples exhibit different degrees of polydispersity, which may be explained by the polydispersity of NaCas micelles in the DLS data of NaCas in acetate buffer, although the NaCas aggregates are dynamic and are likely not fixed in size.

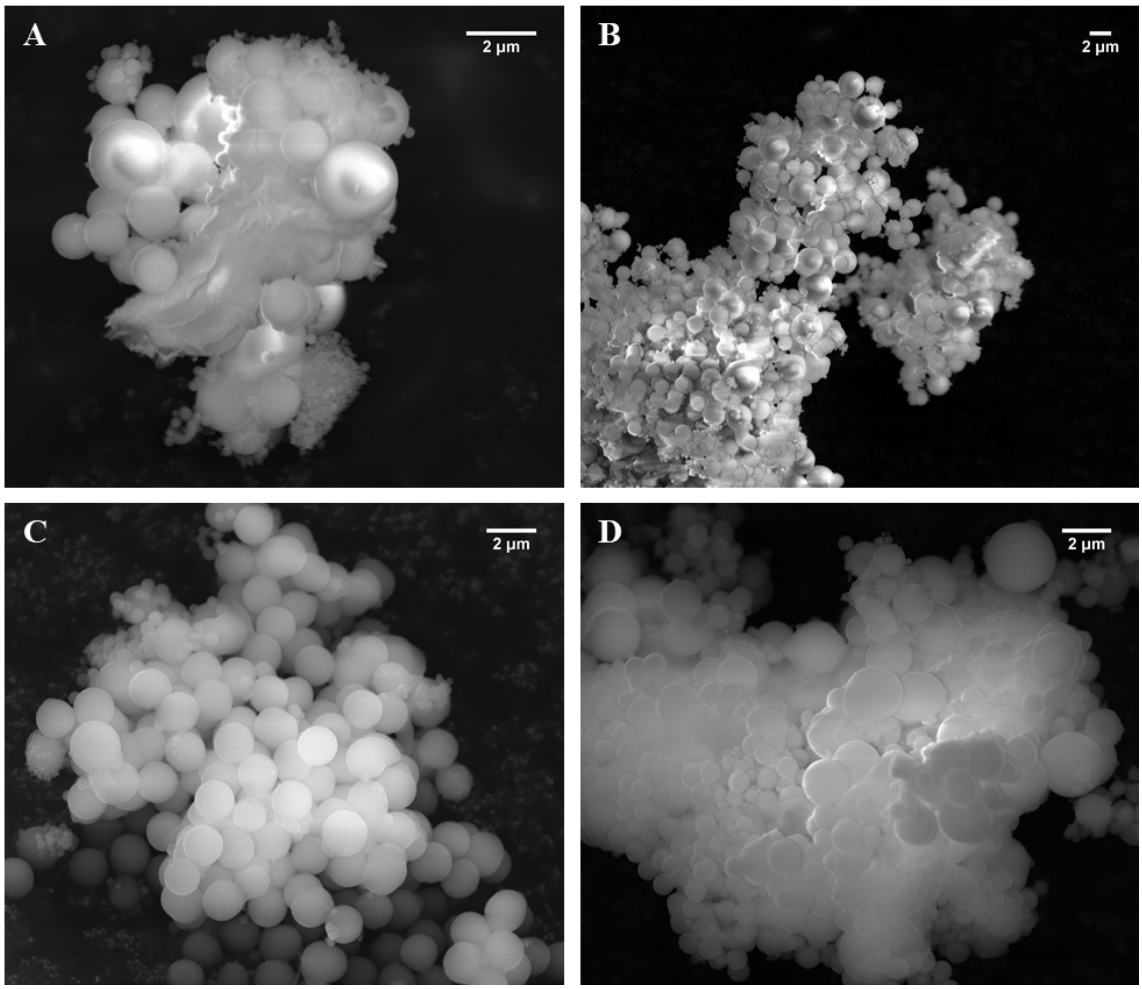


Figure 4.3 *SEM micrographs of silica prepared with (a) 0.2 mg ml^{-1} NaCas (BF1), and (b) 0.4 mg ml^{-1} NaCas (BF2), (c) 162 µL sodium silicate (BF3), and (d) 810 µL sodium silicate (BF4). Scale bars = 2 µm.*

Figure 4.4 shows the PSDs of samples BF1 to BF4. All peaks were determined using goodness of fit statistics. **Figure 4.4A** shows a log-normal distribution (R^2 = 0.97) peak centre of 124 nm. **Figure 4.4B** shows 2 peaks fitted with a combination of log-normal and Gaussian functions (R^2 = 0.92). At 0.2 mg ml^{-1} NaCas, the growth of the particles is through coalescence (log-normal). At 0.4 mg ml^{-1} NaCas, the log-normal peak centre shifts from 124 nm to 258 nm and the emergence of a Gaussian peak is seen at 1423 nm.

Coalescence occurs when particles, often of different sizes, merge to form a single particle. Accordingly, a PSD resulting from this process has a right-skewed tail, characterised by a log-normal function. Ostwald ripening occurs via material transfer from smaller, less thermodynamically stable, particles to larger particles. Larger particles, being more thermodynamically stable, grow at the expense of smaller particles. Lifshitz and Slyozov,[31] and Wagner,[32] provided mathematical descriptions of the Ostwald ripening process. This LSW model describes the PSD of particles grown via Ostwald ripening as having a left-skewed tail, with a sharp cut-off at 1.5 times the mean particle diameter. This cut-off is a consequence of the assumption in the LSW model that the solution is infinitely dilute, meaning no particle interaction takes place. In real systems, this mathematical restraint does not reflect reality, so the LSW model must be adjusted to take particle interaction into accounted. In which case, a Gaussian function provides a better description

It is possible to differentiate between coalescence and Ostwald ripening by the shape of the particle size distribution. Log-normal for coalescence, and Gaussian for Ostwald ripening. However, both processes are not mutually exclusive – they can, and do, coexist and overlap. Therefore, we have fitted the PSDs with a mixture of Gaussian and log-normal functions. The degree to which either process dominates depends on the experimental conditions used. Generally, Ostwald ripening results in particles which are more monodisperse than those produced via coalescence. This is because of the log-normal distribution associated with coalescence. Therefore, analysing the PSDs can allow for optimisation of the polydispersity by understanding the experimental conditions which give rise to an Ostwald ripening-dominated mechanism.

This emergence of a Gaussian peak at higher concentrations of NaCas suggests the growth process shifts from primarily coalescence to a mixture of coalescence and Ostwald ripening, with larger particles produced. As discussed in section **1.4.3**, the presence of adjacent carboxyl and amino groups can significantly enhance the silica dimerisation rate. This may explain why a higher concentration of NaCas results in larger particles. **Figure 4.4C** shows a multimodal distribution fitted with Gaussian functions (R^2 = 0.96) with mean peak diameters of 382 and 1590 nm. **Figure 4.4D** shows a multimodal distribution fitted with a combination of Gaussian and log-normal functions (R^2 = 0.97) with mean peak diameters of 473 and 861 nm. The production of smaller particles at higher sodium silicate concentrations may be due to an increased hydrolysis rate, allowing for the formation of small particles. Thus, at low concentrations of sodium silicate (162 μL) growth occurs via an Ostwald ripening mechanism and at higher concentrations of sodium silicate (810 μL), a mixture of coalescence and Ostwald ripening occurs. From these experiments, in order to promote Ostwald ripening and produce more monodisperse particles, the data indicate that high concentrations of NaCas and low concentrations of sodium silicate are required. However, while spherical silica is formed, the particles are quite polydisperse with multiple peaks in the PSDs. While the analysis and fitting of these peaks with log-normal and Gaussian functions can provide insight into the growth process, caution must be used when fitting a combination of peaks to a distribution. The goodness of fit parameters aim to statistically identify which functions provide the best fit. However, as is the case when fitting multiple peaks, there may be multiple fittings which provide similar goodness of fit statistics. While the data presented here have been analysed carefully, given the overall low quality of the particles in terms of size dispersity,

interpretation of the growth process from the PSDs is difficult. However, the data obtained from this experiment provided an excellent foundation to develop the process further, which is discussed next.

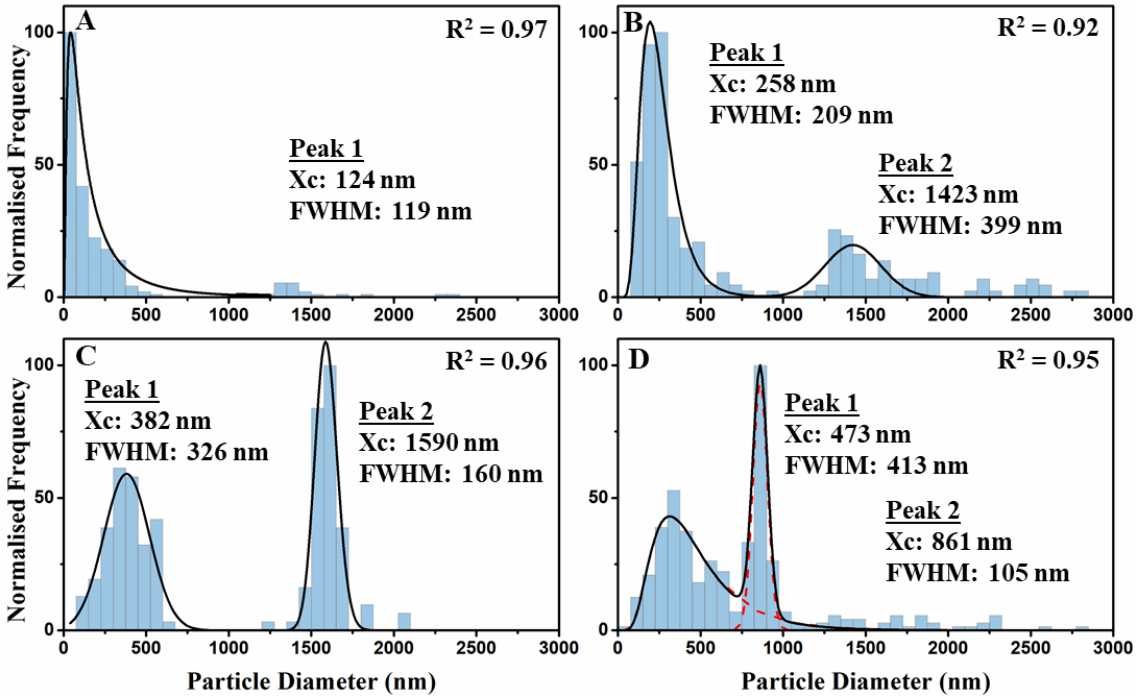


Figure 4.4 *PSDs of particles prepared with (a) 0.2 mg ml^{-1} NaCas (BF1), and (b) 0.4 mg ml^{-1} NaCas (BF2), (c) 162 µL sodium silicate (BF3), and (d) 810 µL sodium silicate (BF4).*

4.4.3 Silica prepared with acetate buffer and calcium chloride

Our third set of experiments focused on optimising our new sustainable process for producing more monodisperse spherical silica particles. Most applications require relatively monodisperse silica. We added calcium chloride to our reaction system to stabilise the NaCas micelle. Calcium chloride has been shown to reform casein micelles from NaCas.[19] Other studies in the literature found the size of casein micelles to be in the range of 50 – 600 nm with an average size of ca. 200 nm.[33,34] Here we report the casein

micelle size to have an average size of ca. 100 nm. However, our system uses a buffer solution of pH 5.94 and acidic pH has been shown to decrease the casein micelle size in milk,[35] which may explain why the size reported here varies slightly from other studies of casein in different systems. **Figure 4.5** shows distribution data from DLS measurements of NaCas with 8 mM $CaCl_2$ added. The data show a marked reduction in micelle size and polydispersity compared to the NaCas system with no added $CaCl_2$ shown in **Figure 4.2**. Addition of $CaCl_2$ stabilises the NaCas micelles at all concentrations of NaCas tested. Whether or not this increase in monodispersity would translate into silica was next investigated.

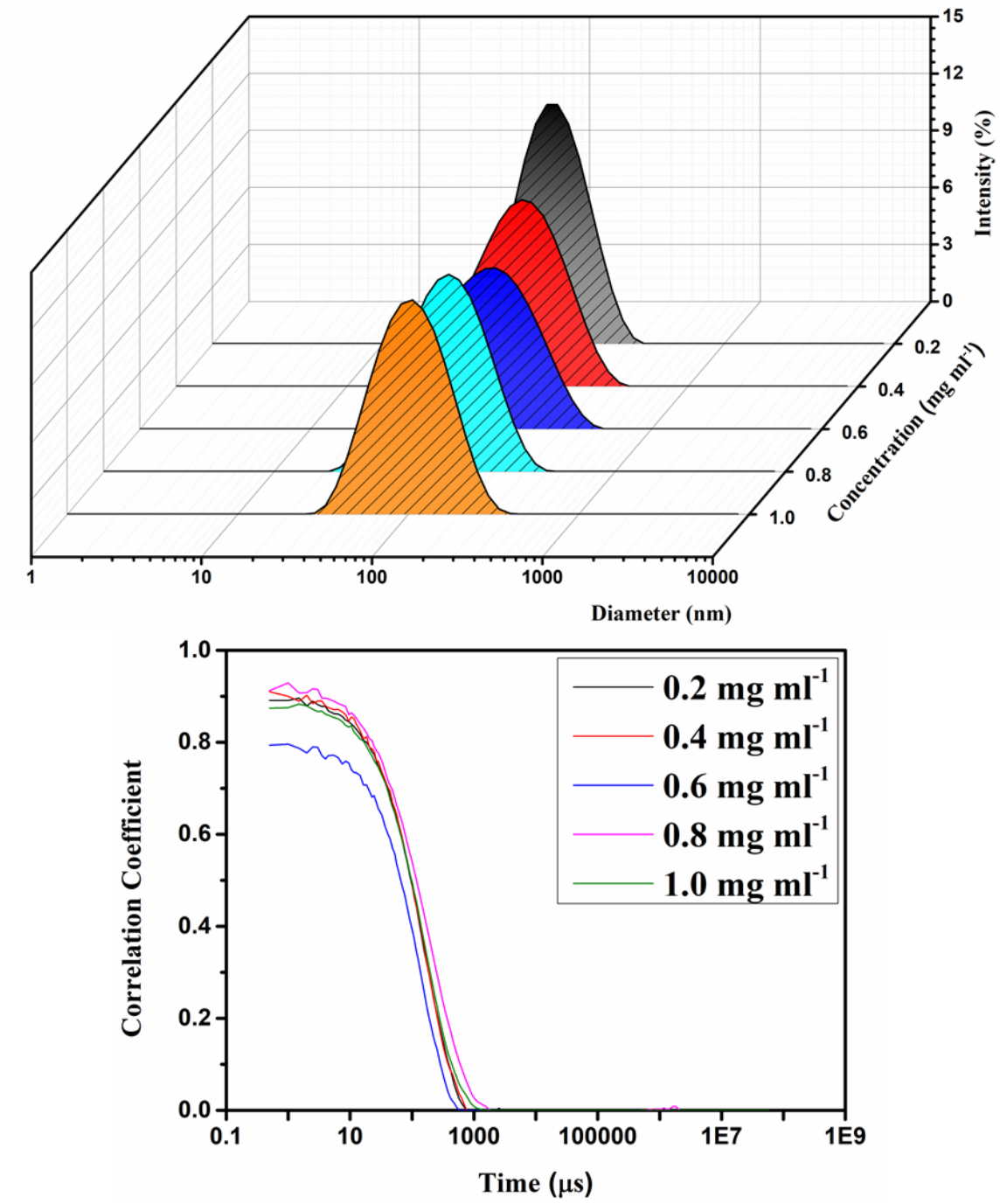


Figure 4.5 *Distribution data from DLS measurements of sodium caseinate at various concentrations with 8 mM $CaCl_2$ in acetate buffer (0.05 M, pH 5.94) (top). Correlograms (bottom).*

In order to optimise the synthesis and understand the influence that NaCas, sodium silicate, and $CaCl_2$ had on particle size, a statistical design of experiments (DOE) was produced to direct our methodologies. **Table A4.1 (**section **4.7 Appendix**) shows the full factorial (2^3) design used for the DOE. The design was free from aliasing, with all primary and higher order interactions analysed. The full factorial design was replicated twice in two blocks with one centre point per block. **Figure A4.4 (**section **4.7 Appendix**) shows the normal probability plot for the residuals. **Figure 4.6** shows the Pareto chart with a significance level of $\alpha = 0.05$. The pareto chart indicates that four variables are statistically significant; sodium silicate, NaCas, $CaCl_2$, and the two-way interaction between NaCas and $CaCl_2$. ANOVA (see **Table A4.2** in section **4.7 Appendix**) also confirms these effects are statistically significant at $\alpha = 0.05$.

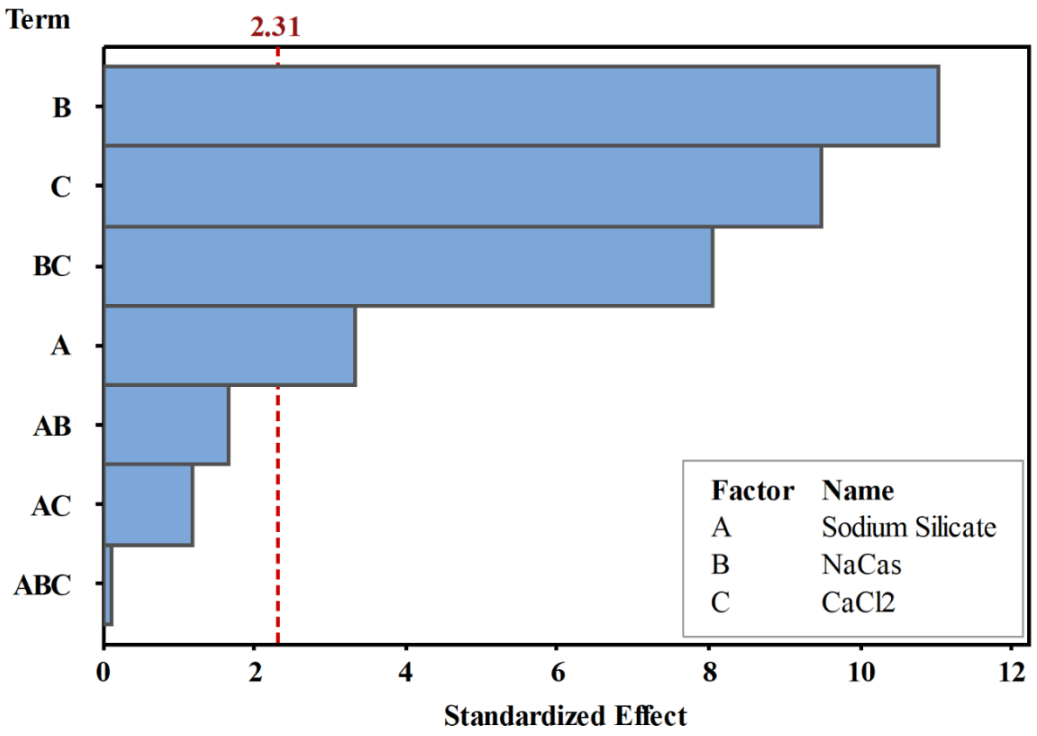


Figure 4.6 *Pareto chart of standardised effects (response is particle size, α = 0.05). Significant effects are those that extend beyond the reference line (2.31).*

Figure 4.7 shows the main effects and interaction plots for particle size. The main effects plot (**Figure 4.7A)** shows the difference in mean response (particle size) between the two levels of the factors sodium silicate, NaCas, and $CaCl_2$. The main effects plot shows that the particles produced with 486 µL sodium silicate were smaller than those produced with 728 µL. Particles produced with 20 mg NaCas were smaller than those produced with 80 mg and particles produced with 6 mM $CaCl_2$ were larger than those produced with 12 mM $CaCl_2$. However, because the two-way interaction of NaCas and $CaCl_2$ was statistically significant, this needs to be accounted for. The interaction plot (**Figure 4.7B**) shows when 20 mg NaCas and 12 mM $CaCl_2$ were used, the smallest particles were produced, while the largest particles were produced when 60 mg NaCas and 6 mM $CaCl_2$ were used.

However, because the slope of the line when using 6 mM $CaCl_2$ is steeper, the interaction between NaCas and $CaCl_2$ has a greater effect on particle size when 6 mM $CaCl_2$ is used. The statistically significant effect that the interaction between NaCas and $CaCl_2$ has on particle size is not surprising. $CaCl_2$ is needed to conformationally change and stabilise the casein micelles in the system, which is seen in the DLS data. Furthermore, while the interaction plot shows that increasing concentration of NaCas increases particle size, the effect is not as large when using 12 mM $CaCl_2$. This suggests that above a certain concentration of $CaCl_2$, the NaCas micelles are sufficiently stabilised such that addition of more $CaCl_2$ has little effect. This is confirmed in the DLS data (**Figure 4.5**) which shows that the diameter of the micelles does not change significantly when NaCas concentration is increased.

Influences on the size polydispersity of the particles is also an important to understand. The polydispersity index (PDI) is a dimensionless parameter that indicates how monodisperse the sample is. The lower the PDI, the more monodisperse the sample. Values of PDI ≤ 0.1 are defined as being highly monodisperse,[36] while values of ≤ 0.3 are considered acceptable for applications such as drug delivery.[37,38] **Figure A4.5 (**section **4.7 Appendix**) shows the polydispersity index (PDI) of the particles synthesised via the DOE protocol. All of the samples have a PDI < 0.24 with the majority of the samples < 0.18, indicating moderate monodispersity. The lowest PDI was 0.104, corresponding to a mean particle size of 215.7 nm, indicating good monodispersity.

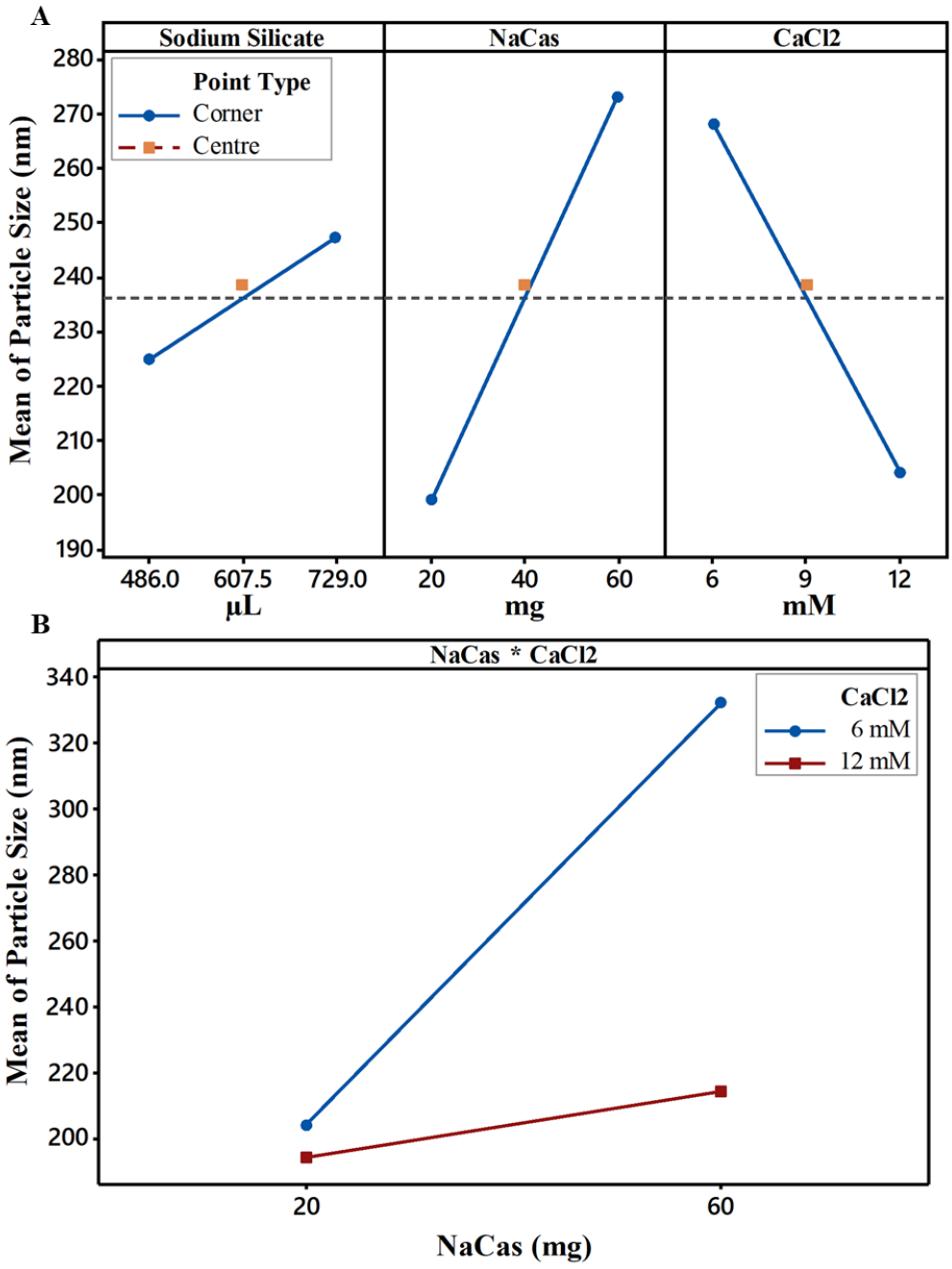


Figure 4.7 *(a) Main effects plots of sodium silicate, sodium caseinate, and calcium chloride and their effect on particle size. Differences between level means are shown for each factor level and are connected by a line. Orange squares are the mean response for the centre point runs. A non-horizontal line indicates a main effect is present. Dashed horizontal line shows the mean particle size for all runs (b) Interaction plot for particle size (fitted means). Non-parallel lines indicate that an interaction effect is occurring. The relationship between particle size and sodium caseinate depends on the concentration of calcium chloride.*

The factorial analysis of the primary and higher-order effects on particle size enables values of particle size to be predicted using regression. The regression equation obtained after stepwise regression is:

$$\text{Particle Size} = 39.5 + 0.09\ \text{Sodium Silicate} + 5.9\ \text{NaCas} + 7.4\ \text{CaCl}_2 - 0.45\ \text{NaCas} * \text{CaCl}_2 \qquad (\mathbf{4.1})$$

(sodium silicate; *μL, NaCas; mg, $CaCl_2$; mM.)*

Equation 4.1 shows that sodium silicate concentration has a minor effect on particle size, which is confirmed in the main effect plot, **Figure 4.7A**. NaCas and $CaCl_2$ both individually and through their interaction, have a larger effect than sodium silicate on particle size. However, practical and physical limitations are presumed to exist for this relationship. As discussed earlier, the interaction effect between NaCas and $CaCl_2$ has a smaller effect on particle size at higher $CaCl_2$ concentrations. Furthermore, DLS data (**Figure 4.5**) indicate that the casein micelle size does not change upon increasing NaCas concentration. However, increasing NaCas concentration increases the number of casein micelles in solution. If the rate of hydrolysis of sodium silicate is slower than the rate of nucleation, this would mean that larger particles would be formed. Furthermore, if electrostatic repulsion between forming particles is minimal and/or smaller particles are thermodynamically unstable, then particle growth could proceed by either coalescence or, Ostwald ripening, or both. Increased NaCas concentration could also lower the electrostatic repulsion between particles by stabilising the negative charge on their surfaces. The increased number of casein micelles could also reduce the interfacial energy allowing particles to grow. However, further work is needed to understand the growth dynamics of this system as other synergistic effects might also be occurring.

Table 4.5 shows a comparison between the predicted values of particle size and the experimental values. **Equation 4.1** was used to predict the particle size based on the input parameters sodium silicate, NaCas, and $CaCl_2$. **Figure 4.8** shows the SEM images of particles obtained from runs R1 to R4 and **Figure 4.9** shows their corresponding PSDs. The experimental values for particle size of R1 and R2 show excellent agreement with the predicted values and are within the 95 % CI. The experimental values of R3 and R4 are outside the 95 % CI of the predicted value, however they still show good agreement. **Table A4.3 (**section **4.7 Appendix**) shows that the R^2 (adjusted) and the R^2 (predicted) is 93.63 and 90.39 %, respectively, meaning that there is still some variation that is unaccounted for by the regression analysis. However, based on the experimental results in **Table 4.5**, the regression equation performs reasonably well in predicting the particle size based on the input factors.

Table 4.5 *Comparison of predicted and experimental values of particle size based on equation 4.1.*

Run	Sodium Silicate (µL)	NaCas[a] (mg)	$CaCl_2$ (mM)	Predicted PS[b] (nm)	Experimental PS (nm)
R1	486	20	8	189.6 [95 % CI (176, 202.3)]	200
R2	567	20	8	197.1 [95 % CI (185.6, 208.6)]	190
R3	648	20	8	204.6 [95 % CI (193.1, 216.1)]	184
R4	729	20	8	212.1 [95 % CI (198.4, 225.7)]	196

[a] NaCas, sodium caseinate
[b] PS, particle size; CI, confidence interval

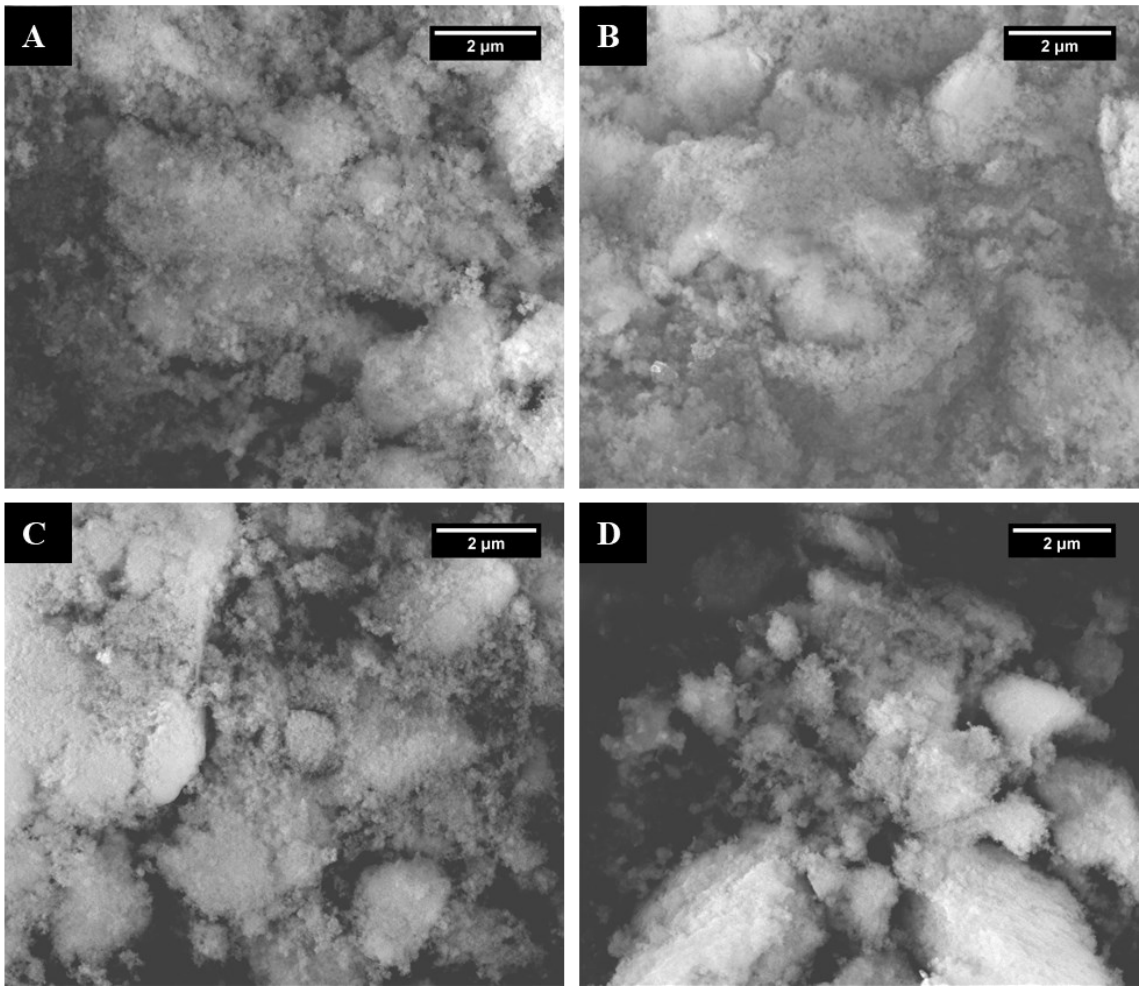


Figure 4.8 *SEM images of silica particles prepared with (a) 486 µL sodium silicate (R1), (b) 567 µL sodium silicate (R2), (c) 648 µL sodium silicate (R3), and (d) 729 µL sodium silicate (R4). All reactions used 20 mg NaCas and 8 mM* $CaCl_2$*, in 50 ml acetate buffer (0.05 M, pH 5.94).*

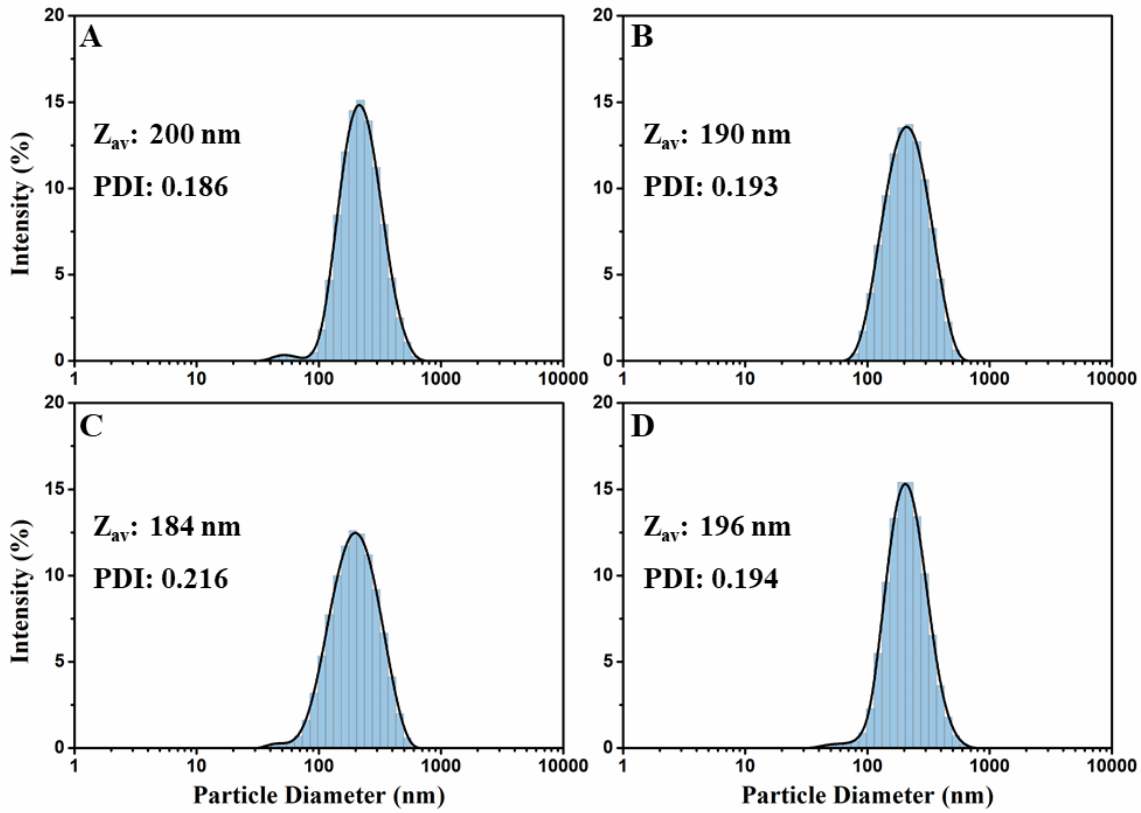


Figure 4.9 *PSDs from DLS measurements of silica particles prepared with (a) 486 µL sodium silicate (R1), (b) 567 µL sodium silicate (R2), (c) 648 µL sodium silicate (R3), and (d) 729 µL sodium silicate (R4). All reactions used 20 mg NaCas and 8 mM $CaCl_2$, in 50 ml acetate buffer (0.05 M, pH 5.94).*

XPS analysis was performed to confirm the presence of silica for the R1 particles (486 µL sodium silicate, 20 mg NaCas, and 8 mM $CaCl_2$). **Figure 4.10** shows the XPS spectrum for R1. **Figure 4.10A** shows the O 1s spectrum with peaks at 532.6 eV and 530.6 eV, corresponding to oxygen atoms of siloxane groups (Si-O-Si) and non-stoichiometric oxides (Si-O_x-Si), respectively.[39] **Figure 4.10B** shows the Si 2p spectrum with two peaks corresponding to Si-O-Si (103.05 eV) and Si-O-H (102.1 eV), which are indicative of SiO_2.[40,41] Overall, the data confirm that SiO_2 is formed. **Figure A4.6 (**section **4.7 Appendix**) shows the nitrogen sorption isotherm and the pore size distribution of the R1 particles. The isotherm is a Type H3 hysteresis loop, which can indicate the presence

of slit-shaped pores.[42] However, there is no limiting adsorption at high P/P_0 values so interpretation of the data is hindered.[43] Thus, the values for surface area, pore volume, and pore width are given for reference only. Further work on the porosity implications of using NaCas as an SDA is needed to identify its role here.

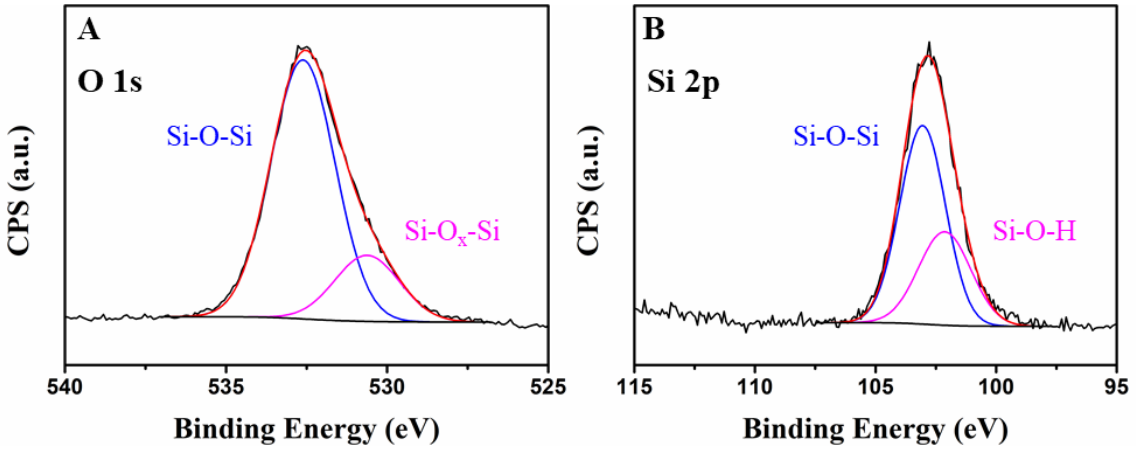


Figure 4.10 *XPS spectra of (a) O 1s and (b) Si 2p peaks of R1 (486 µL sodium silicate, 20 mg NaCas, and 8 mM $CaCl_2$). Red curve is the cumulative fitting.*

They key components of the modified-Stöber process involved in the formation of spherical silica particles are the SDA, such as CTAB and ammonium hydroxide. CTAB forms micelles in solution when the critical micelle concentration (cmc) is reached. The silica precursor is hydrolysed within the core of these micelles and subsequent condensation occurs around these micelles. The ammonium hydroxide acts as a catalyst for hydrolysis and also prevents agglomeration of the formed particles by stabilising the surface of the particles. This templated approach is driven by electrostatic and thermodynamic forces between the hydrolysed silicate species and the SDA.[24] This micellar action of SDAs like CTAB is key to the formation of spherical silica particles. NaCas has similar properties to CTAB. As discussed, NaCas can form micelles in

solution, but gives polydisperse spherical particles. However with the addition of calcium, the micelle structure of casein is stabilised, creating a more monodisperse structure.[44] This is seen in our results. When calcium is added to our system, the monodispersity of the silica particles is greatly increased. In the absence of calcium, the particles exhibit a wide size variation with multiple peaks in the PSD. Addition of calcium to the hydrophobically associated casein clusters, reforms the native micelle structure. This reformation occurs via calcium interaction with the phosphate and carboxylate groups on the protein.[45]

The above DOE analysed the influence NaCas, sodium silicate, and $CaCl_2$ had on particle size while keeping the pH constant. Isolating these factors made for an easier analysis. It is known that sodium silicate undergoes hydrolysis under acidic conditions. From the results of our experiments, it is clear that this occurs at pH 5.94 with subsequent condensation and morphological control provided by NaCas. However, to test whether this was true under different pH conditions, we conducted similar experiments at pH 4.94. **Figure 4.11** shows SEM images of particles formed at pH 4.94. It is not initially clear from the SEM data whether the particles discrete or agglomerated. Therefore DLS measurements were obtained from the samples. **Figure 4.12** shows the corresponding DLS data for these experiments. While DLS cannot give the shape of particles, it can be used to determine if the particles are aggregated. The samples were dispersed in EtOH prior to DLS measurements, giving a stable dispersion with no sedimentation. The DLS data indicate that the particles are discrete. From the SEM and DLS data it can be concluded that the particles are likely spherical. **Figure 4.12A** shows that particles of diameter 264 nm with PDI of 0.223 were formed with 40 mg NaCas. Increasing the amount of NaCas to 80 mg decreases the particle size to 254 nm, while lowering the PDI

to 0.168 (**Figure 4.12B**). Further increasing the amount of NaCas to 120 mg decreases the particle size to 228 nm, with no significant change of the PDI (**Figure 4.12C**). However, increasing the amount of NaCas to 160 mg increases the particle size to 275 nm, while also increasing the PDI to 0.212 (**Figure 4.12D**). While this system also produces relatively monodisperse particles, increasing the amount of NaCas generally results in smaller particles. This is contrary to the system at pH 5.94, where **Equation 4.1** predicts an increase in particle size with increasing NaCas. This difference in particle size response under different pH might be explained by having increased electrostatic repulsion between forming particles at lower pH. However, further work is needed to understand this dependence.

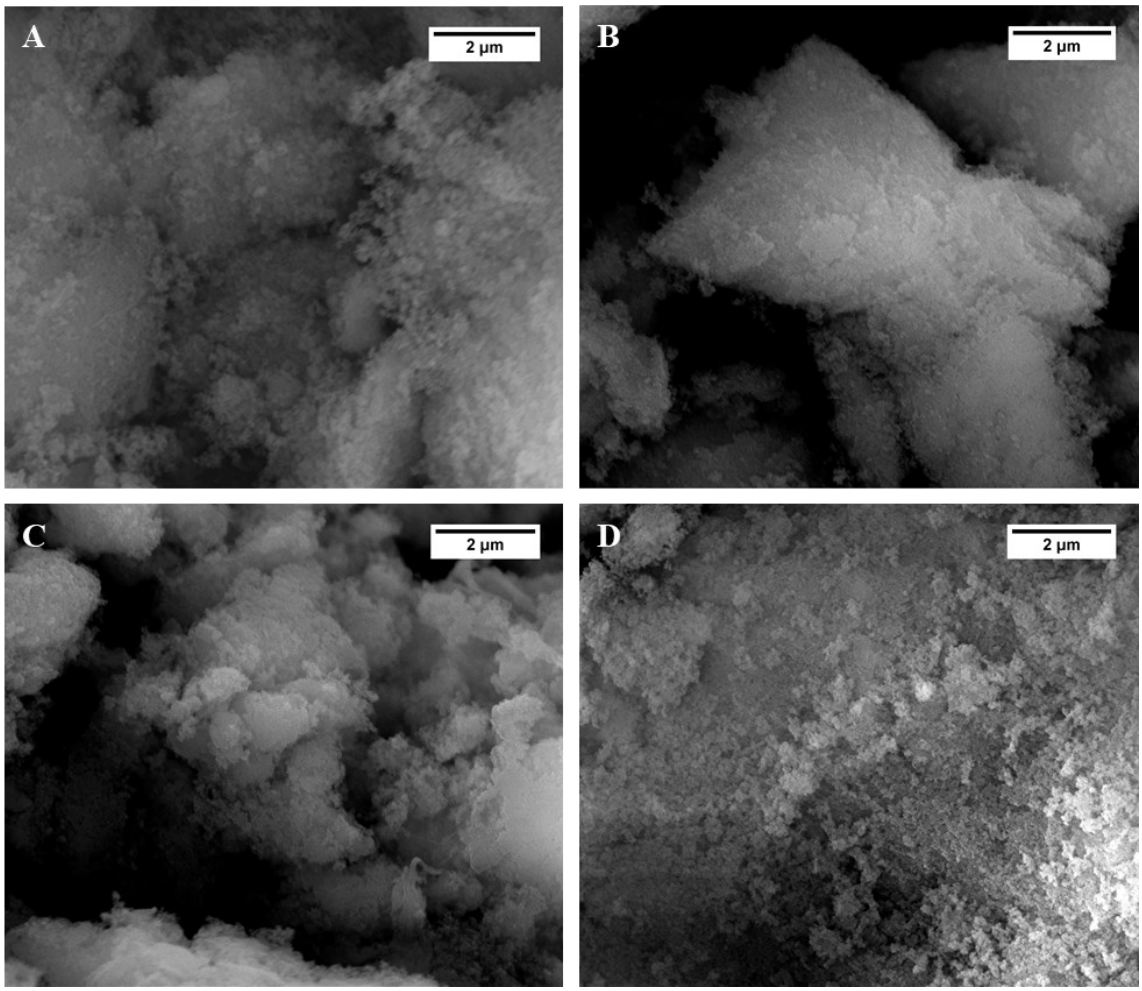


Figure 4.11 *SEM micrographs of silica prepared with (a) 40 mg NaCas (BC1), and (b) 80 mg NaCas (BC2), (c) 120 mg NaCas (BC3), and (d) 160 mg NaCas (BC4). Scale bars = 2 µm. All other reactants kept constant.*

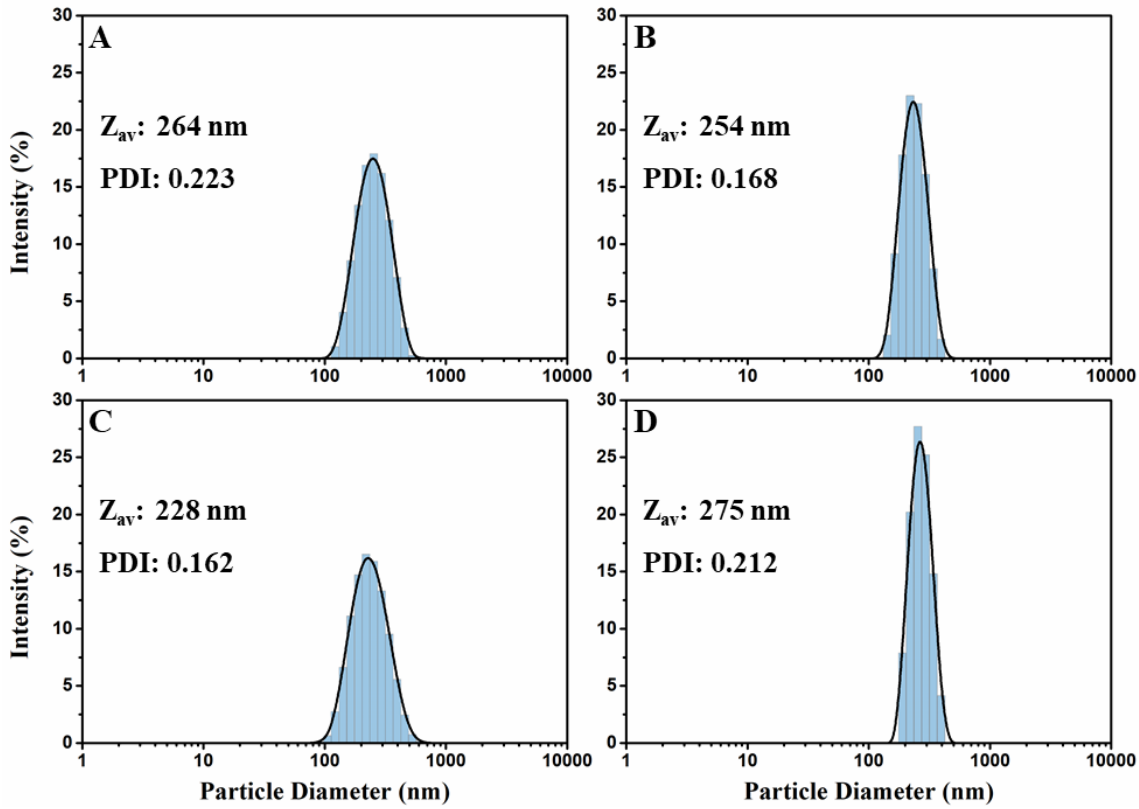


Figure 4.12 *PSDs from DLS measurements of silica prepared with (a) 40 mg NaCas (BC1), and (b) 80 mg NaCas (BC2), (c) 120 mg NaCas (BC3), and (d) 160 mg NaCas (BC4). All reactions used 729 µL sodium silicate and 8 mM $CaCl_2$, in 50 ml acetate buffer (0.05 M, pH 4.94).*

4.5 Conclusion

We have successfully developed a sustainable synthesis for producing size-monodisperse spherical silica particles. Our new synthesis provides renewable, environmentally benign substitutes for each category of component in the current, dominant, and unsustainable industrial processes – the Stöber and modified-Stöber syntheses. With the modified-Stöber process as a starting point, we have created a sustainable process using sodium caseinate in a water-based reaction. Having demonstrated that sodium caseinate can act as a structure-directing agent to form spherical silica, we used it as an effective replacement for petrochemically-derived surfactants such as CTAB. Similarly, we showed that acetate buffered water, which hydrolyses sodium silicate, could be used as a catalyst for our new system. Calcium chloride allowed us to stabilise the casein micelles to produce monodisperse spherical silica nanoparticles. We optimised this process further through a statistical design of experiments that led to the development of a regression equation that we could use to predict particle size based on input concentrations. Our experimentally produced particles were in good agreement (> 90%) with these predicted sizes. Monodisperse particles were produced at pH 5.94 and pH 4.94. Our process uses sodium caseinate, sodium silicate, calcium chloride, and acetate buffer to produce silica nanoparticles in an environmentally friendly and sustainable way. These particles are the most monodisperse and spherical produced with biopolymers that have been documented in the literature to date.

4.6 References

1. Capello, C., Fischer, U. & Hungerbühler, K. What is a green solvent? A comprehensive framework for the environmental assessment of solvents. *Green Chem.* **9**, 927–934 (2007) DOI: 10.1039/b617536h.

2. Isomaa, B., Reuter, J. & Djupsund, B. M. The subacute and chronic toxicity of cetyltrimethylammonium bromide (CTAB), a cationic surfactant, in the rat. *Arch. Toxicol.* **35**, 91–96 (1976) DOI: 10.1007/BF00372762.

3. Nałęcz-Jawecki, G., Grabińska-Sota, E. & Narkiewicz, P. The toxicity of cationic surfactants in four bioassays. *Ecotoxicol. Environ. Saf.* **54**, 87–91 (2003) DOI: 10.1016/S0147-6513(02)00025-8.

4. Knepper, T. P. & Berna, J. L. Surfactants: Properties, production, and environmental Aspects. in 1–49 (2003). doi:10.1016/S0166-526X(03)40004-4 DOI: 10.1016/S0166-526X(03)40004-4.

5. Scully, S. M. & Orlygsson, J. Biological Production of Alcohols. in *Advanced Bioprocessing for Alternative Fuels, Biobased Chemicals, and Bioproducts* 83–108 (Elsevier, 2019). doi:10.1016/B978-0-12-817941-3.00005-X DOI: 10.1016/B978-0-12-817941-3.00005-X.

6. Patwardhan, S. V & Staniland, S. S. Biomineralisation: how Nature makes nanomaterials. in *Green Nanomaterials: From bioinspired synthesis to sustainable manufacturing of inorganic nanomaterials* (IOP Publishing, 2019). doi:10.1088/978-0-7503-1221-9ch6 DOI: 10.1088/978-0-7503-1221-9ch6.

7. Aimé, C., Coradin, T. & Fernandes, F. M. Biomimetic Sol-Gel Materials. in *The Sol-Gel Handbook* vols 1–3 605–650 (2015). DOI: 10.1002/9783527670819.ch19.

8. Sabu, C., Rejo, C., Kotta, S. & Pramod, K. Bioinspired and biomimetic systems for advanced drug and gene delivery. *J. Control. Release* **287**, 142–155 (2018) DOI: 10.1016/j.jconrel.2018.08.033.

9. Sun, Q., Vrieling, E. G., Van Santen, R. A. & Sommerdijk, N. A. J. M. Bioinspired

synthesis of mesoporous silicas. *Curr. Opin. Solid State Mater. Sci.* **8**, 111–120 (2004) DOI: 10.1016/j.cossms.2004.01.005.

10. Demadis, K. D., Pachis, K., Ketsetzi, A. & Stathoulopoulou, A. Bioinspired control of colloidal silica in vitro by dual polymeric assemblies of zwitterionic phosphomethylated chitosan and polycations or polyanions. *Adv. Colloid Interface Sci.* **151**, 33–48 (2009) DOI: 10.1016/j.cis.2009.07.005.

11. Gautier, C. *et al.* Biomimetic dual templating of silica by polysaccharide/protein assemblies. *Colloids Surfaces B Biointerfaces* **65**, 140–145 (2008) DOI: 10.1016/j.colsurfb.2008.03.005.

12. Jia, J., Zhou, X., Caruso, R. A. & Antonietti, M. Synthesis of Microporous Silica Templated by Gelatin. *Chem. Lett.* **33**, 202–203 (2004) DOI: 10.1246/cl.2004.202.

13. Coradin, T., Coupé, A. & Livage, J. Interactions of bovine serum albumin and lysozyme with sodium silicate solutions. *Colloids Surfaces B Biointerfaces* **29**, 189–196 (2003) DOI: 10.1016/S0927-7765(02)00208-4.

14. Coradin, T., Durupthy, O. & Livage, J. Interactions of amino-containing peptides with sodium silicate and colloidal silica: A biomimetic approach of silicification. *Langmuir* vol. 18 2331–2336 (2002) DOI: 10.1021/la011106q.

15. Yerramilli, M. & Ghosh, S. Long-term stability of sodium caseinate-stabilized nanoemulsions. *J. Food Sci. Technol.* **54**, 82–92 (2017) DOI: 10.1007/s13197-016-2438-y.

16. Xi, Y. *et al.* Sodium caseinate as a particulate emulsifier for making indefinitely recycled pH-responsive emulsions. *Chem. Sci.* **11**, 3797–3803 (2020) DOI: 10.1039/C9SC05050G.

17. Ji, J. *et al.* Preparation and stabilization of emulsions stabilized by mixed sodium caseinate and soy protein isolate. *Food Hydrocoll.* **51**, 156–165 (2015) DOI: 10.1016/j.foodhyd.2015.05.013.

18. Bonnet, C., Corredig, M. & Alexander, M. Stabilization of Caseinate-Covered Oil Droplets during Acidification with High Methoxyl Pectin. *J. Agric. Food Chem.*

53, 8600–8606 (2005) DOI: 10.1021/jf0511998.

19. Huppertz, T., Fox, P. F. & Kelly, A. L. *The caseins: Structure, stability, and functionality*. *Proteins in Food Processing: Second Edition* (Elsevier Ltd., 2018). doi:10.1016/B978-0-08-100722-8.00004-8 DOI: 10.1016/B978-0-08-100722-8.00004-8.

20. Belyakova, L. E. *et al.* Effect of sucrose on molecular and interaction parameters of sodium caseinate in aqueous solution: relationship to protein gelation. *Colloids Surfaces B Biointerfaces* **31**, 31–46 (2003) DOI: 10.1016/S0927-7765(03)00041-9.

21. McMahon, D. J. & Oommen, B. S. Casein Micelle Structure, Functions, and Interactions. in *Advanced Dairy Chemistry* 185–209 (Springer US, 2013). doi:10.1007/978-1-4614-4714-6_6 DOI: 10.1007/978-1-4614-4714-6_6.

22. Dickinson, E. *et al.* Analysis of Light Scattering Data on the Calcium Ion Sensitivity of Caseinate Solution Thermodynamics: Relationship to Emulsion Flocculation. *J. Colloid Interface Sci.* **239**, 87–97 (2001) DOI: 10.1006/jcis.2001.7480.

23. Büchel, G., Grün, M., Unger, K. K., Matsumoto, A. & Kazuo, T. Tailored syntheses of nanostructured silicas: Control of particle morphology, particle size and pore size. *Supramol. Sci.* **5**, 253–259 (1998) DOI: 10.1016/S0968-5677(98)00016-9.

24. Alothman, Z. A Review: Fundamental Aspects of Silicate Mesoporous Materials. *Materials (Basel).* **5**, 2874–2902 (2012) DOI: 10.3390/ma5122874.

25. Goretsky, A. V., Beck, L. W., Zones, S. I. & Davis, M. E. Influence of the hydrophobic character of structure-directing agents for the synthesis of pure-silica zeolites. *Microporous Mesoporous Mater.* **28**, 387–393 (1999) DOI: 10.1016/S1387-1811(98)00307-2.

26. Wan, Y. & Zhao, D. On the controllable soft-templating approach to mesoporous silicates. *Chem. Rev.* **107**, 2821–2860 (2007) DOI: 10.1021/cr068020s.

27. Keane, D. A., Hanrahan, J. P., Copley, M. P., Holmes, J. D. & Morris, M. A. A

modified Stöber process for the production of mesoporous Sub 2 micron silica microspheres; applications in HPLC. *J. Porous Mater.* **17**, 145–152 (2010) DOI: 10.1007/s10934-009-9274-7.

28. Trejo, R. & Harte, F. The effect of ethanol and heat on the functional hydrophobicity of casein micelles. *J. Dairy Sci.* **93**, 2338–2343 (2010) DOI: 10.3168/jds.2009-2918.

29. van Dokkum, H. P., Hulskotte, J. H. J., Kramer, K. J. M. & Wilmot, J. Emission, Fate and Effects of Soluble Silicates (Waterglass) in the Aquatic Environment. *Environ. Sci. Technol.* **38**, 515–521 (2004) DOI: 10.1021/es0264697.

30. Sierra, L. & Guth, J. L. Synthesis of mesoporous silica with tunable pore size from sodium silicate solutions and a polyethylene oxide surfactant. *Microporous Mesoporous Mater.* **27**, 243–253 (1999) DOI: 10.1016/S1387-1811(98)00258-3.

31. Lifshitz, I. M. & Slyozov, V. V. The kinetics of precipitation from supersaturated solid solutions. *J. Phys. Chem. Solids* **19**, 35–50 (1961) DOI: 10.1016/0022-3697(61)90054-3.

32. Wagner, C. Theorie der Alterung von Niederschlägen durch Umlösen (Ostwald-Reifung). *Berichte der Bunsengesellschaft für Phys. Chemie* **65**, 581–591 (1961) DOI: 10.1002/BBPC.19610650704.

33. De Kruif, C. G. & Holt, C. Casein Micelle Structure, Functions and Interactions. in *Advanced Dairy Chemistry—1 Proteins* vol. 1 233–276 (Springer US, 2003). DOI: 10.1007/978-1-4419-8602-3_5.

34. Glantz, M. *et al.* Importance of casein micelle size and milk composition for milk gelation. *J. Dairy Sci.* **93**, 1444–1451 (2010) DOI: 10.3168/jds.2009-2856.

35. Sinaga, H., Bansal, N. & Bhandari, B. Effects of milk pH alteration on casein micelle size and gelation properties of milk. *Int. J. Food Prop.* **20**, 179–197 (2017) DOI: 10.1080/10942912.2016.1152480.

36. Bhattacharjee, S. DLS and zeta potential – What they are and what they are not ? *J. Control. Release* **235**, 337–351 (2016) DOI: 10.1016/j.jconrel.2016.06.017.

37. Danaei, M. *et al.* Impact of Particle Size and Polydispersity Index on the Clinical Applications of Lipidic Nanocarrier Systems. *Pharmaceutics* **10**, 57 (2018) DOI: 10.3390/pharmaceutics10020057.

38. Mohammadpour Dounighi, N. *et al.* Preparation and in vitro characterization of chitosan nanoparticles containing Mesobuthus eupeus scorpion venom as an antigen delivery system. *J. Venom. Anim. Toxins Incl. Trop. Dis.* **18**, 44–52 (2012) DOI: 10.1590/S1678-91992012000100006.

39. Lamastra, F. R., Mori, S., Cherubini, V., Scarselli, M. & Nanni, F. A new green methodology for surface modification of diatomite filler in elastomers. *Mater. Chem. Phys.* **194**, 253–260 (2017) DOI: 10.1016/j.matchemphys.2017.03.050.

40. Post, P., Wurlitzer, L., Maus-Friedrichs, W. & Weber, A. Characterization and Applications of Nanoparticles Modified in-Flight with Silica or Silica-Organic Coatings. *Nanomaterials* **8**, 530 (2018) DOI: 10.3390/nano8070530.

41. Li, S., Chen, F., Lin, F., Kong, Y. & Dai, H. Adsorption Performance of SiO2/CPAM Composites for Aqueous Ca(II). *BioResources* **13**, (2018) DOI: 10.15376/biores.13.2.3554-3570.

42. Thommes, M. Physical Adsorption Characterization of Nanoporous Materials. *Chemie Ing. Tech.* **82**, 1059–1073 (2010) DOI: 10.1002/cite.201000064.

43. Sing, K. S. W. & Williams, R. T. Physisorption Hysteresis Loops and the Characterization of Nanoporous Materials. *Adsorpt. Sci. Technol.* **22**, 773–782 (2004) DOI: 10.1260/0263617053499032.

44. Smialowska, A., Merino, L. M.-, Ingham, B. & Carr, A. J. Effect of calcium on the aggregation behaviour of caseinates. *Colloids Surfaces A Physicochem. Eng. Asp.* (2017) doi:10.1016/j.colsurfa.2017.02.074 DOI: 10.1016/j.colsurfa.2017.02.074.

45. Curley, D. M., Kumosinski, T. F., Unruh, J. J. & Farrell, H. M. Changes in the Secondary Structure of Bovine Casein by Fourier Transform Infrared Spectroscopy: Effects of Calcium and Temperature. *J. Dairy Sci.* **81**, 3154–3162 (1998) DOI: 10.3168/jds.S0022-0302(98)75881-3.

46. McMahon, D. J. & Oommen, B. S. Supramolecular Structure of the Casein Micelle. *J. Dairy Sci.* **91**, 1709–1721 (2008) DOI: 10.3168/jds.2007-0819.

47. Dalgleish, D. G., Spagnuolo, P. A. & Douglas Goff, H. A possible structure of the casein micelle based on high-resolution field-emission scanning electron microscopy. *Int. Dairy J.* **14**, 1025–1031 (2004) DOI: 10.1016/j.idairyj.2004.04.008.

4.7 Appendix

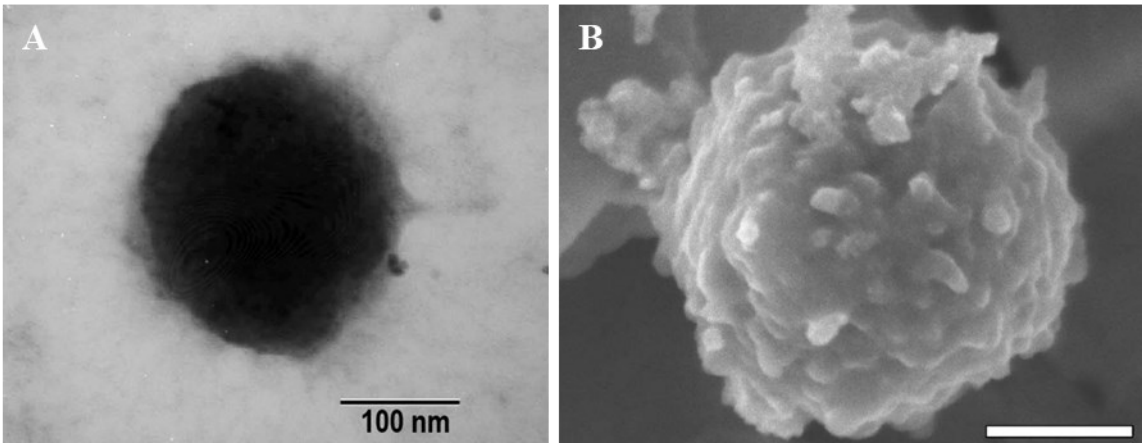


Figure A4.1 *Structure of casein micelle. (a) Transmission electron micrograph of freeze-dried poly-L-lysine immobilised casein micelle fixed with glutaraldehyde (from McMahon et al.*[46] *(b) Electron micrograph of an individual casein micelle, scale bar = 100 nm. (from Dalgleish et al.*[47]

Figure A4.2 shows SEM images of the formed solids obtained when no NaCas is present. These monolithic structures have no defined shape or size. **Figure A4.2A** shows the solids formed in the control experiment using water, sodium silicate, and ammonium hydroxide. **Figure A4.2B** shows the formed solids formed in the control experiment using acetate buffer and sodium silicate. Under acidic conditions, such as those used here, sodium silicate undergoes hydrolysis and subsequent polymerisation to form silica. In the absence of a structure-directing agent, this process is uncontrolled and results in these monolithic structures. This result was as expected, given the lack of a SDA. Therefore, we concluded that spherical particles do not form in our reaction system without the presence of NaCas.

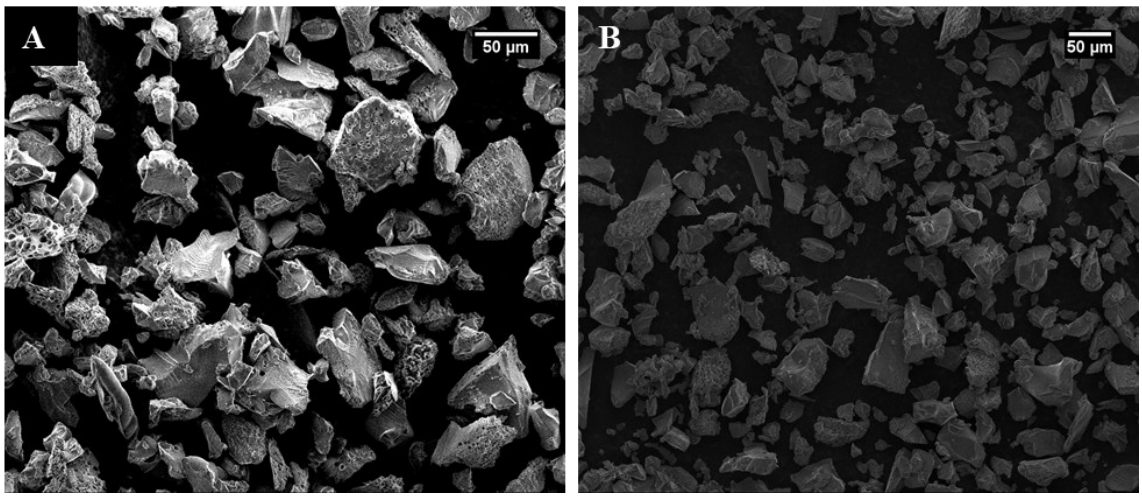


Figure A4.2 *Monolith structures formed when no NaCas is present. (a) 25 ml H_2O, 3.2 ml sodium silicate, 12 ml NH_4OH and (b) 50 ml acetate buffer (0.05 M, pH 5.94), 81 µL sodium silicate.*

Figure A4.3 shows SEM images of the solids formed when distilled water is used instead of acetate buffer. These monoliths have no defined shape or size. This indicates that slightly acidic pH, in the form of acetate buffer (0.05 M, pH 5.94), is needed to conformationally change the NaCas into a form that can facilitate its structure-directing ability.

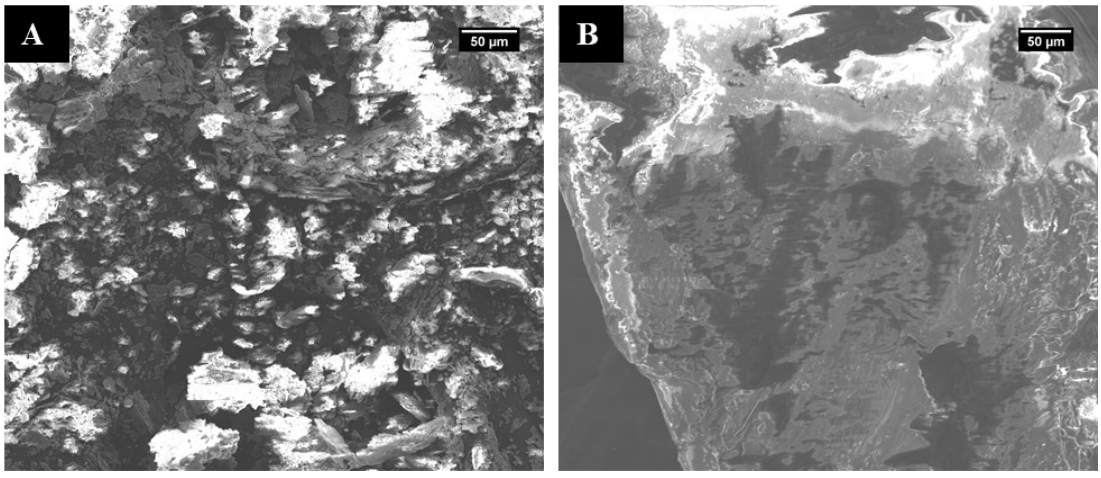


Figure A4.3 *Monolith structures formed when distilled water is used instead of acetate buffer (0.05 M, pH 5.94).*

Table A4.1 *Experimental conditions for 2^3 full factorial design with 2 replicates, 2 blocks, and 1 centre per block. Factors: SS; sodium silicate, NaCas; sodium caseinate, $CaCl_2$. Response variable: PS; particle size. Each factor has two levels and each centre point is midway between these levels. All terms are free from aliasing. Block generators are the replicates.*

RunOrder	CentrePt	Blocks	SS (µL)	NaCas (mg)	$CaCl_2$ (mM)	PS (nm)	PDI
1	1	1	486	60	6	337.9	0.161
2	1	1	486	20	12	174.3	0.143
3	1	1	729	20	6	216.8	0.184
4	1	1	486	20	6	199.3	0.162
5	1	1	486	60	12	210.0	0.167
6	1	1	729	20	12	208.0	0.153
7	1	1	729	60	12	247.9	0.237
8	1	1	729	60	6	329.1	0.211
9	0	1	607	40	9	250.1	0.231
10	1	2	486	60	6	322.1	0.187
11	1	2	486	20	6	183.5	0.167
12	1	2	729	60	12	199.0	0.117
13	0	2	607	40	9	226.9	0.139
14	1	2	729	20	12	222.1	0.128
15	1	2	486	60	12	199.8	0.186
16	1	2	729	60	6	339.5	0.164
17	1	2	486	20	12	171.9	0.158
18	1	2	729	20	6	215.7	0.104

Table A4.2 *Analysis of variance (ANOVA) for particle size. NaCas; sodium caseinate.*

Source	DF	Adj. SS	Adj. MS	F-Value	p-Value
Model	9	53286.3	5920.7	32.80	0.000
Blocks	1	479.5	479.5	2.66	0.142
Linear	3	40352.9	13451.0	74.53	0.000
Sodium Silicate	1	2009.3	2009.3	11.13	0.010
NaCas	1	22030.0	22030.0	122.06	0.000
$CaCl_2$	1	16313.7	16313.7	90.39	0.000
2-Way Interactions	3	12441.3	4147.1	22.98	0.000
Sodium Silicate*NaCas	1	482.9	482.9	2.68	0.141
Sodium Silicate*$CaCl_2$	1	245.7	245.7	1.36	0.277
NaCas*$CaCl_2$	1	11712.7	11712.7	64.90	0.000
3-Way Interactions	1	2.0	2.0	0.01	0.918
Sodium Silicate*NaCas*$CaCl_2$	1	2.0	2.0	0.01	0.918
Curvature	1	10.6	10.6	0.06	0.814
Error	8	1443.9	180.5		
Total	17	54730.2			

Table A4.3 *Factorial regression model summaries. Initial regression model included all terms. Stepwise regression model identified and included terms from the initial model that were less than or equal to α = 0.05 and removed terms that were greater than α = 0.05.*

Initial				After stepwise regression			
S	r-sq	r-sq(adj)	r-sq(pred)	S	r-sq	r-sq(adj)	r-sq(pred)
13.4345	97.36 %	94.39 %	86.64 %	14.3168	95.13 %	93.63 %	90.39 %

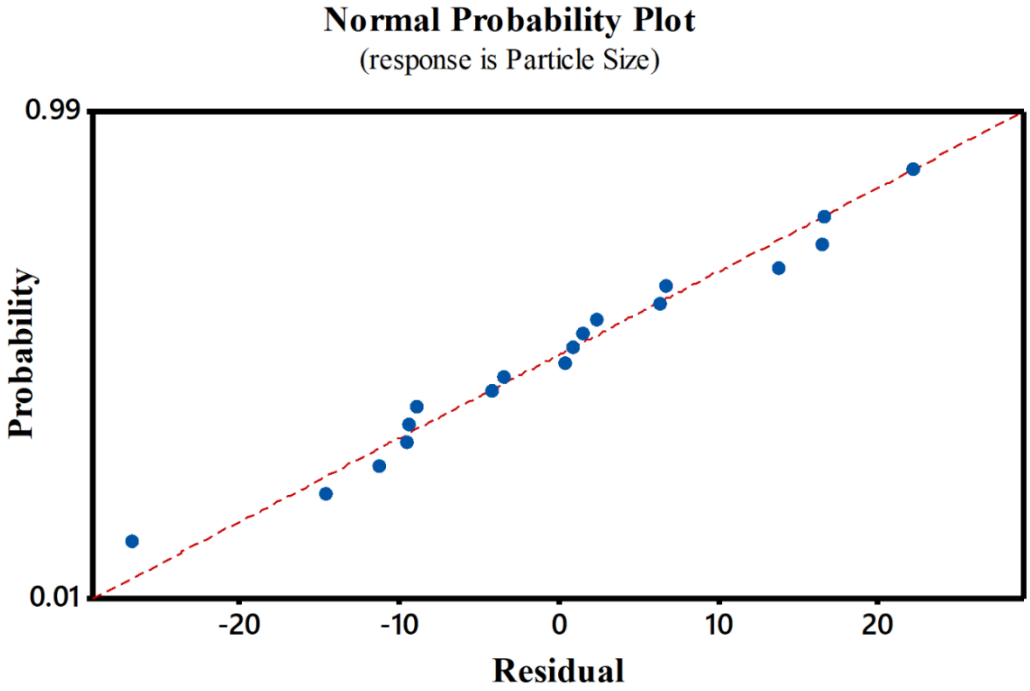


Figure A4.4 *Normal probability plot of residuals (response is particle size).*

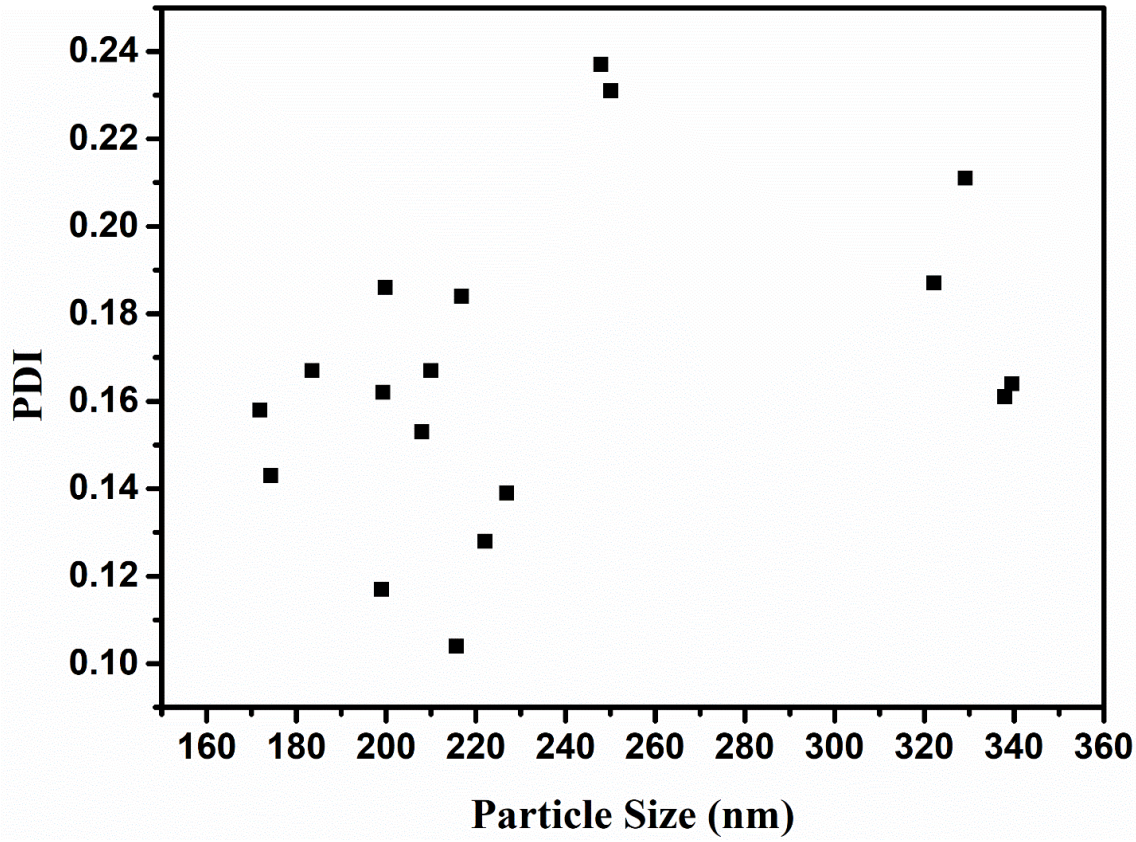


Figure A4.5 *Polydispersity index (PDI) and corresponding particle size of the particles synthesised via the DOE protocol.*

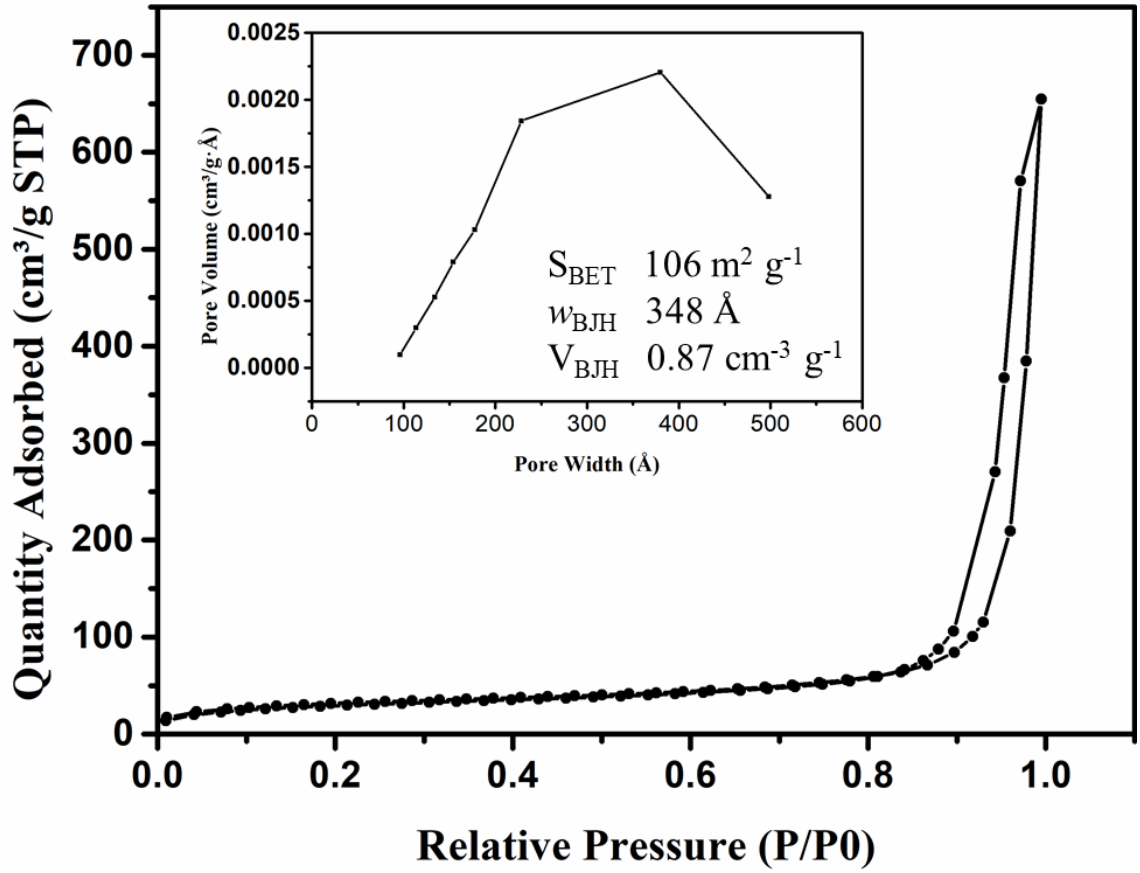


Figure A4.6 *N_2 sorption isotherm and pore size distribution (inset) of R1 silica particles.*

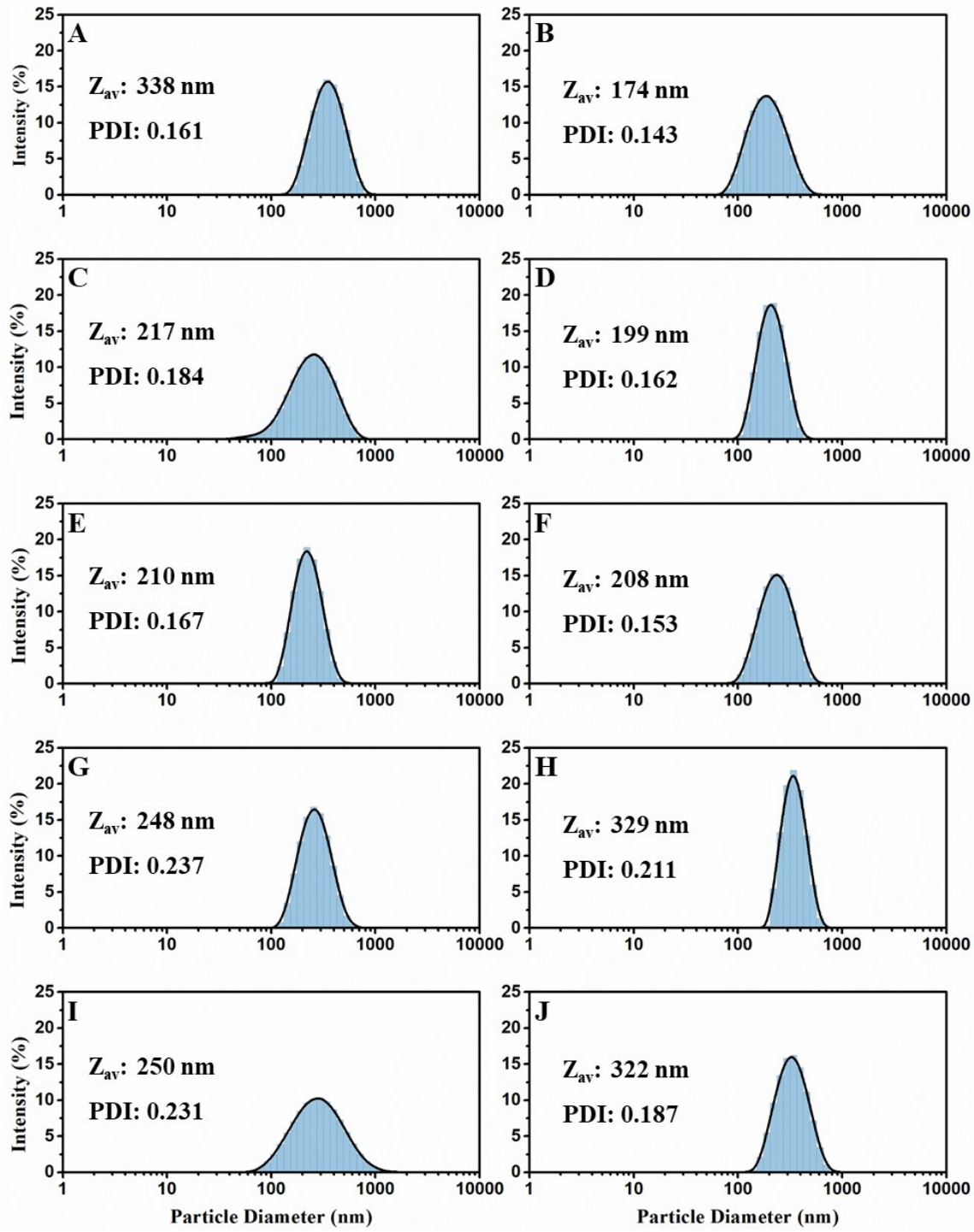


Figure A4.7 *DLS measurements of particles synthesised in factorial analysis (see Table A4.1). (a) Run 1, (b) Run 2, (c) Run 3, (d) Run 4, (e) Run 5, (f) Run 6, (g) Run 7, (h) Run 8, (i) Run 9, and (j) Run 10.*

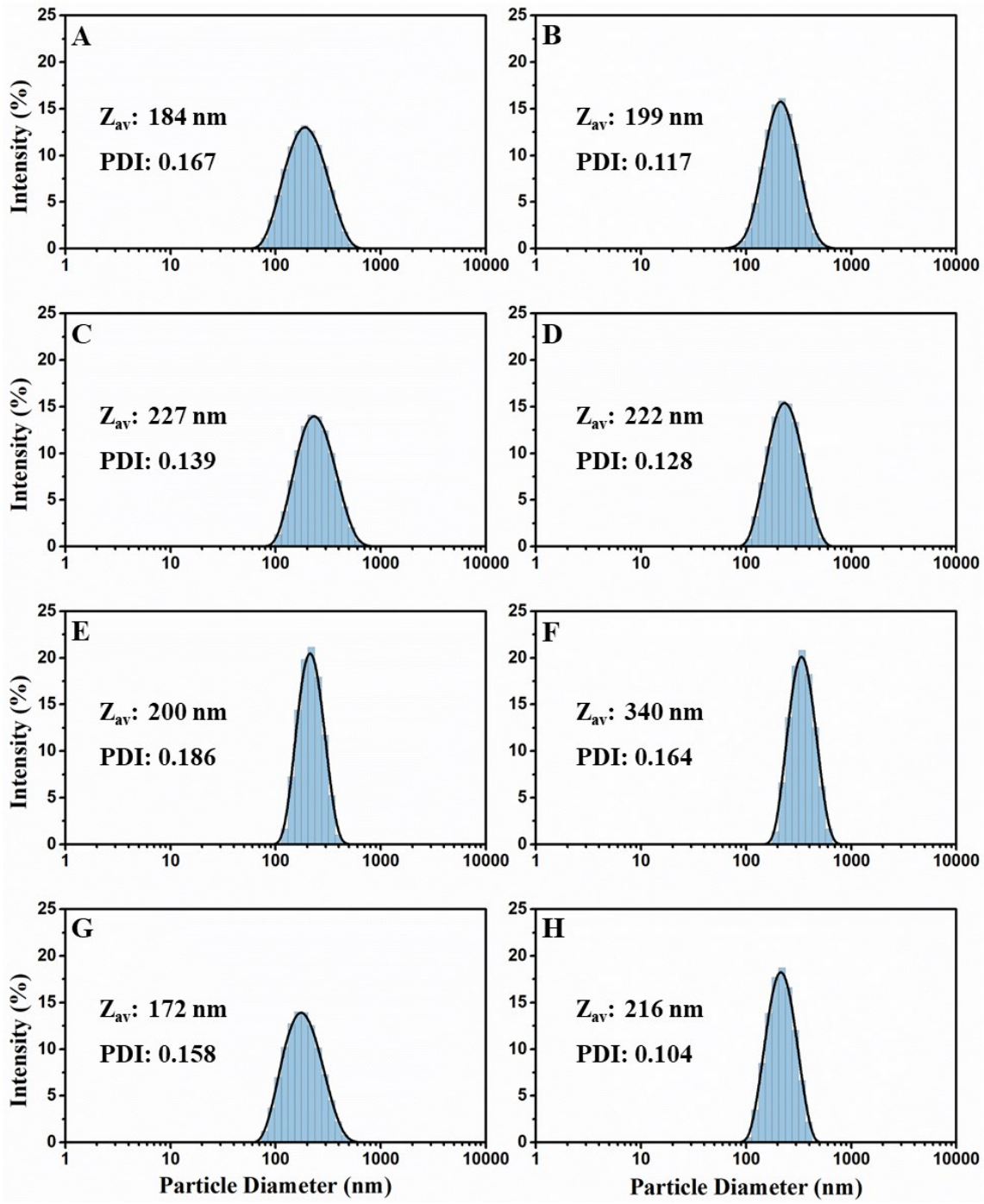


Figure A4.8 *DLS measurements of particles synthesised in factorial analysis (see Table A4.1). (a) Run 11, (b) Run 12, (c) Run 13, (d) Run 14, (e) Run 15, (f) Run 16, (g) Run 17, and (h) Run 18.*

Chapter 5

Conclusion and Future Work

5.1 Conclusion

Spherical silica is one of the most important materials used worldwide. The versatility of these particles is virtually endless. The relative ease with which they can be produced and modified means their application spans a wide range of industries. Due to their widespread use, finding sustainable routes for their production is of particular interest. The traditional Stöber methods are inherently unsustainable and environmentally damaging due to their reliance on petrochemically-derived reagents. Bioinspired synthetic routes which minimise environmental damage and maximise sustainability must be prioritised. To this end, the initial part of this thesis dealt with improving the efficiency of an already established industrial silica process used by Glantreo Ltd. However, such improvements in efficiencies, while having a positive effect on the overall sustainability of the process, are self-limiting due to the inherent unsustainability of the reagents used in the process. Therefore, the latter parts of this thesis focused on developing a sustainable biomimetic process for synthesising spherical silica particles using biopolymers, mild conditions, and water-based chemistries.

Chapter 2 described the statistical analysis of the process used by Glantreo Ltd. to synthesise spherical silica particles. The effect that ethanol, TEOS, water, and ammonia had on particle size was analysed and a method for controlling particle size based on input reagent concentrations was produced. The objective was to analyse the Glantreo Ltd. process by varying the concentration of each reagent and determining their effect on particle size. Increasing the concentration of ethanol results in an increase in particle size. An increase in TEOS concentration also results in an increase in particle size. Similarly, increasing the concentration of ammonium hydroxide results in an increase in particle size

up to 5.1 M ammonium hydroxide. Above 5.1 M ammonium hydroxide, the particle size begins to decrease. Increasing the volume of water results in an increase in particle size up to 0.8 ml water. Above 0.8 ml water, the particle size begins to decrease. The results presented here agree well with other studies in the literature on the Stöber process.

The statistical analysis of this Glantreo Ltd. process enabled the synthesis of silica nanoparticles of controllable dimension, a key requirement for Glantreo Ltd. to subsequently scale-up this process. Information acquired during this analysis allowed for an efficient and high-yielding scale-up. In terms of increasing sustainability, these iterative, small improvements in process efficiencies typify current attempts by industry to reduce greenhouse gas emissions and to pollute less in general. Unfortunately, to this end, such approaches suffer from two basic issues – diminishing returns and the fundamentally toxic nature of the reagents involved. There is only so far one can push these increases in efficiency, before you cannot increase sustainability any further. At that point you are still generating pollution, though less. Those pollutants are highly toxic, often bioaccumulate, and come with large embedded environmental costs that are not addressed by the increases in efficiency within the silica production processes. There is an important place for such methods, and that is to buy us time to more fundamentally address the issues of current industrial production but, they are not an ultimate solution. There have been many studies looking at improving the sustainability of the Stöber processes. Some, like the work presented here, focus on optimising the efficiency of the process by using less reagents or maximising yield. Others focus on altering the process and using more sustainable reagents such as biomolecules and benign experimental conditions. Currently, much of the focus has been on employing the principles of green

chemistry to achieve the goal of sustainable syntheses. The work presented in this chapter represents a first-step approach, which is often used in industry, that minimises the changes to the reaction but maximises efficiency.

Chapter 3 described the use of phosphatidylcholine and soy lecithin to synthesise spherical silica particles. Phosphatidylcholine was combined with soybean oil, acetate buffer, and sodium silicate, yielding polydisperse spherical particles. Soy lecithin was combined with acetate buffer and sodium silicate, giving spherical and more monodisperse particles than the phosphatidylcholine system. DLS data of phosphatidylcholine in acetate buffer and soy lecithin in acetate buffer showed that in the absence of sodium silicate, soy lecithin forms polydisperse bilayer structures, while phosphatidylcholine forms less polydisperse structures. Polydispersity data of the particles obtained in the phosphatidylcholine system correlate with DLS for phosphatidylcholine in acetate buffer. However, the particles obtained in the soy lecithin system were more monodisperse than the DLS data would predict. However, temporal evolution data of the soy lecithin system when sodium silicate is introduced shows that the polydispersity index of the bilayer structures decreases and becomes unimodal. This shows that the presence of sodium silicate reduces the size of the soy lecithin bilayer while also narrowing their size distribution. Sodium ions from the sodium silicate penetrate the headgroup double layer of the phospholipids, enhancing the attractive forces between them, likely resulting in a change in curvature and reduced size. This effect was more prominent in the soy lecithin system, likely because soy lecithin also contains phosphatidylethanolamine and phosphatic acid, which are more sterically accessible to the sodium ions. A mixture of Oswald ripening and coalescence was shown to occur at

low phospholipid concentrations, while Ostwald ripening dominated at higher phospholipid concentrations. Higher phospholipid concentrations also tended to increase particle size. The use of phosphatidylcholine, soy lecithin and water-based chemistries constitutes an increase in sustainability over the Stöber processes. Both phospholipids can be obtained from the waste streams of soybean oil production, thus valorising these by-products. These phospholipids are biodegradable and renewable, which is in stark contrast to the petrochemically-derived surfactants that are traditionally used. Such methods which emphasise sustainability are gaining traction in the area of silica production and beyond. While the quality of the particles presented in this chapter is not comparable to the quality of the particles readily achievable with established Stöber processes, the demonstration that particles can be formed using soy lecithin and phosphatidylcholine in a sustainable synthesis is nonetheless important. The more studies that show that biomolecules can be used to synthesise silica, the faster the adoption and development of such processes become.

Chapter 4 described the use of sodium caseinate to synthesise spherical silica particles in a biomimetic and sustainable way. DLS data showed that sodium caseinate forms micelles in solution and was demonstrated to act as an SDA to form spherical particles. In the absence of sodium caseinate, no spherical particles are formed. Polydisperse spherical silica particles were formed when using acetate buffer (pH 5.94), sodium silicate, and sodium caseinate. The particles were observed to form via Ostwald ripening at low concentrations of sodium silicate and a mixture of coalescence and Ostwald ripening at high concentrations. At low concentrations of sodium caseinate particles form primarily through coalescence, while at higher concentrations of sodium caseinate, a mixture of

coalescence and Ostwald ripening occurs. Addition of calcium chloride to the acetate buffer (pH 5.94), sodium silicate, and sodium caseinate system led to the formation of monodisperse spherical particles. Calcium chloride interacts with the sodium caseinate and stabilises the casein micelles. DLS data confirmed that addition of calcium chloride decreased the size and increased the monodispersity of the casein micelles. Factorial analysis and statistical regression of the calcium chloride system showed that the interaction between calcium chloride and sodium caseinate had a statistically significant effect on particle size. The regression equation obtained from the statistical analysis showed good agreement (> 90 %) between the predicted and experimental particle sizes. Experiments conducted at pH 4.94 also showed that particles with good dispersity could also be produced at lower pH. Sodium caseinate can be obtained from the waste streams of dairy production. Valorisation of such wastes increases the sustainability of silica particle production. The monodisperse silica particles produced using our sustainable biopolymer-based process would make ideal candidates for advanced applications such drug delivery. Residual surfactants remaining in particles produced using traditional Stöber processes can pose health problems when used *in vivo*. Residual sodium caseinate poses no such problems. Apart from this, the spherical silica particles synthesised using our biopolymer-based method could be used in any application in which those synthesised by traditional methods are used. Controlling monodispersity has been the most difficult aspect when using biomolecules to produce silica particles. **Chapter 3** is a good example of this, and many other studies in the literature show that controlling this parameter is difficult. Our results using calcium chloride and sodium caseinate show that achieving relatively good monodispersity is possible using biomolecules in sustainable syntheses.

5.2 Future Work

Our spherical silica particles were produced using biomimetic and sustainable methods and could provide a way of producing such particles on larger scales. Organic solvents and alcohols were shown not be necessary for spherical silica production. Renewable, sustainable, and biodegradable biopolymers were used in lieu of petrochemically-derived surfactants. Purely water-based chemistries remove the need for industrial solvent recovery processes. Overall, producing spherical silica particles by biomimetic and sustainable methods would greatly reduce the environmental damage caused by traditional Stöber processes. Industrial waste streams are a potential source of biopolymers that can act as structural directing agents. Such agents are key to maximising the sustainability of our proposed processes. Controlling the monodispersity of the final particles is dependent on the biopolymer properties and reaction conditions. Finding biopolymers which can mediate and control silica polymerisation while simultaneously controlling morphology is the cornerstone of biomimetic silica synthesis. Identifying more biopolymers that meet these criteria would promote further developments in this field.

Elucidating the structure of phosphatidylcholine and soy lecithin in our acetate buffer system would provide more insight into the specific role these biomolecules have on the morphology of the particles. Small-angle neutron scattering (SANS) or small-angle X-ray scattering (SAXS) would both be useful tools in this regard. Both techniques are routinely used to determine biomolecular structures. This data would help to optimise the synthesis conditions and hopefully improve the monodispersity of the particles produced using phosphatidylcholine and soy lecithin. Determining whether the biomolecules could be

recycled and used again after the synthesis would be an interesting study. If this were the case, then the sustainability of the reaction would increase further. If the biomolecules could be used for multiple syntheses, how many times, and their effect on the particles would be useful to know.

The exact structure of the casein micelle is still debated in the literature, even with SANS and SAXS data. Therefore, further work needed for our sodium caseinate synthesis should focus on providing more detail on the mechanism by which casein controls silica particle morphology. Using these particles produced with sodium caseinate in advanced applications such as drug delivery or biosensors would be interesting further work. It would also showcase that particles produced using such sustainable methods can achieve parity with those made by traditional means. We have shown preliminary results indicating that porosity can be achieved using biomolecular templates. Future work on this should focus on developing and expanding these porous structures which would open up many more applications for sustainably-synthesised particles.

We have shown that it is possible to synthesise spherical silica particles more sustainably than can be done with Stöber processes. Our hope is that such sustainable processes will ultimately succeed the Stöber processes, especially for larger-scale syntheses. However, the work detailed here is only a tentative step in that direction, not least because the quality of our particles is still below that of those made via traditional methods. There are infrastructural barriers around municipal and industrial water treatment and processing that must be addressed for water-based chemistries to be economically feasible at industrial scales. These issues are beyond the scope of our work but are an ongoing focus of the UN Sustainable Development Goals, numerous state circular economy initiatives,

and various governmental and non-governmental green chemistry initiatives. However, using biopolymers from waste streams of global scale industrial processes, such as caseinate from dairy production wastes, provides a source of large amounts of the desired biopolymers. In the case of dairy products, these are subject to increasing global demand year-on-year, guaranteeing a steady supply of the necessary biopolymer. It is important to note, however, that industries like dairy production generate large greenhouse gas emissions, and future, regular life-cycle analyses should be part of any development of circular economies and green chemistries – within silica manufacture and without. This should be done to ensure that valorisation of waste streams does not lead to maintenance of damaging industries that would otherwise fail economically without such valorisation. This would represent a threat to supply of biopolymer sources, making source variety critical. The fact that spherical silica can be achieved with other biomolecules, like lecithin (another waste product), ensures flexibility and robustness of supply. Lecithin can also be obtained from egg yolks, and with hundreds of millions of eggs thrown away every year, this represents another example of a robust supply.

Using valorised waste streams of more than one process for products of increasing demand also removes the need to compete for arable land to grow crops to meet biopolymer demand. This means that no additional embedded environmental costs from fertilisers, pesticides, etc. are incurred. Further, this prevents the wastes from which the biopolymers are obtained from entering landfills or being down-cycled into agricultural feeds where they break down and release methane gas, which has a potent greenhouse effect, far greater than that of CO_2. Yet another benefit is that the use of biopolymers from valorised waste streams and the general reduction of organic reagents in industrial

processes reduces the embedded costs associated with petrochemical production and refinement. This is not to say that there are no greenhouse gas emissions embedded in the production of biopolymers – of course there are. These will arise particularly from processes needed to isolate them from waste streams, and from the use of water-based chemistries, which currently requires far more energy to purify the primary solvent, water, than organic solvents do. Part of the issue here is the lack of development of industrial water purification infrastructures, which could lead to greater efficiencies in this area. Ultimately however, if future life-cycle analyses prove that the use of organic solvents is associated with lower long term greenhouse gas emissions, including all embedded costs, than using water-based chemistries, then the water-based chemistry aspect of our work must be cast aside. Fortunately, this does not mean that the use of biopolymers as structural directing agents in spherical silica synthesis must be cast aside. Many biomolecules, particularly proteins, can, if necessary, be made to work within organic chemistries. This means that the reduced emissions associated with biopolymers valorised from industrial waste streams could be retained and result in vastly decreased greenhouse gas emissions. Should future life-cycle analyses prove this to be the case, then the direction of research into the use of biopolymers for spherical silica production will have to shift in this direction. The use of water-based chemistries, as in our work here, is technically harder to achieve than sticking with established organic chemistries, so pivoting in the direction of the latter would be simple. However, it is the opinion of the of the writer of this thesis that, at this time in history, this does not seem likely to be the future of this research. The highest priority problem to be solved for the planet right now is that of human driven climate change and that means first and foremost we must reduce

greenhouse gas emissions. This thesis shows that producing spherical and monodisperse silica particles is possible using biopolymer-based syntheses and water-based chemistries, and this is a small step towards achieving that.